

Studies of Alkali Metal Compounds in Diesel Fuel and Small Molecule Activation Chemistry

Richard Mackay Gauld

Department of Pure and Applied Chemistry

University of Strathclyde

A thesis submitted to the Department of Pure and Applied Chemistry, University of Strathclyde, in part fulfilment of the requirements for a degree of *Doctor of Philosophy*

2020

This thesis incorporates published work which is the result of the authors original research. It had been composed by the author and has not been previously submitted for examination which has led to the award of a degree.

Signed (Author):

Date:

Signed (Supervisor)*:

Date:

*Confirming the author was primarily responsible for the composition of the published material within the thesis.

Dedicated to my mother, father and late grandfather:

Isabel, Derek and Richard

Acknowledgments

They say that no man is an island and in much the same thread no PhD is ever completed in isolation. The work contained here could never have been successfully completed without the support, encouragement and friendship of many people scattered around the world. It would be remiss of me not to take this opportunity to thank each and every one of them who have encouraged me throughout the past three and a half years, without whom none of this would have been possible.

Firstly, I must thank my supervisor Prof. Robert Mulvey for allowing me the opportunity to join his research group in the first place. His support, ideas, insight and guidance have been instrumental not only to the success of the PhD project but also to my development both as a chemist and a person. I must also say thank you for allowing me the opportunity to represent the group and by extension yourself at the various conferences I have had the pleasure of attending, especially the ICOMC in Florence, definitely the best experience (and steak) I've had! In addition, I must also thank the other academics of the inorganic section, Prof. Eva Hevia, Dr Charlie O'Hara and Dr Stuart Robertson. All of them have given many great suggestions over the years and were always available for a friendly chat about chemistry or life in general. Special thanks must be extended to a few people throughout Strathclyde, starting with Dr Alan Kennedy, who must have the patience of a saint to have dealt with all the X-ray data that I've sent him over the years. Thanks to Dr Chris Dodds for giving me the opportunity to demonstrate in the undergraduate teaching labs, an experience that I have enjoyed immensely over the past three and a half years. Many thanks are also due to Craig Irving, without whom the NMR aspects of the work presented in this thesis simply would not have been achieved. He was also always available for a chat when things were not quite going right in my research which was appreciated. Janie-Anne, who helps keep the lab running with glassware and help also deserves thanks, if only for having to put up with me talking rubbish in the office for the past three years. Finally, thanks to Paul and Billy, who gladly volunteer their

time to help with aspects of departmental life without ever asking for anything in return.

I would hate to miss anyone out who has been part of this PhD journey, so I'd like to thank Alberto, Andy, Annie, Antonio, Callum, Etienne, Florian, Laia, Leonie, Lewis, Maria, Marina, Mark, Michael F, Michael W, Pasquale, Ross, Sam, Scott, Sonia, Stephen, Thomas and Vicky. Special thanks however must go to a few notable people. Dr Ross McLellan, who has made a positive contribution to many, if not all, of the good ideas contained within this thesis, as well as being a source of many practical and theoretical tips on X-ray crystallography. Dr Victoria Pollard (to be formal) was a great source of friendship both in and out of the lab during the time we overlapped, and I shall treasure many of our conversations in the office and in Cranberries, be it about chemistry or not. Dr Sonia Bruna Fernandez, who had the misfortune to share an office with me for her entire time here deserves thanks for putting up with me for so long! There were many days when the greatest source of fun was the conversations we had, especially on the days when Real Madrid had been beaten!

I have also had the pleasure to have worked with several visiting scholars and final year students in my time in the group and all of them deserve praise for making the most of their time both at Strathclyde and Scotland in general. Lara, the best student ever. Becky, who I have no doubt is still jumping up and down in the yellow wall. Lea, who has worked ridiculously hard on about 15 different things. Heather, who shared an office with me for the last few months and has coped with that unfortunate turn of events with good grace and humour. Kaddy, who loved it here so much she came back, and life in the lab was always better when she was around! And last but by no means least, a very special thank you to Jen. She has put up with all of my stress induced ramblings both inside and outside work, as well as finding the time to support me throughout the writing of this thesis and I am sure that whatever she does in the future, she will excel at it.

I must also thank both the EPSRC and Innospec Ltd. for providing the funds to allow me to undertake the research contained within this thesis. Special thanks are also

due to Dr Jim Barker and Miss Jacqueline Reid from Innospec Ltd., for encouraging me before, during and after our industrial meetings. I have learned a lot from our collaboration and sincerely hope our paths cross sometime in the future.

A massive thank you must go to my family: my mum, Isabel and my dad, Derek, both of whom have offered unconditional support and encouragement throughout the PhD and the writing of this thesis. From encouraging me to read as soon as I was able to; to buying me that microscope when I was seven and starting me on my journey towards science, I can never adequately express how much I am forever grateful for what you have done for me.

Finally, I must ensure that I mention my late grandfather, Richard McDowell Mackay. He is the man I am named after, and while he did not live long enough to see me start or indeed complete this PhD, I know that he would be as proud of me now as he was when I first got accepted into university.



Abstract

The study of internal diesel engine deposits is a field that has recently begun to be explored in more depth from a chemistry perspective. The many issues caused within diesel engines related to the formation of insoluble, carboxylate-based deposits demanded insight be gained into the chemical make-up and composition of such deposits in the crystalline state. Such insight is challenging as the long chain nature of these deposits complicates the ability to render them crystalline, hence why no detailed studies had previously been carried out onto such species. Of related interest is the expanding field of small molecule activation chemistry, with CO₂ being a prime example of an environmentally damaging small molecule produced by diesel engines. Despite the worldwide activity in both small molecule activation and alkali metal-based chemistry, no previous studies had sought to combine these two strands of research as undertaken here.

The first part of this project develops the field of diesel deposits in terms of accessing suitable crystals in order to determine the solid-state structures of long chain alkali metal carboxylates, of the type commonly found within diesel engines. The products obtained were characterised by X-ray crystallography and multinuclear NMR spectroscopy. This revealed a remarkable set of structures, ranging from dimeric arrangements in polar solvents to polymeric arrangements in non-coordinating solvents. A highlight is the structure of the long chain sodium 2-ethylhexanoate, **3**, which to the best of our knowledge represents the longest chain solvent-free and donor-free alkali metal carboxylate characterised using single crystal diffraction, showing a novel arrangement composed of a central hydrophobic core, with the long alkyl chains arranged around the periphery of this central core, rather than a simple layering arrangement.

In the second part of this project the activation of the globally important small molecule CO₂ was probed using common alkali metal based reagents. Three novel structures were crystallographically characterised, collectively exhibiting a higher degree of complexity post CO₂ addition than would otherwise be anticipated. For example, addition of CO₂ to LDA was anticipated to occur between the reactive Li-N bond to form a molecular lithium carbamate, however in actual fact addition of CO₂ furnished a more complex dodecameric structure, composed of two open cubanes linked by planar four-membered (LiO)₂ rings. Extension to small isocyanate molecules and NacNac alkali metal reagents revealed a common series of

transformations, leading to products containing new dual imine and amide functionality at the backbone γ -carbon position. The mechanism leading to this dual functionality was explored *via* multinuclear NMR spectroscopic studies. Finally, extension to carbodiimides and phosphine oxide molecules revealed attack at the front of the alkali metal NacNac complex, contrasting with the backbone γ -carbon attack seen with isocyanates and CO_2 .

Peer Reviewed Publications

- “Diverse outcomes of CO₂ fixation using alkali metal amides including formation of a heterobimetallic lithium–sodium carbamato-anhydride via lithium–sodium bis-hexamethyldisilazide”- R. M. Gauld, A. R. Kennedy, R. McLellan, J. Barker, J. Reid and R. E. Mulvey, *Chemical Communications*, 2019, **55**, 1478-1481.
- “Backbone Reactivity of Lithium β -Diketiminato (NacNac) Complexes with CO₂, *t*BuNCO and *i*PrNCO”- R. M. Gauld, R. McLellan, A. R. Kennedy, J. Barker, J. Reid and R. E. Mulvey, *Chemistry: A European Journal*, 2019, **25**, 14728-14734.
- “Structural Studies of Donor-Free and Donor-Solvated Sodium Carboxylates”- R. M. Gauld, R. McLellan, A. R. Kennedy, F. J. Carson, J. Barker, J. Reid, C. T. O’Hara and R. E. Mulvey, *Preliminary drafted manuscript*.

Conference Presentations

Oral Presentations:

- R. M. Gauld, R. McLellan, A. R. Kennedy, J. Barker, J. Reid, R. E. Mulvey; *“Small molecule activation of CO₂ utilising alkali metal amides.”* Universities of Scotland Inorganic Chemistry Conference 2018 (USIC-52), University of Edinburgh, Edinburgh, 3rd-4th September **2018**.

Poster Presentations:

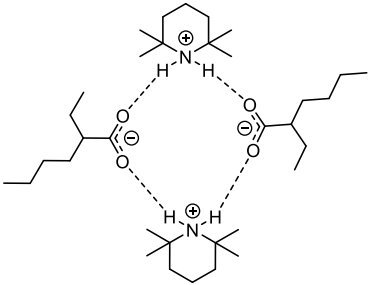
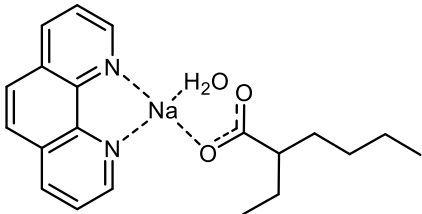
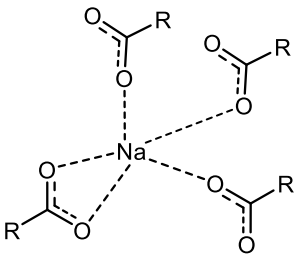
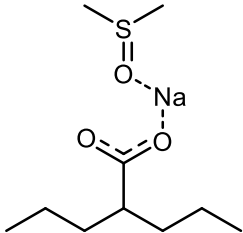
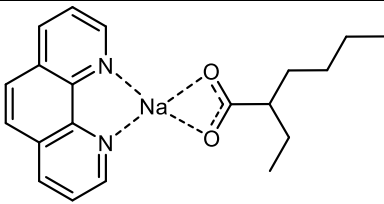
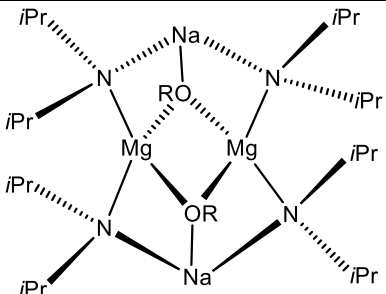
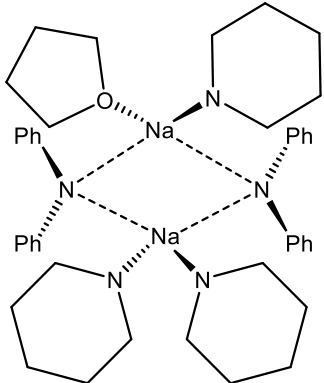
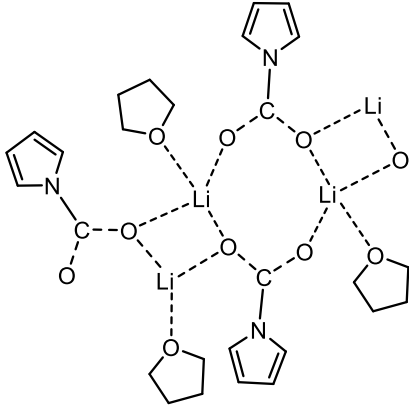
- R. M. Gauld, R. McLellan, A. R. Kennedy, J. Barker, J. Reid, R. E. Mulvey; *“Fixation of small molecules utilising a common β -diketiminato scaffold.”* Dalton Younger Members Event (DYME), University of Cardiff, Cardiff, 5th-6th September **2019**.
- R. M. Gauld, R. McLellan, A. R. Kennedy, J. Barker, J. Reid, R. E. Mulvey; *“Fixation of small molecules utilising a common β -diketiminato scaffold.”* Universities of Scotland Inorganic Chemistry Conference 2019 (USIC-53), University of Glasgow, Glasgow, 29th-30th August **2019**.
- R. M. Gauld, A. R. Kennedy, R. McLellan, J. Barker, J. Reid, R. E. Mulvey; *“Small molecule activation of CO₂ using common utility amides.”* International Conference on Organometallic Chemistry 2018 (ICOMC-28), Florence, Italy, 15th-20th July **2018**.

Abbreviations

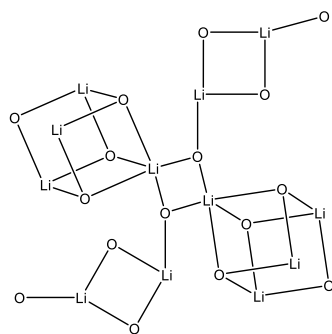
1,10-phen	1,10-phenanthroline
12-crown-4	1,4,7,10-tetracyclododecane
15-crown-5	1,4,7,10,13-pentaoxacyclopentadecane
Ar	Generic aryl group
Bar	Bar (Unit of pressure, 1 bar = 0.987 atm)
C ₆ D ₆	Deuterated benzene
CDCl ₃	Deuterated chloroform
CSD	Cambridge Structural Database
Cy	Cyclohexyl group
d ₈ -toluene	Deuterated toluene
Dipp	2,6-diisopropylphenyl group
DOSY	Diffusion ordered NMR spectroscopy
Et	Ethyl group
FLP	Frustrated Lewis pair
HMDS/HMDS(H)	1,1,1,3,3,3-hexamethyldisilazide/1,1,1,3,3,3-hexamethyldisilazane
HOMO	Highest Occupied Molecular Orbital
<i>i</i> Bu	<i>Iso</i> -butyl group
<i>i</i> Pr	<i>Iso</i> -propyl group
IR	Infra-red
K	Kelvin
LDA	Lithium Diisopropylamide
LUMO	Lowest Occupied Molecular Orbital
Me	Methyl group
Me ₆ -TREN	Tris[2-(dimethylamino)ethyl]amine
MeOD	Deuterated methanol
NacNac	β-diketiminato ligand
<i>n</i> Bu	<i>n</i> -butyl group
ⁿ BuLi	<i>n</i> -butyl lithium
NaO ^t Bu	Sodium <i>tert</i> -butoxide
NMR	Nuclear Magnetic Resonance

	s – singlet
	d – doublet
	t – triplet
	br – broad
	m – multiplet
Ph	Phenyl group
ppm	Parts per million
PMDETA	N,N,N',N'',N'''-pentamethyldiethylenetriamine
R	Generic alkyl group
RT	Room temperature
<i>t</i> Bu	<i>Tertiary</i> -butyl group
THF	Tetrahydrofuran
TMEDA	N,N,N',N'-tetramethylethylenediamine
TMP/TMP(H)	2,2,6,6-tetramethylpiperidide/2,2,6,6-tetramethylpiperidine
TMS	Trimethylsilane
X	Halide

Table of Numbered Compounds

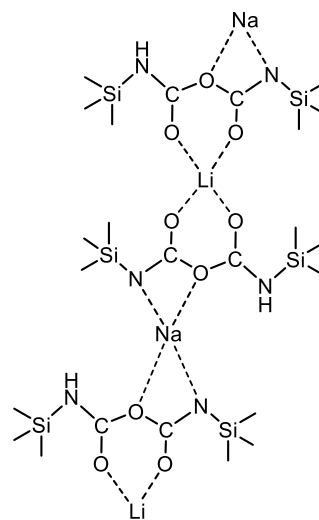
Compound Number	Compound	Compound Number	Compound
1		2	
3	 where R is 2-ethylhexanoate	4	
5		7	 where R is 2-ethylhexanol
9		10	

11

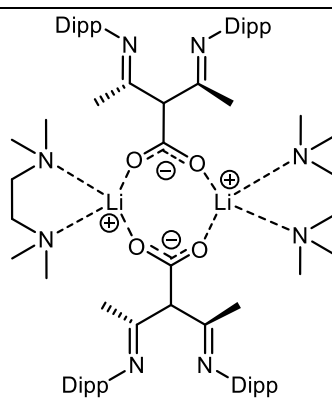


Organic groups omitted for clarity

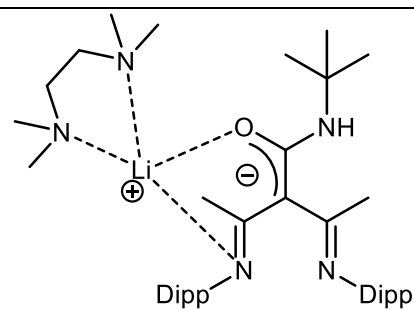
12



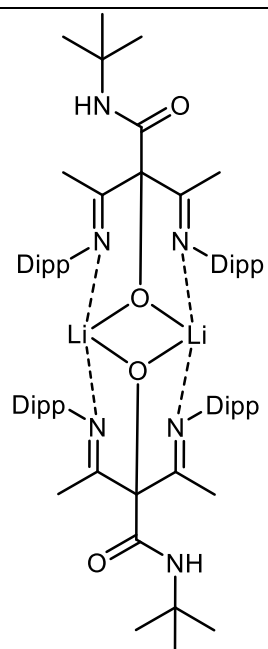
13



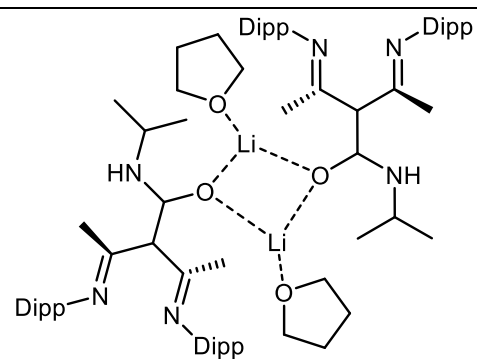
14



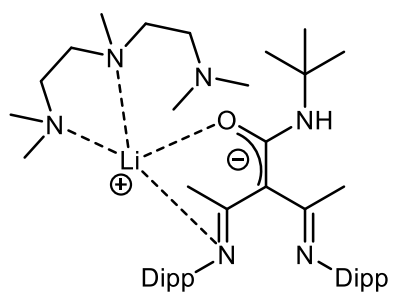
15



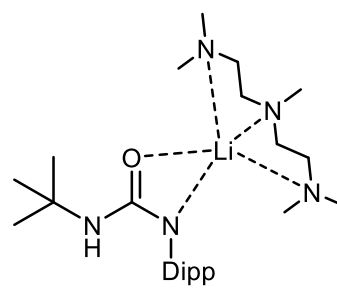
16



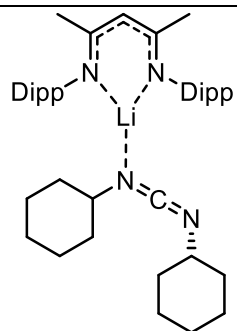
17



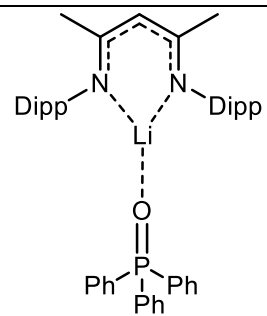
18



19



20



Contents

Acknowledgments.....	iv
Abstract.....	vii
Peer Reviewed Publications.....	ix
Conference Presentations.....	x
Abbreviations.....	xi
Table of Numbered Compounds.....	xiii
Part I: Studies of alkali-metal carboxylates in diesel fuel and deposits.....	1
Chapter 1: Introduction	1
Preface	1
1.1 Diesel composition and the problem of deposits.....	1
1.1.1 Composition of diesel and its properties	1
1.1.2 Diesel additives: Uses and nature.....	8
1.1.3 Identity of diesel engine deposits and associated issues	13
1.2 Carboxylate Group Chemistry.....	16
1.2.1 Types of metal carboxylate and their analysis.....	19
1.3 Overall aims of Part I of the PhD project	24
Chapter 2: Structural Studies of Donor-Free and Donor-Solvated Sodium Carboxylates	26
2.1 Abstract.....	27
2.2 Introduction	28
2.3 Introduction from the Manuscript.....	30
2.4 Results and Discussion	33
2.5 Extended results and discussion.....	45
Part II: Small molecule fixation utilising common molecular architectures	74
Chapter 3: Introduction	74
Preface	74
3.1 Small molecule fixation chemistry.....	75
3.1.1 Fixation of CO ₂	75
3.2 β -diketiminate chemistry.....	84
3.2.1 β -diketimines in organometallic chemistry	86
Chapter 4: Diverse outcomes of CO ₂ fixation using alkali metal amides including formation of a heterobimetallic lithium–sodium carbamate-anhydride via lithium–sodium bis-hexamethyldisilazide.....	98
4.1 Abstract.....	99

4.2 Introduction	99
4.2.1 Organolithium chemistry	100
4.2.2 Utility amides	105
4.3 Project aims.....	119
4.4 Introduction from the manuscript	119
4.5 Results and Discussion	121
4.6 Extended Discussion and Future Work	127
Chapter 5: Backbone Reactivity of Lithium β -Diketiminates (NacNac) Complexes with CO ₂ , tBuNCO and iPrNCO	136
5.1 Abstract.....	137
5.2 Introduction	137
5.3 Project aims.....	137
5.4 Introduction from the manuscript	138
5.5 Results and Discussion	140
5.6 Extended Discussion and Future Work	149
Chapter 6: Conclusions and Outlook	160
6.1 Conclusions	160
6.2 Outlook and Future Perspectives.....	164
Chapter 7: Experimental	167
7.1 General Experimental techniques.....	167
7.1.1 Solvent and reagent purification	167
7.1.2 Analytical techniques	167
7.2 Experimental data for Chapter 2	170
7.2.1 Synthesis of compounds	170
7.3 Experimental data for Chapter 4	177
7.3.1 Synthesis of compounds	177
7.4 Experimental data for Chapter 5	181
7.4.1 Synthesis of compounds	181
7.5 Crystal structure data and refinement details for compounds reported in this thesis ..	189
References	194

Part I: Studies of alkali-metal carboxylates in diesel fuel and deposits

Chapter 1: Introduction

Preface

Of recent concern within the fuel industry is the problem of insoluble deposits coating various components of diesel engines. These deposits, identified as being mostly composed of sodium carboxylates, lead to a variety of issues within the engine and can ultimately lead to complete loss of power to the vehicle. Therefore, the industry has been keen to identify the nature of these deposits and the structures that they adopt both in solution and the solid state. Given the problems that can be caused by such deposits, it is perhaps surprising that no major studies have looked at the nature of them from a purely chemistry viewpoint, with most work looking at diesel engine deposits studying them from an engineering point of view. The first part of this thesis will detail studies carried out attempting to obtain insight into the nature of long chain carboxylates found in diesel fuel, looking at the types of carboxylate structure that may form in diesel fuel as well as during the engine testing process carried out by fuel refineries and retailers. The focus here will be applied to the structures adopted by such species in both solution and the solid state, as well as looking at the type of reactivity such species undergo in the diesel engine itself. Firstly, and in order to set the context for the research presented, a more in-depth introduction to the phenomenon of diesel engine deposits will be presented.

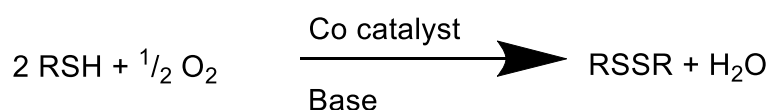
1.1 Diesel composition and the problem of deposits

1.1.1 Composition of diesel and its properties

The complex mixture of components known commercially as diesel is one of many products produced from a common source of crude oil. Diesel, along with petrol, is one of the major fuel sources used to run commercial vehicles, with diesel also being the preferred fuel used in railroad, industrial vehicles and military installations. Advantages of diesel over petrol

include the fact that it is more reliable, more robust and also provides a better fuel economy, as well as the engine itself being less sensitive than petrol to variations between batches of fuel.^{1, 2} This latter point is particularly important given the variation of diesel depending on the blend of additives each supplier adds. Indeed, in the first half of 2016, 49.7% of all new cars registered within Europe ran on diesel, with the figures being 47.9% and 70.4% within the United Kingdom and Republic of Ireland respectively.³ Diesel is produced from crude oil that is extracted from the ground *via* a process called fractional distillation. Put simply, this involves using the different boiling points of the varying chemicals or fractions within crude oil samples to separate them. Once collected, these fractions can then be transformed into new products. This process takes place in a fuel refinery, where the lightest fractions with the lowest boiling point are collected first. These are usually light hydrocarbons such as butane and propane and are collected at the top of the refinery tower.⁴ Gasoline, kerosene and diesel are then collected from successive lower points on the column, due to having successive higher boiling points, with anything left at the bottom of the tower collected as atmospheric bottoms.⁴

The next major process that occurs on the diesel fraction is a desulfurization process to remove the majority of any sulfur containing compounds from the mixture. Sulfur compounds should be removed from fuel as their presence can increase the concentration of soot particles emitted by the engine and the sulfur can also be converted *via* combustion to sulfur oxides, which have a corrosive effect upon the engine.⁵ The removal of sulfur from diesel is also mandated by legislation in many jurisdictions such as the United States and European Union. The process whereby sulfur is removed is sometimes called a mercaptan oxidation process or Merox process.⁶ Within the refinery, thiols are converted into disulfides using a cobalt catalyst such as cobalt tetrasulfophthalocyanine and a base (Scheme 1.0).⁷



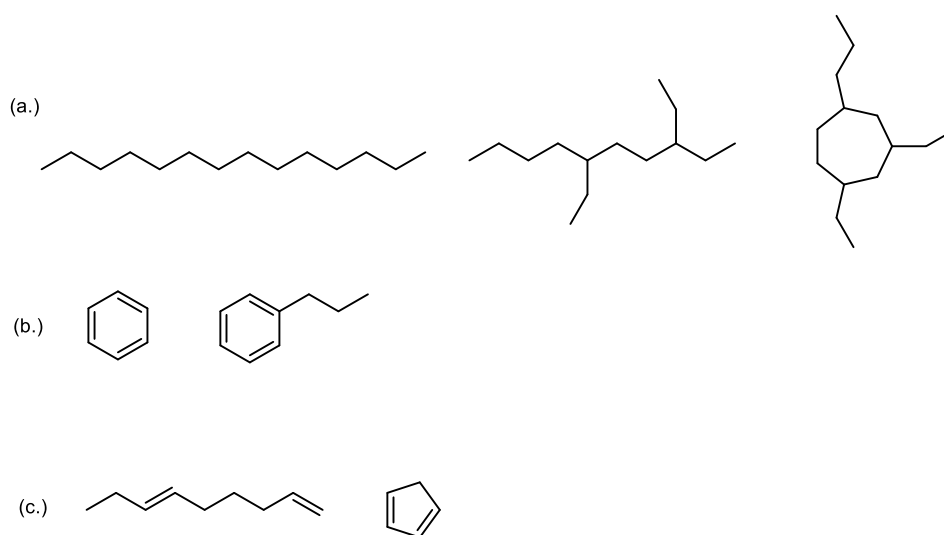
Scheme 1.0: Chemical conversion of thiols (RSH) to disulfides (RSSR) *via* the Merox process.

The base used in this process usually consists of either ammonia or sodium hydroxide, the latter of which can cause deposit related issues if it is not fully removed.⁶ It is also possible that the removal of sulfur from the fuel has contributed to the growing carboxylate salt

deposit problem, with modern low sulfur fuels less able to solubilise the materials that cause such deposits. This is due not to the removal of the sulfur itself *per se*, but instead is due to the Merox process also removing the trace materials that impart lubricity onto the fuel.⁸

It is also possible to get what is known as hydrocracked gas oil, which can be blended with other products to create the diesel that leaves the refinery. This hydrocracked oil is produced by the breaking down of higher mass products into smaller molecules using a catalyst under a hydrogen atmosphere.

What is clear from the refining process is that the diesel that leaves the refinery is a complex mixture of chemicals, each of which confers its own unique properties onto the overall diesel mix. From a purely elemental composition, diesel consists of 84-86% carbon and 13-15% hydrogen, with the remaining 1% consisting of impurities or additives,⁹ which are unsurprising numbers given diesel is a well-known hydrocarbon product. There are generally three main groups of hydrocarbons present within diesel. These are saturated hydrocarbons, composed of alkanes (paraffins), iso-alkanes and cycloalkanes (naphthenes), which make up 66% of diesel, aromatics such as benzene and substituted benzenes which account for 30% of diesel and finally unsaturated hydrocarbons composed of alkenes (olefins) that make up the remaining 4%.^{4, 9} Scheme 1.1 shows chemical structures representative of the type of hydrocarbons that may be found within diesel.



Scheme 1.1: Common compounds present in diesel fuel: (a) shows an alkane, iso-alkane and cycloalkane each consisting of 14 carbon atoms; (b) shows benzene and a substituted benzene; and (c) shows an alkene and a cycloalkene.

Also present in all diesel samples will be a small number of other molecules such as thiophenes that have not been eliminated in the Merox process and carbazoles.⁴ Although such molecules are few in number, they can play a pivotal role in the determination of certain properties of the fuel blend.⁴ There may also be some polycyclic aromatic hydrocarbon (PAH) compounds present. These PAHs are compounds comprising only fused aromatic rings. These will predominantly be 3 fused-ring species such as anthracene, which consists of three benzene rings fused together, but there may be some larger 4- or 6-ring examples.¹⁰ These PAHs have been implicated as a particular outdoor source of pollution and in fact were one of the first atmospheric pollutants identified as potential carcinogens.¹¹

Pertinent to this project, there will be a small number of alcohol and carboxylic acid molecules within the diesel, though the numbers of these molecules are so low they tend not to affect the properties of the diesel, only the refining of the crude product.¹² Indeed many acid species under investigation in this project are in fact deliberately added to the fuel by manufacturers for a variety of reasons (See Chapter 1.1.2 for further details on the additives added to diesel fuel).

There will also be inherent variation in the hydrocarbons present in the diesel. As a general rule, most compounds present will have a carbon number between 9 and 25,¹⁰ that is to say the backbone of the compound will consist of between 9 and 25 carbon atoms. For example, in Scheme 1.1, all the compounds seen in (a) have a carbon number of 14. One of the factors that make the properties of different brands of diesel unique is that each brand will have varying proportions of each class of hydrocarbon present within the overall product.⁴ Important properties to consider about diesel are its viscosity, volatility or boiling point, density and lubricating properties.¹³ There are a series of trends that can be used to predict the properties each class of hydrocarbon will impact upon the fuel. A summary of the main trends of compound classes found in diesel is presented below:

(i) Boiling Point

In general, the boiling point of a compound increases as the number of carbon molecules increases, for example, octane has a higher boiling point than hexane. This is true as long as the class of compound is constant and you are comparing like with like.⁴ If the carbon-number is kept the same and the class of compound is changed, the boiling point decreases in the sequence:

Aromatics > cycloalkanes > n-alkanes > iso-alkanes

It should be noted that iso-alkanes have a lower boiling point than n-alkanes due to the smaller surface area of iso-alkanes when compared to n-alkanes, meaning that dispersion forces are smaller for iso-alkanes and they can subsequently boil at lower temperatures.¹⁴ The boiling point of diesel, due to the variation in compounds that are present within the mixture is not well defined to a single value but instead has a wide range of possible values, generally spanning 170-390 °C.¹⁰ Taking a mid-point of the range as approximately 260 °C, the main compounds that boil at this temperature are C₁₂ aromatics, C₁₃ cycloalkanes, C₁₄ alkanes and C₁₅ iso-alkanes.⁴

(ii) Density

Density is an extremely important property of diesel as it affects the amount of fuel injected into the engine.⁵ If the density of the fuel is higher than normal, the fuel-air ratio in the engine will also be higher and, theoretically at least, the engine will produce more power.⁵ However, the negative aspect of having a dense fuel is that the smoke emissions and particulate matter levels will also increase⁵ and as these are tightly controlled by legislation, the maximum density is generally kept at a middle level. Again as above, hydrocarbon density increases as the carbon-number increases.⁴ If the carbon-number is kept constant, the density decreases in the sequence:

Aromatics > cycloalkanes > alkanes

Of course, density is not a constant value and varies with the environment the fluid is placed in. It is known from two laws that as pressure increases, the density will also increase while as the temperature increases, the density will decrease, known as Boyle(s) and Charles(s) laws respectively.¹⁵ In modern engines, the density will vary significantly under the high temperatures and pressures experienced.¹⁶ Schaschke *et al.* found that there is inherent variation within diesel blends with regards to their density at different temperatures and pressures, with the presence of additives also leading to differences between blends produced by different refineries.¹⁶

(iii) Cetane Number

The cetane number of diesel is a way of quantifying the ignition quality of the diesel fuel being tested.⁵ Essentially it is a measure of how well the diesel will ignite when compressed,

with a fuel having a higher cetane number consequently having a shorter ignition delay.¹⁷ Cetane numbers are the inverse of octane numbers for petrol, with a high octane number indicating a fuel that is more resistant to spontaneous ignition *via* compression.¹⁷ With regards to diesel fuel specifically, the higher the cetane number the better the overall ignition quality, with the long chain hydrocarbon cetane itself (Figure 1.0) being given a score of 100.⁵ Interestingly, recent work carried out by Boot *et al.* has shown that sometimes a high cetane number will actually lead to an increase in the amount of soot and nitrous oxide gas produced which is limited by law to reduce the impact upon human health.¹⁸ The study found that a high concentration of substituted aromatics within the fuel would lead to lower cetane numbers (see below), which would then subsequently lead to a higher level of soot emissions as expected.¹⁸ However, if additives that increase the cetane number were added, the level of soot produced was still higher.¹⁸ While these findings contradict each other, they successfully show the vast complexity found when looking at the most “simple” of diesel samples.

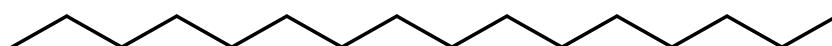


Figure 1.0: Chemical structure of cetane (C₁₆H₃₄).

The cetane number of fuels can be boosted by adding certain cetane boosting compounds, typical examples of which are organic nitrates such as 2-ethylhexyl nitrate (Figure 1.1).¹⁹

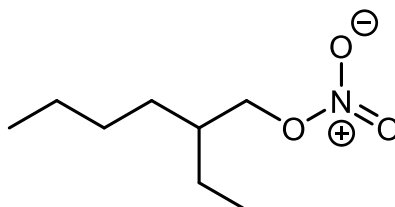


Figure 1.1: Chemical structure of 2-ethylhexyl nitrate.

The secondary advantages of using compounds such as these are improvement of cold-start performance, reduction of both combustion noise and soot emissions.²⁰ The disadvantages of using organic nitrates is that they not only increase the flammability of the fuel, but they also reduce the stability,²⁰ making it more likely that degradation products will be present if the fuel is stored for a long period of time.

The cetane number varies among different classes of hydrocarbons:

n-Alkanes: as the molecular weight of the alkanes increases, the cetane number also increases.⁴

iso-Alkanes: there is a wide range of possible cetane numbers between 10 and 80.⁴ The nature of the iso-alkane can make a difference, with a hydrocarbon possessing many short side chains having a lower cetane number than a hydrocarbon with one side chain of four or more carbon atoms, which will have a higher cetane number.⁴

Cycloalkanes: a much narrower range is seen here, with typical values in the range 40-70.⁴ A high molecular weight hydrocarbon with one long side chain will have a higher cetane number, while a low molecular weight hydrocarbon with a short side chain will have a lower cetane number.⁴

Aromatics: the range here is between 0 and 60.⁴ A benzene substituted compound with a long chain will have a cetane number generally near the upper end of the range, while a benzene substituted with a short chain will be on the lower end of the scale.⁴ Where a number of aromatic rings fused together, as in PAHs, the cetane number will be below 20.⁴

(iv) Viscosity

Viscosity is a measure of how resistant a liquid is to flow across a surface. This property is related to molecular weight, with larger molecules typically being more viscous than smaller molecules. If the carbon-number is kept constant, cycloalkanes are seen to be slightly more viscous than alkanes or aromatics.⁴ In terms of a relationship between viscosity and temperature, it is found that the viscosity of a given fuel decreases exponentially as the temperature increases.²¹ This is an important point, as in engines the fuel will experience much higher temperatures and pressures than it would normally be subjected to, which would therefore have an impact upon the viscosity.

In order to give clarity to all diesel suppliers, a set of standard values for many properties of diesel have been set by governmental organisations worldwide. Within the European Union for example, the European Standards Organisation have developed a set of standards set out in the document BS EN 590, with all EU member countries ensuring that the diesel used within their country abides by these standards.⁴ Table 1 summarises the latest guidance, issued in 2013.

Table 1.0: European standards for diesel fuel, set in BS EN 590, adapted from information contained within reference (4).

<i>Property</i>	<i>Value as set by BS EN 590</i>
Cetane number	Minimum of 51
Density at 15 °C	Minimum of 0.820 g/ml Maximum of 0.845 g/ml
Polycyclic aromatic hydrocarbon content	Maximum of 10% m/m
Flash Point	Temperature > 55 °C
Water Content	Maximum of 250 mg/kg
Lubricity at 60 °C	Maximum of 460 µm
Viscosity at 40 °C	Minimum of 2 mm ² /sec Maximum of 4.5 mm ² /sec
Fatty acid methyl ester (FAME or biodiesel) content	Maximum of 7% v/v

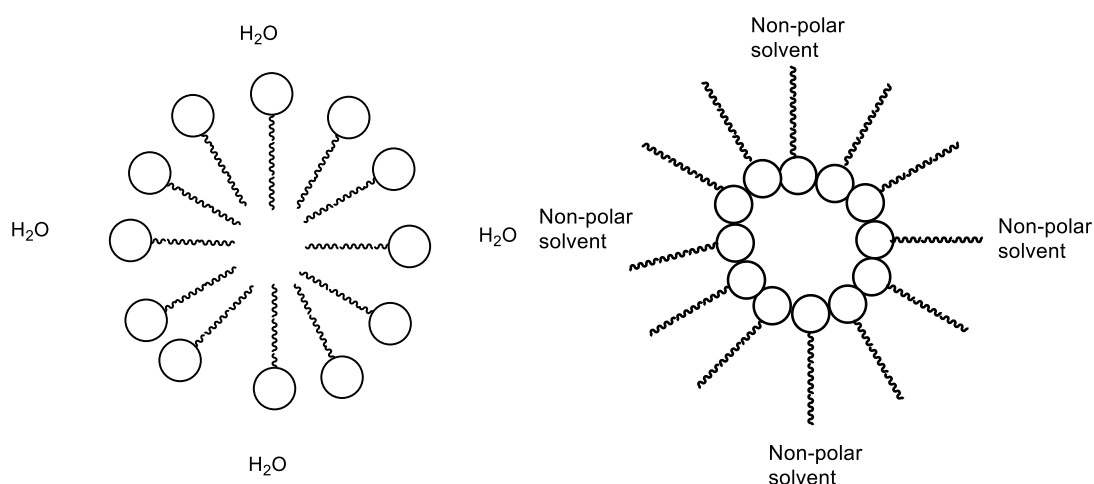
1.1.2 Diesel additives: Uses and nature

The preceding section described the chemical composition of diesel as it leaves the refinery. However, by the time it has been added to the engine of a car, the overall composition will be very different. Each major fuel provider will add a series of additives to their own brand of diesel, with variations in additives common even among the same overall brand, with premium versions having a different additive blend added compared to ‘normal’ batches. These additives are compounds designed to improve upon some aspect of the fuels’ engine performance. They are ubiquitous amongst almost all diesel blends and can range from combustion improvers to anti-icing additives for cold climate countries.¹⁹ The most pertinent additives in this project are deposit control additives, lubricity improvers and corrosion inhibitors. Each of these additive types will now be discussed in turn:

(i) Deposit control additives

Deposit control additives or DCA are widespread in their use throughout diesel engines the world over. Many companies such as Innospec do not specify the exact chemical nature of the DCA they use, instead stating that they use a ‘commercially available additive that is used globally’, with no further details or analysis into what this globally available additive is,

presumably due to industrial confidentiality. However, most DCA will share a common structure, that of a long chain, hydrophobic hydrocarbon tail with a hydrophilic polar head group attached.²² One theory of how these additives are able to control deposits is based on the fact that this polar head will have an affinity for the metal surface of the engine, while the non-polar hydrocarbon tail allows the DCA to remain fuel soluble.¹⁹ Any precursors in the fuel that cause deposits will be attracted to the DCA molecule and they will then become bound together in a resulting inverse micelle.²² A micelle is an aggregate of a specified dimension that exists in an equilibrium with the ions or molecules that make up said aggregate.²³ A pictorial representation of two common micelle types is shown in Scheme 1.2.



Scheme 1.2: Molecular level diagram of micelle classes. Left, a conventional micelle that would form in aqueous solution, with the polar head pointing out towards the solution and the non-polar tails pointing inward; Right, an inverse micelle that forms in non-polar solvents, with the long chain hydrocarbon pointing out towards the solution.

Another theory postulates that the DCA forms a thin liquid film on the metal surface at ambient temperature, meaning any deposits that have already formed will be washed away *via* detergent action.²² There can also be a preventative effect, whereby the DCA will prevent the agglomeration of any deposit precursors.¹⁹ This method is more likely to occur *via* a process known as steric stabilisation. This would involve the polar head of the DCA being attracted to the polar deposit and the long polymeric chain being suitably soluble in the fuel, thus allowing for the prevention of any deposit formation.²⁴ Many of these DCA are based on polymeric molecules such as polyisobutylene succinimide (PIBSI) (Figure 1.2). It is composed of a polyamine 'head' and a long chain polyisobutylene 'tail' that stabilises the structure.²⁵ It is found that by increasing the number of secondary amines within the structure, a greater

attraction occurs between the polar head of PIBSI and the metal surface or, in some cases, for the polar surface of the particle being controlled.²⁵

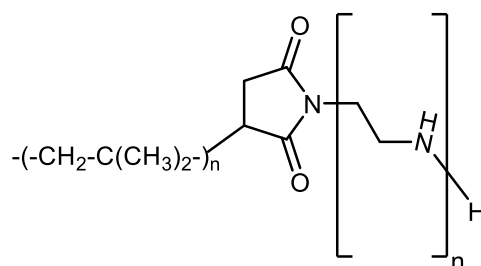


Figure 1.2: Molecular formula of polyisobutylene succinimide (PIBSI).

Generally PIBSI is added to diesel at a concentration range of between 10 and 200 mg/kg.¹⁹ There have been some issues with this additive in the past due to its polymeric nature, specifically centred on if a low molecular weight PIBSI is used within the fuel. Fox and Bennet found that if the PIBSI-type DCA added was of low molecular weight, with polar compounds and carboxylic acid functionality present, deposits could form as a result of this DCA being added.²⁶ Of course, this rather defeats the purpose of adding the DCA in the first place, but research carried out by Barker *et al.* looking specifically at this issue found that, while a low molecular weight PIBSI could cause deposits within diesel engines, provided the PIBSI was of high molecular weight, no problems occurred.²⁷ This would give weight to the theory that the polymeric tail imparts solubility, as a short tail group (associated with a low molecular weight polymer) would be more likely to be insoluble, while a long tail group (associated with a high molecular weight polymer) is more likely to be soluble within the diesel.

(ii) Corrosion inhibitors

Corrosion inhibitors are also designed with a polar head group to enable attachment to the metal surface and a hydrocarbon tail to ensure solubility within the fuel.¹⁹ It is necessary to add them in order to attempt to prevent corrosion, due to the widespread damage that can be done upon an engine through the impact of rust, which can severely block engine components and pipelines.¹⁹ Corrosion inhibitors can be added into fuel either at the refinery stage or as part of an additive package with other chemicals and are generally added at a concentration range of 5-100 mg/kg.¹⁹ One common corrosion inhibitor used is the di-acid dodeceny succinic acid (Figure 1.3).

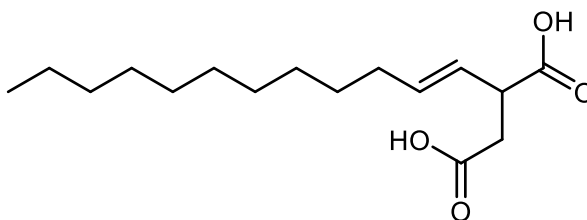
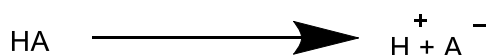
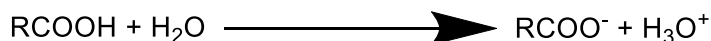


Figure 1.3: Structure of dodecenyl succinic acid (DDSA).

Acid strength is measured by calculating how readily an acid dissociates in water to give a proton (H^+) and a carboxylate anion (COO^-) (Scheme 1.3)



Scheme 1.3 Top: acid dissociation to form protons and carboxylate anions Bottom: simplified representation.

The extent of dissociation, represented by the pK_a can then be measured using the following equations:

$$K_a = \frac{[H^+][A^-]}{[HA]} \quad pK_a = -\log_{10}(K_a) \quad (1.0)$$

where $[H^+]$ is the concentration of protons, $[A^-]$ is the concentration of anions and $[HA]$ is the concentration of original acid, all measured at equilibrium. The lower the pK_a value, the greater extent to which the acid is dissociated in solution and thus the stronger is the acid. For example, hydrochloric acid is almost fully dissociated in solution and thus has a pK_a of -7.

DDSA is likely to have a pK_a of approximately 2.7, indicating that it is a reasonably powerful acid. This di-acid is actually one major acid source for the sodium carboxylate salt forming process, as it appears to form a sodium salt with many fuel soluble sodium sources under various conditions.² Indeed, a recent trend within refinery pipelines is to increasingly focus on good housekeeping thereby limiting the opportunities for water to enter the system and cause damage. This would massively cut down the need to use corrosion inhibitors such as di-acids, which would then by extension also reduce the opportunities for deposits to form within engines.⁸

(iii) Lubricity additives

Before the 1990s, the fuel injection equipment within a diesel engine was lubricated by the diesel itself, with many people theorising that this was due to the presence of sulfur compounds within the fuel.²⁸ Indeed, when the Merox process was introduced to remove these sulfur containing compounds, the subsequent lubricity of the fuel was found to be lower. However, it was discovered that rather than the sulfur containing compounds directly, it was the heavy aromatic compounds that were also removed from the fuel during the Merox process that were responsible for the lubricating properties.²⁸ In order to remedy this issue, the fuel industry had to add a series of chemical lubricity additives.

There are two main classes of lubricity improver, neutral or acidic.⁸ In light of the issues caused by acidic corrosion inhibitors, it would be logical to assume that the neutral additives, based on esters and amides, would be more attractive for use within an engine. However, these additives require a higher treat rate than mono-acidic additives and are therefore more expensive to apply, which leads to the widespread use of mono-acid based additives.⁸

Lubricity improvers based on mono-acids have much of the same design features as corrosion inhibitors. Here, their affinity for metal surfaces reduces the metal to metal contact due to a light film on the surface.²⁹ It has been found in some studies that for the improver to be effective, there should be a polarity-imparting oxygen atom present, as this leads to better engine lubricity.²⁹ Additionally, it was found that acids are the best group to use, as they have a free hydroxide group available, which provides a better enhancement of lubricity in comparison to that of esters,²⁹ as well as having cost benefits. The common lubricity improver oleic acid (Figure 1.4) is a tail oil fatty acid, which is how many lubricity improvers are shown, although a mixture of acids is more likely to be present as opposed to a single species.²

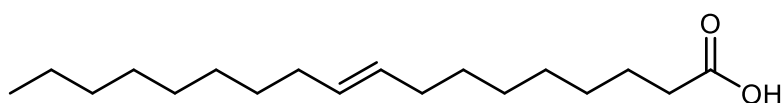


Figure 1.4: Chemical structure of oleic acid.

The pK_a of this acid was found from experiments to be 9.85.³⁰ This is higher than the value for DDSA, indicating that the oleic acid is a weaker acid. This suggests that, as a weaker acid, the mono-acid species would be less likely to cause deposit issues as it would be more difficult to remove the proton from the acid. Another possible reason for the mono-acid to

cause less deposit issues is due to the level of micelle formation possible. The di-acid can form polymeric micelles likely to be insoluble in diesel, while the mono acid is more likely to form smaller monomeric micelles that remain soluble within the fuel and therefore do not contribute to any deposit issues.³¹

As in the case of di-acids, these mono-acids have also been implicated in sodium salt formation within engines, reacting with soluble sodium sources to cause blocking of fuel filters within the system or injector sticking, depending on the sodium source.²

1.1.3 Identity of diesel engine deposits and associated issues

As can be seen from Chapter 1.1.2, diesel starts off as a complex mixture of components, with companies adding to this *via* their use of additives. These additives, while fulfilling a clear need within the engine, are also responsible for the vast majority of the deposit issues seen within diesel fuel over the past few years. While traditionally thought to be a product of fuel degradation or contamination, recent work has shown the main class of deposits to be both inorganic and organic in nature, specifically composed of sodium carboxylates.³²

It should be noted of course that such metal carboxylates are not the sole class of deposits seen within engines. Broadly speaking there are four; metal carboxylate salts, polymeric amides, aged fuel and pyrolyzed fuel.³³ According to the study carried out by Lacey *et al.*, however, it is the metal carboxylate deposits that cause the most concern amongst fuel manufacturers.³³

There is much concern around these deposits due to the multitude of negative effects they have on modern engines. Modern common rail injection systems within diesel engines have several features that are much more sensitive to deposit formation than previous systems.² The common rail injection systems allow for improved fuel atomisation, exact control over injection parameters and multiple injection strategies, but these features, which are advantageous for engine manufacturers as they allow for the development of much more powerful diesel vehicles, are what leads to more overall sensitivity to deposit formation.³⁴ Such systems also subject the fuel to much more exacting conditions than previously experienced, for example the pressures within the system can be up to 300 MPa, as well as having temperatures of up to 150 °C within the main body of the engine, with even higher temperatures at the nozzles.³³ These conditions mean that even the smallest levels of deposits can cause an issue within the engine framework. For example, it has been shown

that just 100 mg of fine dust spread through 50 L of fuel is sufficient to cause significant damage to the internal engine components.¹

Research has also investigated the mechanism of formation of such deposits. For such deposits to form, it is necessary to have two main components present within the diesel, an acid and a source of sodium. The acid sources tend to come from additives, such as those discussed previously. Common acids found in diesel include DDSA and succinic acids, namely hexadecenyl or dodecenyl acid.³³ Such succinic acids are widely used as corrosion inhibitors in fuel pipelines, hence why they appear in diesel fuel.³⁴ It was noted in a study carried out by Almena *et al.* that some deposits have been seen within the internal components of oil heating boilers.³⁴ This is an interesting finding as compared to the components found in a diesel engine, boiler components experience vastly different conditions, including lower temperatures, pressures and entirely different base fuel compositions. This suggests that sodium carboxylate deposits form only through the interaction of sodium and an acidic group, given that vastly different systems can give rise to the same class of deposits even if none of the conditions between the systems are the same.³⁴

Potential sources of sodium that could be present in diesel are many and varied and include sodium chloride, sodium sulfate and sodium hydroxide.⁶ The levels of these sources of sodium should always be minimised, as this will minimise the potential for deposit formation. For example, most manufacturers insist that the levels of sodium should be kept below 0.1 ppm.⁶ However, Joseph has carried out analysis showing on average fuel tanks in the United States contain 2500 ppm of sodium containing compounds.⁶ This is clearly much higher than the recommended level and as such may be contributing to the deposit issues seen. While there is no legal limit for sodium levels within ordinary diesel, there is an upper limit of 5 ppm for biodiesel made using fatty acid methyl esters or FAME.³⁵

Joseph identified three main sources of possible sodium contamination in the United States. These were general operations carried out in the refinery, the manufacture of biodiesel and issues surrounding the transportation of diesel from refinery to fuel station.⁶ As previously stated, the desulfurisation process can lead to the presence of sodium within the system. As previously discussed, the Merox process transforms thiols present in the diesel mixture into disulfides and very often uses sodium hydroxide as a base.⁶ Traditionally this process was applied to jet fuel production, though many refineries are now beginning to apply it to common diesel.⁶ The sodium hydroxide base has to be removed from the diesel product

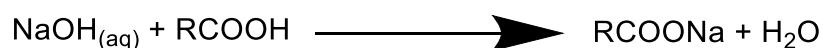
before shipping and this is usually done *via* water wash, which if done ineffectively will leave behind some sodium hydroxide, presenting a source of sodium ions for further reaction.⁶ An alternative method of removing the water involves using salt drying, which can add yet another potential source of sodium to the fuel.⁶

One common form of biodiesel used in the world is FAME.⁶ There are some major issues surrounding the synthesis of esters present in FAME due to the use of sodium based reagents within the process. Many biodiesel components are made *via* a transesterification reaction, where long chain carboxylic acids are reacted with methanol and sodium hydroxide to form the corresponding ester.⁶ Much like the previous mentioned refinery issue, if sodium hydroxide is not all successfully removed from the product, the final FAME blend will contain some trace levels of sodium hydroxide.⁶ To minimise the potential of further reaction, the sodium hydroxide should be removed from the FAME blend *via* a neutralization process, followed by a water wash.⁶

The final main source of sodium contamination is in the fuel transportation process. One interesting potential contamination sources is in marine vessels. As the fuel is pumped out of storage tanks on ships in seaports, it is necessary to fill the tank with water to act as ballast. In seaports, salt water is used as the ballast and if the tank is not cleaned out properly before the next load of diesel is pumped in, the fuel will mix with the residual salt water present within the tank, leading to trace levels of sodium present within the fuel.⁶

It has been suggested that the simplest way to eliminate deposit formation may be simply to reduce the levels of sodium contamination. This is particularly crucial at fuel service stations, where the diesel is likely to be stored for long periods in underground tanks, which can sometimes lead to higher sodium levels being present.⁶

Such sodium compounds then react with the acids present within the fuel to form sodium salts *via* the general acid-base equation (Equation 1.1).



Equation 1.1: General acid-base reaction to form a carboxylate and water.

This long known general reaction is driven by the $\text{p}K_{\text{a}}$ of the species involved. The weakest acid will have the largest $\text{p}K_{\text{a}}$ value and vice versa.³⁶ Thermodynamically, the reaction will always be driven towards the species that is the weakest acid,² and it is this principle that

guides the formation of such deposits within diesel engines, as water has a pK_a of approximately 16, therefore the reactions are always driven towards the formation of a sodium carboxylate and water.³⁶ There is an important caveat to using solely pK_a values when describing this chemistry, which is that pK_a values are determined in aqueous systems. Diesel is clearly not an aqueous system and while it may contain water, the acids of interest are generally insoluble in water.² Not only that, but the water within the fuel will almost certainly not be present as a bulk phase, but rather as either droplets within the fuel or dissolved within the diesel.² Another factor that has contributed to the rise of internal deposits is the increasing use of FAME as a fuel source.³³ The changes in fuel composition and engine design have all contributed to the problem of internal deposits, as they have opened up new opportunities for reactions, which even a few years ago would not have been possible.³³

Sodium carboxylate deposits cause various problems within the engine that in some cases make the use of the engine almost impossible. Such issues can include general poor engine operation, a decrease in the ability to drive using the engine as well as making it impossible to cold-start the engine.³⁴ The deposits themselves tend to be white or off-white in colour and are universally soluble in water.³³ They are predominantly seen on the injectors within the engine, but can also be found elsewhere within the engine due to the recirculation of fuel.³⁷

The various factors at play in a diesel engine can therefore lead to a myriad of different reaction conditions within the fuel and engine system that can potentially lead to deposit formation, and it is this complexity that presents the challenge to the chemist attempting to understand such systems.

1.2 Carboxylate Group Chemistry

One of the simplest reactions that a carboxylic acid can undergo is a deprotonation to produce a salt, known as a carboxylate.³⁸ This reaction involves the removal of the hydrogen atom of the hydroxyl group of the acid, replacing it with a metal atom. The reaction of low molecular weight aliphatic acids to produce such salts are well-known, and the products are well characterised in terms of their preparation and properties.³⁸ Indeed, the alkali metal carboxylates, which are often known as 'soaps', have been known since German tribes first prepared them in the times of Julius Caesar.³⁹ These soaps are generally fully soluble in water,

with a characteristic foam often seen.³⁹ The exception to this rule is seen in short chain lithium carboxylates, which are insoluble in water.³⁹ The lack of solubility of alkali metal carboxylates (excluding lithium) in organic solvents is attributed to their inability to form stable micelles in hydrocarbons, which leads to their precipitation out of solution.⁴⁰ Work carried out by Kissa in the 1960s did however find that if the metal carboxylate was derived from that of a branched acid or an acid containing an acyclic ring, then the solubility of that acid in organic solvents far exceeded that of the straight chain homologue.⁴¹

In contrast to the properties of alkali metal carboxylates, the carboxylates of other metals are generally insoluble in water, with a general formula $M(O_2CR)_n$ where M represents a metal in the n^{th} oxidation state and R represents an organic radical, generally containing between 6 and 7 carbon atoms.³⁹

Three general methods are used to synthesise metal carboxylates, namely the fusion method, the precipitation method and reactions in non-aqueous media.³⁹ An overview of these methods shall be discussed; firstly, however, a brief description of some features of carboxylic acids is presented.

All carboxylic acids by definition contain a carboxyl group.²³ They have a general formula of R-COOH, where R represents the rest of the molecule, either aliphatic or aromatic, and COOH is the carboxyl group. Most carboxylic acids dimerise, both in solution and the solid state, with such dimers formed through hydrogen bonding between two carboxyl groups.³⁹

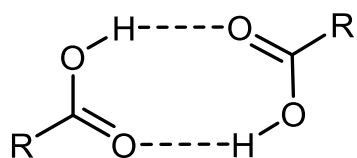


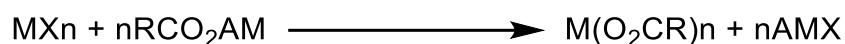
Figure 1.5: General hydrogen bonded dimeric structure of carboxylic acids. The dashed lines represent hydrogen bonds.

As expected, the main feature of carboxylic acids identified in analysis is the carboxyl ($-C=O$) group. This group is visible using a number of analytical methods, such as NMR and IR spectroscopy. For example, in a general IR spectrum, there are two main bands indicative of a carboxyl group, a broad band at about 3300 cm^{-1} and a sharp band at about 1700 cm^{-1} . These bands represent the $-OH$ stretch and carbonyl stretching frequency respectively. Carboxylic acids are also easily detected *via* ^1H NMR, with a broad signal at 10-13 ppm due

to the –COOH proton and a signal in ^{13}C NMR at 170-180 ppm due to the corresponding carbon.³⁹

In terms of their acidity, carboxylic acids tend to have $\text{p}K_{\text{a}}$ values of around 4.8-5.³⁹ The presence of an electronegative substituent will lower the $\text{p}K_{\text{a}}$ and thus will give a stronger acid, due to the electronegative substituent stabilising the carboxylate group *via* its electron withdrawing character.³⁹

As mentioned, there are several methods that can be utilised in the synthesis of metal carboxylates. A popular method is reacting solutions, either alcoholic or aqueous, of metal salts with sodium, potassium or ammonium soaps. This will produce a metal carboxylate *via* a metathesis reaction.³⁹ This produces a soluble alkali-metal or ammonium salt by-product, while the desired metal carboxylate can be obtained by filtration, as it is normally insoluble.³⁹



Equation 1.2: Fusion method of preparing metal carboxylates, where AM is Na, K and X is Cl or NO_3 .

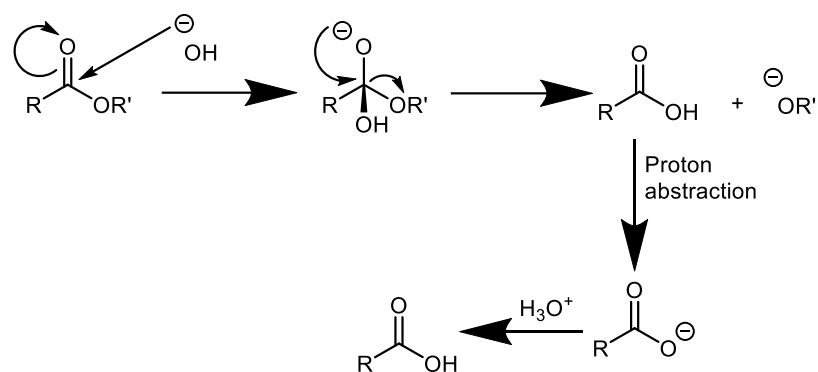
This method has been used to obtain a large number of metal carboxylates such as those of Fe(II), Zn(II), Cr(III) and Mg(II).³⁹ By heating these soaps at 100 °C in a vacuum it is possible to obtain dehydrated soaps, or alternatively crystallisation can be carried out from dry organic solvents.³⁹ For example, Pink was able to obtain magnesium oleate *via* reaction between sodium oleate and magnesium chloride, with the magnesium oleate product (initially hydrated) refluxed in benzene solvent in order to obtain the anhydrous compound.⁴²

Another method used to obtain metal carboxylates is the fusion method.³⁹ This method involves the reaction between metal oxides, hydroxides or carbonates with fatty acids, thereby providing the desired metal carboxylate and the easily removed side products of water and carbon dioxide, depending on the metal source used.³⁹



Scheme 1.4: Fusion method of synthesising metal carboxylates involving metal oxides, hydroxides and carbonates.

This is by far the most common method used in the synthesis of metal carboxylates given how easily the side products can be removed. It is frequently used in industry, where the fatty acid is sometimes replaced with an oil or fat, although such a substitution generally leads to a lower level of the desired carboxylate obtained, with a much higher amount of decomposition products due to the greater complexity of the reaction.³⁹ When the source of the metal is an oxide, the reaction is sometimes called a saponification, though this is usually used when the aim is to hydrolyse an ester to produce a carboxylic acid.³⁸ Rather than the direct displacement of a hydrogen atom with a metal atom to produce a metal carboxylate, a saponification process involves a hydroxide anion attacking the ester carbonyl group, producing a tetrahedral alkoxide intermediate.⁴³ Upon elimination of the alkoxide anion and proton abstraction a source of protons can then be used to quench the reaction and form a free carboxylic acid,⁴³ though of course the mineral acid used could in theory be replaced by a metal oxide to form a metal carboxylate if so desired.



Scheme 1.5: Mechanism of the saponification method of ester hydrolysis.

1.2.1 Types of metal carboxylate and their analysis

Metal carboxylates are found in many other areas of chemistry and indeed have several uses besides that of purely academic interest. For example, some can be used as decorative or protective coatings, within the rubber and plastics industry and in the cosmetic industries.³⁸ The high number of metal carboxylates available for use is unsurprising given the wide number of fatty acids available, each of which can potentially react with each alkali, alkali-earth or heavy metal.³⁸

One common historical use of metal carboxylates was as driers in the area of painting, with lead and manganese soaps used in paints, varnishes and resins since about 1885.³⁸ Indeed,

much of the early advancement in the synthesis of new metal carboxylates was driven by the demands of the paint industry.³⁹ In terms of protective coatings, carboxylates can be used to preserve antique samples of metals from modern atmospheric pollutants. For instance, of particular concern to conservation scientists is the corrosion of lead, found both in old plumbing systems and in pipe organs.⁴⁴ Many old buildings around the world have plumbing systems composed of lead piping, with several negative health effects associated with lead dissolving from the pipes and entering the water, which is then subsequently drunk by the people who occupy those buildings. By immersing the sample into an ethanol or aqueous solution of a metal carboxylate or by spraying such a solution onto the sample, a lead carboxylate is formed upon the surface of the artefact, which affords some level of protection.⁴⁴ Such a coating is found to not only protect the sample from any further corrosion, but for lead pipe organs it also improves the aesthetic appeal of the sample.⁴⁴ It has also been found that such a coating will even provide protection to a sample where the corrosion process has already begun.⁴⁵ The main advantages of using such a carboxylate based treatment is the fact that it is both user-friendly and relatively low-cost, though it should be noted that such a treatment would only be considered as a short term solution.⁴⁵ Due to the fact that the main group carboxylate salts are water insoluble, they can further be used as coatings that impart waterproofing properties onto materials.⁴⁶

Many alkali metal carboxylates have also found uses in the cosmetics industry. For example, the sodium salt of 2-(2-dodecoxyethoxy)acetic acid or laureth-11 is often used in eyeliner products.⁴⁷ Carboxylates are also found in shampoos as primary detergents, owing to the fact that they are both anionic and inexpensive, both considered important factors in the cosmetics industry.⁴⁸

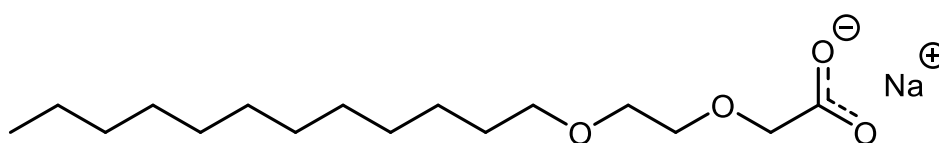
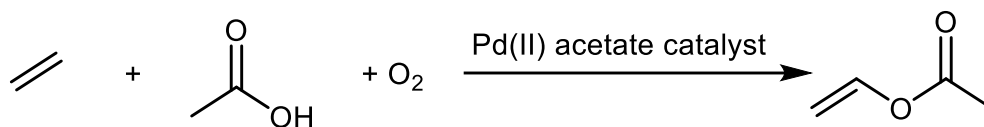


Figure 1.6: Structure of the sodium salt of laureth-11.

There are also some synthetic uses of metal carboxylates, due in part to their relatively high stability.³⁹ One such use is in the synthesis of vinyl acetate from acetic acid and ethylene,

which usually proceeds using a palladium-based catalyst.⁴⁹ This catalyst can be based on a palladium(II) acetate trimer.³⁹



Equation 1.3: Synthesis of vinyl acetate utilising a Pd carboxylate catalyst.

Many other metal carboxylates can be utilised in the soap, textile and paint industries.³⁹ Given that most carboxylates (excluding those of sodium and potassium) are soluble in organic solvents, they have been utilised as stabilisers in the polymer industry, particularly those carboxylates of tin, used to stabilise polyvinylchloride.⁵⁰ A more specialised historical use of zinc carboxylates emerged during the Second World War. Flammable liquids were very often used during the war, having been previously developed during the First World War. The major disadvantage of using them was their excessive dispersion, meaning that commanders would find it very difficult to target specific enemy installations.⁵¹ It was found that the use of zinc stearates solidified the incendiary fuels, allowing them to be more effectively targeted, and thusly zinc stearates became very widely used throughout the war.⁵¹

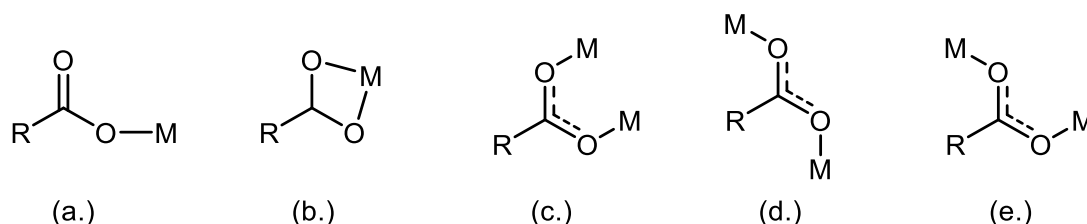
There are generally only a few analytical methods commonly used in the analysis of metal carboxylates. In particular, the analysis of alkali metal carboxylates is dominated by two techniques, those of IR and thermal techniques such as thermogravimetry and differential scanning calorimetry. IR proves to be the dominant technique in both academia and industry, for a number of reasons. It is both relatively cheap and easy to perform, as well as providing a rudimentary insight into some structural aspects of the salts.

The most obvious feature within the IR spectra of sodium carboxylates is the absence of the strong carbonyl stretching band at about 1700 cm⁻¹ and its replacement by two new bands at approximately 1500 and 1400 cm⁻¹.⁵² These two new bands correspond to the asymmetric and symmetric stretching vibrations of the carboxylate group respectively.⁵² Some limited structural information can be gained from such IR spectra. For example, the intensity of the asymmetric stretch is often found to be greater than that of the symmetric stretch, suggesting an asymmetric bonding mode for the metal carboxylate as well as a high degree of tilting in terms of the alkyl chains.⁵² Often the symmetric carboxylate stretching band is split in the IR spectrum, which is ascribed to extensive interactions between carboxylate head groups.⁵² This split is due to the interactions reducing the head group symmetry, which promotes a vibrational decoupling of degenerate vibrations, hence splits the band.⁵²

The difference between the wavenumbers of these bands ($\Delta\nu$) can also give an indication of the metal carboxyl coordination present within the molecule. Using the equation:

$$\Delta\nu = \nu_{\text{asymmetrical}} - \nu_{\text{symmetrical}} \quad (1.4)$$

where $\nu_{\text{asymmetrical}}$ is the wavenumber of the asymmetrical stretch and $\nu_{\text{symmetrical}}$ is the wavenumber of the symmetrical stretch, it is possible to infer the likely bonding mode of the metal atom to the carboxylate group.⁵³ Scheme 1.6 shows some of the common bonding modes available to metal carboxylates.⁵⁴



Scheme 1.6: Common modes of bonding available to the metal atom in metal carboxylates; (a) unidentate (b) bidentate (c) syn-syn bridging (d) anti-anti bridging (e) anti-syn bridging.

It is found that if the mode of coordination is chelating such as in (b)-(e) above, the equal interactions between both oxygen atoms and the metal results in a $\Delta\nu$ value of approximately 100 cm^{-1} .⁵³ If the metal is bonded in a monodentate manner such as in (a), where only one oxygen atom interacts with the metal, then the $\Delta\nu$ value is usually much greater, generally over 200 cm^{-1} .⁵³ This is due to the now larger difference in bond order of the two oxygen atoms, thus leading to a larger difference in frequency and therefore a larger value of $\Delta\nu$.⁵³ In some cases where the metal carboxylate is co-complexed with solvent molecules, the difference in the stretching frequencies is markedly smaller than this, due to the effects of hydrogen bonding between the carbonyl oxygen atom and the solvent molecules. Such hydrogen bonding reduces the intensity of the antisymmetric stretch.³⁹ The same logic is used to explain the $\Delta\nu$ value of $\sim 165 \text{ cm}^{-1}$ observed when the metal atom is bridging.⁵²

Work carried out by Nelson *et al.* showed that for sodium carboxylates up to sodium stearate (a long chain of 18 carbon atoms in the fatty acid backbone), the value of $\Delta\nu$ is between 134 and 139 cm^{-1} . This is below the value seen for monodentate bonding, but also above that seen for bidentate bonding involving both oxygen atoms.⁵² This indicates a hybrid model of bonding, with extensive head group interactions between various carboxylate groups contributing to the IR splitting patterns seen and the intermediate $\Delta\nu$ value seen.⁵² Such a

hybrid model of bonding has been predicted using a combination of IR and powder diffraction, which in combination indicates that such a hybrid model of bonding is likely.⁵³

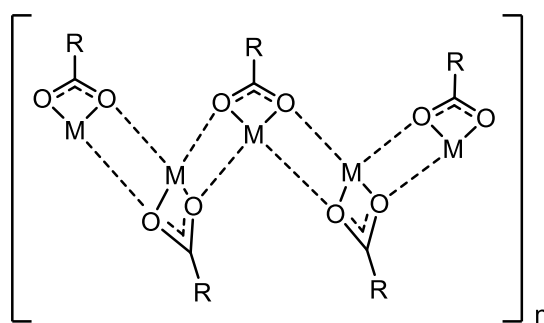


Figure 1.7: Predicted molecular geometry of metal carboxylates where M is Li, Na or K.

IR has also been the foremost technique used in industry engine testing to identify deposits as being carboxylate based. Work carried out by Reid *et al.* showed that deposits formed when sodium naphthenate (a fuel soluble sodium salt) was added to diesel fuel containing a di-acid additive.² The engine components used were removed and subsequently analysed *via* IR, with the characteristic peak present at 1565 cm^{-1} indicative of the deposit being carboxylate based.² Of course it is worth noting that, while IR can identify the carboxylate nature of the deposit, the major disadvantage of analysing deposits solely using IR is that IR alone cannot differentiate between the sodium being associated with the original sodium source or the acid present in the fuel, meaning that in the actual engine tests carried out, it was not known whether a reaction had occurred or if the acid (DDSA in this instance) was simply making the sodium salt (sodium naphthenate in this case) less soluble in the diesel fuel, causing it to potentially precipitate from the diesel as a deposit.²

Energy-dispersive X-ray spectroscopy (EDS) has also been utilised in order to ascertain the chemical make-up of deposits found. This technique uses X-ray beams to excite electrons in various shells in the atoms of the elements that make up the sample. These electrons then return to the ground state, releasing energy in the form of X-rays that can then be assigned to elements that are present within the sample. In this instance, with the deposit being composed of a sodium carboxylate, it would be expected to find such deposits would predominantly be composed of carbon, oxygen and sodium. Indeed, Almena *et al.* analysed an injector coated with deposit and found that the main elements present were indeed carbon and oxygen, with the metal present identified as sodium.³⁴

Differential scanning calorimetry (DSC) has also been used to analyse such long chain sodium carboxylates, allowing for identification of any phase transitions in the sodium carboxylate powder. It would be expected that the temperatures of such transitions would be affected by the extent to which the long chains pack as well as the extent of the intermolecular interactions between the carboxylate head groups.⁵² Rather surprisingly, it is found that for long chain carboxylates there can be up to four transitions observed in the DSC trace.⁵² Some of these transitions have been assigned to the rotation of the long flexible chain around the carbon-carbon bonds present.⁵² Thermogravimetric analysis further suggests that these long chains degrade between 690-750 K, due to the long chains cracking to produce smaller fragments,⁵² akin to the process that occurs in an oil refinery to produce diesel.

Of course, it would be ideal to obtain more accurate structural insights into these fatty acid carboxylates from single crystal X-ray diffraction. However, this type of analysis is very challenging when looking at the alkali-metal carboxylates. When the straightforward neutralization reaction of long chain aliphatic fatty acids is attempted, the products are usually in the form of a powder, rather than the crystalline form necessary for single crystal analysis.⁵⁵ Many of the metallic soaps also form gels in organic solvents,⁴⁶ as well as having a tendency, when crystals are obtained, to be microcrystalline solids and thin needles.⁵² In part these issues arise because the long chain examples of metal soaps have a low molecular symmetry, as well as a high degree of flexibility of the long chain backbone.⁵²

1.3 Overall aims of Part I of the PhD project

As laid out in the preceding sections, the problem of internal diesel injector deposits is currently of major interest to many industrial fuel companies worldwide, with a resolution required as soon as possible. The multitude of problems caused by these deposits means that a study of reaction conditions that lead to their formation, as well as insight into the structures such deposits adopt in solution and the solid state is vital for such a resolution to be achieved.

Recent unpublished work from our industrial partners Innospec has shown that the sodium hydroxide to ligand ratio has a significant effect on injector sticking as a result of the various architectures that can be formed. While this is surprising from a simple ionic carboxylate model, such variation is not unexpected when viewed through the prism of modern

organometallic and coordination chemistry. Consequently, the overall aims for this part of the PhD project were

- Prepare samples of long chain alkali metal carboxylates similar to those found in diesel deposits
- Attempt to gain insight into the structure that such compounds adopt in solution state
- Grow single crystals of such complexes, with or without donor additives, to enable understanding to be grasped of the different effects each of the structures will have in the fuel
- Attempt to extend such work to other systems of relevance such as alkoxides to probe their effectiveness as potential models for carboxylates in the future
- Accrue knowledge into the sodium naphthenate source commonly used as a fuel soluble source of sodium in engine testing to ascertain its chemical make-up and composition

Chapter 2: Structural Studies of Donor-Free and Donor-Solvated Sodium Carboxylates

Preliminary drafted manuscript.

Putting the results into context with the literature an extended introduction, discussion and conclusion to the paper are provided.

Contributing authors to the manuscript and their roles

Richard M. Gauld- Designed and performed the experiments; analysed the data; drafted the manuscript

Ross McLellan- Helped with the data processing; contributed to the drafting of the manuscript

Alan R. Kennedy- Ran and solved the X-ray diffraction data for compound **4**; checked the accuracy of X-ray diffraction data processing

Freya J. Carson- Obtained the preliminary crystal structure of compound **4**

Jim Barker- Industrial collaborator

Jacqueline Reid- Industrial collaborator

Charles T. O'Hara- Academic supervisor of Freya J. Carson

Robert E. Mulvey- Principal investigator

The supporting information can be found in Chapter 7: Experimental; Section 7.2 and Tables 7.5.1 and 7.5.2

2.1 Abstract

Focusing mainly on sodium 2-ethylhexanoate, this study reveals that the carboxylate exists as a dimer in MeOD solution as evidenced by Diffusion Ordered NMR Spectroscopy (DOSY). Two crystalline varieties with distinct polymeric structures have been synthesised and crystallographically characterised. A mixed 1,10-phenanthroline–water solvate $[\{(C_5H_{10})(C_2H_5)COONa.(H_2O)[1,10\text{-phen}]\}_2]_{\infty}$ contains dimeric $[NaO(H)_2]_2$ subunits, which propagate through hydrogen bonds between O atoms of the carboxylate and OH water bonds. Adjacent polymeric chains interdigitate with each other through π - π interactions between 1,10-phen rings. Solvent-free sodium 2-ethylhexanoate has five-coordinate cations comprising one bidentate chelating and three monodentate carboxylate oxygen atoms. Here, the packing arrangement is different with the central hydrophilic $(NaO_2)_{\infty}$ core surrounded by a wrapping of disordered alkyl groups. A similar polymeric structure is observed for the crystalline DMSO-solvated sodium valproate $[\{(C_3H_7)(C_4H_8)COONa.(DMSO)\}]_{\infty}$. This adopts a layered arrangement comprising alternating sodium carboxylate hydrophilic layers and hydrophobic organic bilayers.

2.2 Introduction

As is clear from Chapter 1, there is a great deal of industrial interest within the field of alkali metal carboxylates due to their regular formation within diesel engines. Recent unpublished work carried out by Innospec Ltd. first identified these deposits as carboxylate based, forming due to the interaction between fuel soluble sources of sodium and carboxylic acids added to the diesel fuel as additives. In engine testing the fuel soluble source of sodium is generally sodium naphthenate, a mixture of sodium containing compounds. This is added to the fuel during engine testing runs, whereupon it reacts with the acidic molecules present within the fuel to form deposits. Very often at this point the engine will then fail due to carboxylate-based deposits coating the injector, reducing the amount of fuel injected and therefore causing engine failure. However, the crucial issue when using sodium naphthenate is the dearth of information available relating to its chemical structure and composition. Indeed, given the nature of the sodium naphthenate being a mixture, even something as simple as its molecular weight is not known with any certainty. This seems a bizarre approach given the accuracy with which normal laboratory reactions are carried out, however seems to be the industry standard.

The compound referred to as sodium naphthenate is the sodium salt of naphthenic acid, a generic term for the mixture of cyclopentyl and cyclohexyl carboxylic acids present within crude oil. The molecular weight of such species varies from 120 up to 700 atomic mass units, with chain lengths of between 10 and 15 carbons on average.⁵⁶ It is clear from the literature that there is a paucity of information available on both the conclusive identity of sodium naphthenate species and indeed the parent acids. Both are theorised to be cyclic molecules, whose generic formula is $C_nH_{2n+z}O_2$, where n is the carbon number and z is an even, negative integer.⁵⁷

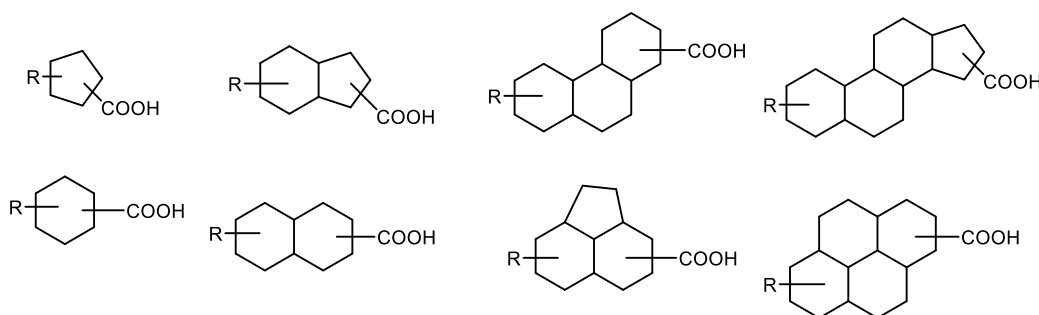


Figure 2.0: Selection of molecules that may be present within samples of naphthenic acid, where R represents an alkyl chain of indiscriminate length.

Given the lack of literature precedent on this compound it would be pertinent to carry out a study to see if any insight could be gained into the structure or chemical make-up of the sample.

While the main thrust of this chapter will be focussed on obtaining crystal structures of comparatively simpler sodium carboxylates (single species as opposed to mixtures), the extended results and discussion will detail our attempts to gain insight into sodium naphthenate through a number of analytical techniques.

2.3 Introduction from the Manuscript

Of vital importance in the toolbox of the synthetic chemist are organolithium reagents such as lithium alkyl and lithium amide compounds, both classes of which are widely utilised throughout synthetic chemistry.⁵⁸⁻⁶⁰ Collum put the extent of this utilisation into some perspective by pointing out that in excess of 95 % of natural product syntheses rely upon a lithium based reagent at some point in their preparation.⁶¹ Organolithium compounds were introduced by Schlenk in 1917,⁶² though perhaps surprisingly given the comparative lack of development, organosodium chemistry actually began even earlier, dating back to the reactions of alkyl halides with sodium metal in the 1840s and 1850s studied by Wanklyn.^{63, 64} Research into organosodium chemistry has been relatively limited, due mainly to the success of their lighter congeners since organolithium compounds in general exhibit higher solubility in commonly used organic solvents, are more stable, have the presence of NMR active lithium isotopes which lends themselves to solution state characterisation and are easier to handle than the heavier sodium congeners.^{65, 66} However, recently there has been an upsurge of interest in organosodium chemistry. This was partly driven by the higher reactivity of the heavier alkali metals when compared to lithium but also by increased focus within the chemical sciences on sustainability. Sodium is the most abundant alkali metal in the earth's crust and oceans, as well as being the sixth most abundant element on earth overall. Sodium also contains several other advantages from a sustainability point of view, such as being non-toxic and inexpensive.⁶⁷ There is therefore an understandable drive towards reducing the reliance on comparatively rare elements such as lithium with more sustainable alternatives such as sodium,⁶⁸ especially given lithium's burgeoning use in the widespread field of lithium-ion batteries,⁶⁹ the subject of the 2019 Nobel Prize in Chemistry,⁷⁰ which further incentivises the development of other alkali metals in areas such as sodium ion batteries⁷¹ and catalysis. Of particular note in the latter area is the recent breakthrough by Takai *et al.* who showed that cross-coupling reactions such as Negishi and Suzuki-Miyaura could be carried out catalytically by organosodium compounds.^{67, 72} This study showed that these cross-coupling reactions could be accomplished in a one pot-reaction starting from inexpensive aryl chlorides, which is attractive from an industrial scale viewpoint.⁷² Insight has also been gained into cyclisation reactions of alkynols, which proceed sluggishly using a mixed lithium magnesiate, but worked more efficiently using a sodium magnesiate and best of all using a potassium based system, showing the potential advantages of investigating heavier alkali

metals further.⁷³ A catalytic system looking at hydrophosphorylation of nitriles and alkenes has also been developed utilising simple alkali metal HMDS complexes (HMDS is 1,1,1,3,3,3-hexamethyldisilazide), which show superior performance when moving to the heavier alkali metals, again highlighting the advantages that sodium and potassium can offer.⁷⁴ In a final example, a NaHMDS catalyst system has also been found to perform aminobenzylolation of aldehydes with toluenes in excellent yields while tolerating a wide variety of functional groups.⁷⁵ Clearly the field of sodium and organosodium chemistry in particular offers a vast untapped scope.

Considering structural studies, our research group has long been fascinated with the structural diversity and variation of sodium-containing complexes. It is known that the structures of alkali metal complexes can vary depending upon the identity of the alkali metal, which in turn can have a profound effect on the outcome of reactions. For example, in the context of trans-metal trapping it has recently been discovered that replacing LiTMP with NaTMP (TMP is 2,2,6,6-tetramethylpiperidide) has a significant effect on the onward reactivity of the trapped species, showing potential advantages in terms of replacement of lithium with sodium as a metallating agent.⁷⁶ We have also shown that changing the alkali metal can unlock fascinating structures depending on the identity of the alkali metal chosen, with the ligand system *trans*-calix[2]benzene[2]pyrrolides showing diverse structural motifs ranging from monomers to tetramers depending on which alkali metal partners them.⁷⁷

Our recent reported work in the field of small molecule activation, particularly on the fixation of CO₂ using alkali metal complexes,^{78, 79} piqued our interest in sodium carboxylate chemistry since they can be produced by such reactions.⁸⁰ Sodium carboxylates are also an industrially important class of compound.³² For example, the sodium salt of 2-(2-dodecoxyethoxy)acetic acid or laureth-11 is often used in eyeliner products.⁴⁷ Carboxylates are also found in shampoos as primary detergents, owing to the fact that they are both anionic and inexpensive, both considered important factors in the cosmetics industry.⁴⁸ Given that many non-alkali metal carboxylates are soluble in organic solvents, they have also been utilised as stabilisers in the polymer industry, particularly those carboxylates of tin, used to stabilise polyvinylchloride.⁵⁰ Interestingly, however, there is also a gap in the literature with regard to the solid state structures of long chain examples (see below).

Sodium carboxylates also have their downsides in an industrial setting. When forming within diesel engines they are thought to be responsible for a myriad of issues such as poor engine

operation, a decrease in the ability to drive using the engine as well as making it impossible to cold-start the engine.³⁴ The presence of these sodium carboxylate deposits is due to interaction between sources of sodium such as sodium chloride, sodium sulfate and sodium hydroxide⁶ and acidic molecules present in the diesel. These acidic molecules are generally long chain examples which are added to the diesel by engine manufacturers in order to improve some aspect of the engine performance.¹⁹ These long chain acids include dodecenyl succinic acid, that is introduced as a corrosion inhibitor and oleic acid, which is used as a lubricity improver to reduce metal on metal contact. The issue is when these acids interact with residual sodium in the diesel, sodium carboxylates form, which block the engines components and contribute to the previously described issues.² Despite the industrial importance of understanding the effect of these deposits, a paucity of general research has been carried out into the structures of long chain examples of sodium carboxylates. This is accounted for mainly by the long chain nature of these compounds, which makes their crystallisation extremely challenging and instead they exist as gels or microcrystalline material which do not lend themselves to single crystal X-ray diffraction study.^{52, 53} Indeed, a search of the Cambridge Structural Database (CSD) shows that while there are 11,840 hits for a sodium containing complex, there are only 295 hits for sodium carboxylates, with long chain examples containing a chain of four or more carbons numbering only 45.⁸¹ Moreover, limiting the elements present to only carbon, hydrogen, oxygen and sodium reveals a meagre 11 hits for a chain length of four or more carbons.

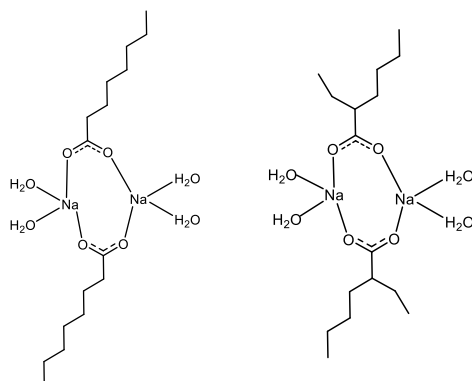
Here, in this contribution we present our results in studying long chain sodium carboxylates, with emphasis on obtaining structural insight into the architectures such compounds adopt in the solid state. We show that changing the nature of the Lewis base donor added can lead to a variety of distinct structural motifs, among which we present the longest chain example (numbering eight carbons in total) of a donor-free sodium carboxylate whose structure has been determined by single crystal X-ray diffraction.

2.4 Results and Discussion

The poverty of available literature on structurally characterised long chain examples of sodium carboxylates, as well as the industrial relevance of such compounds, prompted us to focus our efforts on obtaining relevant crystal structures. The carboxylic acids chosen were 2-ethylhexanoic acid and octanoic acid. Both are representative of the type of acids found in diesel fuel, whilst their relatively moderate chain lengths offer greater opportunity for crystallisation. In order to obtain samples of the sodium salts, the acids were reacted with ethanolic solutions of NaOH in a 1:1 ratio, to produce white powders. These powders proved to be insoluble in many apolar, organic solvents, requiring the use of MeOD for ^1H NMR characterisation. The spectra for both reaction products showed the deprotonation reaction had been successful in each case, with the absence of a resonance at about 12 ppm indicative of lack of a carboxyl proton (See ESI). In order to extract more information on their solution state structures, a Diffusion Ordered Spectroscopy (DOSY) NMR study was carried out, using tetramethylsilane (TMS) as an internal standard. DOSY NMR takes advantage of the fact that different molecular species within a solution will have different diffusion coefficients, which are related to both the shape and size of the molecular species itself.⁸²⁻⁸⁹ By plotting these diffusion coefficients, which are measured during the physical NMR experiment, it can be ascertained how many different species are present within the solution. Using software from Stalke *et al.* it is then also possible to estimate the molecular weight of these species and thereby predict the aggregation state and structure that may be adopted by such species in solution.⁹⁰ Carrying out the DOSY NMR on a sodium octanoate sample, it was seen that there was only one major species present in solution, which had a log diffusion value of -9.0825 m^2/s . This estimates a molecular weight of 433 g/mol, which appears too large a value to represent a monomeric complex of only 166 g/mol. A dimeric sodium carboxylate species, comprising two sodium cations, two carboxylate anions and four solvating water molecules would have a calculated molecular weight of 404 g/mol. This value is within the error limits (an error of only -7 % between the theoretical and calculated molecular weight) of the DOSY software, which suggests that in polar solvents, sodium octanoate is likely to form a dimeric species as shown in Scheme 2.0.

Carrying out a DOSY analysis on a sample of sodium 2-ethylhexanoate also showed the presence of only one major species in solution, which had a log diffusion value of -9.1840 m^2/s . This estimates a molecular weight value of 404 g/mol, again being found to be

consistent with a dimeric structure containing solvating water molecules with an error of 0 % (Scheme 2.0).



Scheme 2.0: ChemDraw representation of predicted dimeric structure of sodium octanoate (LHS) and sodium 2-ethylhexanoate (RHS), as implied by DOSY NMR analysis.

There is some literature precedent for such dimeric structures of alkali-metal carboxylates. For instance, Collum *et al.*, in their studies of lithium enolates, noted how previously it had been difficult to characterise such lithium structures due to their tendency to aggregate in solution and the lack of observed coupling between the oxygen and lithium atoms.⁹¹ In order to study such lithium species in solution, ⁶Li NMR investigations of lithium carboxylates paired with lithium enolates was carried out.⁹¹ It was suggested using such statistical analysis, that TMEDA-solvated lithium carboxylates may form a dimer, though significantly they also noted that “crystallographic guidance is surprisingly absent.”

To try and redress this lack of information, we attempted to prepare examples of long chain sodium carboxylates that could be analysed *via* single crystal X-ray diffraction. Initial experiments were carried out using sodium 2-ethylhexanoate, with a range of common Lewis base donors such as N,N,N',N'',N''-pentamethyldiethylenetriamine (PMDETA), 2,2'-bipyridine (2,2'-bipy) and 4,4'-bipyridine (4,4'-bipy). These donor molecules could in theory have stabilised the sodium carboxylate *via* dative interactions with the sodium cation, allowing for the formation of solvated crystalline products. All nitrogen donors, they range from bidentate rigid species such as 2,2'-bipy to the tridentate PMDETA. Each donor was added to a suspension of sodium 2-ethylhexanoate in hexane, and the mixture was left stirring overnight. Dissolution was never apparent, with the solvent subsequently removed and the powder residue analysed using ¹H NMR spectroscopy. Perhaps surprisingly, ¹H NMR evidence suggested no metal coordination of any donor molecule regardless of the ratio of

donor : acid used. This was evidenced from the non-movement of the donor resonances in the spectra of the product compared to those of the free donor, indicative that free, uncoordinated donor is still present (See ESI). This suggests that such donor intervention cannot break down the strong Na-O bonding within the parent sodium carboxylate.

Next we visited the reaction between 2-ethylhexanoic acid and the secondary amide sodium tetramethylpiperidide (NaTMP), anticipating that this strong base would deprotonate the acid, producing the sodium carboxylate as well as concomitantly forming a bulky TMP(H) donor, which may interact with the sodium carboxylate as it forms and aid a potential crystallisation. To this end NaTMP [synthesised *in situ* from BuNa and TMP(H)]⁹² was suspended in hexane and two equivalents of 2-ethylhexanoic acid were then added to obtain a yellow solution. This solution was concentrated and placed in a freezer at -30 °C, depositing colourless crystals identified by X-ray crystallography as the contacted ion pair complex $[\{\text{TMP(H)}_2\}^+ \{\text{C}_5\text{H}_{10}(\text{C}_2\text{H}_5)\text{COO}\}^-]_2$ (**1**).

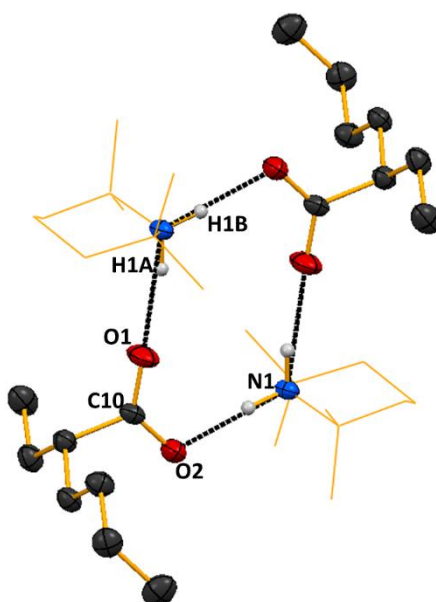


Figure 2.1: Extended molecular structure of $[\{\text{TMP(H)}_2\}^+ \{\text{C}_5\text{H}_{10}(\text{C}_2\text{H}_5)\text{COO}\}^-]_2$ (**1**).

Hydrogen atoms except those of the NH_2 groups are omitted and the organic TMP scaffold is shown as wire frame for clarity. Hydrogen bonds are represented by dashed black lines. Thermal ellipsoids are displayed at 40% probability level. Symmetry transformations used to generate equivalent atoms: 1-x,1-y,1-z.

This sodium-free structure is a hydrogen-bonded dimer, containing a 2,2,6,6-tetramethylpiperidinium cation and a 2-ethylhexanoate carboxylate anion. Graph set notation describes the hydrogen bonding as R(4,4)12.⁹³ A potential explanation for the

absence of the metal is that adventitious hydrolysis had occurred leading to formation of TMP(H) and NaOH, with the former in turn reacting with, and consuming, all the available acid to produce **1**. Alternatively, the remainder of the sodium carboxylate may stay in solution, as **1** was originally obtained fortuitously in a small yield of 16 %. Repeating the reaction rationally using a 1:1 ratio of TMP(H) and 2-ethylhexanoic acid gave a much improved 67 % yield.

A metric feature of note in the structure of **1**, is the C-O bonds, which are intermediate in length between single and double bonds [C10-O1, 1.237(3) Å and C10-O2, 1.253(2) Å]. This is indicative of the total resonance in the carboxylate group. The O1-C10-O2 bond angle also indicates total resonance, lying at 124.3(2)° which is consistent with the literature value for the carboxylate group in sodium formate (124°).^{39, 94} Searching within the CSD for literature precedent of such dimeric structures uncovered only 13 hits for carboxylate groups with TMP(H)₂⁺ related cations.⁹⁵⁻⁹⁸ These were found to be generally short chain carboxylates such as acetates, with the long chain examples generally co-crystallising with a TMP(H) derivative containing hydroxyl substituents rather than just the parent TMP(H) itself.⁹⁶ A further search of the CSD showed only 12 hits for a 2-ethylhexanoate anion, with no examples of a 2-ethylhexanoate complex with a TMP(H)₂⁺ counter ion. Attempts to obtain the corresponding octanoate salt were unsuccessful; hence we switched our attention towards obtaining examples of sodium 2-ethylhexanoate complexes.

We reasoned the use of another nitrogen donor molecule, specifically 1,10-phenanthroline (1,10-phen), may help stabilise the sodium carboxylate. While TMP(H) is bulkier in terms of overall steric factors, it is only a unidentate donor, whereas 1,10-phen is bidentate, with the potential for both nitrogen atoms to coordinate to the same sodium cation given the fact they are 'locked' into one position by the inflexibility of the aromatic 1,10-phen ligand. To this end, one equivalent of 1,10-phen was added to a suspension of sodium 2-ethylhexanoate in hexane and the mixture was stirred overnight. The white powder formed was recrystallized upon addition of THF and gentle warming to give the polymer $[\{(C_5H_{10})(C_2H_5)COONa.(H_2O)[1,10-phen]\}_2]_{\infty}$ (**2**) as colourless crystals.

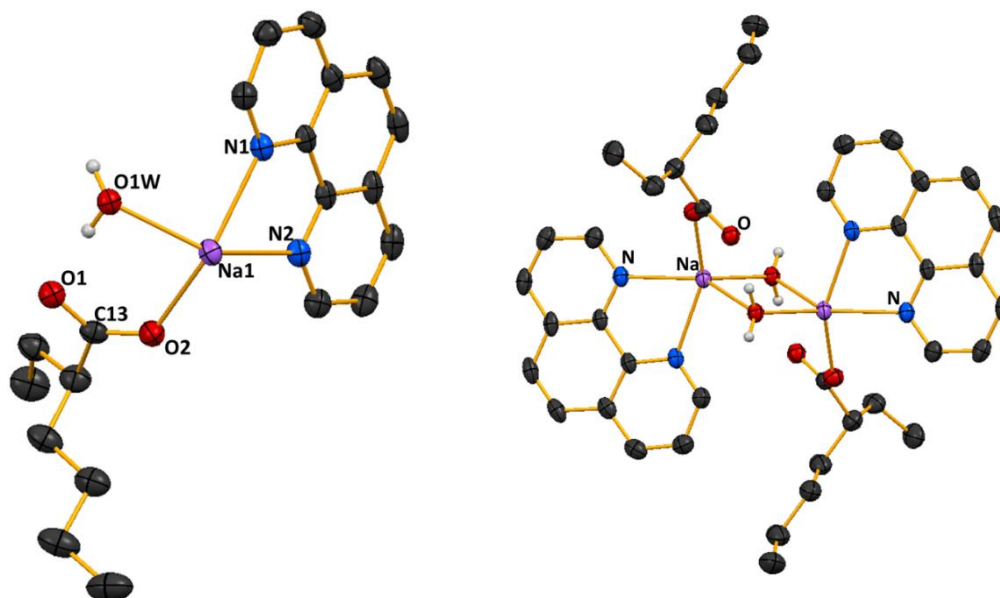


Figure 2.2: (LHS) Contents of the asymmetric unit of $[\{(C_5H_{10})(C_2H_5)COONa \cdot (H_2O)[1,10\text{-phen}]\}_2]_\infty$ (2**). Hydrogen atoms except those of water and disorder in the alkyl chains are omitted for clarity; (RHS) Dimeric coordination unit that is the major structural motif of the hydrogen bonded polymeric structure of **2**. Thermal ellipsoids are displayed at 40% probability level. Symmetry transformations used to generate equivalent atoms: $1-x, 1-y, -z$.**

Polymer **2** adopts a centrosymmetric dimeric coordination substructure comprising two molecules of sodium 2-ethylhexanoate, two molecules of 1,10-phen which chelate the sodium through the nitrogen atoms, and two water molecules that bridge the sodium atoms. The five-coordinate nature of each sodium centre comprises bonding to one carboxylate oxygen, two oxygen atoms of water molecules and two nitrogen atoms from 1,10-phen. This gives sodium a distorted trigonal bipyramidal geometry, as seen in the bond angles subtended at sodium, ranging from $148.16(7)^\circ$ at N1-Na1-O2 (which would be 180° in an idealised trigonal bipyramidal geometry) to $86.07(6)^\circ$ at O1W-Na1-O1W, which would be 90° otherwise.

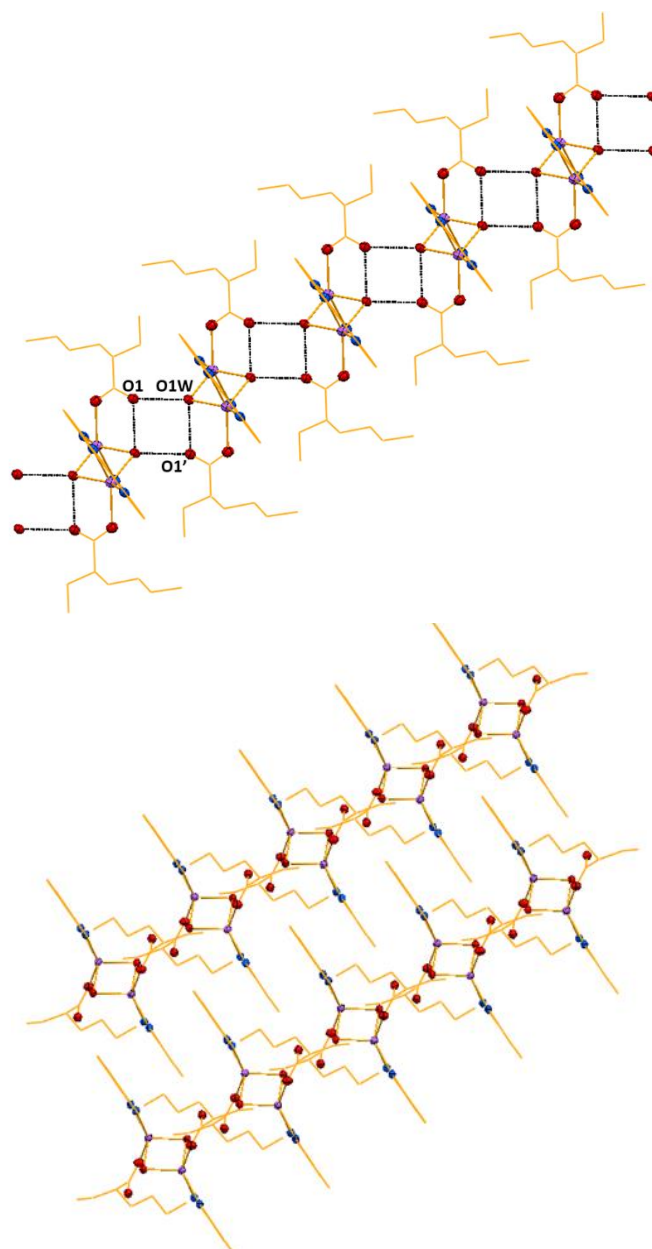
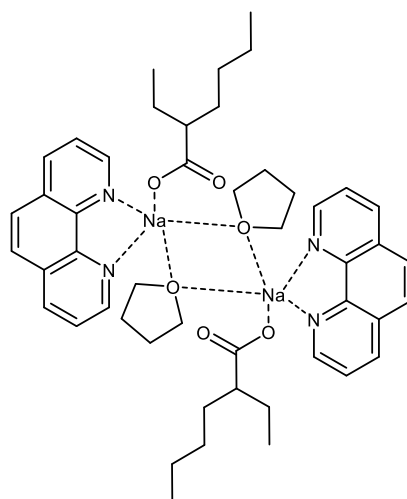


Figure 2.3: (Top) Fivefold section of the polymeric structure of $[\{(\text{C}_5\text{H}_{10})(\text{C}_2\text{H}_5)\text{COONa} \cdot (\text{H}_2\text{O})[1,10\text{-phen}]\}_2]_\infty$ (2) showing hydrogen bonding between dimer units as a black dashed line and (bottom) fivefold section of two interdigitating polymeric chains of $[\{(\text{C}_5\text{H}_{10})(\text{C}_2\text{H}_5)\text{COONa} \cdot (\text{H}_2\text{O})[1,10\text{-phen}]\}_2]_\infty$ (2). These are connected by π - π contacts. Hydrogen atoms are omitted and organic groups are shown as wire frame for clarity. Thermal ellipsoids are displayed at 40% probability level.

The solvating water presumably originates from the commercially obtained sodium 2-ethylhexanoate, which was used as received. Presumably this is made industrially using the parent acid and NaOH, which possibly explains the presence of trace amounts of water. In any case, the water proves to be vital to the architecture of the structure. The water molecule bridges to two sodium cations to create the dimer, while hydrogen bonding between O1W and O1 of adjacent units [O1W...O1 2.786(2) Å and O1W...O1' 2.713(2) Å] forms a rather attractive polymeric structure, composed of linked dimers of **2**. Crystallographically, these hydrogen bonded chains propagate through translation along the *a* direction. This polymer interacts with neighbouring polymers *via* π - π interactions between 1,10-phen rings (centroid...centroid bond lengths between 1,10-phen rings are on average between 3.45 Å and 3.6 Å). Thus adjacent polymeric chains interdigitate with each other. The overall packing is a layered structure with hydrophobic bilayers composed of disordered alkyl groups alternating with layers containing the hydrophilic atoms and the aromatic groups. These layers lie parallel to the crystallographic *ab* plane.

In order to ascertain whether this structure was maintained in solution, a DOSY NMR spectroscopic study was carried out on crystals of **2** in d₈-THF solvent, with TMS as an internal standard. This revealed two distinct species. One species corresponds to a 1:1 mixture comprising free 1,10-phen and THF with an error of -3 % between the theoretical and calculated molecular weights of 252.32 g/mol and 259 g/mol respectively, while the other appears to be a 2:2:2 complex comprising a 1,10-phen solvated sodium 2-ethylhexanoate dimer, bonded THF, and free THF corresponding to an error of 5 % between theoretical and calculated molecular weights (Scheme 2.1). The DOSY suggests a loss of water (from crystalline **2**) and replacement with bridging THF molecules, which though rare have previously been observed crystallographically.⁹⁹⁻¹⁰² The loss of water leads to an absence of hydrogen bonding, meaning a molecular structure such as that in Scheme 2.1 is more likely to be present rather than the polymer witnessed in the solid state, though 100 % definitive identification of the solution state structure remains elusive.



Scheme 2.1: ChemDraw representation of the proposed sodium species present in a solution of 2 as implied by DOSY NMR analysis.

With these results in hand we pondered whether crystals of a donor-free example of sodium 2-ethylhexanoate could be obtained. We therefore attempted several different methods including layering techniques and slow diffusion type reactions with many different solvent systems, all of which were unsuccessful, producing only viscous oils or amorphous solids. Success finally came with the slow diffusion of acetonitrile into an acetone solution of sodium 2-ethylhexanoate that produced a few small crystals suitable for X-ray structural determination. This established their composition to be $[(C_5H_{10})(C_2H_5)COO.Na]_{\infty}$ (**3**).

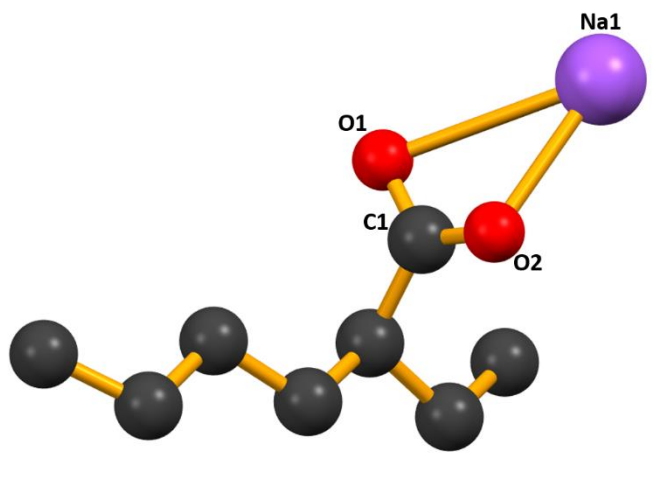


Figure 2.4: Contents of the asymmetric unit of $[(C_5H_{10})(C_2H_5)COO.Na]_{\infty}$ (3**). Hydrogen atoms are omitted for clarity.**

The structure of **3** is revealed to be a unique polymeric form of sodium 2-ethylhexanoate, which is both solvent-free and donor-free. Unfortunately, disorder throughout the long chain backbone rules out a detailed discussion of bond lengths and bond angles; however, the molecular connectivity of the polymer is unambiguous. An infinite chain is observed, with the polymer propagating by action of the 4_1 screw axis parallel to the crystallographic c -direction. Sodium cations within the structure are five-coordinate, made up of two oxygen atoms that attach in a bidentate chelating fashion, and to one carboxylate oxygen atom from three separate carboxylate anions. The long 2-ethylhexanoate chains rotate around a central 'core' composed of sodium cations. Unlike the solvated examples **2** and **4**, the packing arrangement is not a simple layering of hydrophobic and hydrophilic groups. Instead, the hydrophilic polymeric NaO_2 core is surrounded by a wrapping of disordered alkyl groups (Figure 5). This result is unique since to our knowledge it reveals the longest straight chain alkali metal carboxylate characterised *via* single crystal X-ray diffraction. The solid-state structure of sodium 2-ethylhexanoate also contrasts with the structure predicted by DOSY, which suggests that of a dimer. This would make sense given the fact that polar solvents such as water and methanol are likely to deaggregate the structure seen in **3** to that of a simpler dimeric structure.

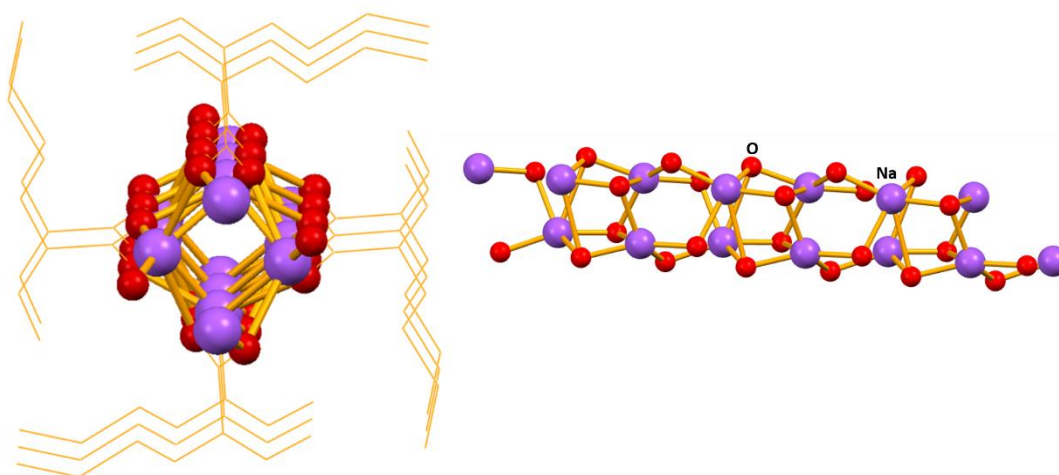


Figure 2.5: (Left) Central Na-O core of 3 with hydrogen atoms omitted, sodium and oxygen atoms drawn as spheres for clarity and organic groups drawn as wire frame for clarity. (Right) Side on view of central Na-O core showing coordination of sodium cations with hydrogen atoms and organic groups omitted and sodium and oxygen atoms drawn as spheres for clarity.

Following these successful results, we then decided to investigate whether such complex architectures could be formed using similarly branched sodium carboxylates. We came across valproic acid as a potential interesting molecule to investigate, as its sodium salt (sodium valproate) and the parent acid are used as Active Pharmaceutical Ingredients (API) to treat a variety of medical disorders such as epilepsy, bipolar disorder and migraines.¹⁰³ To this end, sodium valproate was suspended in 2 ml of a 1:1 mixture of DMF and DMSO and heated until a solution was obtained. This solution was cooled slowly in a hot water Dewar flask over a few days to afford colourless crystals, identified as the solvated polymer $[\{(C_3H_7)(C_4H_8)COONa.(DMSO)\}_\infty]$ (**4**).

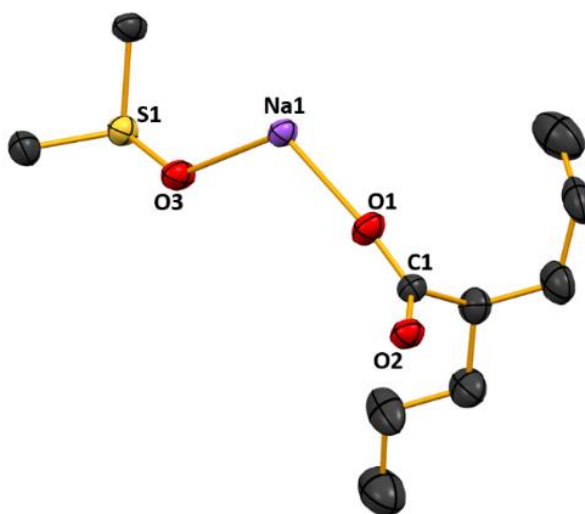


Figure 2.6: Contents of the asymmetric unit of $[\{(C_3H_7)(C_4H_8)COONa.(DMSO)\}_\infty]$ (4**).**

Hydrogen atoms are omitted for clarity. Thermal ellipsoids are displayed at 40% probability level. Symmetry transformations used to generate equivalent atoms: $-x, -y, -z$.

Complex **4** adopts a polymeric structure in the solid state, composed of the long chain sodium carboxylate with the sodium solvated by DMSO. Each sodium cation is five-coordinate, sitting in a markedly distorted square pyramidal geometry. There are also two near perfect squares present in **4**, with each square formed from two sodium cations and two oxygens of two different bidentate chelating carboxylates [$Na_1-O_2-Na_1'$, $91.11(7)^\circ$; $O_2-Na_1'-O_2$, $88.89(7)^\circ$; $O_1-Na_1-O_1$, $85.08(7)^\circ$; $Na_1-O_1-Na_1'$, $94.92(8)^\circ$]. The sodium interacts with two carboxylate unit oxygen atoms in a unidentate manner, one carboxylate unit oxygen atoms in a bidentate chelating manner and one oxygen of DMSO. The C-O bond lengths again confirm the presence of the carboxylate group, with lengths intermediate between single and double bonds [C_1-O_1 , $1.249(3)$ Å and C_1-O_2 , $1.252(3)$ Å]. Once again, the $O_1-C_1-O_2$ bond angle also

indicates total resonance within the carboxylate group lying at $123.7(2)^\circ$, which is consistent with the literature value of carboxylate groups.³⁹ A rather attractive polymeric chain structure is seen, with each chelated carboxylate NaOCO unit bridging to two adjacent sodium cations. Each polymeric motif propagates through translation parallel to the crystallographic a axis. This gives a layered structure with hydrophilic, coordination layers and hydrophobic organic bilayers alternating along the c direction.

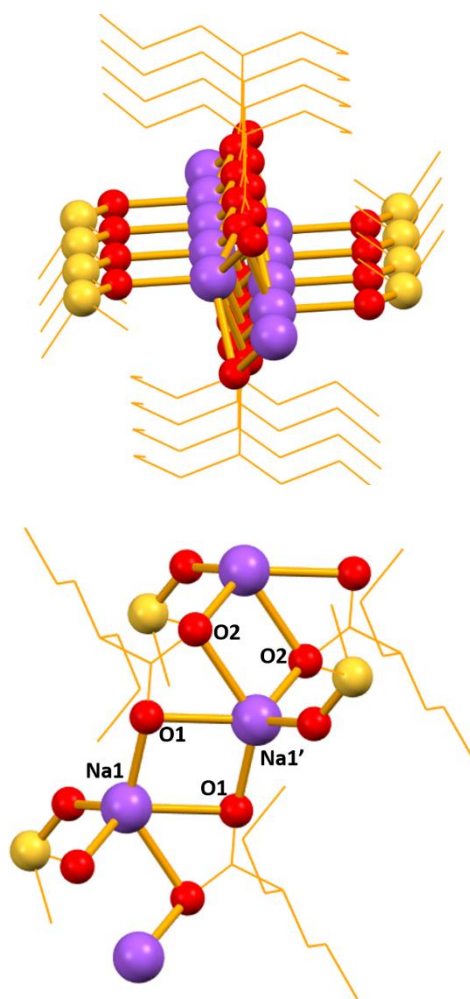


Figure 2.7: (Top) Central Na-O core of 4 with hydrogen atoms omitted, sodium and oxygen atoms drawn as spheres for clarity and organic groups drawn as wire frame for clarity. (Bottom) Repeating polymeric core of 4 showing two fused four-membered rings with hydrogen atoms omitted, sodium and oxygen atoms drawn as spheres for clarity and organic groups drawn as wire frame for clarity.

This study has given a glimpse of the vast array of structures that can be adopted by relatively simple alkali metal carboxylate species in the solid state. Reacting TMP(H) with a long chain branched acid results in the formation of a dimeric hydrogen bonded product, consistent with the predicted structure of sodium carboxylates within polar solvents, as predicted by DOSY NMR.

On reacting sodium 2-ethylhexanoate with 1,10-phenanthroline, a dimeric structure is obtained, with water bridges between the monomer units. This water is crucial to the integrity of the structure, as it provides the means of hydrogen bonding which forms a polymer of dimers featuring interdigitating polymeric chains composed *via* π - π contacts. DOSY NMR analysis suggests the loss of this water in the solution state and its replacement by THF, to construct a molecular structure as opposed to the polymer seen in the solid state.

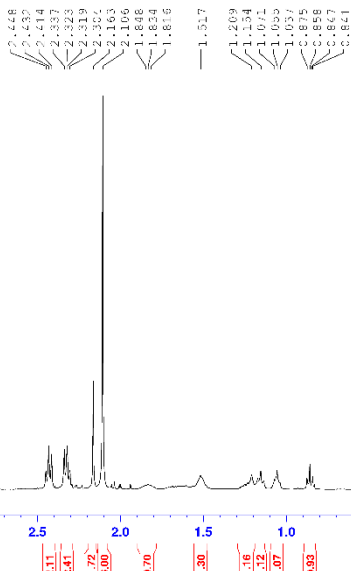
Moving to donor free sodium 2-ethylhexanoate, the solid-state structure of this revealed a more complex than expected polymeric arrangement, composed of a central core of hydrophilic sodium cations with the long, disordered alkyl chains wrapping around this core. This is in stark contrast to the simpler layers of hydrophobic and hydrophilic groups one might expect and is to the best of our knowledge the longest donor-free straight chain alkali metal carboxylate analysed *via* single crystal X-ray diffraction. Finally, we were able to show that similar polymer structures are obtained using donor molecules such as DMSO, with the API sodium valproate also forming a core-based polymer consisting of sodium cation bridged by chelating carboxylates.

Shedding light on metallo structures containing long chain oxygen-based ligands could aid the development and understanding of the use of such ligands in synthetic chemistry. In that regard it is noteworthy that the Knochel group has recently introduced the 2-ethylhexanol derived ligand [sBuMgOR.LiOR], where R is 2-ethylhexyl, into halogen-magnesium exchange methodologies,¹⁰⁴ while sodium 2-ethylhexanoate itself has recently been shown to be a key activator in iron-catalysed hydroboration reactions.¹⁰⁵

2.5 Extended results and discussion

As a starting point for the project, it was decided to explore the effect of introducing common donor molecules to alkali metal carboxylates. This proved to be a more challenging and frustrating avenue of exploration than first expected. While examples of alkali metal carboxylates are used throughout various industries, the structures of their long chain analogues are not as well defined, being mostly predicted through a combination of powder X-ray diffraction, IR and solid-state NMR investigations.^{52, 53, 106} As previously mentioned in Chapter 1, this is due to the long chain being flexible, hence crystals of the long chain analogues tend to form gel-like or amorphous solids, with any crystals that do form likely to exfoliate and thus be unsuitable for single crystal X-ray structural determination.¹⁰⁷ Early experiments carried out therefore focussed on probing the effect/s of donor molecules. Sodium 2-ethylhexanoate or sodium octanoate were initially produced *in situ* using *n*-butylsodium and the respective parent acid. *N*-Butylsodium was chosen over other sources of sodium such as sodium hydroxide as while the latter has the advantage of not being pyrophoric, the former would react with the acid *via* removal of the proton to form the sodium carboxylate of interest while also producing butane gas as a side product, which would leave the reaction and not interfere with the products. If sodium hydroxide was used, the side product would be water, which could subsequently interact with the sodium carboxylate formed and potentially influence the structure adopted by the species. Donor molecules added to the reactions were PMDETA, TMEDA, THF, 15-crown-5, 12-crown-4, diglyme and Me₆-TREN. These donors are nitrogen- or oxygen-based donors, with the expectation that the heteroatoms present would interact with the alkali metal of the carboxylate and stabilise the resulting structure in order to obtain crystals suitable for X-ray crystallographic analysis. In any case, addition of the donor to hexane suspensions of either sodium 2-ethylhexanoate or sodium octanoate was not accompanied by formation of solutions. Instead, the thick white suspensions remained intractable, with only slight colour changes seen, for example, from pure white to off cream, with no major change to the consistencies of the suspensions. Since no solutions were formed crystals could not be obtained, therefore the solvent was removed *in vacuo* and the residues left behind (generally off-white solids or thick viscous oils) were analysed by ¹H NMR spectroscopy. This surprisingly showed no evidence for coordination of the donors, with the resonances corresponding to the donors in the product spectra unchanged when compared to the resonances for the free,

108-113



ethylhexanoate and PMDETA in C₆D₆ solution.

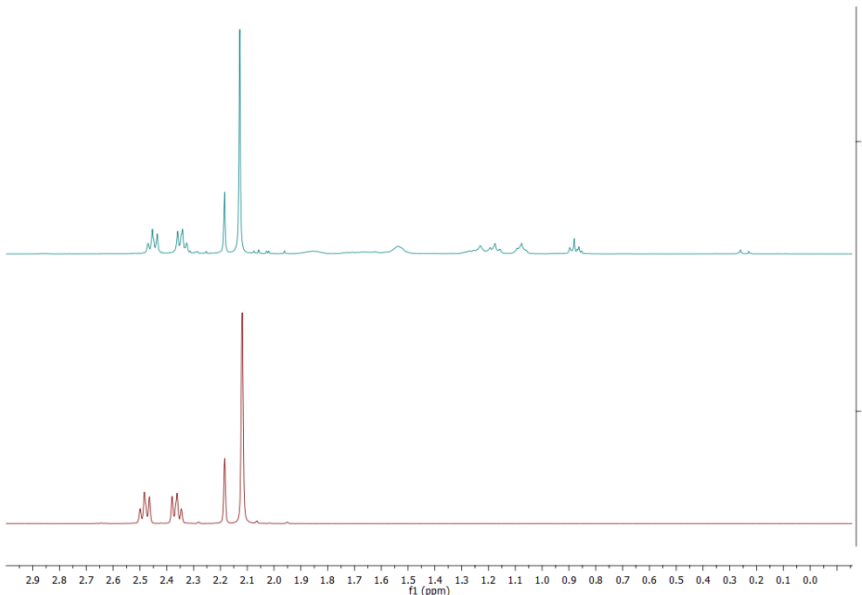


Figure 2.9: (Top) Inset of ^1H NMR spectrum of solid formed from reaction between sodium 2-ethylhexanoate and PMDETA in C_6D_6 and (Bottom) Inset of ^1H NMR spectrum of standard of PMDETA in C_6D_6 .

This presumably is due to the sodium carboxylates forming a stable polymeric structure, with the donors used unable to break down this polymeric structure and hence unable to solubilise the sodium carboxylate. Such solubility issues were not a unique feature of the sodium analogues, with reaction of the parent acids and *n*-butyllithium also producing thick white suspensions, which again did not break down or change upon introduction of donors, presumably due to the same polymeric structure forming. Solvent effects were also investigated, with initial reactions carried out in non-polar hexane. It was reasoned that perhaps a more polar solvent medium for the reactions would lend itself more readily to dissolution of the suspensions, presumably *via* deaggregating the polymer to the dimeric structure predicted to form in polar solvents by DOSY NMR. However, moving to increasingly more polar mediums as toluene and THF respectively did not make any difference to the solubility of the products, with thick suspensions forming regardless of the reaction conditions (such as heating to reflux) or ratios of solvents used (for example using a mixture of toluene and hexane). This is unsurprising given the crux of the issue under investigation in this project is the fact that these deposits form within the diesel engines and are subsequently insoluble. Since diesel fuel is a mixture of hydrocarbons it is to be expected that the deposits formed in the lab environment would also be insoluble. One interesting result obtained during this time was found on varying the ratio of acid : ⁿBuNa used. Suspending one equivalent of ⁿBuNa in methylcyclohexane and adding three equivalents of octanoic acid produced a colourless solution. This was concentrated and placed at -30 °C overnight, where potentially white crystals had formed. These unfortunately melted extremely quickly during an attempted X-ray crystallographic study; therefore, no structural determination could be made. The solvent was subsequently removed, and the white solid left analysed *via* ¹H NMR spectra. These revealed a resonance corresponding to the hydroxyl proton, indicating that some of the parent acid was still intact and had not been deprotonated. This is to be expected given that it had been added in excess, with the solution forming possibly as a result of the acid solvating the resulting sodium carboxylate *via* hydrogen bonding interactions, hence the presence of the hydroxyl proton. However, given the nature of the long chain acids involved it is unlikely that any such acid solvated carboxylate structure can ever be crystallographically characterised.

Next, we moved on to investigate the effects of more rigid donor systems such as 1,10-phenanthroline (1,10-phen). This donor molecule, while still containing nitrogen atoms to interact with the alkali metal is much more rigid than donors such as TMEDA or PMDETA,

owing to its π -system conformationally locking the nitrogen atoms into a single position, allowing for both these atoms to interact with the cation. To this end, sodium 2-ethylhexanoate was generated *in situ* in hexane solvent by reacting $^n\text{BuNa}$ and 2-ethylhexanoic acid. This formed an off-cream coloured suspension, to which was added one equivalent of 1,10-phen. This was left to stir overnight, after which time a white powder had formed, of different consistency to the sodium 2-ethylhexanoate suspension. This powder was isolated by filtration and a ^1H NMR spectrum was ran. This showed the powder was composed of aliphatic protons consistent with the long 2-ethylhexanoate chain, and resonances corresponding to the aromatic protons of the 1,10-phen ligand. When compared to the spectra of free uncoordinated 1,10-phen, the product spectra showed a significant change in the resonances corresponding to the 1,10-phen ligand. For example, the quartet that is present at 6.93 ppm has shifted downfield to 7.03 ppm in the powder, with the doublet of doublets at 9.03 ppm in the standard also shifting considerably, with the corresponding resonance in the powder being at 9.27 ppm.

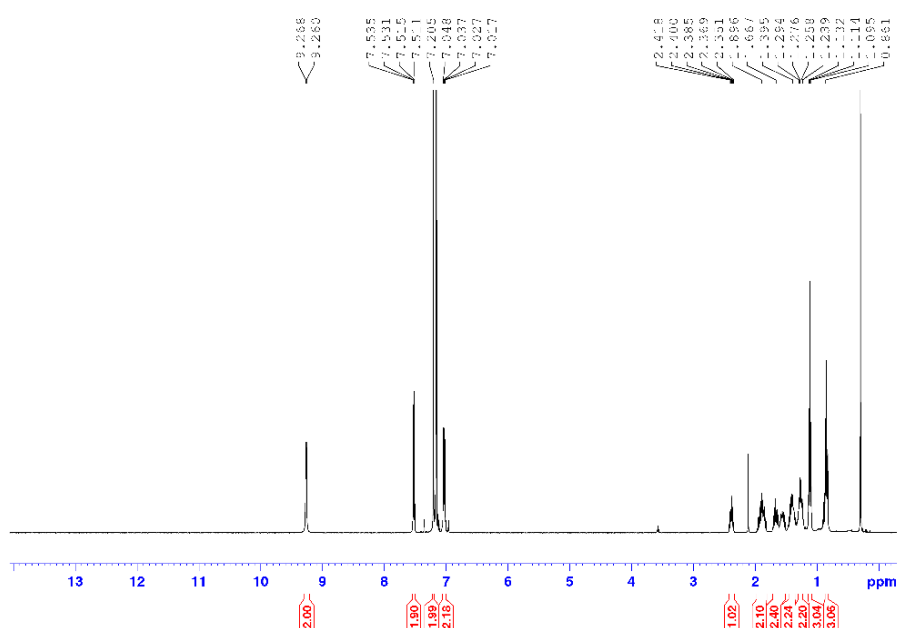


Figure 2.10: ^1H NMR spectrum of powder formed from reaction between sodium 2-ethylhexanoate and 1,10-phen in C_6D_6 .

These changes in the 1,10-phen resonances suggest that the 1,10-phen may be coordinated to the sodium carboxylate. Therefore, an attempt was made to obtain crystals of this potential sodium carboxylate aggregate. The powder was first suspended in hexane then THF was added with gentle heating until a transparent solution was formed. This was left in a hot water Dewar overnight, with colourless crystals subsequently forming. An X-ray crystallographic study uncovered the structure to be the polymer $[(C_5H_{10})(C_2H_5)COONa(1,10\text{-phen})]_{\infty}$ (**5**). This polymeric structure adopts a monomeric substructure composed of one molecule of sodium 2-ethylhexanoate, where the sodium is chelated by one molecule of 1,10-phen. Noticeably, in contrast with structure (**2**) presented in Chapter 2.4, there is no water molecule present in this new structure. Each sodium centre thus interacts with each carboxylate in a rarely seen bidentate chelating bonding mode.³⁹ Despite all attempts to find a suitable model, disorder within the alkyl chains rules out a detailed discussion of bond lengths and bond angles, although the molecular connectivity is unambiguous.

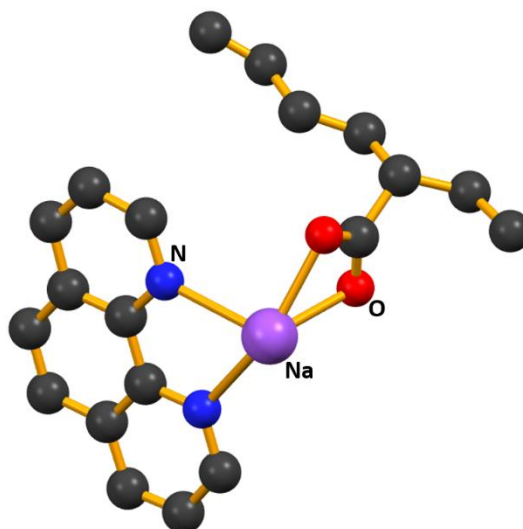


Figure 2.11: Contents of the asymmetric unit of $[(C_5H_{10})(C_2H_5)COONa(1,10\text{-phen})]_{\infty}$ (**5**). Hydrogen atoms and disorder in the alkyl chain are omitted for clarity. Symmetry transformations used to generate equivalent atoms: $\frac{1}{2}+x, -y, z$; $\frac{1}{2}+x, \frac{1}{2}+y, \frac{1}{2}+z$; $x, \frac{1}{2}-y, \frac{1}{2}+z$.

Each symmetrically equivalent sodium cation is five-coordinate, interacting with two oxygen atoms from one carboxylate unit in a bidentate manner, two nitrogen atoms from the 1,10-phen ligand and one oxygen atom from an adjacent 2-ethylhexanoate anion in a unidentate manner. It is this monodentate carboxylate interaction that propagates the polymer chain, with the long alkyl chains disposed in a zig-zag arrangement relative to each other. The

polymer also contains stacked rings of the 1,10-phen ligand, which are off-centre with respect to each other in that the bottom ring of one 1,10-phen ligand lies above the top two rings of the adjacent 1,10-phen ligand. Interestingly, replication of this result proved to be challenging, with all later attempts resulting in the formation of complex **2** as described in the previous section. The structures share similarities in that they are both polymeric, but in **2** the polymer propagates through hydrogen bonding between water molecules and π - π stacking between interdigitating 1,10-phen rings, while in **5** the polymer propagates through the action of unidentate carboxylate bonding.

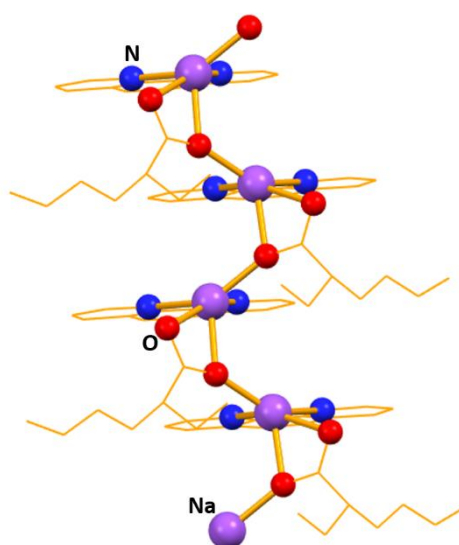
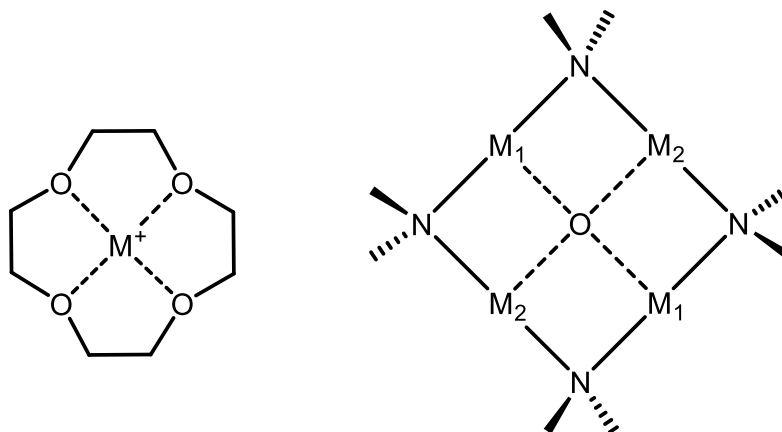


Figure 2.12: Four fold section of the polymeric structure of $[(C_5H_{10})(C_2H_5)COONa(1,10\text{-phen})]_{\infty}$ (5**). Hydrogen atoms and disorder in the alkyl chain are omitted for clarity. Organic groups are shown as wire frame for clarity. Symmetry transformations used to generate equivalent atoms: $\frac{1}{2}+x, -y, z$; $\frac{1}{2}+x, \frac{1}{2}+y, \frac{1}{2}+z$; $x, \frac{1}{2}-y, \frac{1}{2}+z$.**

With these results in hand, we pondered whether other rigid donor systems could be utilised in the crystallisation of long chain acids. Our attention turned to inverse-crown chemistry, which was developed in large part within the inorganic section at Strathclyde.¹¹⁴⁻¹¹⁶ These inverse crowns can be thought of as special classes of heterobimetallic complex, with their composition inverted with regards to conventional crown ethers, in that where in crown ethers the oxygen atoms trap cations *via* interactions, in inverse crowns oxygen or related cations are trapped within the central core of a positively-charged host ring featuring a mixture of electropositive metals (Scheme 2.2).¹¹⁵ The field of inverse-crown chemistry can therefore be considered as a subclass of inverse coordination chemistry.¹¹⁷ Metals featured within these inverse crowns include Li, Na or K (from alkali metal amides) and Mg or Zn (from

bisamides). The combination of these metals leads to a synergistic effect within the systems, in that the chemistry carried out by these inverse crowns cannot be carried out by complexes that contain each of the metals individually.¹¹⁸ There are many examples of inverse crown ethers within the literature and they are well known as oxygen scavengers, with adventitious oxygen or moisture being very efficiently trapped within the inverse crown, even if standard precautions to remove oxygen and moisture are followed.¹¹⁹



Scheme 2.2: Comparison between the motifs of generalised (LHS) crown ether and (RHS) inverse crown ether complexes.

Of particular relevance to this part of the project was work carried out by Mulvey *et al.* exploring alkoxide binding within inverse crown chemistry in 2002.¹²⁰ In this contribution it was shown that a mixed sodium-magnesium diisopropylamide based inverse crown could react with a long chain alcohol to produce a crystalline sodium-magnesium-alkoxide-diisopropylamide inverse crown product.¹²⁰ This product was formed *via* formation of the pre-inverse crown *in situ* (from reaction of ⁿBuNa, Bu₂Mg and addition of iPr₂NH in hexane), followed by addition and subsequent deprotonation of the appropriate alcohols, butanol and octanol. Products crystallised from non-polar aprotic solvents, either toluene or hexane. Figure 2.13 shows the structure of the octoxide product.

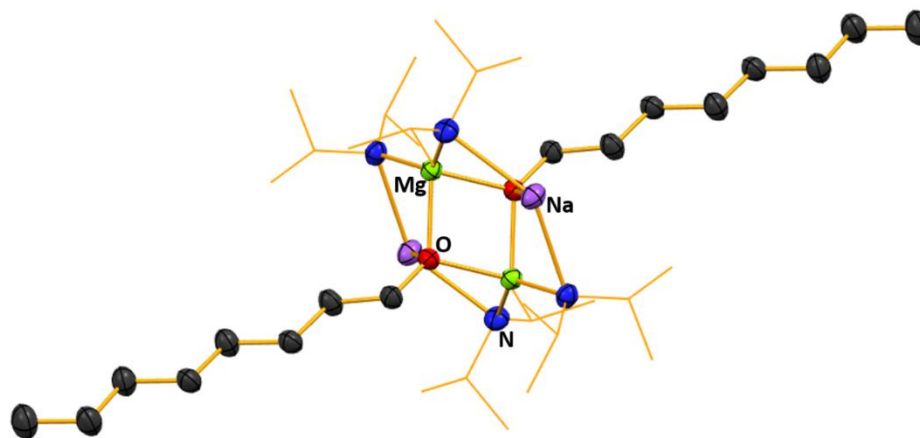


Figure 2.13: Structure of $[\{NaMg[N(iPr)_2]_2OOct^n\}]_2$ (6). Hydrogen atoms and organic fragment of inverse crown scaffold shown as wire frame for clarity. Thermal ellipsoids are set at 40 % probability level.

Both structures consist of an eight-membered $[Na(N)_2Mg]_2$ cationic ring, with the core of the ring occupied by two oxide anions from the alcohol. Of particular note is the overall shape of this ring, being described as chair-shaped, with the Na cations displaced from the plane defined by $NMgN...NMgN$, with this displacement being greater in the octoxide case when compared to the butoxide.¹²⁰ These alkoxide based structures could prove to be useful models for carboxylate based inverse crowns, with the octoxide being suitable for the long chain octanoic acid in particular. However, the butoxide example would be a poor model for the longer chain branched 2-ethylhexanoic acid. Therefore, it was decided to attempt to synthesise an inverse crown based on 2-ethylhexanol, which could prove to be a useful model. To this end, $nBuNa$ was suspended in methylcyclohexane, to which was added Bu_2Mg and three equivalents of iPr_2NH , forming a yellow solution. To this was added 2-ethylhexanol, which formed a colourless solution. This was concentrated *in vacuo* and placed at $-30\text{ }^{\circ}C$. After a few days, colourless crystals had formed, identified as the alkoxy based inverse crown $[\{NaMg[N(iPr)_2]_2OC_2H_3(C_2H_5)C_4H_9\}_2]$ (**7**).

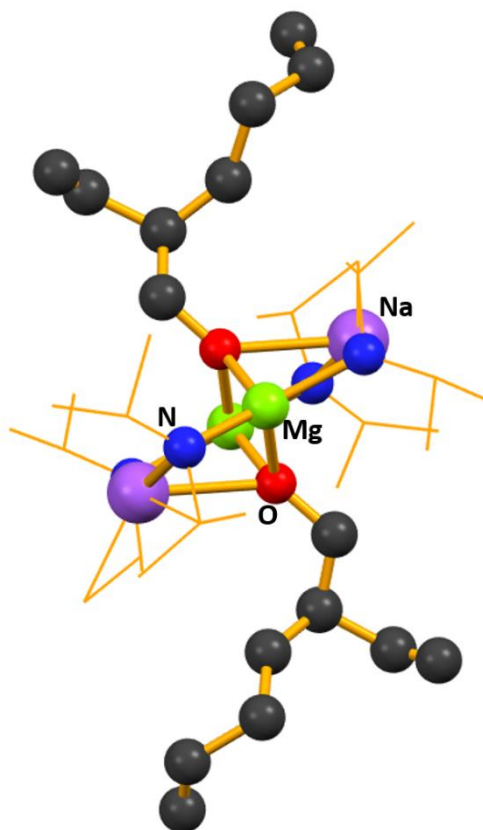


Figure 2.14: Structure of $[\{\text{NaMg}[\text{N}(\text{iPr})_2]_2\text{OC}_2\text{H}_3(\text{C}_2\text{H}_5)\text{C}_4\text{H}_9\}_2]$ (7**). Hydrogen atoms and disorder within the complex omitted for clarity. Organic fragment of inverse crown scaffold shown as wire frame for clarity. Symmetry transformations used to generate equivalent atoms: $-x, y, -z$; $\frac{1}{2}+x, \frac{1}{2}+y, \frac{1}{2}+z$; $\frac{1}{2}-x, \frac{1}{2}-y, \frac{1}{2}-z$.**

Disorder within the structure of **7** make a detailed discussion of its bond lengths and bond angles impractical, however the molecular connectivity shows a similar structure to that recorded by Mulvey *et al.* in their work.¹²⁰ The inverse crown scaffold is composed of a central eight-membered $[\text{Na}(\text{N})_2\text{Mg}]_2$ ring, with two molecules of 2-ethylhexanoate within the central cavity. The 2-ethyl portion of the chains are arranged in a trans-fashion with respect to each other, presumably as a result of sterics. In contrast to that structure obtained by Mulvey *et al.*,¹²⁰ there appears to be agostic interactions²³ between the sodium cation and two carbons from two separate iPr_2N groups. This is presumably due to the shorter bonds between the Na and the N of the iPr_2N groups in **7** when compared to the octoxide structure **6** (Na-N bond distance of 2.39(1) Å in **7** compared to Na-N bond distance of 2.478(2) Å in **6**) which would bring the iPr_2 groups into closer proximity with the Na cation. This structure would be an ideal model for carboxylate based inverse crowns, however despite several attempts no such structure could be obtained. When forming the inverse crown as per the literature procedure¹²⁰ and adding in an equivalent of either 2-ethylhexanoic or octanoic

acid, a solid would initially form. This solid subsequently dissolved upon stirring to leave a clear homogenous solution. Unfortunately, cooling of this solution always resulted in the formation of colourless oils, which proved to be difficult to get back into solution once formed. ^1H NMR analysis of this oil showed apparent breakdown of the inverse crown structure, with a broad resonance between -0.4 and -0.7 ppm indicative of the continued presence of alkyl groups adjacent to the magnesium centre. While failure to form the inverse crown structure cannot be ruled out, given the successful reaction to produce **7** above it seems more likely that addition of the acids somehow causes the breakdown of the crown to its constituent parts.

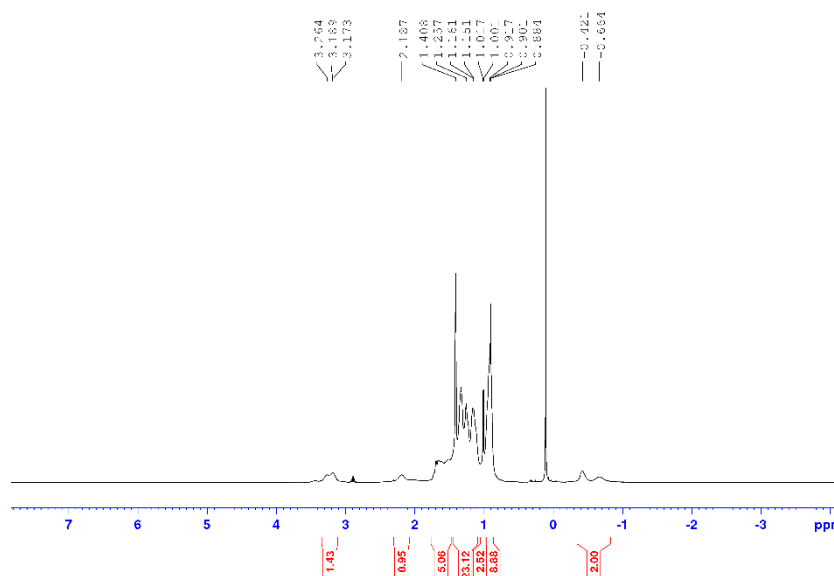


Figure 2.15: ^1H NMR spectrum of oil formed from reaction between sodium 2-ethylhexanoate and inverse crown in C_6D_{12} .

Looking for alternative ways to crystallise out long chain examples of carboxylates, an investigation by Mulvey *et al.* from 2000 was recalled.¹²¹ This was looking into metal-metal exchange reactions between alkali metal alkoxides and alkali metal amides. While this may seem to be simple reaction on the surface in fact it hides a myriad of complexity.¹²¹ For instance, the transmetallation reaction between $n\text{BuLi}$ and $t\text{BuOK}$ may seem to be simplistic, however together these complexes form an aggregate of indeterminate composition referred to as Lochmann-Schlosser or LICKOR superbase.¹²² This complex is capable of enhanced, synergistic reactivity; for example, toluene and benzene react slowly with alkyllithiums and not at all with potassium alkoxide reagents, however there is extreme reactivity when a mixture of the two are present.¹²³ The ultimate identity of the reactive

species remains a mystery, though several attempts have been made to obtain reliable evidence for the chemical make-up of these species. An example includes the work of Klett *et al.*, who combined neopentyllithium with potassium *tert*-butoxide to obtain a crystallographically characterised example of a LICKOR superbase, which exists as a mixture of various aggregates.¹²⁴ While the structure obtained was heavily disordered, molecular connectivity was conclusive, revealing the aggregate to be a combination of a $[\text{Li}_4(\text{O}^t\text{Bu})_3]^+$ unit and a $[\text{K}_3\text{Np}_3(\text{O}^t\text{Bu})]^-$ unit, arranged in a Li_3K_3 octahedron capped by *tert*-butoxide groups. The work carried out by Mulvey *et al.* in 2000 was related to this field as the resulting structure, obtained *via* reaction of either lithium anilide and sodium *tert*-butoxide or sodium anilide with lithium *tert*-butoxide with 4-methyl pyridine (4-Me-py) as coordinating solvent, is reminiscent of those structures likely to be found within the realm of superbases, in that it combines both alkali metal amide and alkali metal alkoxide components.¹²¹ The structure in question was determined by X-ray crystallography, which showed its mixed-metal composition to be $[\text{Li}_4\text{Na}_4(\text{tBuO})_4\{\text{PhN}(\text{H})\}_4(\text{NaOH})(4\text{-Me-py})_4]$ (**8**).

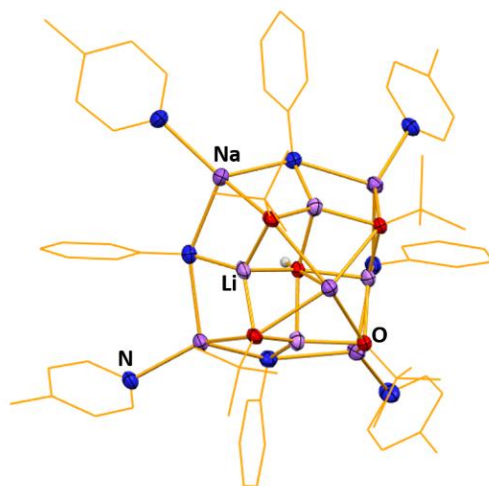


Figure 2.16: Structure of $[\text{Li}_4\text{Na}_4(\text{tBuO})_4\{\text{PhN}(\text{H})\}_4(\text{NaOH})(4\text{-Me-py})_4]$ (8**). Hydrogen atoms apart from that in the OH group omitted for clarity. Organic fragments shown as wire frame for clarity. Thermal ellipsoids are displayed at 40 % probability level.**

The structure is composed of an eight-membered $(\text{Na}\{\text{N}(\text{H})\text{Ph}\})_4$ ring, with a smaller but still eight-membered $(\text{LiO})_4$ ring above this. The structure adopts an attractive dome shape comprised of 17 vertices, with the top of the dome being a Na cation. Encapsulated within this architecture is a hydroxide molecule, presumably arising from adventitious hydrolysis, although a definitive origin is not certain.¹²¹ The sodium atoms at the base of the dome architecture are solvated by the 4-Me-py molecules, with the Na at the apex of the structure

bonded to the hydroxide encapsulated within, with the short Na-O bond of the Na-OH compared to Na-OtBu bond (2.349(5) Å vs 2.557 Å respectively), suggesting that the NaOH molecule perhaps acts as the 'seed' around which the complex is formed.¹²¹

With these results in mind, it was decided to attempt to synthesise a similar type of complex but with the simple *tert*-butoxide alkoxide unit replaced by the longer chain 2-ethylhexanolate. This may prove to be a useful model for the crystal behaviour adopted by the carboxylate systems of interest, as both this alcohol and the acids are composed of long chains. 2-Ethylhexanol and ⁿBuLi were reacted in hexane, forming the lithium alkoxide *in situ*. To this mixture was added NaNPh₂ and two equivalents of pyridine to form a green suspension. Pyridine was chosen over its 4-methyl derivative (4-Me-py) as it was thought the latter donor may have contained too much steric bulk given the alkoxide unit has significantly increased in sterics going from *tert*-butoxide to 2-ethylhexanolate. THF and gentle heating formed a green solution. Upon cooling the solution to -20 °C, colourless crystals formed, the structure of which was revealed by X-ray crystallography to be [(PhNNa)₂(Py)₃.0.5(THF/Py)] (9).

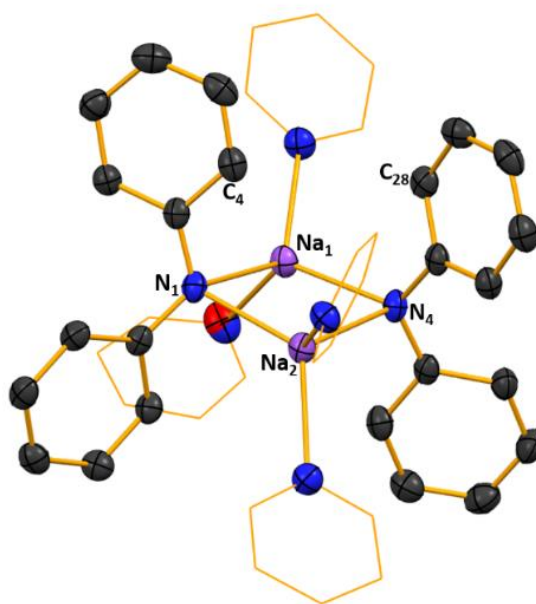


Figure 2.17: Molecular structure of [(Ph₂NNa)₂(Py)₃.0.5(THF/Py)] (9). Hydrogen atoms and disorder within the complex omitted for clarity. Organic fragment of solvating pyridine and THF shown as wire frame for clarity. Thermal ellipsoids are displayed at 40 % probability level. Symmetry transformations used to generate equivalent atoms: -x, ½+y, -z.

The structure is a dimer consisting of two molecules of sodium diphenylamide, with one of the sodium atoms solvated by two molecules of pyridine and the other sodium atom solvated by one pyridine and one solvent site containing both pyridine and THF in an approximately 50:50 ratio. Each sodium cation therefore has a coordination number of four, made up of one nitrogen atom from both diphenylamide units and two donor atoms (nitrogen in the case of pyridine and oxygen in the case of THF). The bond angles around Na₁ range from the acute of 99.0(1)° to the obtuse 125.6(1)°, giving a τ_4 value of 0.86.¹²⁵ Those around Na₂ range from 92.0(1)° to 123.6(1)°, with τ_4 = 0.84.¹²⁵ Therefore both sodium cations occupy a distorted tetrahedral environment. There are also agostic interactions present, with each sodium cation interacting with an additional *ipso* carbon atom from one phenyl ring of the diphenylamide. These are long contacts, being approximately 3 Å in length (Na₁-C₄ 2.924(3) Å; Na₂-C₂₈ 3.038(3) Å) in both instances. The (NaN)₂ ring forms a near-square at the dimers centre, with internal angles of 81.09(9)° at N₁, 98.0(1)° at Na₂, 80.85(9)° at N₄ and 99.0(1)° at Na₁.

Clearly within **9** there is no long chain alkoxide present within the structure, with the alkoxide lithium 2-ethylhexanoate presumably remaining in solution without being incorporated into the dimeric structure, with ⁷Li NMR of crystals of the structure showing no resonance, giving weight to the possibility that the lithium alkoxide remains in the solution. It could be that the dimer is so stable that the alkoxide unit cannot break it apart in order to be incorporated or alternatively it may be that the sterics of the longer chain 2-ethylhexanoate molecule in comparison to the *tert*-butoxide molecule seen in the structure of **8** precludes the formation of a similar dome-like architecture. Alternatively, the lack of hydroxide molecule in **9** that can potentially act as a seed could be another reason for the formation of a different architecture.

All the previously discussed reactions were carried out using standard Schlenk techniques, which also means they were all carried out under atmospheric pressures. However, as should be clear from Chapter 1, the chemistry that takes place within diesel engines takes place at much higher temperatures and pressures than would ordinarily be experienced on the bench. These extreme conditions may influence the structures adopted by the alkali metal carboxylates of interest. For example, high temperatures and pressures are very often standard conditions for the synthesis of metal organic frameworks or MOFs. These MOFs are compounds composed of organic linkers and voids, which through cross-links can form one-

, two- or three-dimensional structures.¹²⁶ The organic linkers in many examples of these MOFs are based on carboxylates, with di- and tricarboxylic acids particularly common. One of the most desirable properties of these acids is a rigid backbone, with aromatic carboxylic acids often used for this reason. In terms of synthetic procedures, solvothermal synthesis techniques are used, which are chemical reactions that take place in a reaction vessel (generally in an autoclave) at temperatures that are above the boiling point of the solvent and at pressures greater than 1 bar.¹²⁷ These conditions allow for the effective dissolution of the reaction products, and by introducing a cycle of heating and cooling, very often the MOF products are observed as crystals.

While the acids used in this project do not have the rigid backbone characteristic of traditional MOF linkers, in engines the conditions these carboxylates would experience would be rather similar to the conditions used to synthesise MOFs. Therefore, it seemed pertinent to attempt some reactions at conditions more akin to those experienced in the field. This would allow for a more accurate representation of the kinds of structures adopted by alkali metal carboxylates at these harsh interfaces if crystals could be obtained, given that by heating reactions within an autoclave high pressures are also generated. In this regard, a series of reactions were set up and heated within high pressure tubes. These tubes can be sealed and heated to 120 °C without damage, with a high pressure of 10 bar also produced within the tube, thus replicating more closely real-world engine conditions within the laboratory. Table 2.0 shows a summary of some of the reactions performed under these conditions.

Table 2.0: Selection of high-pressure reactions carried out

<i>Reaction</i>	<i>Solvent</i>
NaOH + 2-ethylhexanoic acid	H ₂ O
NaOH + 2-ethylhexanoic acid + 1,10-phen	H ₂ O
NaOH + Octanoic acid	H ₂ O
NaOH + Octanoic acid + 1, 10-phen	H ₂ O
4NaOH + DDSA	H ₂ O
4 NaOH + DDSA + 2 1, 10-phen	H ₂ O
NaOH + 2-ethylhexanoic acid	MeOH
NaOH + 2-ethylhexanoic acid + 1, 10-phen	MeOH

NaOH + Octanoic acid	MeOH
NaOH + Octanoic acid + 1, 10-phen	DCM
Sodium naphthenate + 1, 10-phen	DCM

All high-pressure reactions were carried out at 120 °C in an oil bath. Each reaction was heated at this temperature for 64 hours, before being cooled to room temperature over a period of 24 hours.

A general procedure would involve dissolving 1-2 mmol of the reactants in 3-5 ml of the solvent. These solutions were added to the high-pressure tubes and the vessel was then placed in an oil bath at 120 °C. After 3 days the tube was slowly cooled to room temperature and the material left in the tubes was analysed. In many cases the solutions had changed colour dramatically (Figure 2.18), transforming from colourless to pale yellow or dark orange, which may be suggestive of an assortment of reactions having taking place.

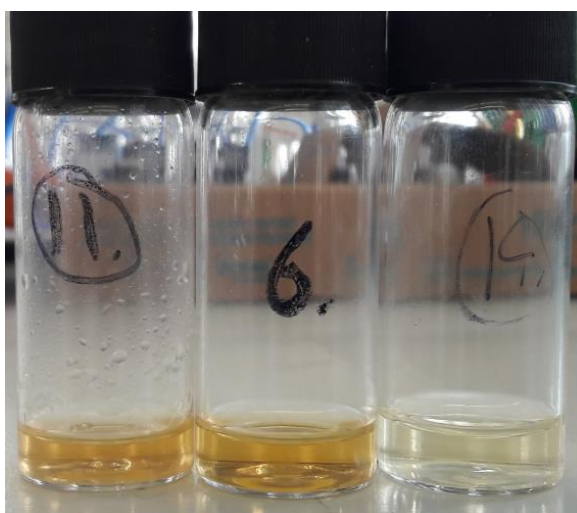


Figure 2.18: Solutions from high-pressure reactions. Note the various shades of yellow present in these solutions.

IR analysis was carried out on the solutions to ascertain if the formation of carboxylate species could be evidenced. The IR spectra shows the characteristic peaks associated with the asymmetric (1567 cm^{-1}) and symmetric (1413 cm^{-1}) stretching of the carboxylate group, indicating that the deprotonation reaction was successful. The solutions were then left to see if slow evaporation could produce any crystals. After a period of a few weeks, in all cases, no crystal formation was evident. The samples were then used to set up various slow diffusion experiments, however once again no crystals could be formed, with the only products being amorphous solids and powders.

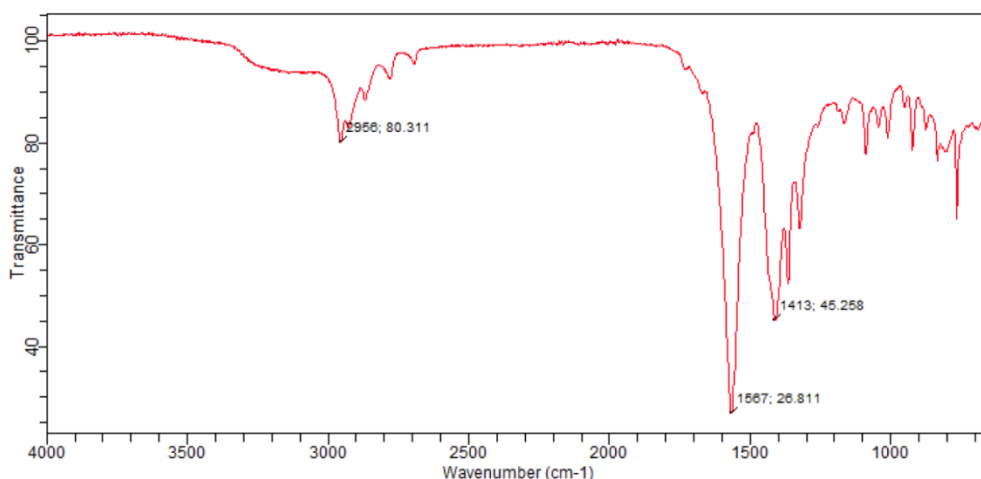


Figure 2.19: IR spectrum of reaction product of 2NaOH and DDSA.

An interesting result was seen when sodium naphthenate and 1, 10-phen were heated to 120 °C in DCM solvent. While sodium naphthenate on its own is not fully soluble in DCM (see later), upon addition of the 1, 10-phen a yellow solution is immediately formed. Upon heating this for three days, a black solid formed in an otherwise yellow solution. ^1H NMR analysis of this powder seemed consistent with coordination of the 1, 10-phen, due to the movement in the resonances associated with the ligand, as seen previously for structures **2** and **5**.

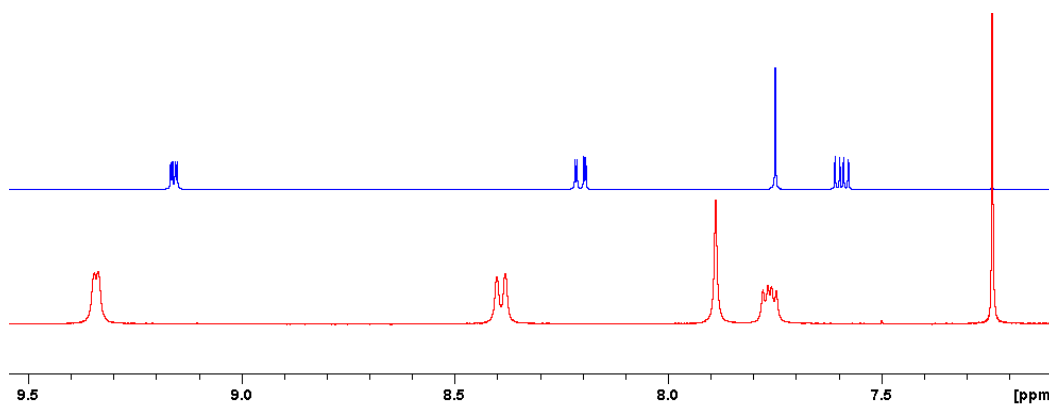


Figure 2.20: Comparative ^1H NMR spectra showing (top) standard of 1,10-phen in CDCl_3 and (bottom) reaction product of sodium naphthenate and 1,10-phen in DCM in CDCl_3 .

Upon leaving this solution, crystals suitable for X-ray analysis were obtained, but these were of a protonated 1, 10-phenanthroline chloride hydrate.

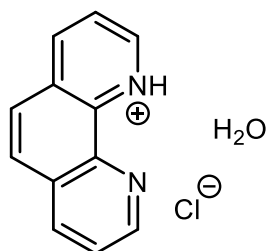


Figure 2.21: ChemDraw of reaction product of sodium naphthenate and 1,10-phen in DCM as identified *via* X-ray crystallography.

This result is consistent with both IR and ^1H NMR data of the solution, which while showing a movement in the 1, 10-phenanthroline resonances also showed the presence of the free naphthenic acid, characterised by the resonance at 12.02 ppm corresponding to the hydroxide group.

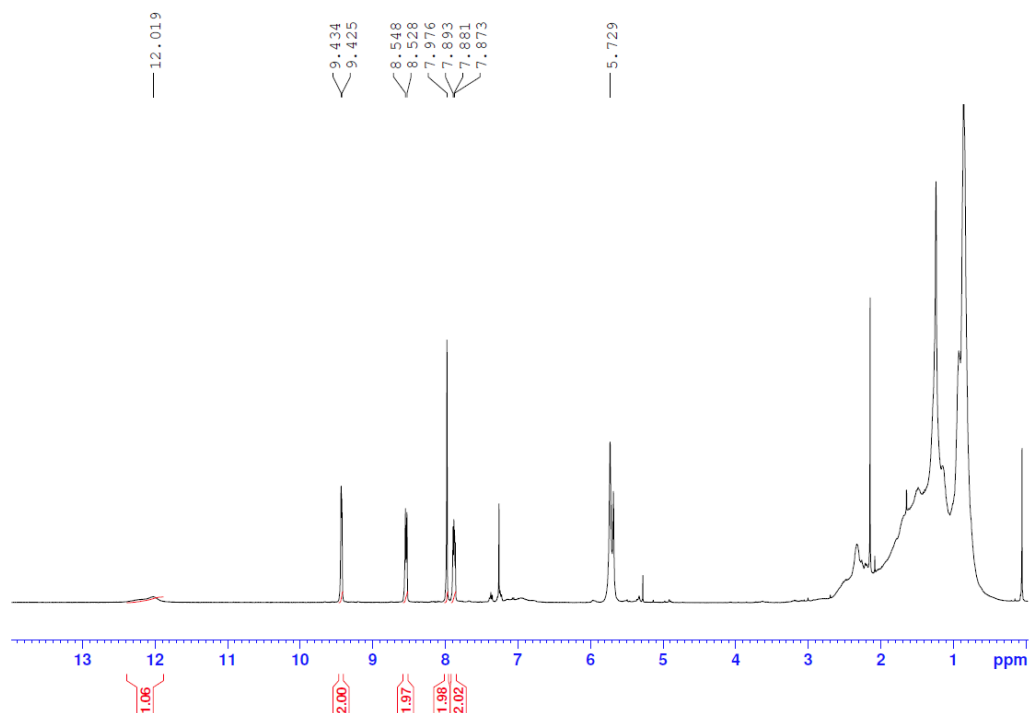


Figure 2.22: ^1H NMR spectra of reaction product of sodium naphthenate and 1,10-phen in CDCl_3 .

The reason why insight into sodium naphthenate would be useful is due to its role as an important sodium source within the fuel industry. This is a consequence of its use as the principal source of sodium within diesel engine testing. However, given the lack of information on sodium naphthenate, including something as vital as its molecular weight, it

would be advantageous to attempt to provide some sort of insight into the overall composition of the mixture, with the attempts in this project summarised over pages 62-73.

Initial solubility tests of sodium naphthenate

Initially it was decided to test the solubility of the sodium salt species, to discern in which solvents any studies or crystallisation tests could be carried out. Various solvents were tried, ranging from non-polar to polar. Results are summarised in Table 2.1, with the polarity of the solvent increasing as the table is descended.

Table 2.1: Solubility tests involving sodium naphthenate and a selection of solvents

<i>Solvent</i>	<i>Solubility</i>
Hexane	Insoluble, forms yellow gel
Petroleum ether	Insoluble, forms a pale white gel
Diethyl ether	Insoluble, forms a white powder
Chloroform	Soluble, forms a colourless solution
Dichloromethane	Only partially soluble, still some powder remaining
THF	Soluble, forms a yellow solution
Acetone	Insoluble, forms a white powder
Ethyl acetate	Insoluble, forms a white powder
Isopropanol	Only partially soluble, forming a yellow solution
Ethanol	Soluble, forms a pale-yellow solution
Methanol	Soluble, forms extremely pale-yellow solution
Water	Soluble, forms yellow solution

What is apparent from this table is that there is no real 'cut-off' point, where solvents more polar than this point dissolve the sample and solvents below this point do not. For example, sodium naphthenate is fully soluble in chloroform and THF, but it is less soluble in the more

polar ethyl acetate and isopropanol. This seemingly suggests that the polarity of the solvent has no discernible impact on the solubility and naturally complicates solution state analysis.

Spectroscopic studies

IR spectroscopy was the simplest way to identify the main functional groups present within the sodium naphthenate sample, obtained from TCI and identical to the type used by Innopsec in engine testing reactions. The IR spectrum (Figure 2.23) shows vibrations at $\sim 2900\text{ cm}^{-1}$, characteristic of aliphatic C-H stretches, and at 1556 and 1411 cm^{-1} , characteristic of the asymmetric and symmetric carboxylate stretches respectively. The asymmetric stretching vibration is more intense than the symmetric stretching vibration, which can suggest a more asymmetric bonding mode within the sample.⁵² The intense stretching vibration representative of the aliphatic CH stretches suggests that the majority of the sodium naphthenate sample is aliphatic in nature, with low levels of aromatic compounds present. These findings are consistent with the paucity of literature precedent that is available on sodium naphthenate.⁵⁷

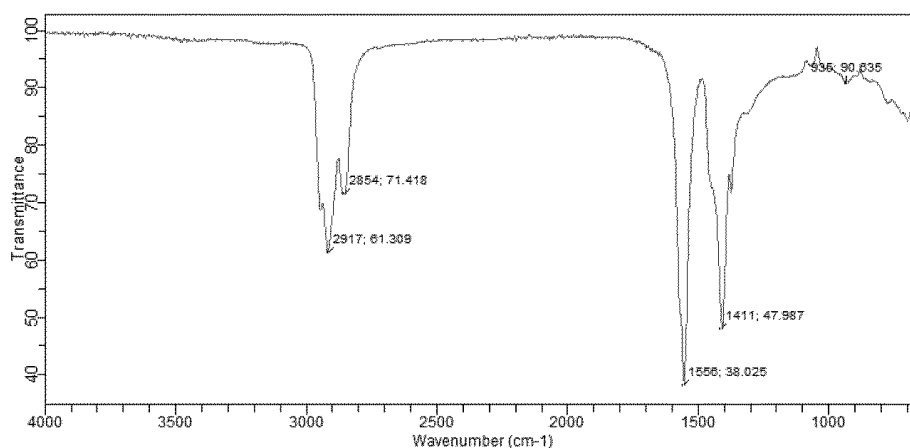


Figure 2.23: IR spectrum of sodium naphthenate.

Next, NMR spectroscopy was attempted. However, this proved to be more challenging than initially thought. As seen in Table 2.1, sodium naphthenate is insoluble in many commonly used solvents, with the insolubility hampering attempts to get informative NMR information. Initial testing looked at C₆D₆, which did provide a spectrum, however it is important to note that not all the sodium naphthenate sample dissolved in the C₆D₆ solvent. This showed what was broadly expected, with a series of very broad resonances between 0.89 and 2 ppm, indicative of aliphatic hydrogen atoms, which served to confirm the largely aliphatic nature of the sample.

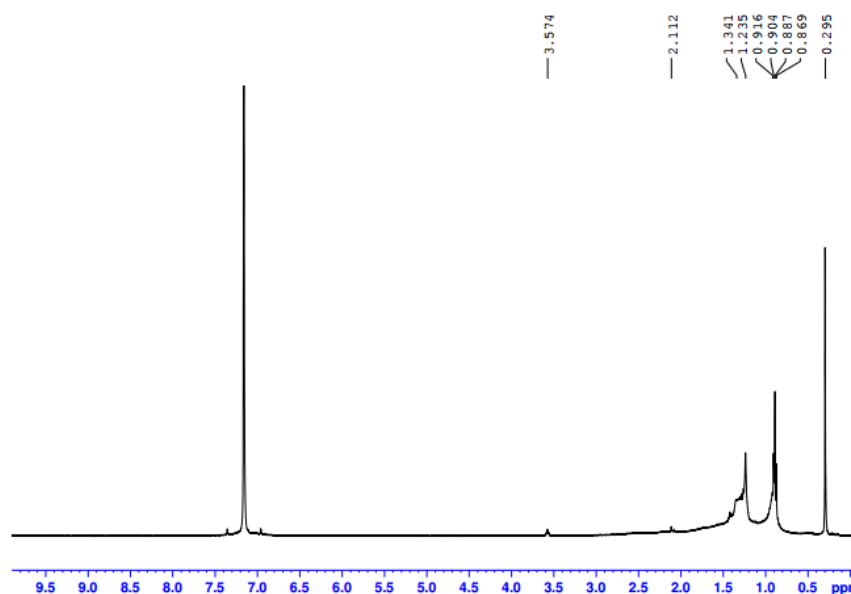


Figure 2.24: ^1H NMR spectrum of sodium naphthenate in C_6D_6 , with the large resonance at 7.16 ppm corresponding to C_6D_6 solvent.

The broadness of these resonances gives some indication of the complexity of the sample, with several similar hydrogen environments likely contributing to each of the resonances.

The NMR experiment was then repeated using d_8 -THF as solvent, reasoning that hopefully the increased solubility of the sodium naphthenate in THF would allow for an improved spectrum quality. Unfortunately, this was not seen, with the resonances associated with the aliphatic protons in fact becoming broader and poorer quality in comparison to those seen in Figure 2.24. When recording a ^{13}C NMR spectrum in d_8 -THF, prolonged experiment scan times were necessary to see even the smallest relevant resonances, with 8192 scans required to see the faint carboxylate carbon resonance at 181.9 ppm.

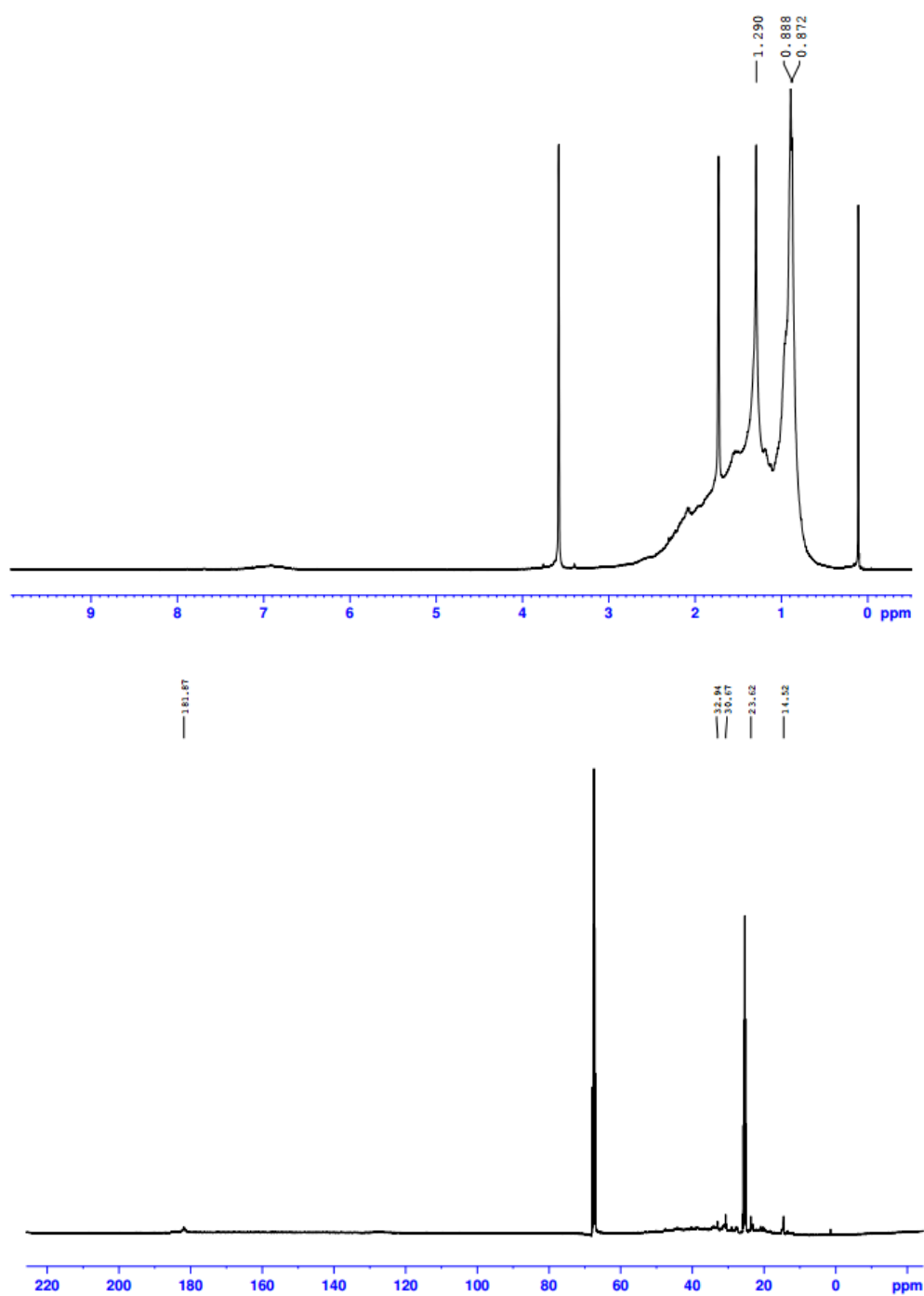


Figure 2.25: (Top) 1H NMR spectrum of sodium naphthenate in d_8 -THF; (Bottom) ^{13}C NMR spectrum of sodium naphthenate in d_8 -THF.

To attempt to gain more insight into the structure or potential structures of the sodium naphthenate, a sample was reacted with the chelating donor molecule 1, 10-phen. Previous success has been had where the nitrogen atoms of this donor have donated to sodium cations of sodium carboxylates, enabling both spectroscopic analysis and structural

determination to be achieved. To this end, 1 mmol of 1, 10-phen and sodium naphthenate were mixed in hexane and left stirring overnight to afford a white powder. ^1H NMR studies suggested coordination of the 1, 10-phen to some component of the sodium naphthenate mixture. This could be inferred by the downfield shift of the resonances associated with the 1, 10-phen protons when compared to a 1,10-phen standard.

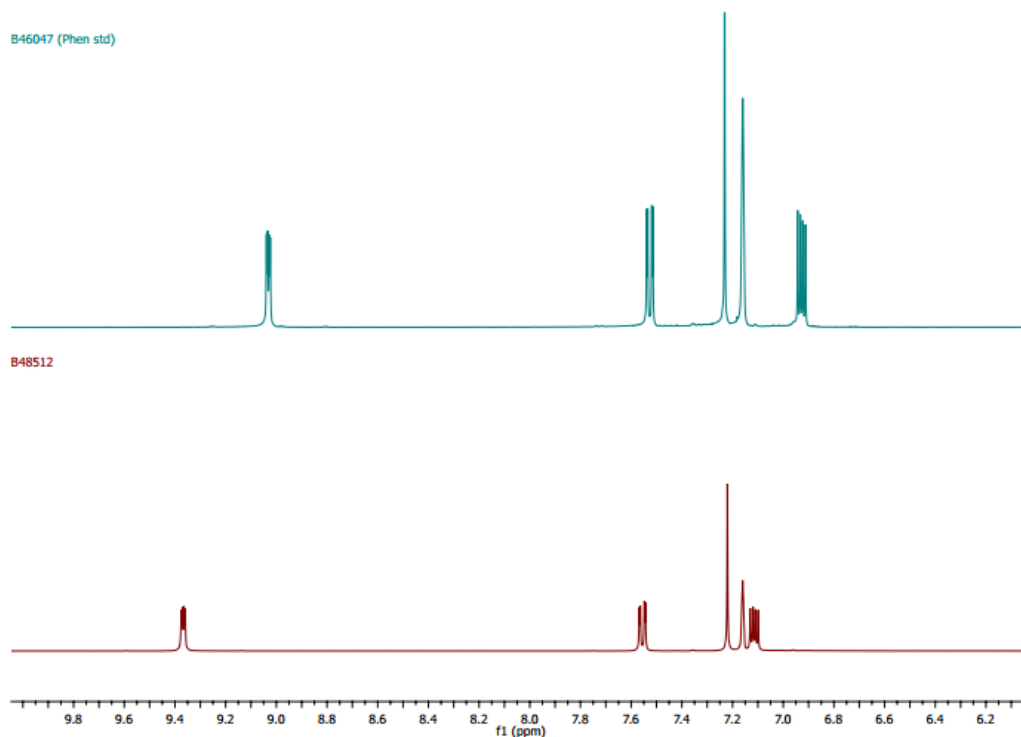


Figure 2.26: Comparative ^1H NMR spectra showing (Top) 1, 10-phenanthroline standard in C_6D_6 and (Bottom) reaction product of sodium naphthenate and 1, 10-phenanthroline in C_6D_6 .

Diffusion ordered spectroscopy or DOSY NMR was then tried. This is a technique exploiting the fact that molecules of different molecular weights will diffuse at different rates in solution. This can then be utilised using calculations to allow for an estimate of the molecular weight of the species in solution, thus providing insight into the structures adopted. The DOSY NMR of the reaction product between 1, 10-phen and sodium naphthenate is shown in Figure 2.27.

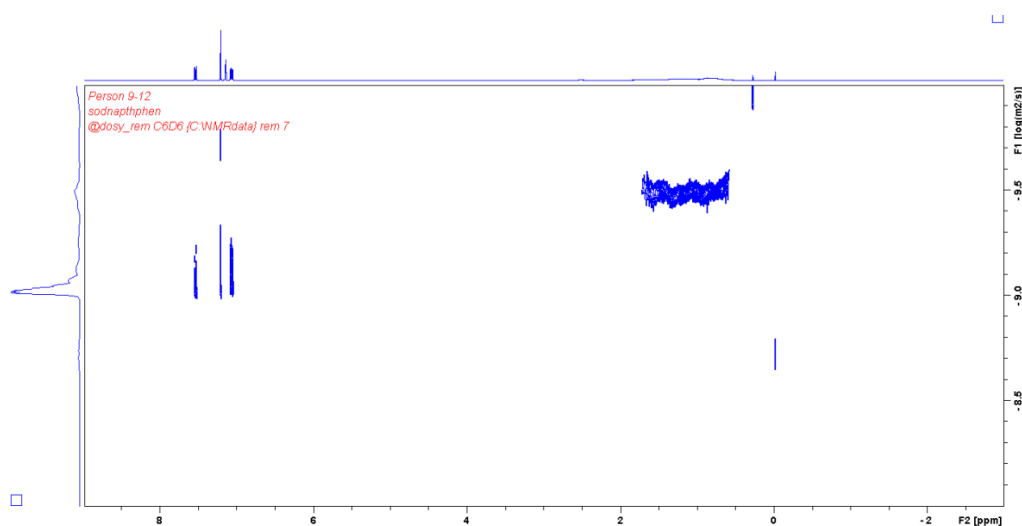


Figure 2.27: ^1H DOSY NMR spectrum of powder formed on reacting sodium naphthenate with 1, 10-phenanthroline.

The diffusion coefficient, the numerical value given to each fragment of different molecular weight is calculated and then entered into software developed by Stalke *et al.*⁹⁰ The diffusion coefficient for the 1, 10-phen fragment was calculated as $9.823 \times 10^{-10} \text{ m}^2/\text{s}$, giving a log value of $-9.0078 \text{ m}^2/\text{s}$. Using the software, in conjunction with the log value of the diffusion coefficient of the TMS internal standard, this gives a predicted molecular weight of 305 g/mol. This is too large to represent an uncoordinated free 1, 10-phen molecule, which would only have a molecular weight of 180.21 g/mol. If the 1, 10-phen was coordinated to a single sodium cation, the molecular weight would increase to 203 g/mol, however this gives an error of -33 %, which would indicate that this is still not the species seen in solution.

When the formula for 1, 10-phen coordinated to a sodium carboxylate species that may be present in sodium naphthenate, namely sodium cyclopentanoate (Figure 2.28), the molecular weight is calculated as 317 g/mol. This gives a much lower error of only 4 %, which is within the limits for the software. Therefore, the DOSY data suggests that there is some sort of coordination between 1, 10-phen and at least one component that may be present within the sodium naphthenate mixture. Looking at the naphthenate fragment, the software predicted a molecular weight far in excess of 3500 g/mol, indicating the complex nature of the sample under investigation, with a forest of molecular species contributing to the overall composition.

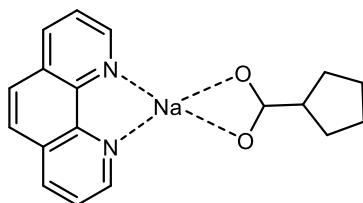


Figure 2.28: Proposed structure of 1, 10-phen-sodium cyclopentanoate complex on the basis of DOSY NMR data.

Endeavours to obtain a more accurate picture of the structure/s of sodium naphthenate itself or a 1,10-phen coordinated complex *via* single crystal X-ray diffraction were made but unfortunately only oils or amorphous solids were ever obtained each time.

We then thought to simplify the sodium naphthenate mixture, to see if any of the components of the overall sample could be separated out and its specific composition established. The first and simplest way of doing this would be through a series of washing experiments, whereby a sample of the sodium naphthenate powder was washed with a solvent that the overall bulk was insoluble in to see if some soluble component could successfully be separated. To this end a sample of sodium naphthenate was washed with a series of solvents ranging from non-polar hexane all the way to acetone. This washing was generally accompanied by a colour change, with the powder turning from yellow to white. This powder was then kept, and the solvent removed from the washings *in vacuo*, with the residue analysed *via* ^1H NMR spectroscopy. All the resultant NMR spectra appeared similar, with the broad set of signals between 0.5 and 2 ppm remaining, with unfortunately very little resolution observed.

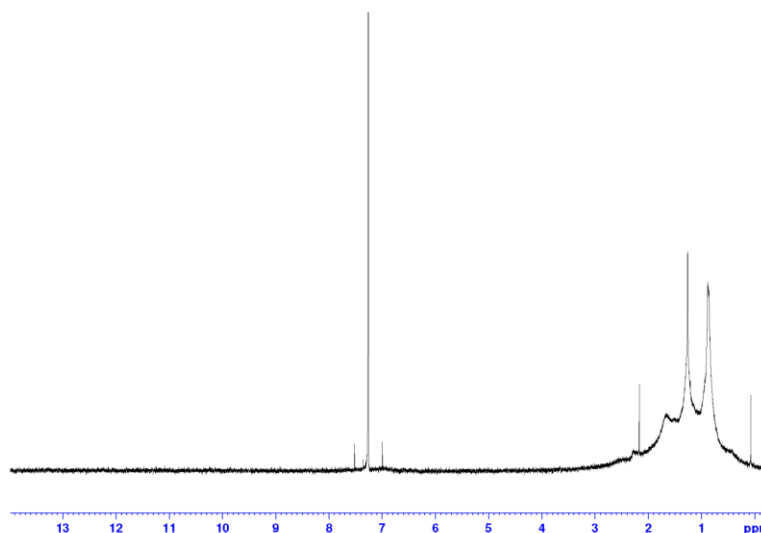


Figure 2.29: ^1H NMR spectrum of the isolated solid from the acetone wash of sodium naphthenate in CDCl_3 .

Another attempt was made to separate the parts of the mixture out chemically *via* exploitation of the common ion effect.¹²⁸ This is an effect that takes advantage of the fact that when a common ion, which is an ion that is already in the solution, is added to a solution the equilibrium shifts and in general the solubility of the species decreases. This process is sometimes referred to as salting out, which is utilised in the production of soap. In this case, NaCl was added to aqueous solutions of sodium naphthenate until a solid began to precipitate out. This was filtered off and the process repeated until several batches of solid had been isolated. Shown in Figure 2.30 are ^1H NMR spectra from the first and third batches of solid produced, which show very little change from either the parent spectra or indeed from each other, meaning that no separation of the various components of the mixture seems possible.

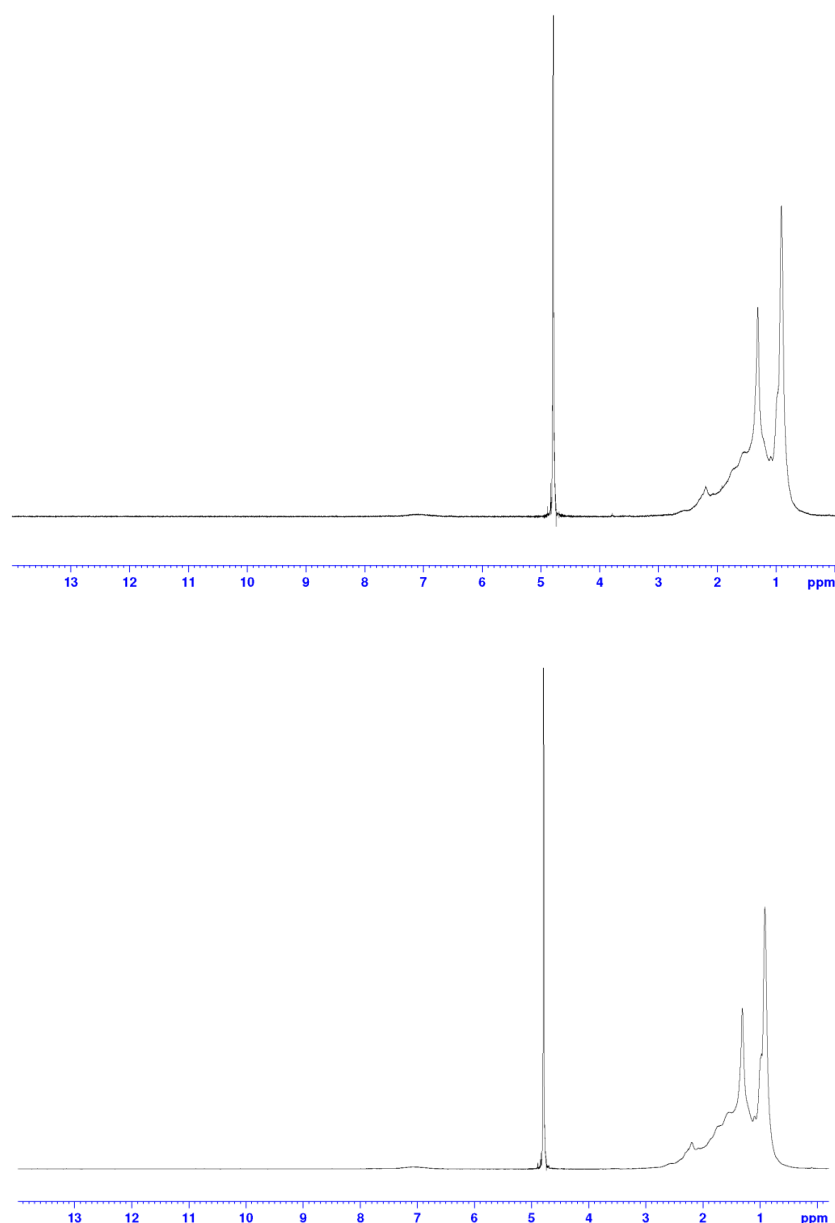


Figure 2.30: (Top) ¹H NMR spectrum of the first batch in CDCl₃ and (Bottom) ¹H NMR spectrum of the third batch in CDCl₃.

Reactivity of sodium naphthenate and DDSA

In order to try to replicate within the laboratory the engine testing carried out in industry, sodium naphthenate and dodecenylsuccinic acid (DDSA) were mixed in various ratios within hexane solvent, with the ratios ranging from an acid : sodium naphthenate ratio of 1:0.5 to 1:3. This is more reminiscent of the sort of testing carried out within fuel companies when

investigating the formation of sodium carboxylates.² Accordingly, sodium naphthenate was suspended in hexane, forming a yellow gelatinous material. DDSA was then added as a xylene-based solution in the appropriate ratio and the mixture left stirring overnight. The solvent was then removed, and the solid left analysed *via* ^1H NMR spectroscopy. Figure 2.31 shows the collated spectra for 0.5, 1 and 1.5 equivalents of sodium naphthenate.

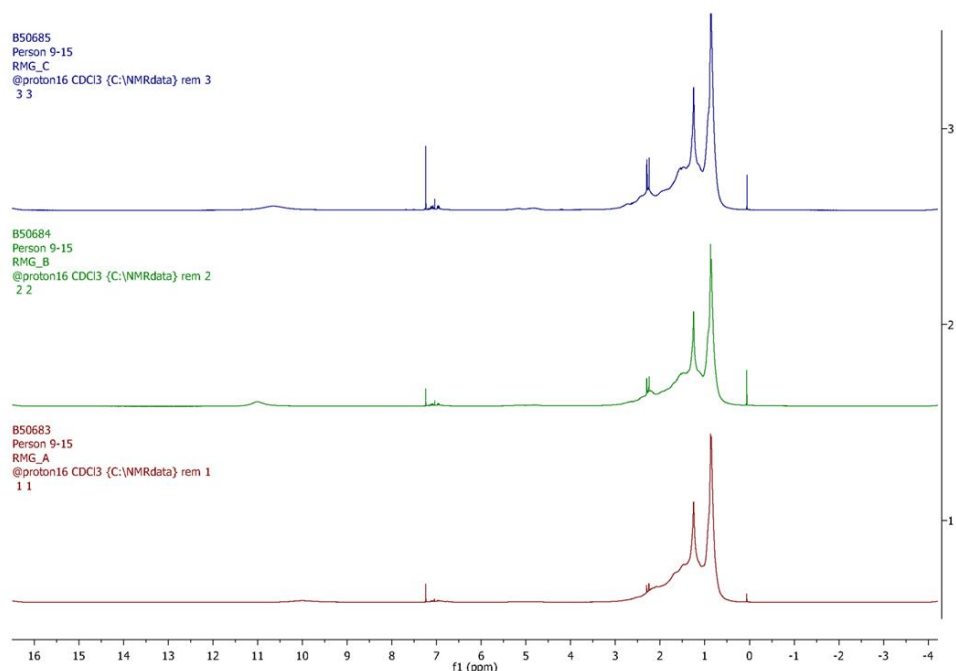


Figure 2.31: Comparative ^1H NMR spectra showing (top) reaction product of DDSA:Sodium naphthenate in a 1:1.5 ratio; (middle) reaction product of DDSA:Sodium naphthenate in a 1:1 ratio and (bottom) reaction product of DDSA:Sodium naphthenate in a 1:0.5 ratio.

It can be seen from the NMR spectra that in all cases the carboxyl proton is still present, though the intensity is much less when the ratio of acid to sodium naphthenate is 1:0.5. This is unsurprising in some respects as each single DDSA molecule will contain two carboxylic acid groups and therefore will need a minimum of two equivalents of sodium naphthenate in order to fully neutralise the acid. Therefore, it would be expected that the carboxyl proton would still be visible given that there will be acid groups that have not been deprotonated by the action of the sodium naphthenate. Figure 2.32 shows the ^1H NMR analysis of reactions involving 2 and 3 equivalents of sodium naphthenate relative to DDSA.

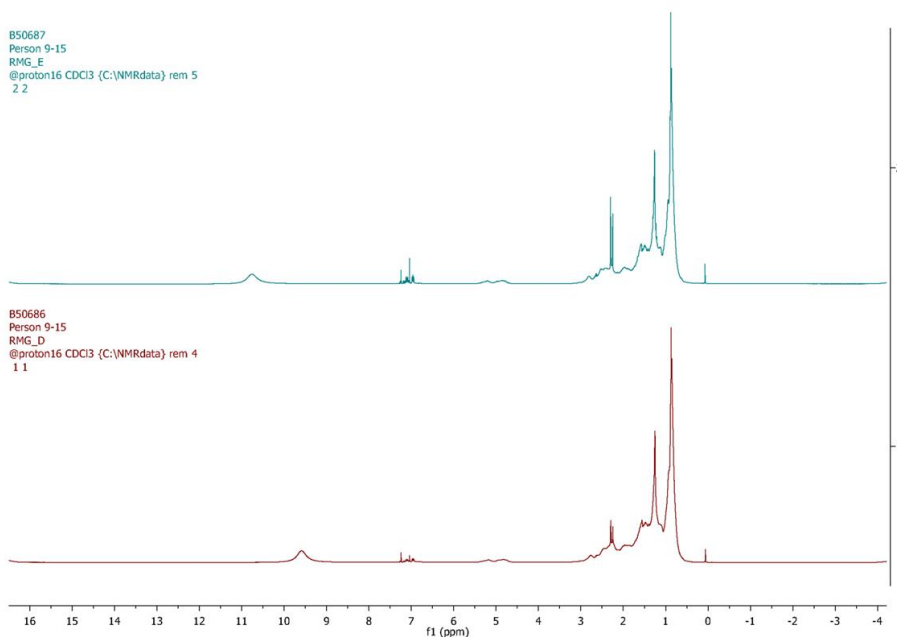


Figure 2.32 Comparative ^1H NMR spectra showing (top) reaction product of DDSA:Sodium naphthenate in a 1:3 ratio and (bottom) reaction product of DDSA:Sodium naphthenate in a 1:2 ratio.

Again, the characteristic resonance of a carboxyl proton is present in both NMR spectra (between 9-10 ppm in both instances), indicating that some acid groups are still present in the residue. The resonances in both instances seem more intense when compared to those seen in Figure 2.31 for the lower ratios, which may indicate the formation of a different acid species present in the sample, perhaps due to the sodium cation transferring from the sodium naphthenate to DDSA, with concomitant formation of naphthenic acid.

Indeed, the major drawback of IR spectroscopic analysis in this instance is that it is impossible to tell if the sodium cation has transferred from the sodium naphthenate to the DDSA or the sodium cation is still bonded to the naphthenate fragment. Both species within the equilibrium are likely to have similar pK_a values given that both are carboxylic acids. This means that, given the similarity between the two values, there is likely to be little thermodynamic driving force for the reaction. Therefore, total transfer of the sodium cation from the sodium naphthenate fragment to DDSA to form a DDSA carboxylate species is unlikely to occur to any great extent, with a constant equilibrium in place, therefore it is impossible to predict with any real certainty where the Na cation is in relation to any of the compounds present.

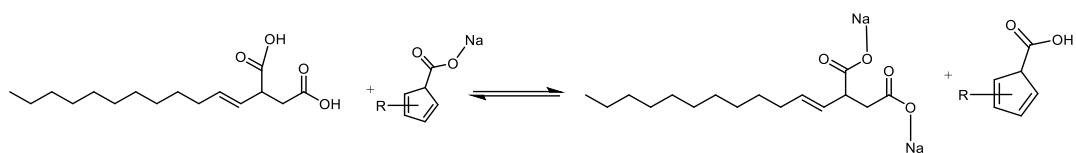


Figure 2.33: Equilibrium formed when DDSA and sodium naphthenate are reacted together.

Part II: Small molecule fixation utilising common molecular architectures

Chapter 3: Introduction

Preface

Small molecule activation, which can lead to the transformation of abundant small molecules typically CO_2 , H_2O , O_2 or N_2 into higher value chemical feedstocks such as methanol in the case of CO_2 , is at the forefront of research in many fields of chemistry. For some groups, the reason for focusing on such a field is a purely academic venture, while others are driven by the prospect of using oxygen and nitrogen as a cheap chemical feedstock for the formation of new C-O or C-N bonds. For all however, the fundamental challenge to be overcome is to transform the reasonably unreactive and usually strong bonds within these small molecules into viable candidates for onward reactions. Of particular attention within this part of the PhD project is CO_2 . This is an attractive molecule to consider activating given the major environmental issues that CO_2 contributes to, with attempts to capture and sequester CO_2 a major focus of many research groups worldwide. There are many ways in which CO_2 can be sequestered, but of interest to us was the fixation of CO_2 using reactive alkali metal complexes, which may provide a route to new molecular architectures in which to store the CO_2 molecule. There are many commonly used alkali metal based reagents that are used every day within synthetic laboratories, many of which possess a reactive alkali metal-nitrogen bond, which would open up the possibility of CO_2 insertion reactions into this bond. Reagents in this category include the 'utility amides' such as lithium diisopropylamide and lithium 2,2,6,6-tetramethylpiperidide as well as lithium β -diketiminato complexes, which have recently begun to emerge as one of the most widely used ligand systems throughout chemistry. In order to provide context for the reasoning behind this research idea, a general introduction to small molecule fixation and β -diketiminato chemistry will now be presented.

3.1 Small molecule fixation chemistry

3.1.1 Fixation of CO₂

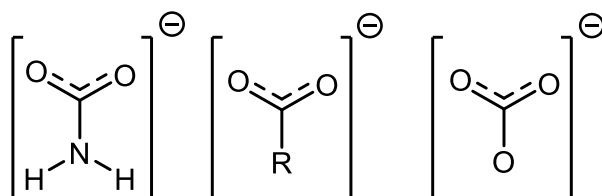
The fixation of CO₂ is a fascinating topic of research for many diverse reasons. Investigations into CO₂ actually date back to the 18th century, when it was shown that CO₂ could be produced upon heating of MgCO₃ or CaCO₃.¹²⁹ In the modern era, one major reason for continued and increased interest in CO₂ chemistry is due to the gas being a major contributor to the so-called greenhouse effect, with the link between increased levels of CO₂ and increased heating at the surface of the earth having been confirmed.¹³⁰ This leads to CO₂ being by far the most well-known environmentally hazardous pollutant, with several countries having signed up to various protocols committing to the reduction of CO₂ levels in the atmosphere. Indeed, with the aforementioned legislation, as well as the scientific consensus that the effects of global warming are now being felt, there is a much higher awareness of environmental issues within the chemical community.¹³¹ There is technology available to remedy the release of CO₂ from anthropogenic sources, divided into three main categories; pre combustion CO₂ capture, post combustion CO₂ capture and oxy-fuel combustion.¹³²

Notwithstanding the environmental issues surrounding CO₂, it is also a vital building block for life on earth, as atmospheric carbon dioxide is the source of available carbon in the carbon cycle.^{133, 134} There is also potential for supercritical CO₂ to be utilised in several ways throughout organic process chemistry, all of which demonstrates the vast scope of CO₂ chemistry.¹³⁵

Despite appearing to be on the surface a relatively simple molecule, the chemistry of CO₂ can be rather complex. Its basic shape is that of a linear, triatomic molecule composed of two terminal oxygen atoms, bonded to a central carbon atom *via* two equivalent, but short, carbon-oxygen double bonds.¹³⁶ Due to the electronegativity difference between carbon and oxygen, there is a partial positive charge on the carbon atom and partial negative charge on the oxygen atoms, allowing CO₂ to behave as both a Lewis acid and a Lewis base, with the molecule exhibiting many of the characteristics of polar species, namely that of an electrophilic carbon and nucleophilic oxygen atom.¹³⁷ Despite this, the linearity of the molecule means that overall it is non-polar.¹³⁸ Activation of the CO₂ molecule is challenging on account of a large kinetic energy barrier.¹³⁹ The LUMO of CO₂ lies very low in energy, much

lower than that of the similar C(O)(S) or CS₂ molecules.¹³⁸ This means that upon reduction, electrons are added to the LUMO, which subsequently becomes more energetically favoured than the HOMO if the molecule is in a bent geometry, hence when CO₂ is coordinated at metal centres a distortion from linearity is almost always seen.¹³⁸

Several classes of compound that occupy a pivotal role within chemistry have a CO₂ fragment within their structure. These include carbamates, carboxylates and carbonates (Scheme 3.0), some of which will be discussed further below.



Scheme 3.0: Selection of anionic species containing a CO₂ fragment.

Nonetheless, there are several methods available in order to utilise CO₂. For example, in nature several enzymes use CO₂ (or the hydrated form HCO₃⁺), to carry out a carboxylation reaction and form a new C-C bond, for example the formation of a carboxylic acid moiety, with a metal cation often being required as a co-factor.¹³⁷ CO₂ can also be utilised in the synthesis of polymers, with its reaction with cyclohexane oxide and a zinc catalyst investigated by Zimmer and Darensbourg.¹⁴⁰

Such reactivity allows for the formation of strongly covalent bonds between the central Lewis acidic carbon atom and a donor atom of a Lewis base, which is the most common method of activation in the literature.¹⁴¹ A rare type of CO₂ activation is that found in CO₂ inclusion complexes, a class of complex where the CO₂ becomes physically adsorbed onto the porous surface of the material. These are comparatively rare due to the CO₂ remaining in a linear non-activated form.¹⁴¹ Metal organic frameworks and porous coordination polymers have been designed to be able to physically adsorb the CO₂ without altering the overall original framework, with one of the first such examples of a CO₂ inclusion complex dating from the 1980s.¹⁴² Development of such frameworks has focussed on producing materials capable of selectively adsorbing CO₂ over other gases, which has advantages in many industries ranging from steel to natural gas mining.¹⁴³

Metal-free inclusion complexes involving CO₂ have also been developed, with a *tert*-butylcalix[4]arene (tBC) complex capable of absorbing either one or two molecules of CO₂ to

form ($t\text{BC} \cdot \text{CO}_2$).¹⁴⁴ If one molecule of CO_2 is adsorbed, it resides within the central cavity of the structure, while the second molecule if present lies in the space between the arene molecules. This complex was also found to lose its second molecule of CO_2 over time.¹⁴⁴

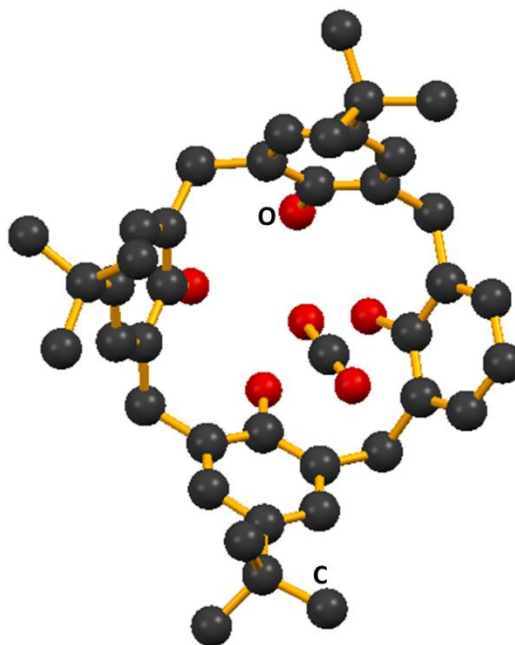
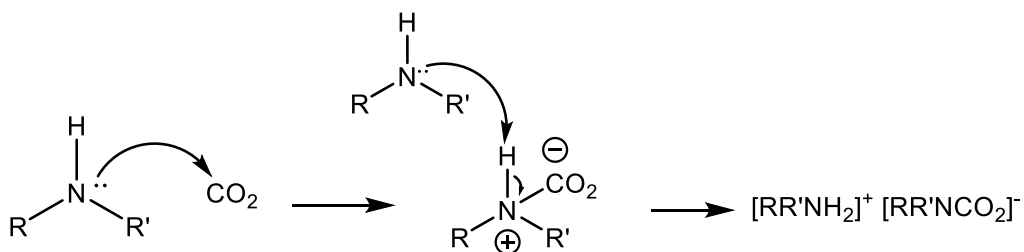


Figure 3.0: Molecular structure of ($t\text{BC} \cdot \text{CO}_2$), showing one linear CO_2 molecule adsorbed in the central cavity, with hydrogen atoms omitted for clarity.

Other groups have captured CO_2 using amines, resulting in the formation of carbamate species, a reaction that has been known for several decades.¹⁴⁵ This reaction proceeds with initial formation of a zwitterionic carbamate. However, this is unstable and a rapid proton transfer occurs, generally to a second equivalent of amine.¹⁴¹ In industry the standard amine used for CO_2 capture is monoethanolamine, $\text{H}_2\text{N}(\text{CH}_2)_2\text{OH}$ (MEA), which generates a discrete cation-anion pair upon reaction with CO_2 .¹⁴¹



Scheme 3.1: Reaction of an amine with carbon dioxide, followed by proton transfer from a second amine equivalent to form a discrete carbamate salt.

An alternative to MEA has recently been developed, namely 2-amino-2-methyl-1-propanol, $(\text{CH}_3)_2\text{C}(\text{NH}_2)\text{CH}_2\text{OH}$ (AMP).¹⁴¹ The crystal structure of the CO_2 derived carbamate salt of this amine was elucidated in 2010.¹⁴⁶ It has been suggested by the researchers behind this work that AMP may prove to be a superior amine for use in CO_2 capture, as theoretical calculations have shown the AMP-carbamate CO_2 bond is weaker than the MEA-carbamate CO_2 bond, thus the energy needed to release the captured CO_2 would be less for AMP, which is an industrial cost advantage.¹⁴⁶

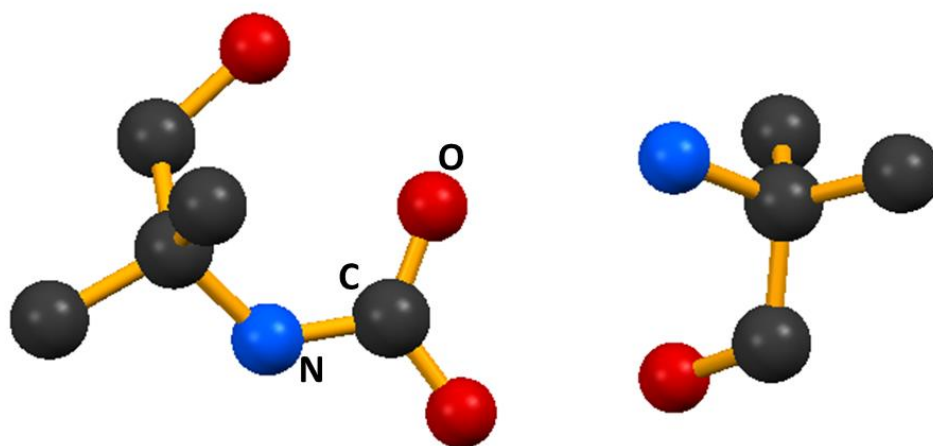
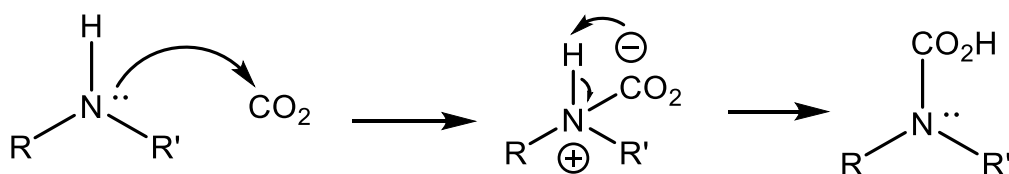


Figure 3.1: Structure of AMP-carbamate ion pair with hydrogen atoms omitted for clarity.

It is rare to find a carbamic acid species that forms *via* proton transfer to the carbamate group formed when CO_2 is inserted. Such carbamic acids are unstable towards hydrolysis, with only a few select cases where they have been isolated and characterised.^{147, 148}

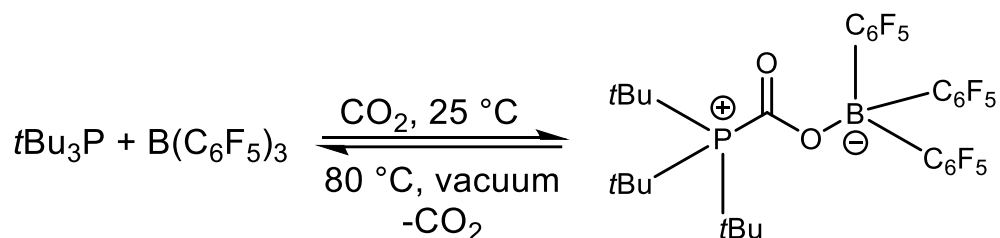


Scheme 3.2: General reaction of an amine with carbon dioxide, followed by proton transfer to generate a carbamic acid.

The final main class of CO_2 activated products are carbamate and carboxylate complexes. Carbamate complexes are formed through the formal addition of CO_2 to a bond between nitrogen and usually a metal atom.¹⁴¹ The most common metal used in this regard is

magnesium, resulting in the formation of magnesium-carbamate complexes, which provide a model for magnesium containing enzymes that are capable of biologically fixing CO₂.¹⁴⁹ Other metals studied include Li and Al, as well as the semi-metal B, all of which form polynuclear carbamate complexes containing multiple oxygen-element bonds.¹⁵⁰⁻¹⁵³ Further examples include Cu, Zn and Sn, with more than one carbamate ligand bound to the central metal in these cases.^{154, 155}

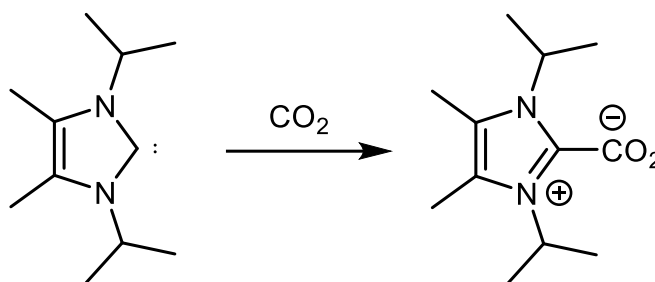
CO₂ activation is also important in the emerging field of frustrated Lewis pairs or FLPs, with the successful activation of CO₂ being one of the ‘tests’ performed to assess potential FLP activity.¹⁴¹ Given the plethora of Lewis acid/Lewis base combinations available, there are vast numbers of FLP systems that may be capable of activating CO₂. In terms of Lewis bases, phosphines, amines and carbenes have been used, with the Lewis acids of choice typically being alanes or boranes.¹⁴¹ In some cases, the adducts formed not only activate and bind the CO₂, but do so in an irreversible manner, with this stability playing an important role in any subsequent reactivity at the CO₂ centre, as this is accomplished without the release of CO₂, allowing for its reduction to carbon monoxide or methanol.^{156, 157} The irreversibility of the CO₂ binding is well illustrated using borane FLPs, with many of the adducts requiring forcing conditions such as heating under a vacuum in order to release the CO₂, such as the now classical system developed by Stephan and Erker (Equation 3.0).¹⁵⁸



Equation 3.0: Example showing complexation of CO₂ using an FLP system.

Another class of compound able to activate CO₂ is that of *N*-heterocyclic carbenes (NHCs). These reactive species, first isolated in a stable crystalline form by Arduengo and co-workers in 1991,¹⁵⁹ form adducts with CO₂ that have very small bond dissociation energies. For example, it was as recently as 1999 that the first NHC-carboxylate prepared through CO₂

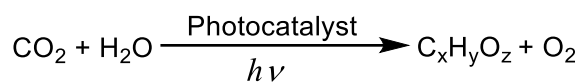
activation was isolated and characterised, the product of the reaction between 2,3-dihydro-1,3-diisopropyl-4,5-dimethylimidazol-2-ylidene and CO₂.



Equation 3.1: Synthesis of the first isolated NHC-carboxylate.

Further use of these complexes as ligands proved to be limited, so efforts focussed on understanding the nature of the newly formed C-C bond. Indeed, Duong *et al.* in their study found that the C-C bond is relatively weak, with CO₂ binding being reversible under certain conditions, an important consideration in the field of NHC and ionic liquid research.¹⁶⁰

Another way in which CO₂ can be activated is over catalyst surfaces. In these systems the CO₂ molecule is generally distorted in some way, either in terms of geometry, in that it is taken from a linear conformation to one that is bent, or in terms of transferring an electron to the CO₂ molecule, thus transforming it to a radical anion, which has been identified as a key intermediate in many of the catalytic processes used.¹⁶¹ One such process is activation through metal sites. Here the metal transfers an electron to the CO₂ molecule to form CO₂^{•-}. Interestingly it was found that the presence of alkali metals on the metal site had a beneficial effect on the transformation of the CO₂, with the presence of potassium decreasing the binding energy of the absorbed CO₂ and promoting the formation of carbamate anions.¹⁶² The species formed on the metal surface are key intermediates in the production of carbon monoxide, methane and methanol from CO₂, which is of course the ultimate goal of small molecule activation chemistry.¹⁶¹ Alternative routes that still involve the interaction between CO₂ and a surface include photocatalytic activation, which essentially attempts to create artificial photosynthesis. This is a promising avenue of research for its ability to take CO₂ and convert it using a source of protons (generally water given its abundance on earth) and a photocatalyst, which harvests the light and converts it to chemical energy, which in turn activates the CO₂ and transforms it into valuable chemicals.¹⁶¹



Equation 3.2: General reaction carried out in artificial photosynthesis.

Despite the potential of such artificial photosynthesis systems, their efficiency remains low, with problems to be overcome including maximising light utilisation, aid in charge separation and migration as well as reduce the electron-hole recombination that takes place.¹⁶¹

CO₂ has also been shown to be activated by electroinduction using *aza*-macrocyclic ligands, which are generally bifunctional compounds that possess both nucleophilic and electrophilic sites, allowing the reversible carrying of the CO₂ molecule.¹⁶³ Such examples are well known for Cu(II) complexes, leading to the characterisation of a binuclear μ -carbonato complex.¹⁶⁴

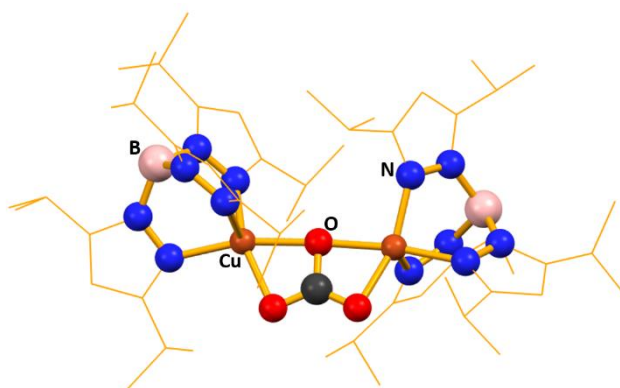


Figure 3.2: Molecular structure of Cu carbonato complex, with organic fragments apart from central carbonato carbon represented as wireframe for clarity.

Despite this plethora of research into CO₂, few studies have considered its insertion into reactive metal-nitrogen bonds. This is perhaps surprising given the ease with which CO₂ can be handled within the laboratory. Such insertion reactions that provide access to carbamate functionalities may not only deliver a route to effective CO₂ capture technologies,¹⁴¹ but also may be utilised in diverse fields ranging from the industrial synthesis of isocyanates to uses in agricultural chemistry.¹⁶⁵ It would also allow for synthesis of carbamic acid derivatives without the use of the toxic gas phosgene.¹³⁷

Previous work has examined the insertion of CO₂ into aluminium-nitrogen¹⁶⁶ and magnesium-nitrogen bonds.¹⁶⁷ The insertion of CO₂ into the reactive Al-N bond has been known since the late 1990s when (TMP)₂AlMe was reacted with CO₂ to form [MeAl(O₂CTMP)₂]₂.¹⁶⁸ This

complex contained two eight-membered $(\text{AlO}_2)_2$ rings, connected *via* a five-coordinate aluminium.¹⁶⁸

The group of Paine *et al.* investigated the chemistry of CO_2 insertion into $\text{TMP}_2\text{AlP}(\text{SiMe}_3)_2$, anticipating that insertion reaction would occur at either the Al-P bond or the Al-N bond, with the possibility of the CO_2 inserting into both.¹⁶⁶ To their surprise, they found that the CO_2 only inserted into the Al-P bond, with the Al-N bond remaining intact.¹⁶⁶

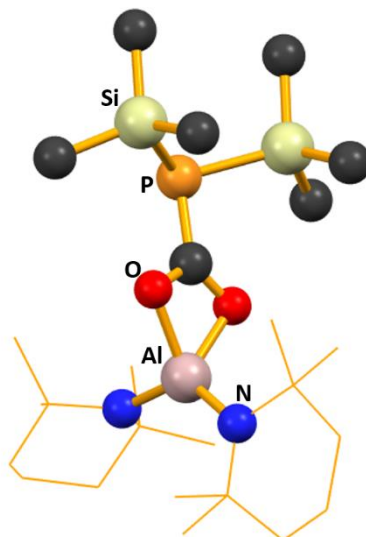


Figure 3.3: Molecular structure of $\text{TMP}_2\text{Al}(\text{O}_2\text{C})\text{P}(\text{SiMe}_3)_2$, with organic TMP fragment drawn as wireframe for clarity.

In terms of insertion into the Mg-N bond, the group of Chang *et al.* recently investigated the reaction between CO_2 and the bisamide $\text{Mg}(\text{N}^i\text{Pr}_2)_2$, discovering that two separate products formed, dependent on the recrystallisation solvent conditions.¹⁶⁷ Using $\text{Mg}(\text{N}^i\text{Pr}_2)_2$ in THF and bubbling through CO_2 for five minutes, a colour change was observed which resulted in the formation of $[\text{Mg}_6(\mu_4\text{-O})(\text{O}_2\text{CN}^i\text{Pr}_2)_{10}]$, containing hexanuclear assemblies of Mg atoms linked by bridging oxo and diisopropylcarbamato groups.¹⁶⁷ However, upon extending the period of CO_2 addition to 30 minutes and recrystallizing from HMPA/toluene, a different product, $[\text{Mg}_5(\mu_5\eta^6\text{-CO}_3)(\text{O}_2\text{CN}^i\text{Pr}_2)_8(\text{HMPA})_2]$, was isolated.¹⁶⁷ This features a pentanuclear Mg assembly linked by oxo and diisopropylcarbamato bridges.¹⁶⁷

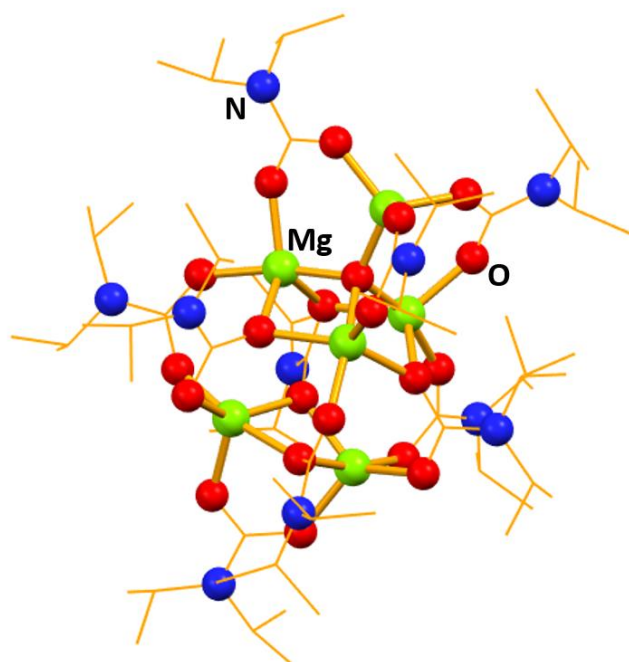


Figure 3.4: Molecular structure of the magnesium hexamer $[\text{Mg}_6(\mu_4\text{-O})(\text{O}_2\text{CN}^i\text{Pr}_2)_{10}]$, with the organic fragment drawn as wireframe for clarity.

3.2 β -diketiminate chemistry

The first β -diketimines were synthesised in the 1950s however it was not until the late 1990s that such ligands began to be explored by synthetic chemists in more depth.¹⁶⁹⁻¹⁷¹ The name β -diketimines refers to a class of anionic bidentate ligands formulated as $[\text{ArN}(\text{H})\text{C}(\text{R})\text{CHC}(\text{R})\text{NAr}]$; where Ar are aryl groups and R is an organic fragment such as a CH_3 group. They are commonly abbreviated to 'NacNac' or 'NacNac(H)', which is derived from their similarity to 1,3-diketones or Acac (ACetylAcetone) compounds. Where Acac compounds contain oxygen atoms, the corresponding NacNac compound contains nitrogen atoms and other R groups as shown below.

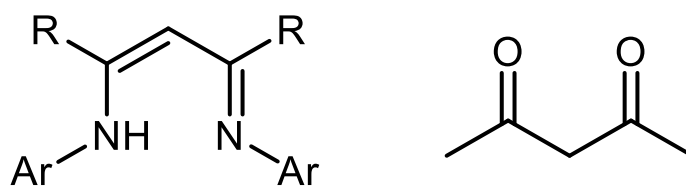
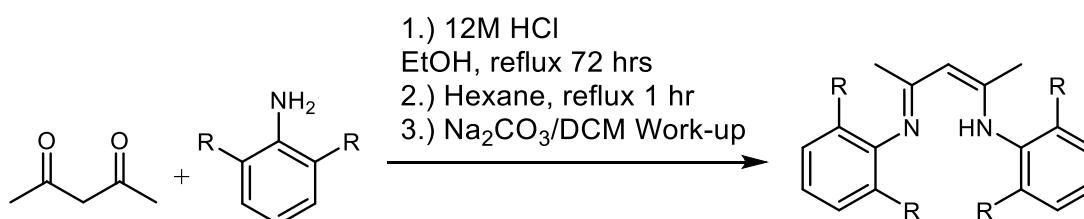


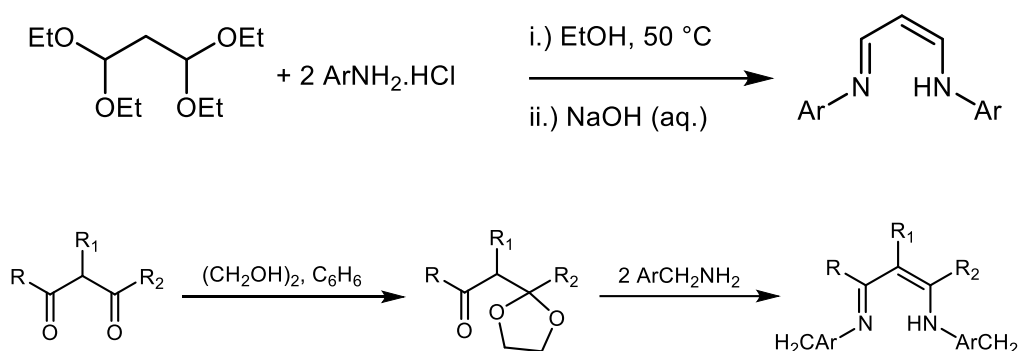
Figure 3.5: General comparison between (LHS) NacNac and (RHS) Acac ligands.

The parent NacNac(H) ligand can be easily synthesised through an acid catalysed condensation reaction between an amine and a β -diketone (Equation 3.3).¹⁷²



Equation 3.3: General synthesis of NacNac(H) ligands *via* acid-catalysed condensation.

There are other methods that have been used previously to synthesise NacNac ligands. For example it is possible to treat a β -diacetal with an aromatic amine hydrochloride salt in hot ethanol, followed by work up with sodium hydroxide to produce the NacNac ligand.¹⁷³ Another alternative synthesis involves the conversion of 1,3-diketone starting material to the NacNac scaffold *via* an intermediate ketoketal.¹⁷⁴



Scheme 3.3: Alternative synthesis of NacNac(H) ligands.

One reason why NacNac(H) ligands are ubiquitous within chemistry is that they can produce unique coordination environments as well as acting as bulky spectator ligands to stabilise reactive metals through bidentate coordination of the nitrogen atoms of the NacNac ligand.¹⁷⁰ NacNac ligands can accomplish this through the vast scope for variation in the bulk of their architecture. For example, by adapting the basic NacNac framework *via* different pendant groups, various steric and electronic properties can be tuned to whatever system is required for the specific metal. Figure 3.6 shows how variation can be imparted on the NacNac architecture at the substituent positions R_1 to R_3 .

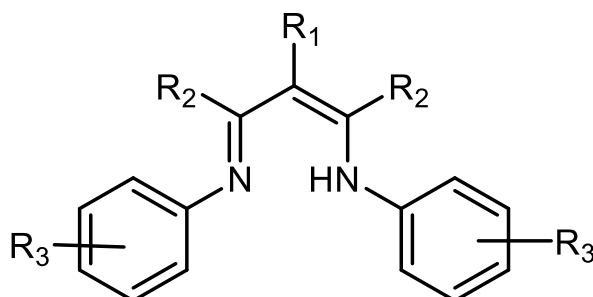


Figure 3.6: Schematic showing the variation that can be imparted on the NacNac ligand at positions R_1 to R_3 .

Steric properties of the NacNac are mostly affected by changing the groups at the R_2 and R_3 positions. R_3 substituents commonly face towards the metal and thus provide most of the steric shielding. The effect of R_2 substituents in terms of steric factors can be to push the R_3 substituents further towards the metal centre, with common substituents in this R_2 position including methyl-, *t*-butyl and phenyl-systems. As the substituent size increases this effect becomes more pronounced, pushing the metal centre deeper into the binding pocket of the NacNac. The electronic properties can be strongly influenced by the R_1 and R_2 substituents

with smaller effects from the R_3 substituents, unless no *ortho*-substituents are present and the aryl ring rotates to become planar with the backbone. These effects cause a change in the electron density at the metal centre, which in turn leads to changes in IR, UV and NMR spectra.¹⁷⁵ For example, the more electron-withdrawing groups present then the lower field the NMR resonances are and the lower the backbonding to the ligand.¹⁷⁵ The position that mostly affects the electronic properties is R_1 , with most ligands having a proton as the substituent here, though there are exceptions where electron-donating groups such as alkyls or electron-withdrawing groups such as trifluoromethyl are present.^{169, 176}

A popular NacNac ligand is formulated as $\text{Dipp}_2\text{NacNac(H)}$, where Dipp is 2,6-diisopropylphenyl, $2,6\text{-}^i\text{Pr}_2\text{C}_6\text{H}_3$. This ligand has played a prominent part in the development of NacNac chemistry since it is convenient to make on a multi-gram scale and it can efficiently stabilise a broad portfolio of different metals.¹⁷² One system showing the remarkable ability of the NacNac ligand to stabilise metals was synthesised by Roesky *et al.* in 2000, which was a monomeric aluminium(I) compound, which was considered as a stable analogue of a carbene.¹⁷⁷ The steric bulk of the NacNac ligand proves to be vital here as it provides kinetic protection to the aluminium centre, preventing disproportionation to Al(III) and Al(0) species as well as giving thermal stability up to 150 °C. In terms of reactivity, this species exhibits amphiphilic behaviour, acting as both a Lewis acid and a Lewis base due to it possessing both electrophilic and nucleophilic character.¹⁷⁷

A description of some of the organometallic chemistry of $\text{Dipp}_2\text{NacNac(H)}$, and other related NacNac ligands will now be given.

3.2.1 β -diketiminates in organometallic chemistry

Lithium NacNac complexes are widely used as the most important NacNac transfer agents,¹⁷² allowing for the synthesis of different metal NacNac systems through salt metathesis approaches. It is remarkable given their synthetic importance that it was not until 1994 that the first synthetically characterised crystalline lithium NacNac species was reported.¹⁷⁸ In this case the lithiating agent was LiR [where $\text{R} = \text{CH}(\text{SiMe}_3)_2$]. However, the majority of lithium NacNac species are synthesised using the parent NacNac(H) ligand and $^n\text{BuLi}$.¹⁶⁹ This results in the removal of the acidic NH hydrogen atom and the formation of the desired LiNacNac species, with concomitant elimination of butane gas. An interesting example of a more unusual reaction product was seen in the lithiation of malonaldehyde bis(phenylimine)

monohydrochloride using two equivalents of $t\text{BuLi}$ to dimetallate the parent hydrochloride salt in the presence of the strong donor molecule hexamethylphosphorictriamide (HMPA).¹⁷⁹ Following the lithiation, the LiNacNac product dimerises through HMPA oxygen bridges.

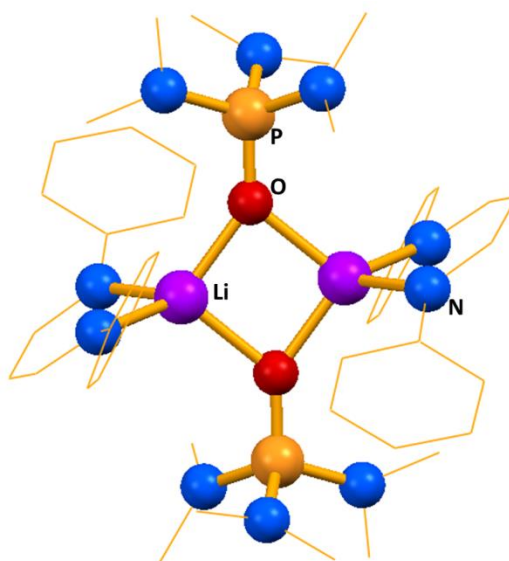


Figure 3.7: Molecular structure of dimeric malonaldehyde bis(phenylimine) based complex with hydrogen atoms omitted and organic fragments drawn as wireframe for clarity.

As previously mentioned, lithium NacNac species are widely used as NacNac ligand transfer agents, generally *via* reaction with metal chlorides.¹⁶⁹ Of these ligand types, the $\text{Dipp}_2\text{NacNacLi}$ complex is the most utilised transfer agent.¹⁷² Their importance inspired efforts to establish the structures of these key intermediates in common solvents such as hexane, THF and diethyl ether. The crystal structures of the THF and Et_2O solvates are shown in Figure 3.8. Both have similar geometric parameters so only a brief description will be given.

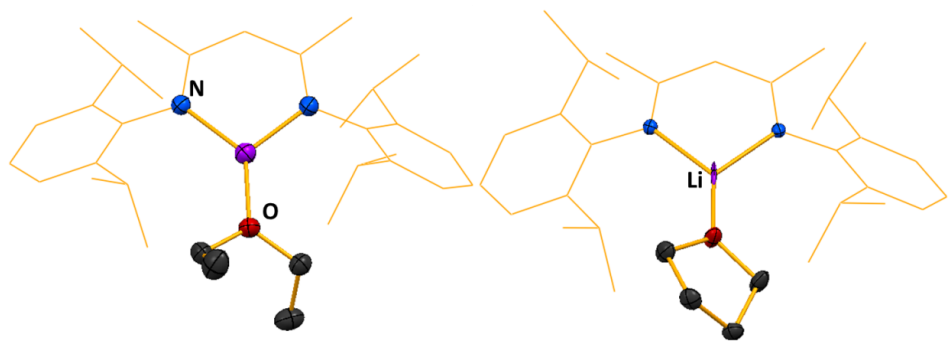


Figure 3.8: Molecular structure of (LHS) $\text{LiNacNac.Et}_2\text{O}$ and (RHS) LiNacNac.THF , with hydrogen atoms omitted and the NacNac scaffold shown as wire frame for clarity. Thermal ellipsoids are displayed at 40% probability level.

In both cases deprotonation does not affect the C_3N_2 planar ring, which remains intact, but within the six-membered C_3N_2Li ring, C-C and C-N bonds become more symmetrical in length, indicating π -bonding delocalisation within the system. Unsurprisingly, the NacNac ligand itself does not see any major geometric changes going from Et_2O solvation to THF solvation, with the only minor distinction being that of Li-O bond lengths, which are shorter by about 0.12 Å in the THF case.¹⁷² This is indicative of the greater donor strength of THF in comparison to Et_2O , which increases the electron density at the lithium centre and subsequently leads to a weaker Li-N interaction, which is borne out experimentally.¹⁷²

When no donor solvent is present, $LiNacNac$ adopts two possible arrangements in the solid state, where $n = 2$ or 12 in $(Dipp_2NacNacLi)_n$ (Figure 3.9). In $(Dipp_2NacNacLi)_2$, there is only slight perturbation from planarity in the C_3N_2Li ring, with few other structural features significantly different from either the THF or Et_2O solvate. The dimerisation comes about *via* long interactions between the lithium cation of one unit and one of the carbons within the Dipp ring of another unit.¹⁷² This mode of dimerisation differs significantly from those of two previously seen examples, in $[{(Me_3N)_3PO}Li\{(Ph)NCH\}]_2$ and $[{(Me_3Si)N(Ph)CH}_2CH)Li]_2$.^{178, 179} In the former it is the NacNac nitrogen atoms that lead to the dimerisation, while the latter has oxygen bridges (Figure 3.7) to form a Li_2O_2 central core. From the same hexane solvent, the complex may also crystallise as a dodecameric $(Dipp_2NacNacLi)_{12}$ variant. This ladder-type complex is formed *via* interactions between Li and C centres from adjacent molecules. The differences between these Li-C interactions arise from the different modes of coordination. In $(Dipp_2NacNacLi)_2$, the interaction is described as ‘face-to-face’, where the lithium cations interact with the front face of the NacNac, while in $(Dipp_2NacNacLi)_{12}$ the interactions are at the back end of the aryl rings, which leads to less steric crowding and hence higher aggregation.¹⁷²

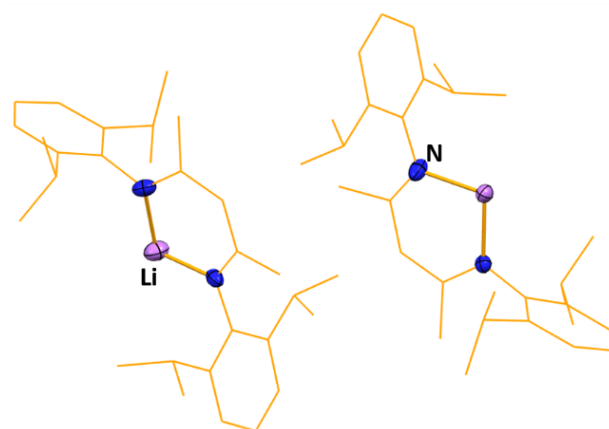


Figure 3.9: Molecular structure of (Dipp₂NacNaLi)₂ with hydrogen atoms omitted and the NacNac scaffold shown as wire frame for clarity. Thermal ellipsoids are displayed at 40% probability level.

Though LiNacNac complexes are used widely as transfer agents, it was noted in a review by Lappert that it can actually be more practical to use the heavier sodium and potassium analogues as transfer agents, as the heavier NaCl and KCl salt by-products of these reactions are easier to separate from reaction solutions than LiCl.¹⁶⁹ Searching through the literature, there is a paucity of research focusing on crystalline examples of sodium NacNac complexes, with the only mentioned example consisting of unpublished work by Lappert *et al.* of the type [NacNacNa(THF)₂], though no evidence of this species could be seen within the CSD.¹⁶⁹ There has been slightly more research carried out on potassium NacNac species, especially with regard to the solid state structures. In 1998, Mair and co-workers isolated an example of KNacNac toluene solvate, but they noted that while a toluene molecule was present “in this instance the toluene remained uncoordinated”.¹⁸⁰

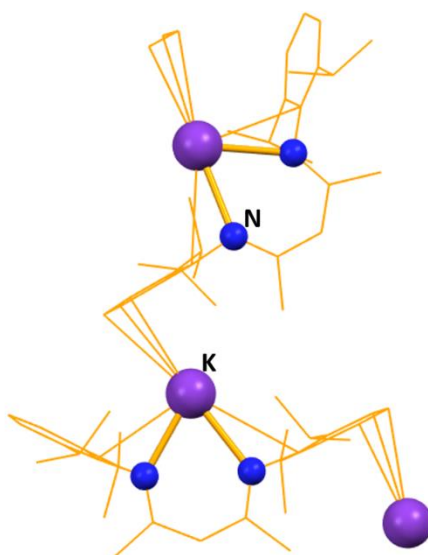


Figure 3.10: Molecular structure of KNacNac toluene solvate with hydrogen atoms omitted and organic fragments drawn as wireframe for clarity, showing the η^5 coordination.

This molecule is essentially monomeric in nature, however a weak η^5 coordination between the potassium cation and 2,6-diisopropylphenyl groups is visible, leading to a pseudo 1-D polymeric zig-zag structure.¹⁸⁰ It has been noted that such weak ligation may have an important role to play in biochemistry, in particular in the field of potassium ion selectivity within cells.¹⁸¹ Almost a decade later, Hill and co-workers crystallised a solvent-free variant from hexane solution.¹¹³ Again, the structure was found to consist of a chain of monomers held together by weak intermolecular interactions between the aryl rings and potassium cations, with the structural parameters essentially identical to that crystallised by Mair *et al.*¹¹³

Moving on to group two examples, the most prevalent of these metals used in NacNac chemistry is magnesium. NacNac ligands have been a key factor in the expansion of magnesium chemistry from the dominate +2 oxidation state to the more unusual low valent magnesium compounds featuring Mg(I). Prior to the utilisation of NacNac ligands, the only evidence for such low valent magnesium compounds was found in certain magnesium containing bimetallic hydrides such as Mg_3RuH_3 and Mg_4IrH_5 .¹⁸² The evidence for this was that these crystalline compounds contained relatively short Mg-Mg distances, suggesting the presence of a bond between them.¹⁸² It was not until 2007 that the first stable examples of such low valent Mg compounds were successfully isolated and synthesised, stabilised by utilising NacNac ligands.^{183, 184} This was achieved by reducing Mg(II) iodide NacNac complexes

with potassium metal in toluene, with the products taking the form L_2Mg_2 , where L was the bulky monoanionic NacNac ligand.¹⁸⁴ It was noted that while the products were air- and moisture-sensitive they were thermally stable up to 300 °C. The Mg centres in the complex are distorted trigonal planar, with a Mg-Mg bond length of 2.8457(8) Å, within the range for calculated Mg-Mg bond distances.¹⁸³ The Mg-N bond distances are also longer than those seen in complexes where NacNac ligands coordinate to Mg(II) centres, another indication of the presence of Mg(I).¹⁸³ Recent advances by Jones and co-workers have shown that it is possible to synthesise these Mg(I) compounds in multigram scale utilising alkali metals supported on alkali metal chlorides as the reducing agents.¹⁸⁵

These Mg(I) dimers proved not only interesting structures from a scientific curiosity perspective, but also due to their potentially interesting reactivity. Initially they were studied as reducing agents, with several properties making them an attractive prospect in this regard such as their striking thermal stability and solubility in a wide range of solvents.¹⁸⁴ Magnesium based reagents have been utilised as reducing agents for many decades. For example, Grignard reagents have been used in many countless synthetic transformations¹⁸⁶ and while not conventionally thought of as reducing agents, some of these transformations are thought to occur *via* a single electron transfer from the organomagnesium compound to the substrate in question, as for example in the pinacol coupling of ketones.¹⁸⁴

Of particular note within the magnesium-based examples of NacNac compounds are NacNacMgⁿBu, synthesised and used in insertion and catalytic reactions by Hill *et al.*^{187, 188} and NacNacMgTMP, first synthesised by Hevia *et al.* in 2013.¹⁸⁹ The former has been shown to be an excellent catalyst for hydroboration of carbodiimides,¹⁸⁷ while the latter has been utilised in C-H activation and deprotonation reactions.¹⁹⁰ The TMP example (Figure 3.11) is the first characterised example of a NacNac based complex of any metal containing the commonly used TMP moiety.¹⁸⁹ The magnesium centre in NacNacMgTMP is distorted trigonal planar, coordinated to two nitrogen atoms from the NacNac ligand and one from the TMP. The large steric demand of TMP can be quantified by the various bond angles subtended at the magnesium centre, with those involving the TMP ligand much more obtuse when compared to the angle of the NacNac ligand [131.18(5)° and 134.97(5)° for TMP vs 93.85(5)° for the NacNac ligand].

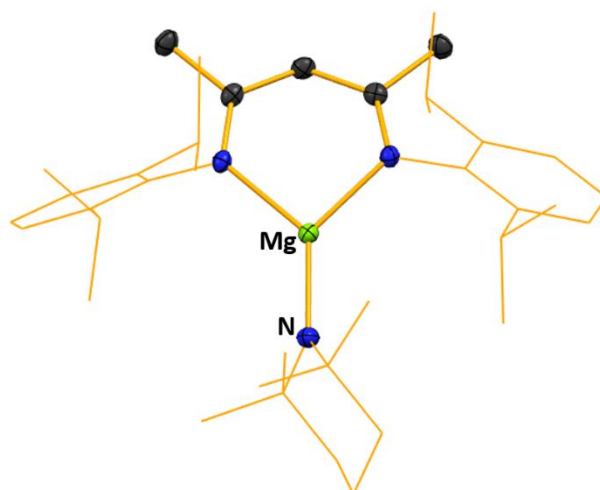


Figure 3.11: Molecular structure of NacNacMgTMP with hydrogen atoms omitted and organic fragments drawn as wireframe for clarity. Thermal ellipsoids set at 40 % probability level.

The development of such group 2 based catalysts has developed at a rapid pace over the previous decade, with examples from Hill, Harder, and Crimmin at the forefront of this development.¹⁹¹⁻¹⁹³ Hill and co-workers in particular have advanced the uses of magnesium NacNac complexes in the field of hydroboration, with recent contributions showcasing the ability of such complexes to catalyse the hydroboration of a range of substrates under mild conditions and in good yields.^{187, 194, 195} The TMP complex (Figure 3.11) can complement the reactivity of NacNacMgⁿBu or display variation. For example, Hevia and co-workers have shown that both NacNacMgⁿBu and NacNacMgTMP are capable of deprotonating benzoxazole to give the same magnesiated and ring-opened product.¹⁸⁹ However, extending the reactivity to *N*-methyl benzimidazole resulted in different products depending on which NacNac complex was employed. If NacNacMgTMP is used, a direct magnesiation results, with the deprotonated benzimidazole bridging between two MgNacNac centres. In contrast, carrying out the same reaction with NacNacMgⁿBu does not lead to this product, even under forcing reflux conditions. Instead, a substitution product, where the solvating THF in NacNacMgⁿBu is replaced by a molecule of non-deprotonated *N*-methyl benzimidazole, results.¹⁸⁹ This shows the variation of reactivity possible simply by varying what is bonded to the MgNacNac architecture and that whereas a Bu ligand is stronger than TMP in conventional alkali metal chemistry, it seems reversed in this Mg NacNac system.

Considering group 2 NacNac ligands that have been not only crystallographically characterised but show potential as catalysts in several areas, the recent advances by the Harder group have proved to be among some of the most promising. For example, in contrast to the ‘solvated’ examples of MgNacNac complexes described above, in 2018 Harder *et al.* described Lewis base free NacNac complexes of both Mg and Ca, with the Mg example showing particularly strong Lewis acidity.¹⁹⁶ While the magnesium centre is ‘naked’ in that it is not coordinated to anything other than a NacNac ligand, the crystal structure was isolated as a $B(C_6F_5)_4^-$ salt.¹⁹⁶ Reaction of this salt with 3-hexyne gave a crystalline complex, with a η^1 -bonded $B(C_6F_5)_4^-$ anion and the alkyne asymmetrically bonded to the Mg, in a practical demonstration of the complexes high Lewis acidity.¹⁹⁶

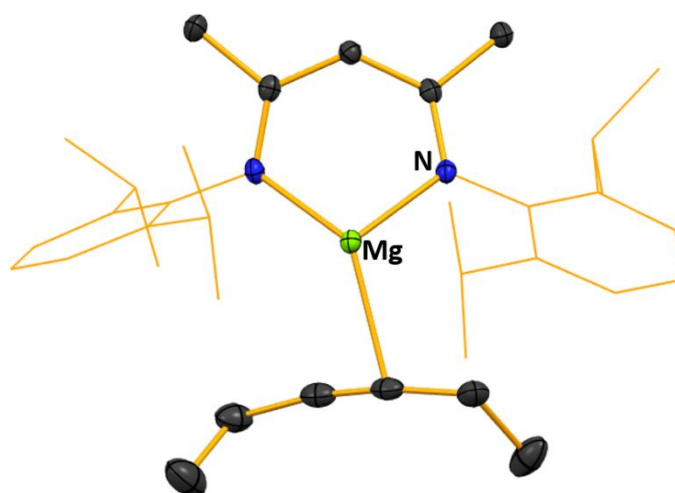


Figure 3.12: Molecular structure of $[NacNacMg^+.EtCCEt][B(C_6F_5)_4^-]$, with hydrogen atoms and counter anion omitted and organic Dipp groups drawn as wireframe for clarity. Thermal ellipsoids set at 40 % probability level.

It was also shown that the addition of arenes to the parent $[NacNacMg]^+ [B(C_6F_5)_4]^-$ complex leads to product complexes featuring η^3 coordination between small arenes such as benzene and toluene, with additional interactions between the Mg centre and $B(C_6F_5)_4^-$ counter ion.¹⁹⁷ When moving to the larger, more substituted arene such as mesitylene, a η^6 coordination is seen, hence there is no space around the Mg centre for any additional interaction with the $B(C_6F_5)_4^-$ counter ion.¹⁹⁷ Aside from their structural interest, such naked MgNacNac ligands have also been shown to take part in reactivity with alkynes and phosphines, as well as being an effective catalyst for the hydrophosphination of phenylacetylene with Ph_2PH .¹⁹⁸ Results such as these highlight the potential untapped reactivity possessed by MgNacNac complexes.

Such reactivity is not limited exclusively to magnesium analogues, with CaNacNac complexes also recently coming to the fore. Recently, Harder and co-workers showed that reacting CaNacNac in the form of its $\text{B}(\text{C}_6\text{F}_5)_4$ salt with AlNacNac in benzene leads to the solvents dearomatization and formation of a $\text{NacNacCa}^+(\text{C}_6\text{H}_6)\text{Al}^{\text{III}}\text{NacNac}$ complex.¹⁹⁹ The dearomatized benzene molecule is trapped between the Ca and Al centres of the complex in a boat conformation, with two short and four long C-C bonds, with the double bonds of the $\text{C}_6\text{H}_6^{2-}$ anion strongly coordinating to the calcium centre.¹⁹⁹

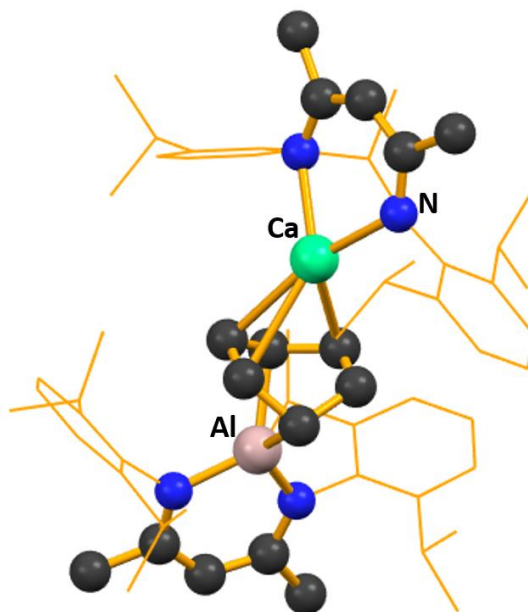
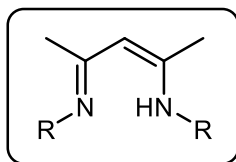
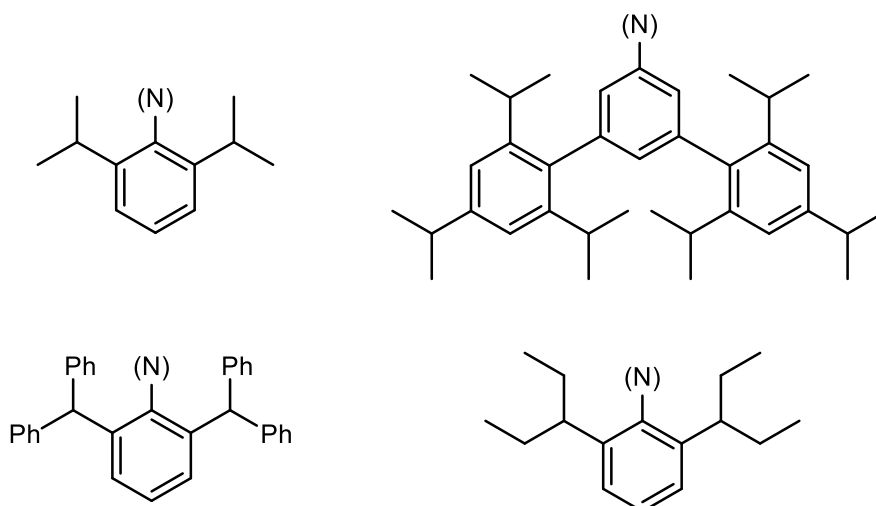


Figure 3.13: Molecular structure of $[\text{NacNacCa}^+(\text{C}_6\text{H}_6)\text{Al}^{\text{III}}\text{NacNac.C}_6\text{H}_5\text{F}][\text{B}(\text{C}_6\text{F}_5)_4^-]$, with hydrogen atoms, counter anion and disorder omitted and organic Dipp groups drawn as wireframe for clarity.

Such complexes can also be formed further down group 2, with the steric bulk of the NacNac ligand exploited in the synthesis of the first Sr alkyl complex, which in turn came from the development of a Sr hydride complex stable towards ligand exchange.²⁰⁰ It is also worth noting that many of the developments relating to heavier alkali-earth metal complexes coincided with the development of even bulkier alternatives to the NacNac ligand, which were termed DIPEP NacNac ligands (DIPEP = 2,6-diisopentylphenyl). This involved the replacement of the isopropyl substituents in Dipp with isopentyl groups in DIPEP.²⁰¹ Indeed, there are several bulkier alternatives to the Dipp substituents that can be used, with a selection drawn in Scheme 3.4.^{202, 203}



where R can be examples of the groups shown below



Scheme 3.4: Selection of bulky NacNac ligands that can be used in synthesis.

The use of this superbuly DIPEP derivative has also been extended to barium chemistry, with the isolation and characterisation of the barium complexes in particular showing the importance of agostic interactions between the metal and the *iso*-pentyl groups of the DIPEP ligand.²⁰⁴ Group 2 NacNac complexes featuring the bulky DIPEP show high levels of stability in comparison to their Dipp counterparts, with ligand scrambling and decomposition visible in the Sr and Ba Dipp complexes at 50 °C and 20 °C respectively, while the same examples involving the larger DIPEP ligand system are indefinitely stable in toluene at 140 °C for up to two weeks.²⁰⁴

In 2006 Harder showed that it was possible to utilise the common NacNac scaffold to synthesise and characterise a molecular calcium hydride complex.²⁰⁵ Indeed, it was noted that the steric bulk and strong coordination of the NacNac ligand was of crucial importance in stabilising this complex.²⁰⁵

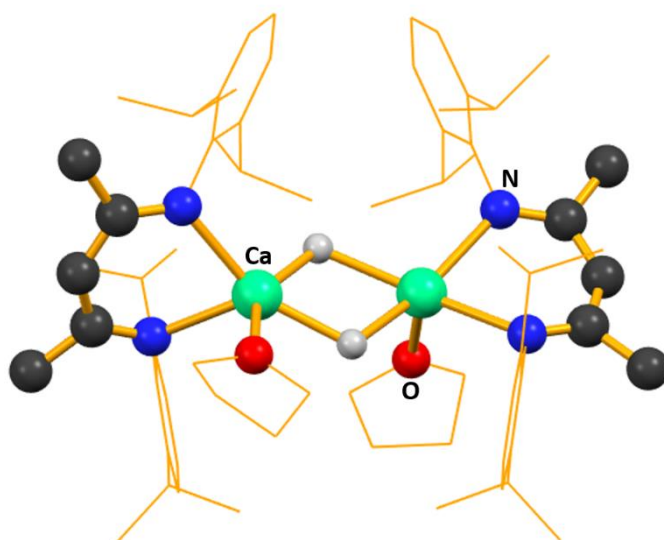
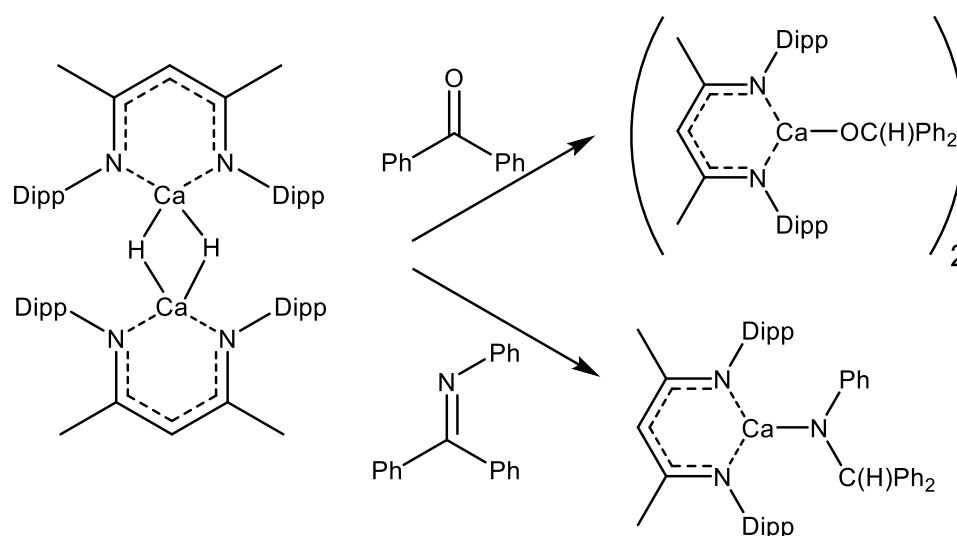


Figure 3.14: Molecular structure of $[(\text{NacNac})\text{CaH}(\text{THF})]_2$, with hydrogen atoms excluding hydrides omitted and organic Dipp groups and THF fragments drawn as wireframe for clarity.

This complex was able to carry out a number of reactions with a series of substrates including addition of the complex to compounds containing carbonyl or imine functionalities, providing an easy route to Ca alkoxide and imide complexes respectively.²⁰⁶



Scheme 3.5: Reaction of carbonyl and imine substrates with CaNacNac hydride complex to provide alkoxide and imide complexes. Solvating THF omitted for clarity.

This reactivity lies in stark contrast to that of binary CaH_2 itself, which is insoluble, inert and subsequently primarily used only as a generic drying agent in organic chemistry.²⁰⁶

Collectively, these results show the increasing impact of NacNac ligands in organometallic chemistry, which hints at a vast untapped potential in future developments, particularly those involving the alkali metals.

Chapter 4: Diverse outcomes of CO₂ fixation using alkali metal amides including formation of a heterobimetallic lithium–sodium carbamato-anhydride via lithium–sodium bis-hexamethyldisilazide

This chapter is based on a published article:

Chemical Communications, 2019, **55**, 1478-1481

Putting the results into context with the literature an extended introduction, discussion and conclusion to the paper are provided.

Contributing authors to the manuscript and their roles

Richard M. Gault- Designed and performed the experiments; analysed the data; drafted the manuscript

Ross McLellan- Helped with the data processing; contributed to the drafting of the manuscript

Alan R. Kennedy- Checked the accuracy of X-ray diffraction data processing

Jim Barker- Industrial collaborator

Jacqueline Reid- Industrial collaborator

Robert E. Mulvey- Principal investigator

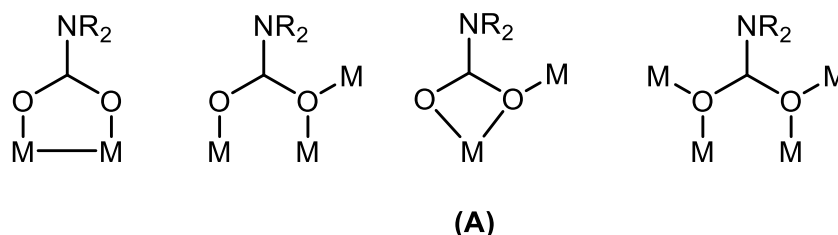
The supporting information can be found in Chapter 7: Experimental; Section 7.3 and Table 7.5.3

4.1 Abstract

Fixation of CO₂ by lithium amides derived from pyrrole and diisopropylamine generates a lithium carbamate polymer and dodecamer respectively. Moving to lithium–sodium hexamethyldisilazide produces a more complicated, intriguing reaction, where unusually the bimetallic composition is maintained in the product but its composition contains both carbamato and anhydride functionalities.

4.2 Introduction

Given the nature of the work described in part I of the thesis on alkali metal carboxylates, it was decided to investigate alternative routes of synthesising such compounds. On account of the widespread use of organolithium reagents within synthetic inorganic chemistry, we pondered whether such reagents had potential uses as CO₂ capture agents. A closely related chemical group to that of the carboxylate is the carbamate group. This group, as in the carboxylate, contains two oxygen atoms bonded to a central carbon. However, whereas a carbamate has a nitrogen atom simultaneously bonded to the central carbon, a carboxylate would have a second carbon atom. The carbamate group is derived from carbamic acid, with an inorganic example of such a carbamate being ammonium carbonate, often used as smelling salts. Much like the arrangement seen with metal carboxylates, there are four main coordination modes that can be adopted by metal carbamates and although there are some examples of unidentate and bridging modes of coordination, the chelating bonding mode (**A** in Scheme 4.0) is by far the most commonly observed.⁵⁴



Scheme 4.0: The four main coordination modes reported for metal carbamates.

When reacting organolithium reagents with CO₂, this would presumably involve insertion of the CO₂ unit into the reactive C-Li bond present, hence leading to the formation of lithium carboxylates. Related to such a reaction, taking lithium/alkali metal amides, another commonly used series of reagents, and reacting them with CO₂ should lead to the insertion of the CO₂ into the reactive N-Alkali metal bond, leading to the formation of lithium/alkali

metal carbamate species. Such species could potentially be crystallographically characterised and their structures explored. In order to further set the context for the research presented in this section, a brief introduction to the common structural motifs adopted by organolithium compounds and alkali metal amides will now be presented.

4.2.1 Organolithium chemistry

First discovered as a new element in 1817 in Sweden by Johan August Arfvedson, the name lithium is derived from the Greek 'lithos' meaning stone, since in contrast to sodium and potassium, lithium had been discovered as a solid mineral rather than in animal blood and plant ash as the others had been respectively.²⁰⁷ Lithium is relatively light and possesses the highest melting and boiling points of the alkali metals.⁵⁴ It is also the smallest of the alkali metal cations, with a radius of only 1.52 Å in comparison to sodium and potassium, which have radii of 1.86 Å and 2.27 Å respectively.⁵⁴ This smaller size has an impact on the reaction of lithium with oxygen. When burnt in air or oxygen at 1 atmosphere pressure, lithium will form Li_2O , with only small traces of Li_2O_2 , while the other alkali metals will react further to form either peroxides or in the case of the heavier analogues superoxides.⁵⁴

One common use for lithium metal is in the synthesis of organolithium compounds, which are very reactive towards water and air, generally being spontaneously flammable under these conditions.⁵⁴ It is therefore unsurprising that it took many years to uncover the solid state structures of organolithium reagents *via* X-ray crystallography, this being a challenge well into the mid-20th century. Indeed, it was not until 1963 that Dietrich uncovered the solid-state structure of ethyllithium.²⁰⁸ Despite the simpler nature, it was not until the following year that Weiss and Lucken uncovered the crystal structure of methyllithium.²⁰⁹ The structure of this and several other alkali metal alkyl complexes were discussed by Weiss in a comprehensive 1993 review article, where it was confirmed *via* neutron diffraction experiments that MeLi forms a tetrameric aggregate, composed of $\text{Li}(\text{CH}_3)_4$ tetramers.²¹⁰ Each of these tetramers interacts with its neighbours, thus producing a three-dimensional network that accounts for the low volatility of MeLi.²¹⁰

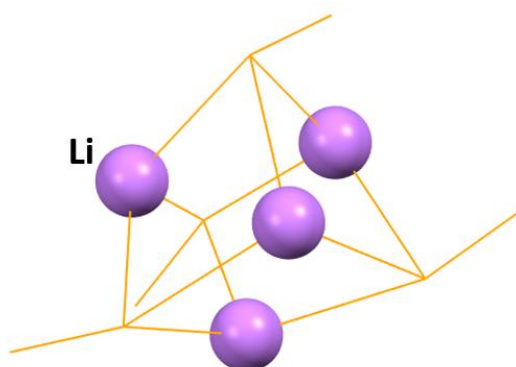


Figure 4.0: Molecular structure of ethyllithium, showing the cubane at the core of the structure. Organic framework shown as wireframe for clarity.

Ethyllithium adopts a solvent- and donor-free arrangement in the solid state, composed of four $\text{Li}(\text{C}_2\text{H}_5)$ units linked to form a (C_6Li_4) heterocubane scaffold. It was not until 30 years after this breakthrough that the structures of two more common lithium alkyl reagents, namely $^t\text{BuLi}$ and $^n\text{BuLi}$, were first uncovered by Kottke and Stalke through the use of specialised crystallographic apparatus.^{211, 212}

$^t\text{BuLi}$ adopts a tetrameric arrangement in the crystal, with two Li_4 and C_4 tetrahedra interpenetrating each other. The four lithium centres are arranged as one tetrahedron, with each face of this tetrahedron capped by a carbon centre from a ^tBu group, which in turn forms a second, larger tetrahedron. This arrangement leads to Li-C bond lengths of 2.246 Å within the structure, with secondary interactions also potentially leading to stabilisation of the Li centre.²¹¹ Unsolvated $^n\text{BuLi}$ in contrast forms a hexameric structure in the solid-state, with six lithium centres present in a distorted octahedral arrangement. The Li...Li separation is varied between six longer Li...Li contacts of average length 2.939 Å and six shorter Li...Li contacts of average length 2.429 Å. This leads to the formation of eight triangular faces within the core of the structure, with six of these capped by ^nBu groups. There are also short distances between the lithium centre and the β -carbon [average of 2.287 Å], suggesting a degree of electrostatic interaction being present.²¹¹

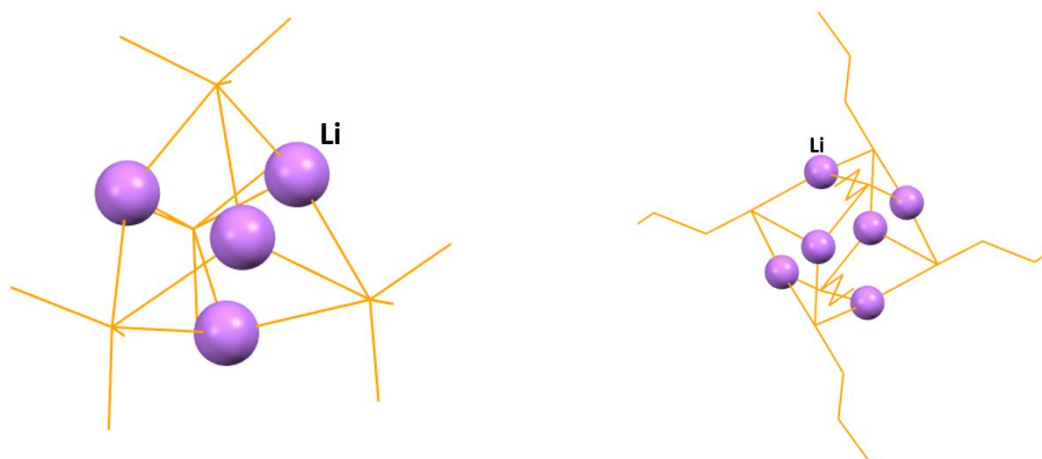


Figure 4.1: (Left) Structure of *tert*-butyllithium and (Right) Structure of unsolvated *n*-butyllithium. Organic framework shown as wireframe for clarity.

Both $n\text{BuLi}$ and $t\text{BuLi}$ exist as discrete electron-deficient structures, with the structures adopted by each species partially explaining the difference in reactivity between them. In $t\text{BuLi}$ the organic groups have greater steric bulk when compared to the organic groups of $n\text{BuLi}$, meaning the former cannot pack so closely together, hindering aggregation and leading to a more open structure. In addition to these steric factors, electronic factors also play a part, with two extra alkyl groups on the carbon centre of $t\text{BuLi}$. These groups are electron donating and therefore increase the electron density on this carbon centre, which in turn increases the polarity of the M-C bond and increases the reactivity of the compound. It is for this combination of reasons that $t\text{BuLi}$ exhibits enhanced reactivity over that of $n\text{BuLi}$.

These organolithium reagents are soluble in organic solvents, a key reason behind their prolific exploitation in synthesis. The simplest lithium alkyl reagent, MeLi bucks this trend though, as it is insoluble in all common organic solvents without the presence of a donor. This lack of solubility is directly related to its structure, which is that of a polymer composed of connected cubanes. First uncovered in 1964, this polymer propagates through agostic interactions between the methyl groups, hence its insolubility in aliphatic and aromatic solvents.²⁰⁹

As is well established, the structure of organometallic species can play a major part in the subsequent reactivity. The aggregation state of the organolithium reagents plays a crucial role in their reactivity, with the presence of electron donors often deaggregating the structures seen above to smaller, simpler alternatives. This deaggregation exposes the $\text{R}^{\delta-}$ component of the reagent, which increases its reactivity and basicity. For example, focussing

on $^n\text{BuLi}$, it has been seen that adding donors such as THF, TMEDA and PMDETA will decrease the aggregation state in various ways. Addition of THF breaks apart the hexamer into more kinetically active smaller tetramers,²¹³ while addition of TMEDA, which has a greater donor capacity being bidentate in comparison to the monodentate THF, gave different structures depending on the ratio of $^n\text{BuLi}$ to TMEDA used. Specifically, the aggregate adopts a general arrangement represented by $[(^n\text{BuLi})_x(\text{TMEDA})_y]$. If there is a stoichiometric deficiency of TMEDA compared to $^n\text{BuLi}$ a polymer of composition $[(^n\text{BuLi})_4\cdot\text{TMEDA}]_\infty$ is observed. In this polymer there is insufficient TMEDA to solvate every Li centre, giving a zig-zag arrangement which propagates through interactions between monodentate TMEDA molecules linking adjacent $^n\text{BuLi}$ tetramers.²¹³

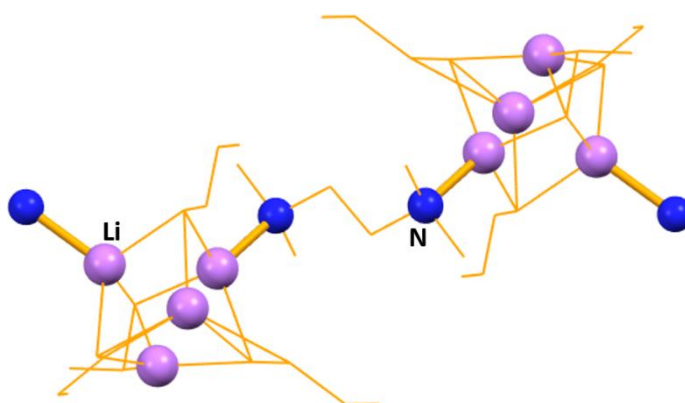


Figure 4.2: Section of the infinite chain structure of $[(^n\text{BuLi})_4\cdot\text{TMEDA}]_\infty$. Organic framework shown as wireframe for clarity.

If, however, the TMEDA donor is added in a slight excess a different structure of composition $[(^n\text{BuLi})_2\cdot(\text{TMEDA})_2]$ is obtained, where the TMEDA acts as a bidentate donor and breaks the $^n\text{BuLi}$ hexamer into dimeric subunits.²¹³

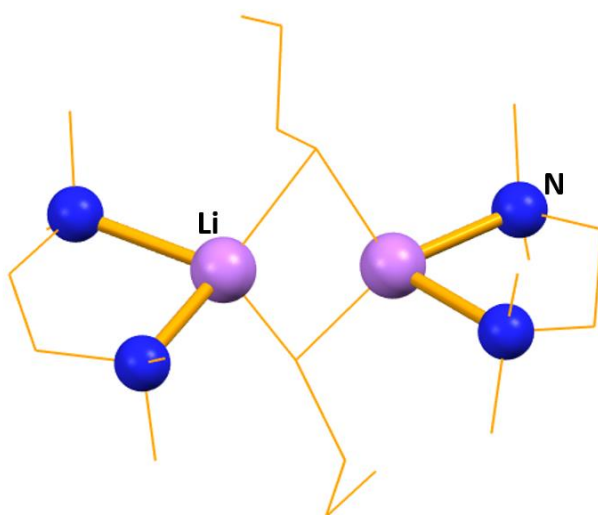


Figure 4.3 Discrete dimeric structure of $[(^n\text{BuLi})_2\cdot(\text{TMEDA})_2]$. Organic framework shown as wireframe for clarity.

Extending this to the trifunctional donor PMDETA reveals a hemi-solvated variant of composition $[(^n\text{BuLi})_2\cdot\text{PMDETA}]_2$.²¹⁴ This unusual complex can be considered as a dimer of $^n\text{BuLi}$ units at the core, with stabilisation provided by two terminal $^n\text{BuLi}\cdot\text{PMDETA}$ units.²¹⁴ It was noted in the paper that low temperatures had to be used in preparing this complex, or else the PMDETA donor itself would undergo lithiation.

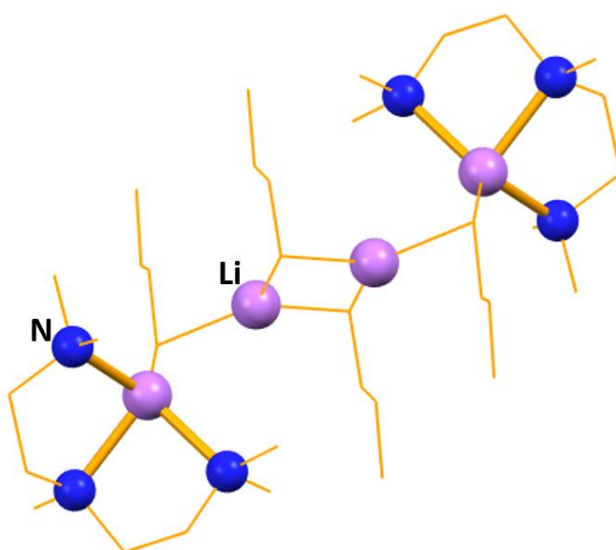


Figure 4.4: Molecular structure of $[(^n\text{BuLi})_2\cdot(\text{PMDETA})_2]$. Organic framework shown as wireframe for clarity.

4.2.2 Utility amides

One facet of structural chemistry that has received considerable attention over the years is that of alkali metal amides based on common or 'utility' amides.²¹⁵ The most popular examples of the parent secondary amines that lead to such amides are diisopropylamine (DA), *tert*-butylamine, 1,1,1,3,3,3-hexamethyldisilazane [HMDS(H)] and 2,2,6,6-tetramethylpiperidine [TMP(H)]. Various studies have been carried out probing the solid state and solution structures of the alkali metal amide species derived from these amines and a discussion of their solid state structures for the most commonly used alkali-metal derived amides, namely those derived from DA, HMDS(H) and TMP(H), will now be presented. Alkali metal derivatives of DA have been known for several years. By far the oldest and most widely used form is lithium diisopropylamide or LDA. This strong base is used in synthetic chemistry due to its ability to deprotonate suitable carbon acids. Indeed, it was noted by Collum that lithium dialkylamides are the preferred reagent when forming ketone enolates.⁶¹ The structure of this amide has been elucidated both in its pure donor free form and in the presence of various donors. Its solvent-free form was first structurally characterised by Mulvey *et al.* in 1991 and was found to be an unusual helical polymer, with N-Li-N segments that are almost linear in appearance, alternating between slightly shorter and slightly longer Li-N bonds [1.939(4)/1.934(5) Å vs 1.956(4)/1.957(5) Å].²¹⁶ Interestingly, it was found that while TMEDA is necessary in order to form a solution from which the crystals are obtained, there is no TMEDA present within the structure, though it was theorised that the molecules probably play a role in chain termination of the polymer.²¹⁶

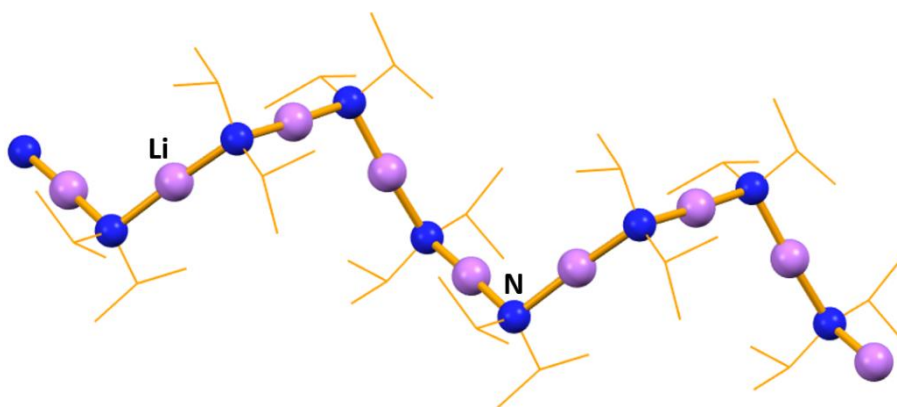


Figure 4.5: A section of the structure of unsolvated LDA showing its helical arrangement. Organic framework shown as wireframe for clarity.

In the presence of the strong donor solvent THF, the polymeric LDA deaggregates to a dimeric structural motif of a type widely seen in alkali metal chemistry, with a 1:1 stoichiometric ratio of LDA to THF ligands within the structure.²¹⁷ This cyclic dimer is composed of a four-membered (LiN)₂ ring. One THF donor molecule solvates each alkali metal, giving an overall coordination number of three for the lithium centre.²¹⁷

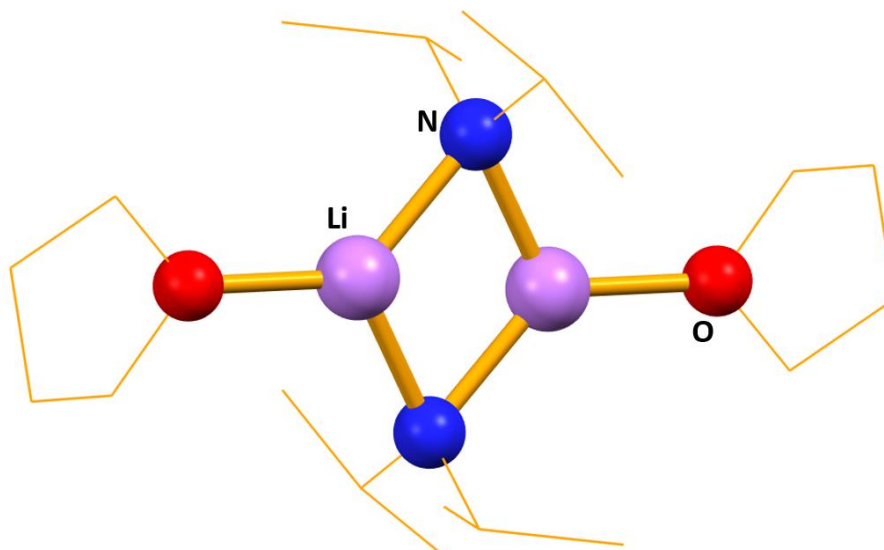


Figure 4.6: Dimeric structure of (LDA.THF)₂ in the crystal state. Organic parts of the structure are shown as wire frame for clarity.

When the donor is changed to TMEDA, a polymeric structure composed of an infinite array of dimeric units similar to those seen with THF is the result.²¹⁸ Here TMEDA fulfils a monodentate bridging role, leading once again to a three coordinate lithium centre. In terms of structural parameters, there is no significant difference between the (LiN)₂ ring formed in (LDA.THF)₂ and that seen in (LDA.TMEDA)_∞. NMR spectroscopic studies carried out on this complex indicate that adding one equivalent of THF will displace the TMEDA to form a dimeric (LDA.THF)₂ structure (Figure 4.6).²¹⁸ This displacement is backed up by structural evidence, with the Li-N_{TMEDA} bond in (LDA.TMEDA)_∞ much longer, and hence weaker, than the Li-O_{THF} bond in (LDA.THF)₂ (2.163 Å on average vs 1.965 Å on average respectively).

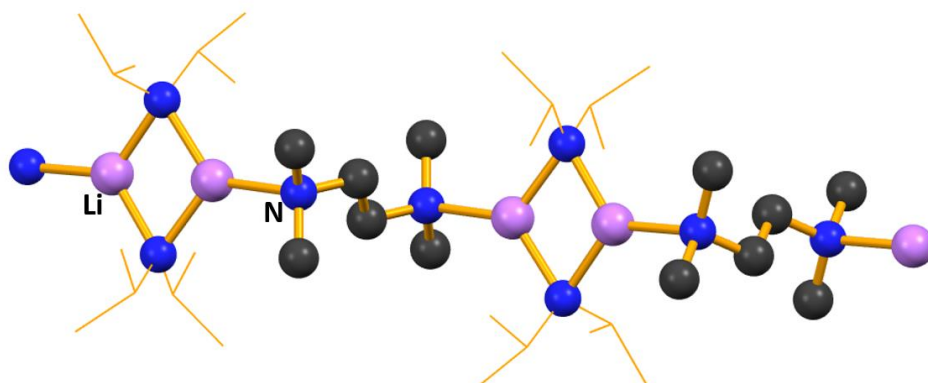


Figure 4.7: A section of the polymeric structure with dimeric subunits adopted by $(\text{LDA.TMEDA})_{\infty}$. Organic DA groups shown as wire frame for clarity.

TMEDA was also utilised by Andrews *et al.* in 1996 when they presented the first synthesis of the sodium congener of LDA.²¹⁹ Again, this complex adopts the common dimeric motif, comprising a central four atom core composed of two sodium cations in a distorted tetrahedral environment and two nitrogen atoms, with a bidentate TMEDA completing the sodium coordination.²¹⁹

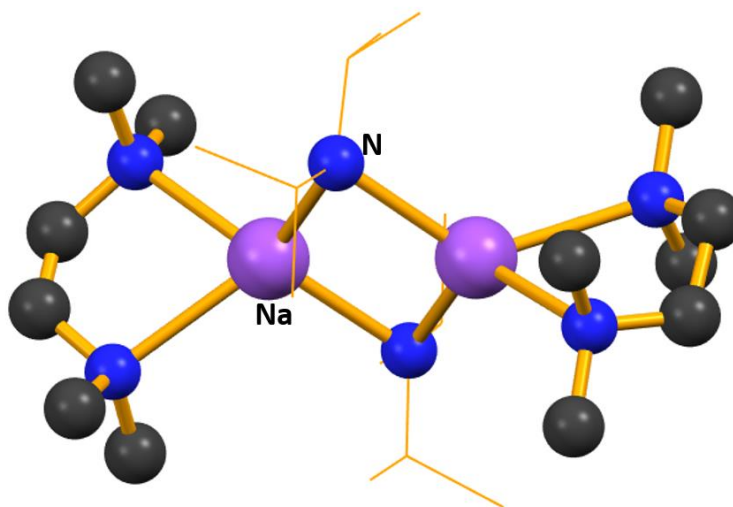


Figure 4.8: Dimeric structure adopted by $(\text{NaDA.TMEDA})_2$ in the crystal state. Organic DA groups are shown as wire frame for clarity.

A similar structure was reported by Clegg *et al.* for the potassium analogue, which again was isolated as the TMEDA solvate. This structure also contains short agostic K...C intermolecular contacts between the potassium and the methyl units of the diisopropylamide molecule.²²⁰ Here, the four-membered (KN)₂ ring is slightly asymmetric, with a pair of long [2.827(2) Å] K-N bonds and a pair of shorter [2.706(2) Å] K-N bonds.²²⁰ While the potassium is four coordinate formally, the intermolecular contacts ensure a higher coordination environment is actually present, with three intermolecular contacts bringing the total coordination environment up to seven, with the potassium interacting with two iPr groups from one DA unit and one iPr group from the other DA unit.²²⁰

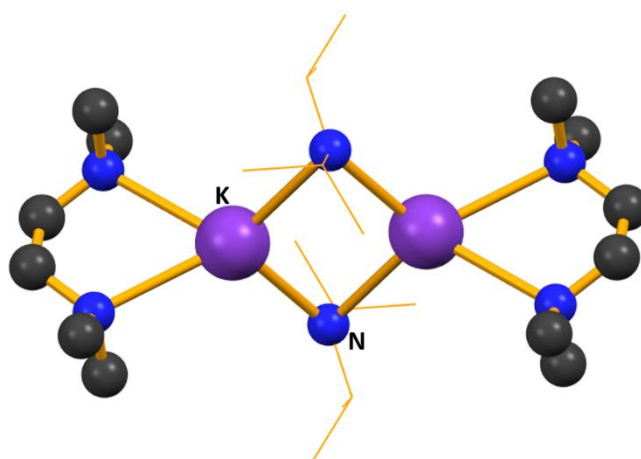


Figure 4.9: Dimeric structure adopted by (KDA.TMEDA)₂ in the crystal state. Organic DA groups are shown as wire frame for clarity.

HMDS(H) was first synthesised in the mid-1940s by Sauer, *via* ammonolysis of trimethylchlorosilane,²²¹ with the lithium derivative following in 1959 and the sodium and potassium versions synthesised by 1961.²¹⁵ In terms of pK_a values, while there is some debate over the exact numerical values, which of course have several variables that must be considered including identity of the alkali metal, solvent choice and temperature, there is a general consensus that LiHMDS is the lowest of the three commonly used amides, with LDA having a much higher value, only slightly below that of LiTMP.²¹⁵ For example, Streitwieser and co-workers, using advanced density functional theory calculations, worked out the pK values to be 24.37, 35.41 and 35.53 for LiHMDS, LDA and LiTMP respectively.²²² It is important to consider the pK values of these amides when looking at reactivity, as their effectiveness as effective deprotonating agents is derived from their high pK values.²¹⁵ The low value for LiHMDS in comparison to those of the others can be explained through a combination of steric and electronic effects, with the longer Si-C and N-Si bonds in HMDS reducing the steric

protection afforded to the nitrogen atom in comparison to the shorter N-C bonds seen in LiTMP.²¹⁵ With regards to the structure of the alkali metal HMDS complexes, LiHMDS was first structurally elucidated in 1969 by Böttcher *et al.*, making it the first crystallographically characterised alkali metal utility amide.²²³ It adopts a trimeric arrangement in the solid state when no solvating donor is present, with each lithium coordinated to two nitrogen atoms of HMDS in a triangular arrangement. A decade later, a more detailed study carried out by Atwood *et al.* revealed more insight into the metrics of this cyclic trimer.²²⁴ For example, they established that the central six-membered Li_3N_3 ring is essentially planar to within 0.01 Å.²²⁴ They also noted that the shortest $\text{Li}\cdots\text{H}$ interaction was 2.56(1) Å, which is to be expected given the polarisation present in the N-SiMe_3 unit, with the Si atom possessing a δ^+ charge, which results in the methyl group possessing a δ^- charge and subsequently it then interacting with the lithium cation.²¹⁵

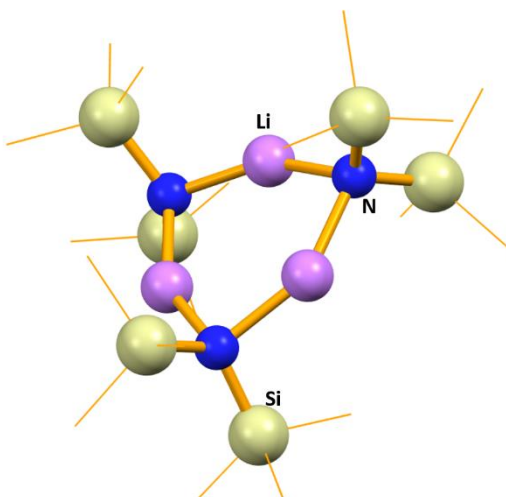


Figure 4.10: Trimeric structure adopted by LiHMDS in the crystal state. Organic groups are shown as wire frame for clarity.

In the presence of THF, this trimer partially deaggregates to form a $(\text{LiHMDS} \cdot \text{THF})_2$ dimer, which features THF solvation of the lithium centre, making it three coordinate.²²⁵

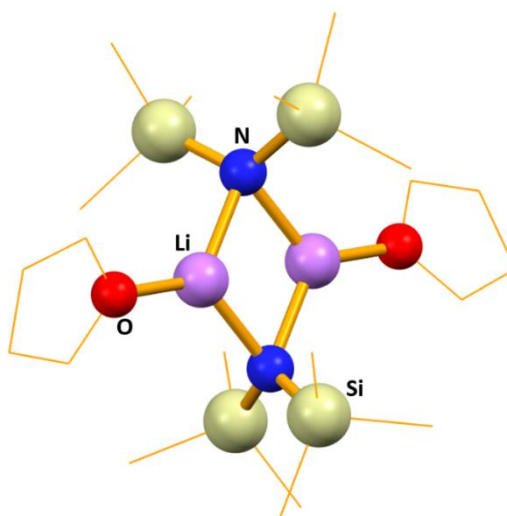


Figure 4.11: Trimeric structure adopted by $(\text{LiHMDS} \cdot \text{THF})_2$ in the crystal state. Organic groups are shown as wire frame for clarity.

The lithium solvation leads to slight elongation of the Li-N bonds, as well as forcing the Li-N-Li angle to a less obtuse value $[106.3(6)^\circ]$ in $(\text{LiHMDS} \cdot \text{THF})_2$ vs $147(3)^\circ$ in the unsolvated LiHMDS trimer].²¹⁵ Moving from monodentate THF to bidentate TMEDA sees a different structural motif emerge, namely that of a rare monomeric alkali metal amide.²²⁶ Lithium is again three-coordinate here, with TMEDA chelating through the nitrogen donor atoms, and the complex is also noted for having a very short Li-N_{HMDS} bond at only $1.893(4) \text{ \AA}$.²²⁶

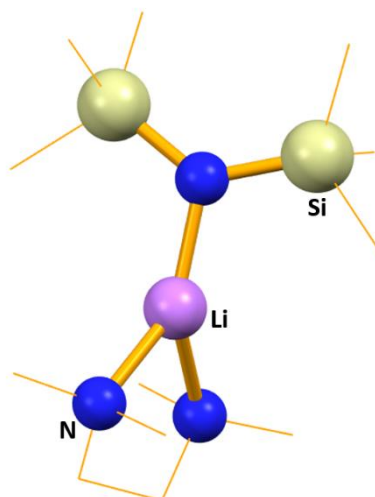


Figure 4.12 Trimeric structure adopted by $(\text{LiHMDS} \cdot \text{TMEDA})$ in the crystal state. Organic groups are shown as wire frame for clarity.

The heavier sodium congener NaHMDS was first structurally characterised by Atwood and Grüning in 1977.²²⁷ It was revealed to be a polymer, with the infinite chain composed of alternating sodium and nitrogen atoms, with average bond lengths within this chain of 2.36 Å.²²⁷ Two decades later a polymorph of unsolvated NaHMDS was uncovered by two groups simultaneously, namely those of Nöth and Driess.^{228, 229} This polymorph comprises a cyclic trimer, akin to that of unsolvated LiHMDS, with bond lengths marginally increased compared to those seen in the polymeric form of NaHMDS, presumably due to ring strain. There are also short agostic interactions in this trimer (Na...H interactions range between 2.384 and 2.616 Å), which presumably aid in the stabilisation of the two-coordinate sodium centres.²¹⁵

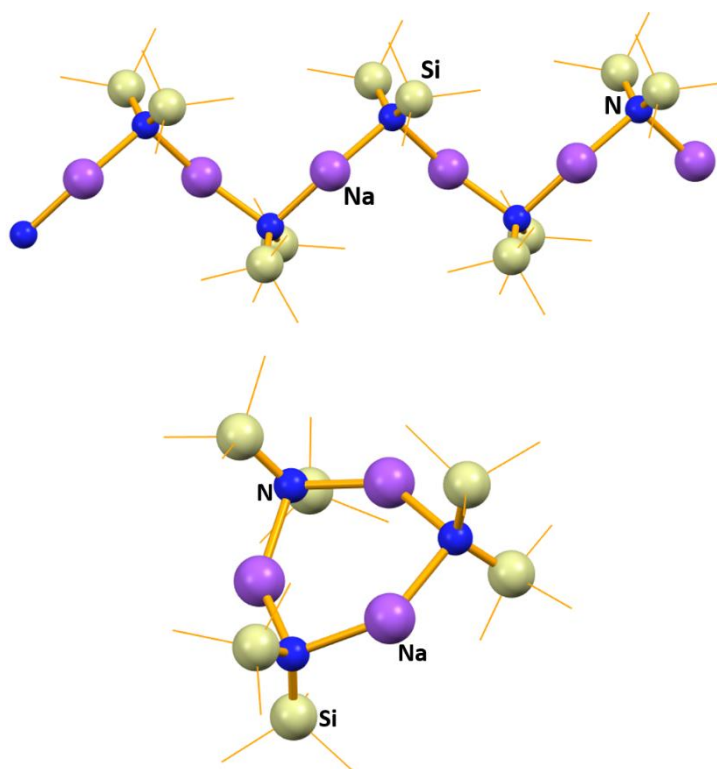


Figure 4.13: (Top) Fivefold section of the polymeric structure adopted by NaHMDS and (Bottom) Polymorphic trimeric structure adopted by NaHMDS. Organic groups are shown as wire frame for clarity.

There are also two polymorphs of the THF solvate of NaHMDS. The first example reported by Dehnicke in 1999 and consists of a dimeric (NaHMDS.THF)₂ complex, with one THF solvating each sodium centre in an arrangement similar to that seen for (LiHMDS.THF)₂.²³⁰ In 2006, Bochmann *et al.* characterised a donor deficient variation, akin to that seen by Dehnicke but with only one THF molecule within the structure, hence only one sodium centre was solvated.²³¹ While both polymorphs feature a four-membered (NaN)₂ ring, the latter has one

sodium centre three-coordinate and one two-coordinate, while the former has two three-coordinate centres. Despite this difference, the metrics of both sodium cations are similar with regards to bond lengths.

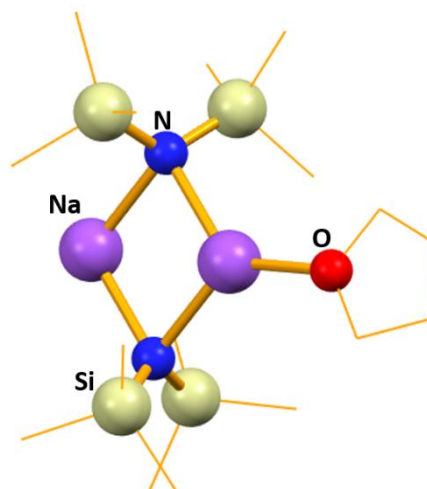


Figure 4.14: Donor deficient example of NaHMDS₂·THF as uncovered by Bochmann *et al.* in 2006. Organic groups are shown as wire frame for clarity.

Despite the previous examples showing effective solvation of alkali metal amides with THF and TMEDA donors, there is no known crystallographically characterised examples of KHMDS with these donors, though such structures have been alluded to within the literature.²³² However, there are two examples of donor-free KHMDS complexes. The first was obtained by Williard and while formally a toluene solvate,²³³ can be considered as unsolvated due to no interactions between the potassium and the toluene, despite such interactions being known from previous research.^{234, 235} The second example of KHMDS was obtained by Hanusa *et al.* and has no solvent of crystallisation within the structure, being genuinely unsolvated.²³⁶ Both structures contain a planar four-membered (KN)₂ ring, with slight asymmetry present *via* the slightly shorter K-N_{HMDS} bonds on one side compared to the other. Noticeably, no agostic interactions are present in these potassium analogues.

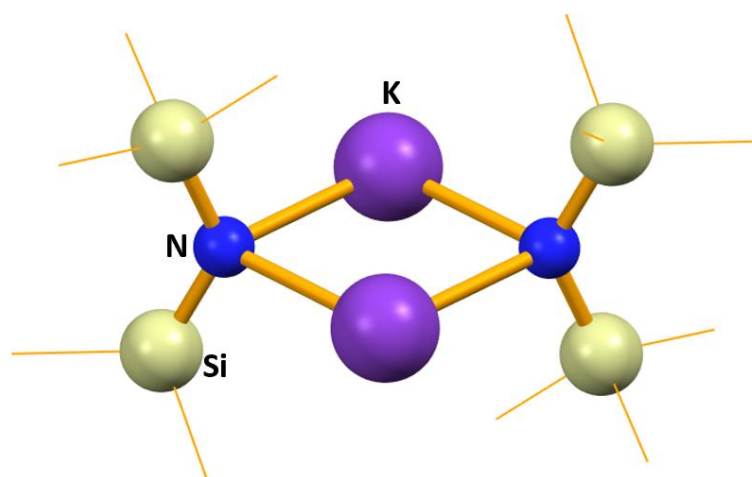
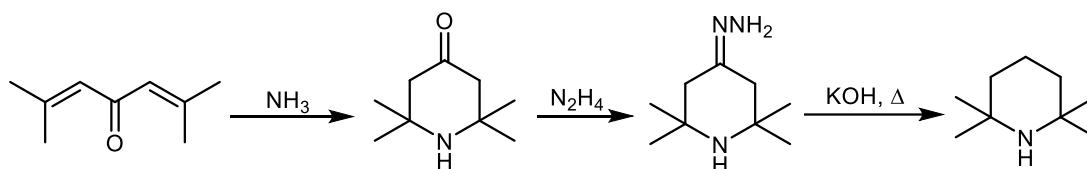


Figure 4.15: Molecular structure adopted by (KHMDs)₂. Organic groups are shown as wire frame for clarity.

Moving to consider TMP(H) and its alkali metal amides, it is worth noting that the parent amine is the most expensive of the three utility amines, with prices generally in the region of £201 per 100 ml from Sigma-Aldrich, which equates to £342.06 per mole. The more expensive price of TMP(H) is attributed to its more complex synthesis in comparison to HMDS(H) and DA(H).²¹⁵ First synthesised in 1905 by Franchimont and Friedmann in a pure form²³⁷ from reduction of 4-bromo-tetramethylpiperidine with a copper/zinc couple, it is now more commonly prepared *via* a Wolf-Kishner-Huang reduction of 2,2,6,6-tetramethyl-4-piperidone.²³⁸



Equation 4.0: Wolf-Kishner-Huang reduction used to access TMP(H).

Unsolvated LiTMP adopts a cyclic tetrameric structure in the crystal, as described by Lappert and Atwood.²³⁹ The central feature is an essentially planar eight-membered (LiN)₄ ring, with bond angles at the lithium and nitrogen centres of this ring larger in comparison to those in LiHMDS, which is thought to be due to the greater steric demands of anionic TMP in comparison to those of HMDS.²¹⁵ In THF, this tetramer deaggregates to a cyclic dimer, as revealed by Mulvey and co-workers in 2011.²⁴⁰ Each lithium centre is solvated by THF, making an overall coordination number of three in a distorted trigonal planar geometry.²⁴⁰ Here, the

solvation by THF is arguably the weakest of the THF solvates of the utility amides discussed (Li-O_{THF} distances on average 1.974 Å here vs 1.882(14) for LiHMDS.THF and 1.963 Å on average for LDA.THF), presumably due to the greater steric shielding of lithium by the bulky TMP ligand.²⁴⁰

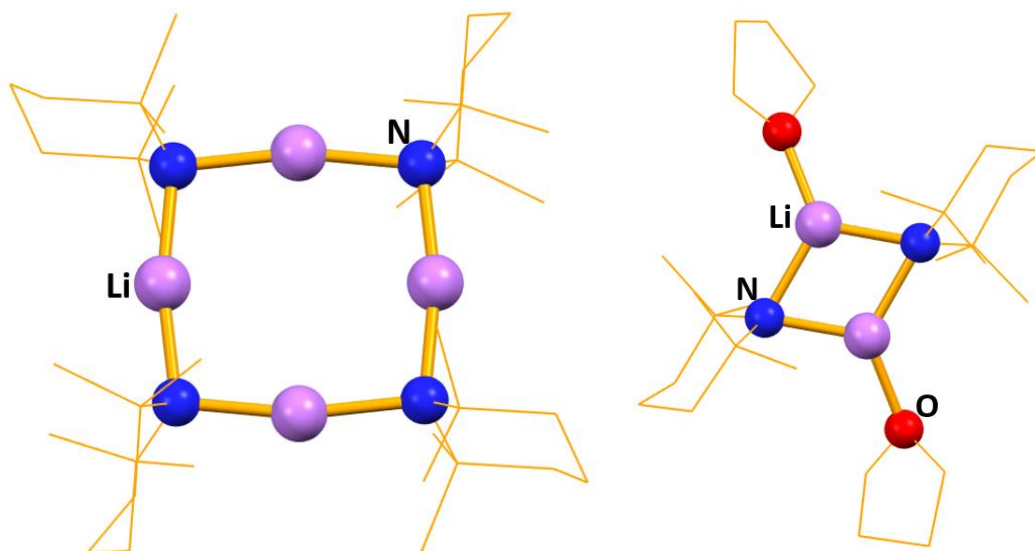


Figure 4.16: (Left) Tetrameric structure of (LiTMP)₄ and (Right) Dimeric structure of (LiTMP.THF)₂ with organic groups shown as wire frame for clarity.

An interesting arrangement is seen for the TMEDA solvate, which has been characterised as an ‘open dimer’.²⁴¹

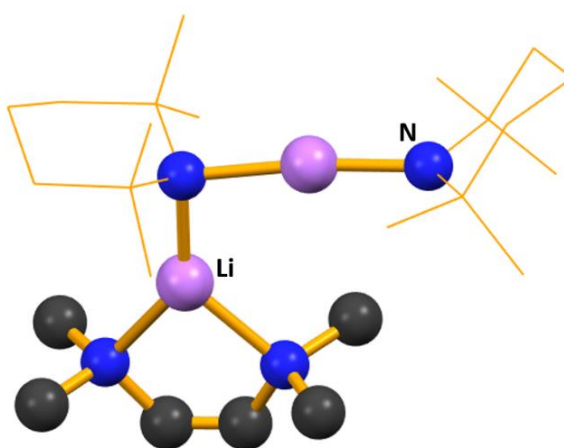


Figure 4.17: Molecular structure adopted by [LiTMP₂.TMEDA]. Organic TMP fragments are shown as wire frame for clarity.

This unique arrangement leads to two different lithium environments within the structure, one being two-coordinate and the other being three-coordinate, as well as a rare terminal amide-based ligand comprising only one M-N bond.²¹⁵ The N-Li-N bond angle is very close to linear, being 172.5(3)°, with the Li-N bonds also unsurprisingly varying depending on the lithium centre of interest, with the bridging nitrogen providing longer Li-N bonds than the terminal nitrogen [bridging N has bond lengths of 1.950(5) Å and 2.049(6) Å to the lithium centres, while the terminal N has a bond length of 1.885(6) Å to the lithium centre]. This short terminal Li-N bond is presumably due to the absence of a second Li-N interaction, which therefore concentrates the negative charge of the nitrogen centre into this bond.²⁴¹

The structures of unsolvated and solvated NaTMP are related in form to those discussed for the other utility amides and therefore to avoid unnecessary repetition only a brief overview of the structures will be presented here. Unsolvated NaTMP adopts a cyclotrimeric arrangement as seen previously for the lithium and sodium congeners of HMDS. First characterised crystallographically by Lappert and Mulvey *et al.* in 1999, there is a greater symmetry in NaTMP than that seen in NaHMDS, therefore only two distinct Na-N bond distances are seen in NaTMP, as opposed to six in NaHMDS.⁹² The sodium cation lies slightly closer to one nitrogen over the other (2.306 Å vs 2.362 Å), with the presence of close contacts between the Na...C of adjacent trimeric units reasoned to stabilise the two-coordinate sodium cations.⁹² As to be expected, addition of THF deaggregates this trimer to a dimer, similar to that seen previously for NaHMDS.²⁴⁰ In contrast to the structure of THF-solvated NaHMDS, there is a distortion in the Na-N bond lengths that make up the central (NaN)₂ ring, with parallel sides having significantly different bond lengths [2.364(2) Å vs 2.350(2) Å and 2.413(2) Å vs 2.438(2) Å].²⁴⁰ Finally, in 2008 O'Hara *et al.* revealed the structure of the TMEDA solvate of NaTMP to be a dimer, with each sodium coordinated to two nitrogen atoms from two different TMP units and two nitrogen atoms from solvating TMEDA.²⁴² Of note in the structure of (NaTMP.TMEDA)₂ are the bond angles within the central ring, which are smaller at sodium when compared to corresponding angles in (NaTMP.THF)₂, being 102.92(6)° and 101.20(6)° vs 105.83(7)° and 107.09(7)° respectively. This change in bond angle is presumed to originate from a sodium coordination number change, from three to four-coordinate going from (NaTMP.THF)₂ to (NaTMP.TMEDA)₂.²¹⁵

In a similar vein to that of KDA, there is only a single solvated structure for KTMP, which was uncovered by O'Hara and co-workers.²⁴² It is isostructural with $(\text{NaTMP.TMEDA})_2$, with similar bond angles, if elongated bond lengths, which is to be expected given the larger alkali metal present. These are on average 0.322 Å longer in the potassium TMEDA solvate when compared to the sodium TMEDA solvate.²¹⁵

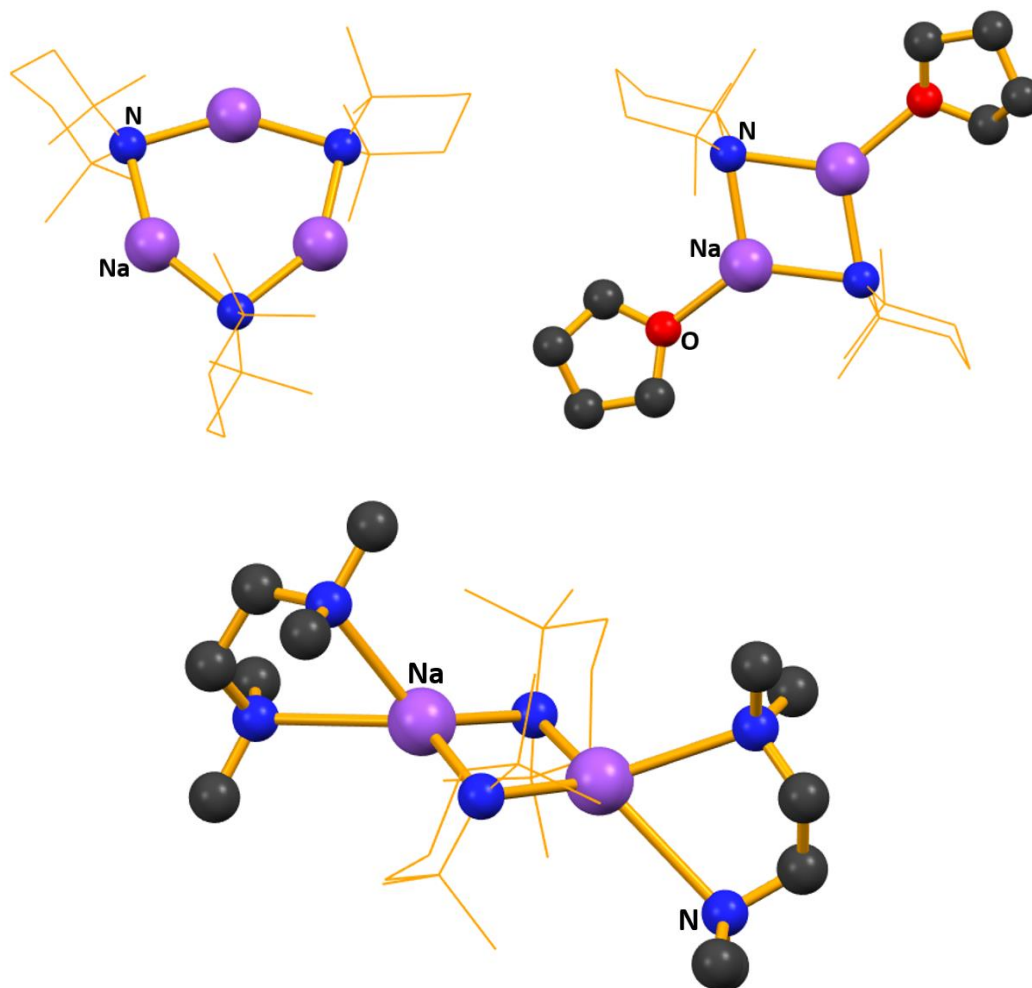


Figure 4.18: (Top Left) Trimeric structure of $(\text{NaTMP})_3$; (Top Right) Dimeric arrangement of $(\text{NaTMP.THF})_2$ and (Bottom) Dimeric structure of $(\text{NaTMP.TMEDA})_2$ with organic TMP groups shown as wire frame for clarity and disorder omitted in all examples.

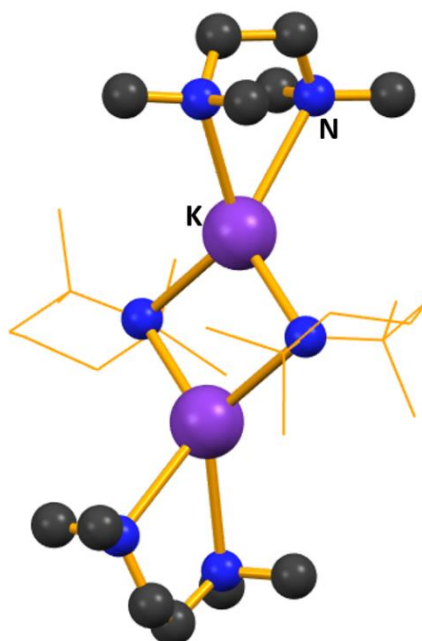


Figure 4.19: Dimeric arrangement of (KTMP.TMEDA)₂ with organic TMP groups shown as wire frame for clarity.

All the utility amides discussed above contain a reactive alkali metal-nitrogen bond, which could lend itself to the formation of carbamate complexes. By far the most common route to the synthesis of carbamate complexes is through the insertion of CO₂ into a metal-nitrogen bond, with insertion into Mg-N bonds the most common.¹⁴¹ This leads to the formation of a magnesium carbamate. Note that while metal carbamates are relatively common, with lithium, aluminium and gallium examples all known,^{141, 243} there has been much less research carried out on the sorts of compounds obtained *via* the insertion of CO₂ into a pre-formed Li-N bond, with few examples of such species characterised.¹⁶⁵ The insertion of CO₂ into alkali metal-nitrogen bonds to form alkali metal carbamates is of particular interest given the wide range of applications of such compounds, ranging from heterocyclic carbamates use as effective herbicides²⁴⁴ to the synthesis of isocyanates from carbamate esters.²⁴⁵ However, despite the widespread interest and structural insight gained into the various alkali metal amides mentioned previously, there are surprisingly only a paucity of examples within the literature of alkali metal carbamates based on these utility amides. This is perhaps unexpected given the relative ease with which CO₂ can be inserted into the system, though of course obtaining crystalline examples of such reaction products may be challenging. A search of the CSD for any alkali metal carbamate returns a mere eight results.⁸¹ Of these, only

three could be considered as the carbamates of commonly encountered utility amides, with significantly all of them being lithium hits.^{150, 246, 247}

Clearly given the lack of literature on alkali metal carbamates of utility amides this is an underdeveloped area of chemistry, with much scope to extend the structural understanding of these types of complexes in solution and solid state.

Another amine that has recently been studied by the Mulvey group is pyrrole. This five-membered aromatic heterocycle, while not considered a utility amine, is important in a range of fundamental fields of chemistry, with the basic skeletal arrangement seen in many different contexts, ranging from agrochemistry²⁴⁸ to polymeric-based materials.²⁴⁹ The sodiopyrrole complex in Figure 4.20 was first synthesised by Mulvey *et al.* in 2011.²⁵⁰

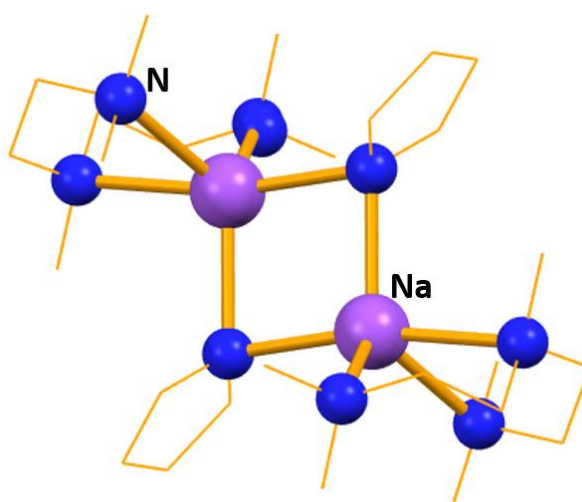


Figure 4.20: Molecular structure of $[(\text{PMDTA})\cdot\text{Na}(\text{NC}_4\text{H}_4)]_2$.

This adopts a type of dimeric structure frequently encountered in alkali-metal amide chemistry, containing a central ring composed of alternating (pyrrole) nitrogen and sodium atoms, with PMDETA raising the sodium coordination number to five.²⁵⁰

4.3 Project aims

Given the paucity of literature on alkali metal carbamates of type $[R_2NCO_2AM]$, where R represents an organic fragment and AM represents an alkali metal, and the ease in which they can be formed from reactions between CO_2 and alkali metal amides, we pondered whether crystalline examples of carbamates derived from commonly used amides could be obtained. Further, frustrated by the difficulty in obtaining crystalline long chain examples of sodium carboxylates (described in more detail in Part 1), it was reasoned that the insertion of CO_2 into organolithium complexes could provide an alternative route to acquiring examples of carboxylates, which could then be analysed for insight into their structures. In addition, given the widespread use of NacNac ligands through many areas of chemistry, it was perhaps surprising that no previous study considered the effects of alkali metal NacNac complexes on small molecules, despite containing a polar, reactive alkali metal nitrogen bond and being widespread throughout chemistry.

Therefore, the aims of this part of the project were to:

- Explore the effects of introducing CO_2 to organolithiums, to establish whether alkali metal carboxylates could be produced and to determine the structures adopted by these species
- Expand the field of small molecule insertion into reactive alkali metal amides, with the goal of realising crystalline examples of the subsequently formed carbamate complexes

4.4 Introduction from the manuscript

The activation and fixation of small molecules is a fertile field of research currently at the cutting edge of inorganic and organometallic chemistry.^{129, 139, 251} Along with fundamental interest, the goal of small molecule activation is to convert common small molecules such as N_2 , O_2 and CO_2 to higher value products, achieved through a variety of chemical means.²⁵¹ For example, Arnold recently demonstrated small molecule activation of N_2 , CO and CO_2 using a uranium based tris(aryloxy), giving a range of complexes such as $[U(OAr)_3]_2(\mu-N_2)$ and the ynediolate complex of the form $[U(OAr)_3]_2(\mu-\eta^1:\eta^1-C_2O_2)$.²⁵² Transition metals such as iron and manganese have been used to activate molecular oxygen, both in synthetic

chemistry²⁵³ and in nature with the best known example in the transport of oxygen in blood of vertebrates by the iron protein haemoglobin.^{254, 255}

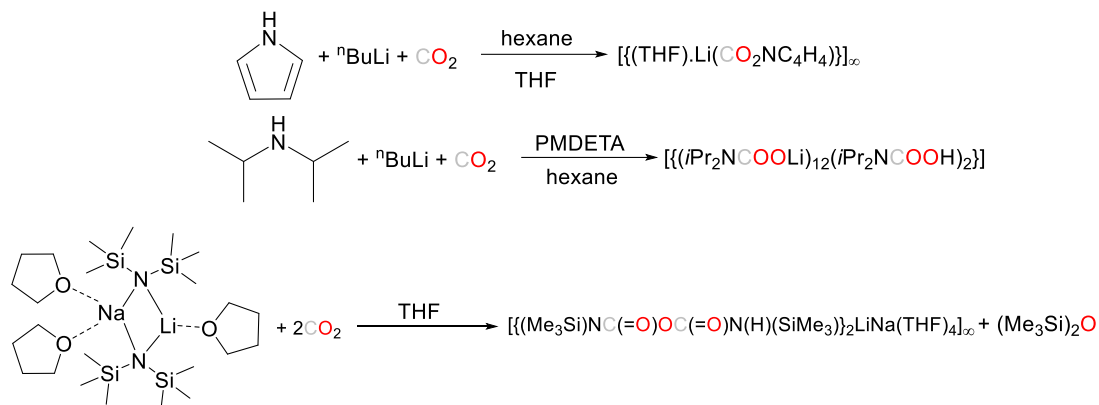
Carbon dioxide is a molecular Jekyll and Hyde, famous as it is the primary carbon source for life on earth; but infamous because of its role as a greenhouse gas. Attempts to capture and sequester CO₂ are currently the focus of many scientific efforts worldwide.¹³⁸ The stability of CO₂ presents a significant challenge in terms of its activation due to the strong C-O double bonds present, exemplified by the high enthalpy value of -393.51 kJ mol⁻¹.^{139,137} Nonetheless, there are many methods available in this regard. For example, nature uses enzymes that employ CO₂ or its hydrated form to carry out a carboxylation reaction to form a new C-C bond.¹³⁷ CO₂ can also be utilised in the synthesis of polymers, as in the reaction with cyclohexane oxide catalysed by zinc crotonate.¹⁴⁰

In spite of this widespread interest, few studies have looked at CO₂ insertion into reactive alkali metal-nitrogen bonds,²⁵⁶ with much greater attention being paid to transition metals and group 14 elements. Such insertion reactions and concomitant formations of carbamate functionalities adds to the diversity of CO₂ chemistry, which attracts widespread interest across capture technologies,¹⁴¹ industry and agriculture.²⁵⁷ The paucity of work carried out on alkali metal amides is perhaps surprising given the widespread utility of these amides in synthesis. Lithium diisopropylamide (LDA) is the most common utility amide, first utilised in 1950 in reactions with esters.²⁵⁸ The structure of LDA in the solid state was elucidated in 1991, revealing an eye-catching helical arrangement with near-linear N-Li-N-Li units,²¹⁶ with a more recent study establishing an equilibrium of trimers and tetramers in toluene.²⁵⁹ Another class of compound that has received much synthetic interest are pyrroles. This is due to the prevalence of the five-membered ring in areas ranging from agricultural chemistry²⁶⁰ to the pharmaceutical industry.²⁶¹

Herein we report the different outcomes of the insertion reactions of CO₂ into common utility lithium amides, namely LDA and lithium pyrrolide. Extending our study to reactions between CO₂ and the mixed lithium-sodium 1,1,1,3,3,3-hexamethyldisilazide (HMDS) system, THF.Li(μ-HMDS)₂Na.2THF, reveals a remarkable carbamato-anhydride product, which retains both lithium and sodium in its polymeric chain structure.

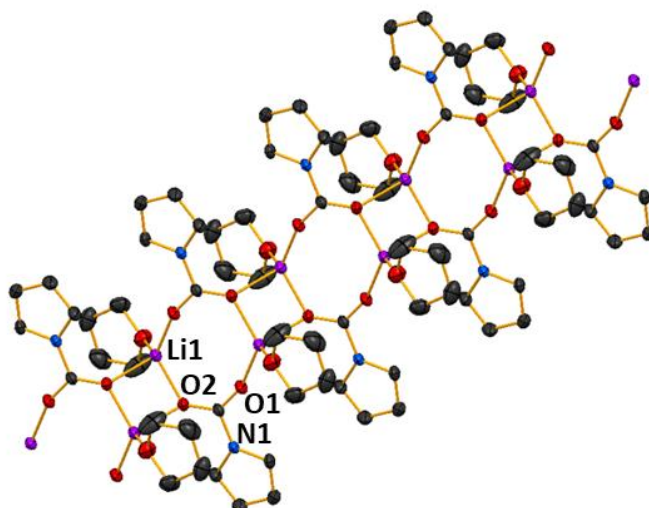
4.5 Results and Discussion

The lithium–nitrogen bonding in pyrrolyl lithium has recently been elucidated, and suggests that the insertion of CO₂ into lithium pyrrole should be possible.²⁶² To this end, pyrrole was reacted with ⁿBuLi in hexane at 0 °C, then CO₂ was bubbled through the resulting suspension for 30 minutes. Adding THF produced colourless crystals of the polymeric carbamate [{(THF).Li(CO₂NC₄H₄)}]_∞ (**10**) (Scheme 4.1), as determined by X-ray crystallography (Figure 4.21).



Scheme 4.1: CO₂ activation reactions carried out in this work.

Carbamate **10** adopts a polymeric ladder of alternating, fused 4-membered (LiO)₂ and 8-membered (LiO)₄ rings, with a THF donor ligand completing the Li coordination. The structure contains only one Li environment, confirmed both in the solid and solution state (See ESI).



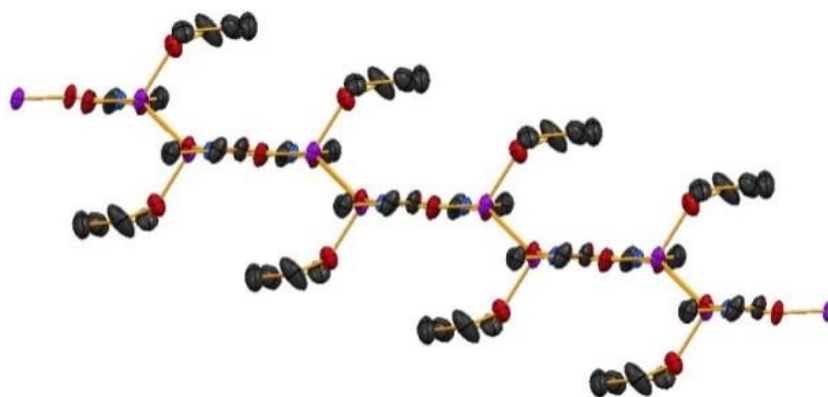


Figure 4.21: (Top) Threefold section of the polymeric structure of $[(\text{THF})\cdot\text{Li}(\text{CO}_2\text{NC}_4\text{H}_4)]_\infty$ (10**); and (bottom) step-ladder arrangement of its 8-atom rings. H atoms are omitted for clarity and thermal ellipsoids are displayed at 40% probability level. Symmetry transformations used to generate equivalent atoms: $-x$, $-y$, $-z$.**

This environment comprises four oxygen atoms in a distorted tetrahedron, three from the carbamate units and the fourth from THF. The mean Li-O-Li bond angle is 109° , ranging from $123.8(3)^\circ$ to $90.5(2)^\circ$ ($\tau_4 = 0.81$)¹²⁵. The $(\text{LiO})_2$ ring forms a near perfect square, with internal angles of $90.5(2)^\circ$ and $89.5(2)^\circ$ at Li and O respectively. Least squares planes through the 4- and 8-membered rings make a dihedral angle of 138° . Though ladder motifs are well known in lithium amide chemistry^{111, 263-266} to our knowledge this is the first such ladder motif found in lithium carbamate chemistry. The Li cation is μ_3 with respect to the carbamate oxygens (Li-O range 1.870(5)-2.020(6) Å) and is effectively equidistant between the carbamate O atom and THF O atom [Li1-O2 and Li1-O3 distance 1.943(5) vs 1.959(6) Å respectively]. The carbamate C-O distances are longer than those seen in the parent CO_2 molecule¹³⁸ and are intermediate between C-O single and double bonds. Robertson *et al.* probed the reaction products of CO_2 insertion into LiTMP observing a similar distance for the C-O bond as seen in **10** [values of 1.255(2) and 1.261(2) Å].¹⁵⁰ Snaith *et al.* also observed similar distances to those of **10** when studying CO_2 insertion products of diphenylamine, with values of 1.251(7)/1.256(7) Å for one carbamate unit and 1.264(7)/1.243(7) Å for the other.²⁴⁷ Due to the widespread nature of the five membered ring, it should come as no surprise to find that N- CO_2 based structural motifs such as that seen in polymeric **10** are present in a variety of biologically active compounds, which have found use as potential cyclotoxic antitumor agents to antiretroviral therapies.^{267, 268}

Next, we turned to LDA, the reactive Li-N bond present would be ideal for use in CO₂ activation presumably furnishing the corresponding lithium carbamate complex. To this end, diisopropylamine was deprotonated with ⁿBuLi in hexane, (PMDETA) N,N,N',N'',N''-pentamethyldiethylenetriamine was introduced and CO₂ was bubbled through this solution for 10 minutes. Cooling the resulting solution to -33 °C gave crystals identified as $[(i\text{Pr}_2\text{NCOOLi})_{12}(i\text{Pr}_2\text{NCOOH})_2]$ (**11**) (Scheme 4.1 and Figure 4.22) by X-ray crystallography.

The centrosymmetric structure of **11** is a discrete dodecanuclear cluster comprising 12 lithium diisopropylamido-carbamate units and two carbamic acids that occupy terminal positions. Note there is no PMDETA present in the structure, though subsequent experiments have shown that PMDETA addition is necessary in order to obtain crystals. The Li cations are bonded to three, four or five oxygen atoms, depending upon their position in the structure. Those bonded to three oxygen atoms (Li1) occupy a slightly distorted trigonal environment (average angle of 119 °). The four coordinate Li centres are all in a distorted tetrahedral environment, with τ_4 values ranging from 0.80-0.84 (Li2). There are two lithium centres in the molecule bonded to five oxygen atoms (Li3), both in a distorted square pyramidal molecular geometry (average bond angle of 94.7 °).

The two carbamic acid groups present at the terminal positions of the Li-O core presumably result from adventitious hydrolysis, likely due to the CO₂ source being dry ice. However, the reaction is reproducible, and the CO₂ is passed through a CaCl₂ drying tube prior to addition. This is a relatively rare example of such a feature, with only a few examples of carbamic acid groups structurally characterised.^{269, 270} In **11** the metallic core skeleton shows a distorted Li₄O₄ cubane that is linked to a perfect central Li₂O₂ planar square (all internal angles 90 °) *via* a μ -(O-N) bond. The corner oxygen atoms of the cubane are connected to the remaining Li of the Li₂O₂ square by a carbamate in a $\kappa\text{O};\kappa\text{O}^1$ bridging mode. The C-O distances in the carbamate units within the cubane section of **11** are consistent with those seen in **10**, with values generally in the range of 1.25-1.26 Å, again longer than in the parent CO₂ molecule.¹³⁸ The bridging carbamates have slightly different bond lengths, with one generally shorter than the other (1.235(4) vs 1.275(5) and 1.267(3) vs 1.288(3) Å), presumably due to the bridging nature.

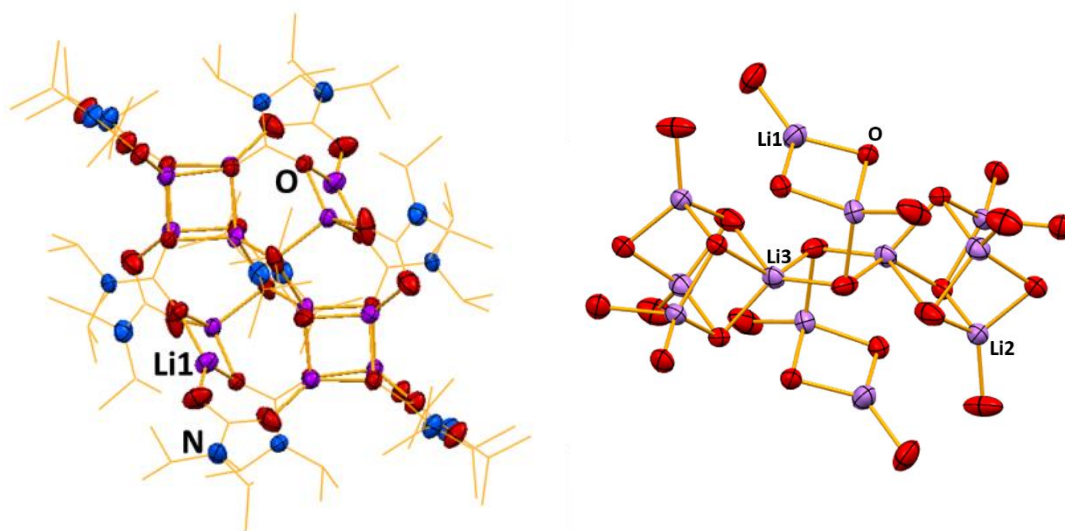


Figure 4.22: (Left) Molecular structure of $[(i\text{Pr}_2\text{NCOOLi})_{12}(i\text{Pr}_2\text{NCOOH})_2]$ (11). Hydrogen atoms are omitted and organic groups are shown as wire frame for clarity; (Right) structure of its Li-O core with organic groups omitted for clarity. Thermal ellipsoids are displayed at 40% probability level. Symmetry transformations used to generate equivalent atoms: $-x, -y, -z$.

The carbamic acid molecules have bond lengths that would be expected for a carboxylic acid derived species, with a C-O double bond of 1.227(3) Å and a C-OH single bond of 1.321(4) Å, though the OH group is not visible in either IR or NMR spectra, perhaps due to the lower number of such groups in comparison to the carbamate groups within the complex.

Diisopropylamide species have been used in CO₂ activation before, notably by Sperrle who obtained a hafnium carbamate complex.²⁷¹ Interestingly, the structure of this complex is simpler than the Li analogue here, having an 8-coordinate hafnium atom bound by four DA-derived carbamate units.²⁷¹

We next attempted to expand fixation of CO₂ into another major class of utility amide; namely those based on alkali metal HMDS compounds.²⁷² Previous studies have shown M-HMDS species are able to activate CO₂. Insertion into U-(HMDS)₄ is followed by a series of silyl migration steps, furnishing an isocyanate complex.²⁷³ The presence of an isocyanate is also implicated by Kemp *et al.*, who probed the insertion reactions of CO₂ into group two complexes based on a HMDS core.²⁷⁴ We wanted to probe the effects of CO₂ addition specifically on mixed alkali metal species, based on work carried out by Williard which disclosed the structures of these mixed alkali metal HMDS complexes to be dimeric.²³² As such, these species would be primed for CO₂ insertion in two distinct sites within the same molecule, between the Li-N bond and Na-N bond for example. However, to the best of our

knowledge it is exceptionally rare to generate a mixed alkali metal product from a mixed alkali metal starting material.^{275, 276}

To this end, a 1:1 NaHMDS:LiHMDS mixture was dissolved in THF, and then CO₂ was bubbled through it for 10 minutes at -78 °C. On warming to room temperature, a yellow solution formed. Cooling this solution to -33 °C deposited crystals, revealed by X-ray crystallography to be the unique lithium-sodium carbamate-anhydride polymer $[\{(Me_3Si)NC(=O)OC(=O)N(H)(SiMe_3)\}_2LiNa(THF)_4]_{\infty}$, (**12**) (Scheme 4.1 and Figure 4.23). Repeated attempts confirmed the reproducibility of this reaction with yields spanning the range 45-51 %. Disorder in THF and Me₃Si groups in **12** rules out a discussion of its bond angles and lengths though its molecular connectivity is unambiguous. Interestingly, when LiHMDS and NaHMDS were reacted separately with CO₂, only intractable gels were formed, implying the origin of **12** is synergistic.

The structure of **12** exists as an infinite chain of silylamido-substituted anhydride units held together by alternating Li and Na cations. The Li cations are four-coordinate in a distorted tetrahedral environment ($\tau_4=0.78$), each coordinated to four oxygens from two chelating anhydride molecules. The Na cations are six-coordinate, bonded to two oxygen and two nitrogen atoms from two individual anhydride units. The nitrogen and oxygen atoms are in the backbone of the anhydride, thus directing polymer formation. The Na coordination sphere is completed by two THF ligands. Therefore, the anhydride unit adopts a ditopic arrangement in terminally binding to Na through one O centre and chelating the Li through two oxygen centres on the opposite face.

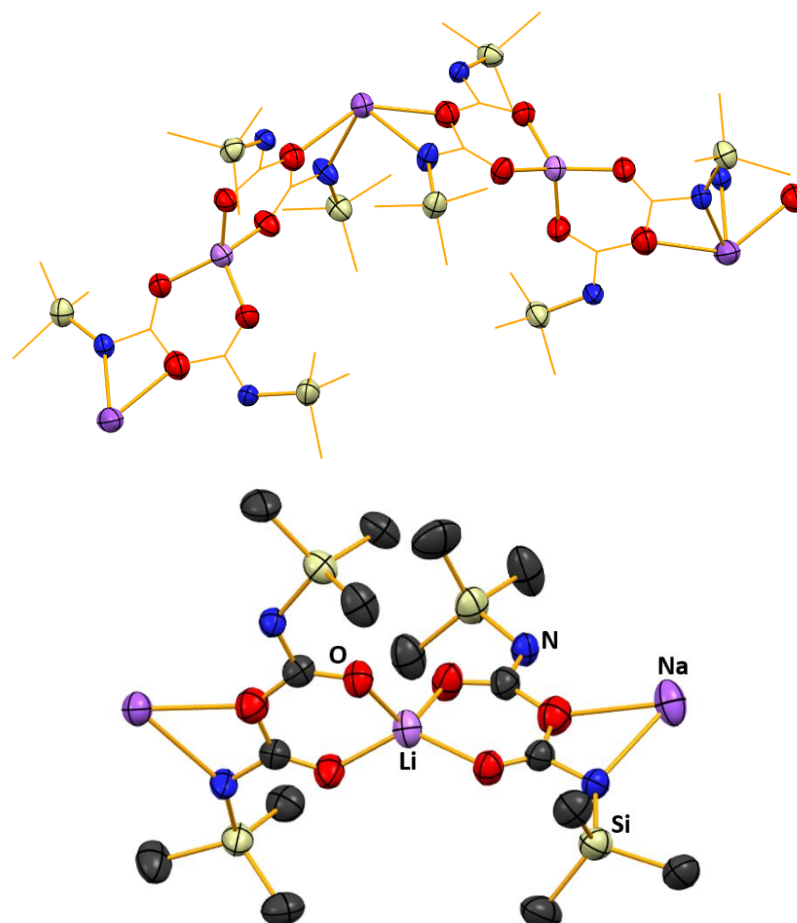


Figure 4.23: Section of the polymeric structure of alkali metal carbamato-anhydride $[\{(\text{Me}_3\text{Si})\text{NC}(=\text{O})\text{OC}(=\text{O})\text{N}(\text{H})(\text{SiMe}_3)_2\}\text{LiNa}(\text{THF})_4]$ (**12**). H atoms and THF molecules are omitted for clarity and organic fragment drawn as wire frame for clarity; the bottom image also has non-carbamate carbon atoms omitted for clarity. Thermal ellipsoids are displayed at 40% probability level. Symmetry transformations used to generate equivalent atoms: $-x, y, -z$; $\frac{1}{2}+x, \frac{1}{2}+y, z$; $\frac{1}{2}-x, \frac{1}{2}+y, -z$.

Given the unexpected nature of **12**, a literature search was done which found no evidence for crystallographically characterised alkali metal anhydrides. However, CO_2 has previously been used in the synthesis of an anhydride derived compound, namely hexahydro-4,7-dimethyl-1-oxatetrazonine-2,9-dione.²⁷⁷ The synthesis involved the addition of CO_2 to either a mixture of the parent dihydrazine and $\text{HN}(\text{SiMe}_3)_2$ or directly reacting CO_2 with the corresponding disilane.²⁷⁷

Based on the stoichiometry of **12**, it appears that two trimethylsilyl units and one oxygen atom has been lost from the reaction, which also shows the formation of a new NH group. As for how compound **12** may have formed, Maron and Mazzanti investigated the conversion

of CO₂ to isocyanates at uranium centres, postulating that multiple N-Si bond cleavage reactions occurred, leading to the release of hexamethyldisiloxane.²⁷³ This could be a potential pathway in this reaction, explaining the loss of both the oxygen atom and the silylamido groups. The NH group present within the polymer backbone could have been formed either through adventitious hydrolysis or the presence of some HMDS(H) within the reaction. In any case, the anhydride can also be isolated in its hydrolysed form using H₂O work-up, with the parent compound featuring two NH groups in the backbone.

In conclusion, we have demonstrated that common utility alkali metal amides can be utilised in CO₂ insertion reactions, providing a route to the formation of alkali metal carbamate species. Through judicious choice of amide, differing molecular architectures can be obtained, ranging from polymeric through to discrete species. A novel alkali metal anhydride species is also presented through the activation of CO₂, revealing an exceptionally rare reaction where a mixed lithium-sodium precursor produces a mixed lithium-sodium product, itself a rare example of a heterobimetallic alkali metal polymer.

4.6 Extended Discussion and Future Work

Our initial interest in CO₂ chemistry stemmed from the possibility of developing a simple alternative route to carboxylate chemistry. As discussed in Chapters 1 and 2, it is exceptionally difficult to obtain crystalline examples of long chain carboxylates. Given this difficulty, it was decided to explore alternative ways of producing said carboxylates with the use of gaseous CO₂. It was reasoned that this greenhouse gas could insert into these reactive compounds and would thus produce lithium carboxylates. A search of the literature revealed that CO₂ has previously been combined with ⁿBuLi and other organolithium reagents in order to produce carboxylic acids post workup.²⁷⁸⁻²⁸⁰ This opened up the possibility of isolating lithium carboxylates pre-workup and characterising them to ascertain their structure. As a proof of concept, the focus of initial efforts was on shorter chain examples of organolithiums, in view of both the difficulty experienced getting longer chain analogues to crystallise and the commercial availability of short chain organolithium compounds. This methodology could also be expanded to short chain sodium compounds, *via* transmetallation of short chain organolithium compounds with NaO^tBu. To this end, the organolithium compound investigated was *n*-propyllithium, with the addition of CO₂ hopefully furnishing lithium butanoate. *n*-Propyllithium was therefore added to a Schlenk tube containing hexane solvent

and subsequently cooled to -50 °C. This had CO₂ bubbled through it *via* dry ice from an adjacent Schlenk tube, forming a white precipitate. This mixture was warmed to room temperature and the solvent removed *in vacuo* to leave behind a white powdery residue, initially analysed by ¹H NMR spectroscopy. Due to the insolubility of the sample in non-polar solvents, this had to be carried out in deuterated methanol, which revealed three sets of resonances characteristic of the successful formation of lithium butanoate. In order to confirm this definitively, a ¹H DOSY NMR spectroscopic study was carried out using naphthalene as an internal standard (Figure 4.24). This would allow a molecular weight to be determined for the species in solution, which should confirm that the CO₂ had inserted to form the lithium butanoate. Shown in Figure 4.24 is the ¹H DOSY spectrum of the sample.

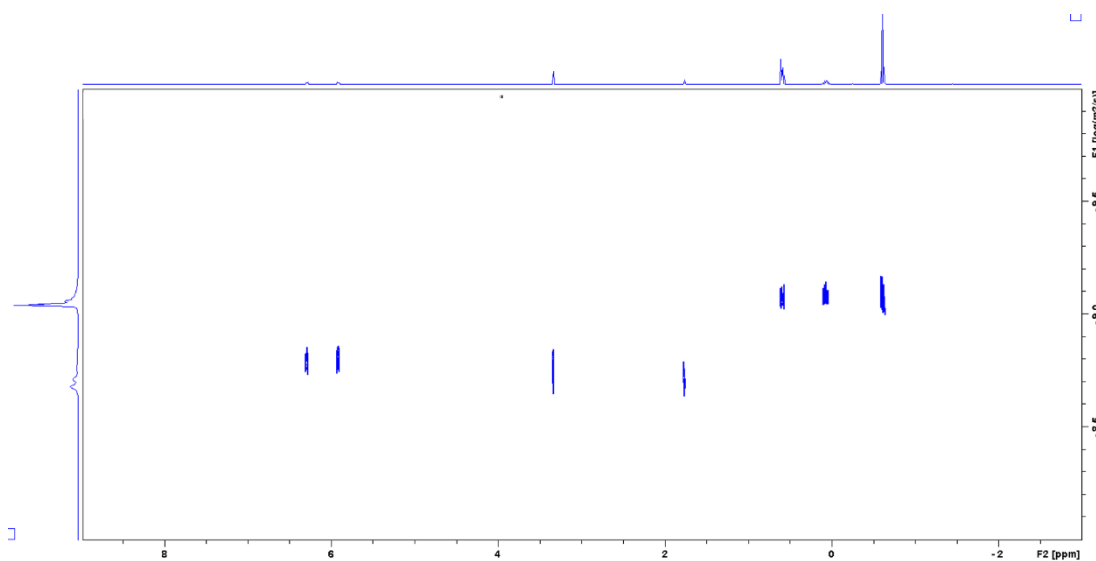


Figure 4.24 ¹H DOSY NMR spectrum of lithium butanoate powder in MeOD.

As can be seen, there is only one major species within the solution, discounting the solvent and the internal standard resonances. The diffusion coefficient for this species was calculated as $8.775 \times 10^{-10} \text{ m}^2/\text{s}$, corresponding to a log value of -9.0568 m²/s. Using the software made available by Stalke *et al.*⁹⁰ and in conjunction with the log value of -8.7719 m²/s for the naphthalene standard, the predicted molecular weight of the species in solution is determined to be 306 g/mol. This is too large to simply be monomeric lithium butanoate, which would only have a molecular weight of 94.04 g/mol. However, on the evidence of the results obtained in Chapter 2.4, where it was established alkali metal carboxylates dimerise in the presence of polar solvents, a dimeric lithium butanoate species with four solvating methanol molecules (two on each lithium centre) $[(\text{C}_5\text{H}_{10})(\text{C}_2\text{H}_5)\text{COOLi}(\text{MeOH})_2]_2$ gives a

molecular weight of 316.24 g/mol. There is only a 3 % difference between this calculated molecular weight and the molecular weight determined in the ^1H DOSY experiment. In contrast to the dimers predicted previously, the lithium butanoate is likely not solvated with water. Replacing the solvating methanol with water reduces the calculated molecular weight to only 260 g/mol, giving an error of -15 %, which is outside the error limits for the software. This can be explained in that in this instance the reagents were completely moisture free, being dry ice and propyllithium. In the previous examples, the alkali metal source was sodium hydroxide, which would react with the acids of interest to produce sodium carboxylate and water, with the latter then solvating the sodium carboxylate. In the case of lithium butanoate, the only polar solvent able to solvate the alkali metal is the methanol, hence the structure predicted by the DOSY experiment.

It was next decided to extend such CO_2 capture chemistry to organosodium compounds to ascertain whether similar structures could be formed. To this end, propylsodium was synthesised *in situ* from the reaction of propyllithium and NaO^tBu in hexane. This was isolated by filtration and subsequently suspended in hexane. To this was added CO_2 at $-50\text{ }^\circ\text{C}$, forming a thicker suspension when compared to the sodium propanoate starting material. The solvent was removed *in vacuo* and the isolated solid analysed by ^1H NMR spectroscopy. Again, due to insolubility in non-polar solvents this was carried out in MeOD. The ^1H NMR spectrum showed resonances associated with the successful formation of sodium butanoate, which indicated successful CO_2 insertion into the parent organosodium species, with the triplet at 2.18 ppm indicative of the CH_2 group adjacent to the carboxylate functionality of the sodium butanoate. In order to gain more insight into the structures adopted by this alkali metal carboxylate species in the solution, a ^1H DOSY NMR study was carried out. The spectrum (Figure 4.25) shows there is again only one major species in the solution, excluding internal standard, solvent and grease resonances.

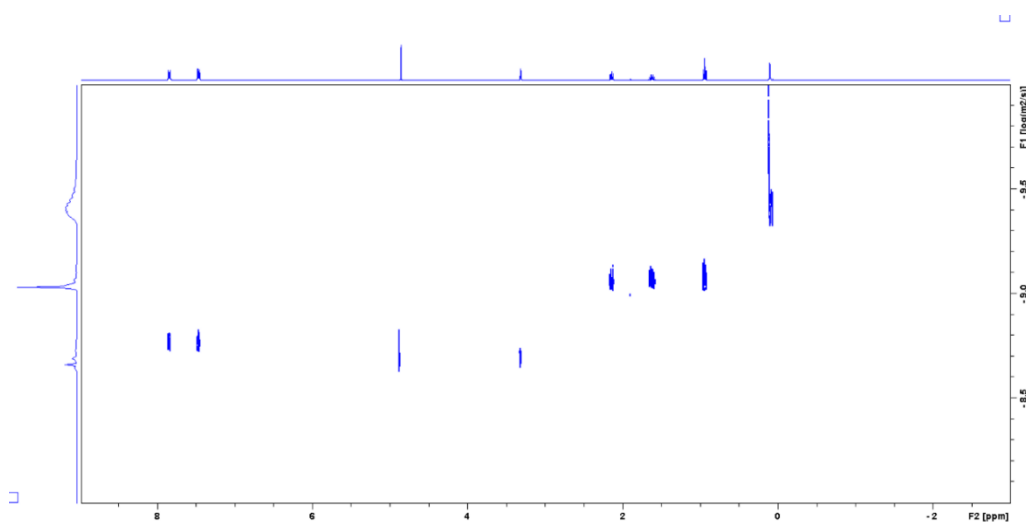


Figure 4.25: ^1H DOSY NMR spectrum of sodium butanoate powder in MeOD.

When calculating the diffusion coefficient of the sodium butanoate species, a value of $9.090 \times 10^{-10} \text{ m}^2/\text{s}$ is obtained, corresponding to a log value of $-9.0414 \text{ m}^2/\text{s}$. Using the software as previously described,⁹⁰ a molecular weight of 307 g/mol is determined. This is again too large for a simple monomeric sodium butanoate, which would only have a value of 110 g/mol. However, upon considering a monomeric sodium butanoate with six solvating methanol molecules a molecular weight of 302 g/mol is determined. This is within the error limits of the software ($\sim 2\%$ discrepancy between calculated and determined molecular weight). This suggests that in contrast to the result obtained with lithium butanoate, sodium butanoate remains in monomeric form. This can be explained through the greater coordination sphere of sodium compared to lithium, which would allow for an increased number of solvating methanol molecules around the sodium centre. These results provide strong further evidence for either the dimerisation or complete solvation of short chain alkali metal carboxylates in polar solvents.

With these results in hand, we pondered whether CO_2 could successfully be inserted into reactive Li-N bonds. Successful insertion into such species would result in the formation of lithium carbamates, with the insertion of CO_2 a simple and relatively cheap way to synthesise such species. If they could be crystallographically characterised this would also be a positive, given the paucity of literature on structurally defined examples of alkali metal carbamate complexes. This led to the results obtained in the previous chapter, some of which are discussed in more depth below.

Considering $[(i\text{Pr}_2\text{NCOOLi})_{12}(i\text{Pr}_2\text{NCOOH})_2]$ (Figure 4.22, page 124) it is clear that there is a greater degree of complexity present compared to just a simple insertion of CO_2 into the Li-N bond of LDA to form a diisopropylamide based carbamate, which may have been expected. This complexity can be seen in the ^7Li NMR spectroscopic studies carried out, with the room temperature ^7Li spectrum showing a broad resonance between 0.41 and 0.62 ppm. The broadness of this signal suggests that there are multiple lithium environments within the solution state, which would agree with the solid-state structure, which shows five lithium coordination environments. To attempt to gain some more detailed insight into the solution state behaviour, a variable temperature ^7Li NMR spectroscopic study was carried out. Upon heating the sample from room temperature to 75 °C, this broad signal showed some resolution, with three distinct resonances appearing at 0.58 ppm, 0.45 ppm and 0.36 ppm visible. This result more accurately reflects the various lithium environments within the structure of **11**. There is still some broadness within the spectra, though presumably this is due to being unable to heat the sample any further as well as the fact that there are several lithium centres contributing to each resonance. Figure 4.26 shows the ^7Li NMR spectrum of the sample at room temperature and that at 75 °C.

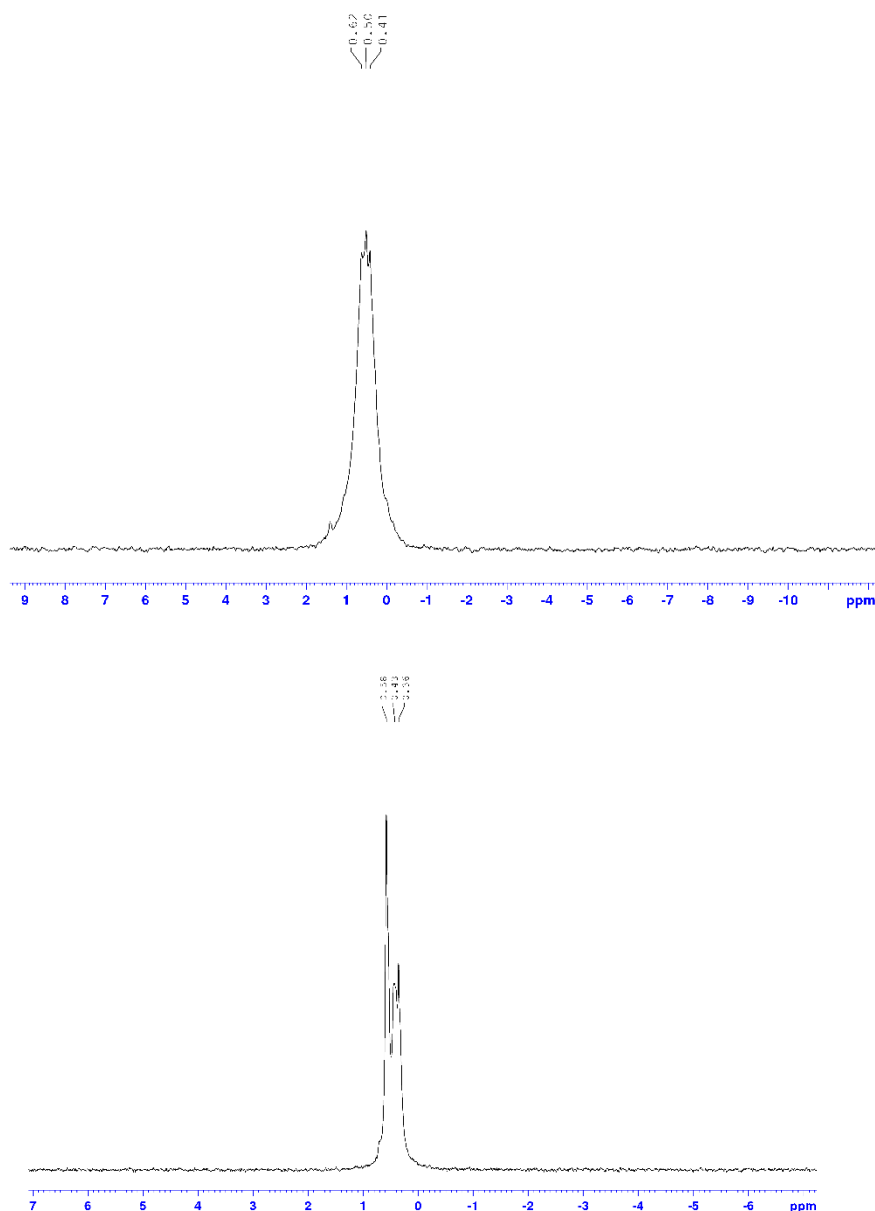


Figure 4.26: (Top) ^7Li NMR spectrum of $\{[(i\text{Pr}_2\text{NCOOLi})_{12}(i\text{Pr}_2\text{NCOOH})_2]\}$ at 300 K and (Bottom) that recorded at 350 K in d_8 -toluene.

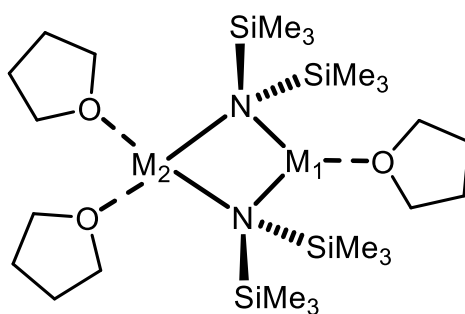
In terms of **12**, the carbamate-anhydride $\{[(\text{Me}_3\text{Si})\text{NC}(=\text{O})\text{OC}(=\text{O})\text{N}(\text{H})(\text{SiMe}_3)]_2\text{LiNa}(\text{THF})_4\}_\infty$ (Figure 4.23, page 126) it is of interest that this is a bimetallic product obtained from bimetallic starting materials. These starting materials are specifically mixed alkali metal HMDS complexes, first reported by Williard and Nichols in 1991.²³² The pairings obtained were Li and Na, Li and K, and finally Na and K, all of general composition $[\text{THF} \cdot \text{M}_1(\mu\text{-HMDS})_2\text{M}_2 \cdot 2\text{THF}]$, where M_1 is the smaller alkali metal and M_2 is the larger alkali metal, which

is different to the structural motifs observed for the monometallic HMDS complexes discussed in Chapter 4.2.2 previously.²³² Each species adopts a four-membered ring conformation, with two HMDS bridges and terminal THF molecules. The central four-membered ring is distorted when compared to the symmetrical four-membered ring seen in the parent Li and K HMDS complexes. This is due to the different metal sizes contained within each complex. The four-membered rings within each pairing are planar, with all endocyclic angles totalling 360°. The larger of the metals will be solvated by two THF molecules, while the smaller metal will be solvated with only one. This is due to the sterics of the complex, with the larger metal inducing longer metal-nitrogen bonds to the bridging HMDS units. This in turn induces the Me₃Si to move closer to the smaller metal in order to maintain tetrahedral geometry at the nitrogen centres, meaning the smaller metal is more sterically protected and hence can only be solvated by a single THF ligand, while the larger metal has less steric bulk around it and can therefore be solvated by two THF molecules.²¹⁵

Table 4.0: Comparison of bond lengths and angles in heterobimetallic HMDS complexes

Metal combination within complex	Bond distances (Å)			
	M ₁ -N	M ₂ -N	M ₁ -O	M ₂ -O
M ₁ /M ₂				
Li/Na	2.024(6)	2.509(4)	1.964(9)	2.433(3)
Li/K	2.053(5)	2.832(3)	1.926(9)	2.689(3)
Na/K	2.365(3)	2.810(3)	2.292(3)	2.709(3)

Metal combination within complex	Bond angles (°)			
	N-M ₁ -N	M ₁ -N-M ₂	N-M ₂ -N	M ₂ -N-M ₁
M ₁ /M ₂				
Li/Na	116.6	78.4	86.7	78.4
Li/K	119.6	81.5	77.54	81.5
Na/K	109.7	81.8	86.68	81.8



Scheme 4.2: General structure adopted by heterobimetallic HMDS complexes, showing the distortion within the central four-membered ring.

In contrast to the result obtained with the bimetallic complexes above, when attempting the CO₂ insertion reactions with homometallic HMDS complexes, no crystals were ever obtained. Indeed, no solutions were ever formed in these reactions post CO₂ addition. Dissolving the individual HMDS alkali metal complexes in THF led to the formation of yellow solutions initially, however the addition of CO₂, even at low temperatures, led to the formation of an intractable gelatinous material.

This material proved to be impossible to solubilise or analyse in any way. Despite these pitfalls, forming the Li/Na heterometallic complex *in situ* and bubbling through CO₂ at low temperatures did not form such an intractable material, instead the solution became only slightly more turbid.

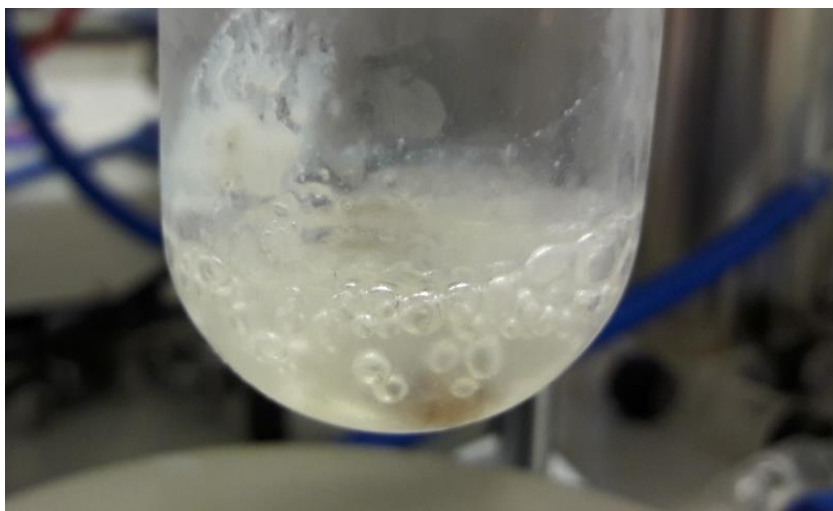
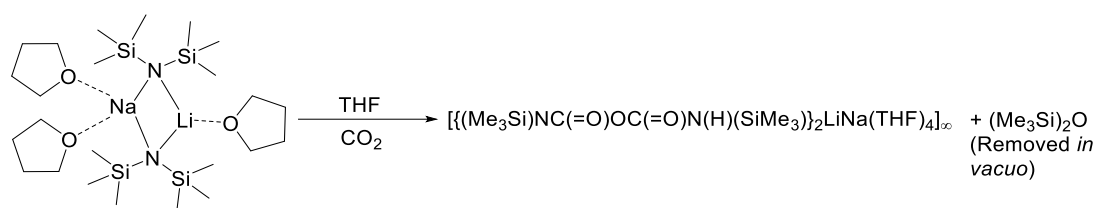


Figure 4.27: Image showing gelatinous material formed when CO₂ is bubbled through a solution of LiHMDS in THF.

This implies that the origin of **12** could be synergistic, in that when the individual components of the starting materials are reacted with CO₂, no reaction takes place, while exposing the heterobimetallic analogue to CO₂ results in the formation of a polymeric carbamato-anhydride. This is one of the few instances to the best of our knowledge when a heterobimetallic starting material leads to a heterobimetallic product. While the exact mechanism by which this product forms is unknown, presumably the two equivalents of CO₂ reacts with the bimetallic HMDS species and forms the polymeric product, with concomitant formation of (Me₃Si)₂O, which presumably is so volatile it is removed from the reaction upon concentration of the solution.



Scheme 4.3: Formation of heterobimetallic product 3, with concomitant formation of (Me₃Si)₂O.

Chapter 5: Backbone Reactivity of Lithium β -Diketimate (NacNac) Complexes with CO₂, tBuNCO and iPrNCO

This chapter is based on a published article:

Chemistry A European Journal, 2019, **25**, 14728-14734

Putting the results into context with the literature an extended introduction, discussion and conclusion to the paper are provided.

Contributing authors to the manuscript and their roles

Richard M. Gauld- Designed and performed the experiments; analysed the data; drafted the manuscript

Ross McLellan- Helped with the data processing; contributed to the drafting of the manuscript

Alan R. Kennedy- Checked the accuracy of X-ray diffraction data processing

Jim Barker- Industrial collaborator

Jacqueline Reid- Industrial collaborator

Robert E. Mulvey- Principal investigator

The supporting information can be found in Chapter 7: Experimental; Section 7.4 and Tables 7.5.4 and 7.5.5

5.1 Abstract

Though alkali metal NacNac (β -diketiminate) complexes have been utilised in synthesis as NacNac-transfer agents, studies of them in their own right with small molecules are exceptionally rare. Here, the lithium compound of the common 2,6-diisopropylphenyl- β -methyldiketiminato [NacNac(Dipp, Me)] ligand is investigated with carbon dioxide and isocyanates. In all four cases studied reaction occurs at the backbone γ -C atom of the NacNac ligand, which redistributes electronically into a diimine. Insertion of CO_2 gives an eight-atom carboxylate ($\text{Li}_2\text{O}_4\text{C}_2$) ring at the γ -C site in a dimer. Insertion of tBuNCO gives a secondary amide at the γ -C site in a monomer with TMEDA chelating lithium. Double insertion of tBuNCO and (adventitious) oxygen gives a dimer with a $(\text{LiO})_2$ central core involving the latter source. Insertion of less bulky (iPrNCO) gives a dimer with dimerisation through the $\text{C}=\text{O}$ bonds of the emergent secondary amide function.

5.2 Introduction

As can be seen from Chapter 3.2, the NacNac ligand is in demand in several areas of modern chemistry. Despite the widespread use of LiNacNac as a NacNac transfer agent, and its burgeoning use in catalysis as an alternative to d-block metal NacNac complexes for some processes,²⁸¹ there is a lacuna within the literature on its ability to react with small molecules such as CO_2 and isocyanates. To this end, it was decided to attempt the reaction of a common LiNacNac ligand with a series of small molecules in order to ascertain the outcomes of reactions and where appropriate to determine what structures such products would adopt in the crystal state. Potentially this could open avenues towards the possibility of establishing cheap and easy ways of obtaining functionalised NacNac ligands, which in turn may bring new reactivities and new properties in the field of catalysis.

5.3 Project aims

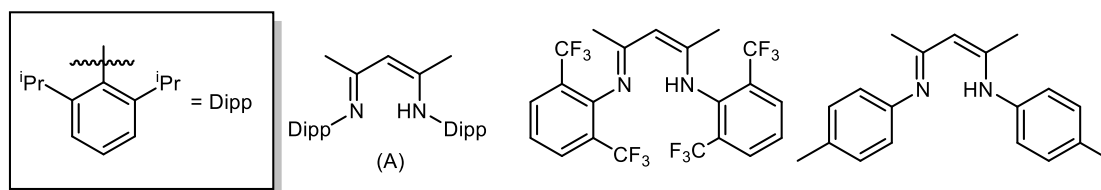
As discussed within previous chapters, there is a lack of previous research into the reactions of CO_2 and other small molecules towards commonly used alkali metal NacNac complexes. Such reactions were anticipated to occur selectively at the polar alkali metal-nitrogen bond

present within such systems, with the products potentially amenable to be worked up into some sort of functionalised NacNac. To this end the overall aims of this project were to:

- Document examples of insertion reactions involving CO₂ and the commonly used transfer agent LiNacNac, exploring any effects introduced by a variety of donor additives and other heavier alkali metals.
- Further develop this concept by extending the investigation to other small molecules, notably isocyanates, which while isoelectronic to CO₂ could provide different reaction outcomes.
- Expand to a wider scope of potential electrophiles, to determine whether the reactivity obtained using CO₂ and isocyanates is shared by other electrophiles.

5.4 Introduction from the manuscript

Now well established in the premier league of ligands,^{171, 282} β -diketiminate (BDI or NacNac) molecules exhibit a wide ranging chemistry, with extensive applications spanning the main group, transition metal and lanthanide blocks of the periodic table.²⁸³⁻²⁸⁵ The NacNac class of ligands are distinguished by a highly versatile structure capable of supporting metal ions in a number of oxidation states and chemical environments.^{175, 286} This versatility, reviewed by Lappert in 2002,¹⁶⁹ is a consequence of the huge variation that can be introduced into the system *via* changing the pendent groups attached to the NCCCN backbone, with varying degrees of steric bulk and electronic effects able to be implanted in this way.



Scheme 5.0: Selection of common NacNac(H) proligands previously utilised in synthesis.

A simple procedure for the high yielding synthesis of the parent NacNac(H) proligand was developed in 2001 by Power *et al.*, who also synthesised and characterised the deprotonated lithium salts, either unsolvated or solvated with THF or Et₂O.¹⁷² Other examples of s-block complexes featuring the NacNac ligand include NacNacMgⁿBu utilised by Hill *et al.* in catalytic and insertion reactions^{187, 188} and NacNacMgTMP (TMP is 2,2,6,6-tetramethylpiperidide)

synthesised by Hevia *et al.*^{189, 190} Both complexes have been structurally characterised and their reactivity probed, with the latter complex being a stronger base, showing proficiency in C-H deprotonation reactions. The former meanwhile is proficient in C-F activation reactions, as well as exhibiting catalytic activity in hydroboration reactions of internal and terminal alkynes.^{190, 287} In deprotonation reactions the NacNac ligand is not involved directly in the metallation (C-H to C-M transformation) step, but its role as a bulky ligand is to help magnesium trap and stabilise the emergent anions.¹⁹⁰

Other examples of NacNac complexes have been synthesised and crystallographically characterised containing metals from across the periodic table, including aluminium,²⁸⁸ scandium^{289, 290} and, magnesium examples other than those above.^{185, 197, 291} The magnesium complexes exhibit remarkably diverse reactivity, spanning cycloaddition reactions, deprotonation reactions and addition reactions of alkynes to the backbone NacNac γ -carbon atom. They can also display interesting coordination modes, for example, η^3 coordination to toluene and benzene.^{198, 291} Aluminium NacNac species have also been shown to engage in fixing small molecules such as white phosphorus and sulfur,²⁸⁸ and can react with elemental oxygen to form alkyl(alkoxy)aluminium complexes, or aluminium oxide species.^{292, 293}

In many of these examples, the NacNac ligand is utilised as a protective scaffold upon which the reactive centre of the complex rests. However, the NacNac ligand does not always act as an inert sterically bulky spectator, with some studies reporting decomposition products, redox non-innocence and cooperative activity between metal complexes and substrates.¹⁷⁰ Germane to the present study, in 2012 Piers *et al.*²⁹⁴ exposed a scandium NacNac complex to an excess of CO₂, resulting in a dimeric scandium carboxylate wherein the CO₂ addition occurred at the central carbon atom of the NacNac backbone, as evidenced by ¹³C NMR spectroscopic investigations using ¹³CO₂.

Recently our group joined the growing number of scientists interested in the field of CO₂ activation/fixation chemistry. Despite the many studies probing CO₂ fixation, we noted how few considered the insertion of CO₂ into reactive Li-N bonds,^{247, 256} even though such bonds are found in synthetically important lithium (and sodium) amide reagents. Our study showed that reaction between a series of common utility metal amides and CO₂ resulted in insertion into the M-N bonds affording a range of new metal carbamate complexes with interesting structural motifs (polymeric ladders, carbamate anhydride mixed sodium lithium polymers).⁷⁸ Inspired by this study, we decided to expand our efforts into researching the

popular NacNac ligand, to examine the effects of CO₂ fixation on their lithium derivatives, anticipating CO₂ insertion into the reactive N-Li bonds present in these species. The fact that alkali metal complexes are agents supreme for transferring the NacNac anion,²⁹⁵⁻²⁹⁷ and numerous other ligands, adds an extra incentive for elaborating fully the chemistry of alkali metal NacNac complexes. Reported herein are our results focusing on the fixation of small molecules with lithium NacNac complexes of the commonly studied 2,6-diisopropylphenyl-β-methyldiketimate [NacNac(Dipp, Me) or (DIPPBDI) **A** Scheme 5.0]. A novel lithium β-diimine based dimer, where CO₂ is inserted into the backbone of the NacNac ligand is reported. Surprisingly to the best of our knowledge this is first such crystallographically characterised backbone insertion of CO₂ with an alkali metal NacNac salt. Extension of small molecules used to isocyanates, results in a series of backbone fixated products featuring dual imine and amide functionality, providing straightforward access to potentially useful ditopic ligands.

5.5 Results and Discussion

The parent NacNac(H) proligand **A** was synthesised as per the literature procedure.¹⁷² Following isolation, the proligand was reacted with *n*-butyllithium in hexane at 0 °C, generating *in situ* the lithium NacNac complex. The common chelating donor *N, N, N', N'*-tetramethylethylenediamine (TMEDA) was then added to the suspension resulting in a dark solution. CO₂ was then bubbled through the mixture for 30 minutes and the resulting solution concentrated and cooled to -20 °C, resulting in the formation of colourless crystals of the dimeric product [$\{(\text{MeCN-2,6-}i\text{Pr}_2\text{C}_6\text{H}_3)_2\text{CH}(\text{CO}_2)\}\text{Li.TMEDA}\}_2$] in 46% yield (**13**). Determined by X-ray crystallography, the centrosymmetric structure of **13** is composed of deprotonated NacNac units, linked by the backbone of the NacNac framework, *via* an eight-membered carboxylate (Li₂O₄C₂) ring (Figure 5.0). The single lithium environment present in the solid-state structure is further confirmed in solution state NMR studies (see ESI for details).

The lithium centre is four coordinate, bonded to two oxygens from the carboxylate unit and two TMEDA nitrogen atoms in a distorted tetrahedral environment, with bond angles ranging from 84.6(2)° to 127.0(3)°. The level of distortion can be quantified by the parameter τ_4 introduced by Houser *et al.*¹²⁵ In **13** $\tau_4 = 0.84$ (a value of 1 relates to a perfect tetrahedral geometry and 0 to a square-planar geometry). The lithium centre is bonded to an oxygen from each symmetry equivalent carboxylate unit [Li-O₁ 1.867(7) Å; Li-O₂' 1.923(5) Å]. C-O bond distances in the carboxylate unit are elongated compared to those in the parent CO₂

molecule (1.1615 Å),¹³⁸ indicating significant π -delocalisation within the CO₂ moiety [C₃₀-O₁ and C₃₀-O₂ distances are 1.245(4) and 1.250(4) Å respectively]. Such elongation of C-O bonds has been observed in several studies of carboxylates, all of which contained bonds of similar length to those in **13**.²⁹⁸⁻³⁰⁰

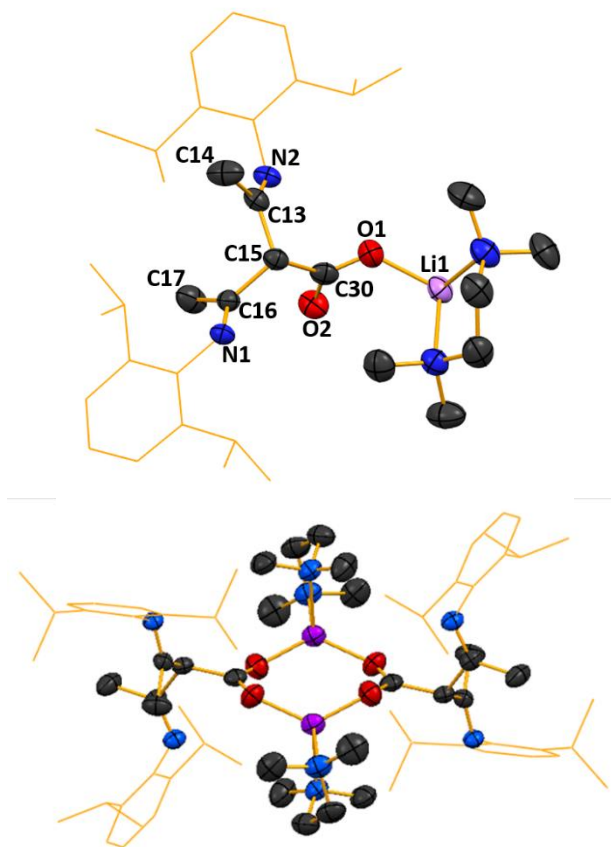


Figure 5.0: Top: Molecular structure of the asymmetric unit of $\{[(\text{MeCN-2,6-}i\text{Pr}_2\text{C}_6\text{H}_3)_2\text{CH}(\text{CO}_2)]\text{Li.TMEDA}\}_2$ (13**) with key atoms labelled; and bottom: Dimeric structure of (**1**). Hydrogen atoms are omitted and the NacNac Dipp groups are shown as wire frame for clarity. Thermal ellipsoids are displayed at 40% probability level. Symmetry transformations used to generate equivalent atoms: $-x, -y, -z$.**

Of special interest in **13** is the fact that the CO₂ does not insert into the seemingly more reactive Li-N bond present in the alkali metal complex, instead redistributing to the NacNac backbone and forming a new carbon-carbon bond, providing on one hand carboxylate functionality in the backbone at the γ -carbon position, and on the other hand diimine (C=N) functionality in the main body of the NacNac ligand (Figure 5.1). The presence of the imine components were confirmed in the solid state *via* the C-N bond lengths [C₁₃-N₂, 1.268(3) Å and C₁₆-N₁, 1.269(3) Å] which compare favourably with the average C-N bond lengths in imines of 1.279 Å (Table 5.0).³⁰¹ The carboxylate functionality is detectable in ¹³C NMR

experiments, with the central carboxylate carbon resonance at 170 ppm. IR spectroscopy confirms the symmetrical carboxylate stretching and imine C=N stretching at 1636 and 1591 cm^{-1} respectively. The NacNac ligand itself is also heavily distorted in this structure relative to the parent amine or lithium salt, presumably a consequence of the loss of resonance across the NCCCN unit compared with the parent ligand. For example, in **A** the methyl groups lie 2.50 Å from the γ -carbon, whereas in **13** the methyl groups are elongated ($[\text{C}_{15}\text{-C}_{17}]$ 2.577(5) Å and $\text{C}_{15}\text{-C}_{14}$ 2.560(5) Å]. The $\text{N}_1\cdots\text{N}_2$ separation distance also shows a marked distinction, being 2.685(3) Å in the parent amine, compared to 4.513(3) Å in **13**, a consequence both of the loss of conjugation and a lack of lithium with which to bond. Further, the bond angles in the NacNac backbone, of $\text{C}_{13}\text{-C}_{15}\text{-C}_{16}$ narrow in **13** [112.6(3)° compared to 125.9(3)° in the parent NacNac(H)].

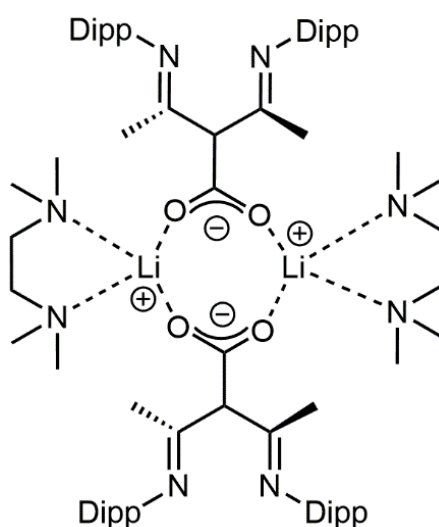


Figure 5.1: ChemDraw representation of the structure of $[(\text{MeCN-2,6-iPr}_2\text{C}_6\text{H}_3)_2\text{CH}(\text{CO}_2)]\text{Li.TMEDA}]_2$ (13**) showing the diimine conformation.**

To the best of our knowledge this is the first example of backbone attack on CO_2 using an alkali metal NacNac complex, despite the widespread synthetic utilisation of such complexes. The most relevant related study is that carried out by Hayton *et al.* probing the fixation of CS_2 via a bimetallic nickel-potassium complex, resulting in redistribution of the CS_2 unit to the backbone of the NacNac ligand.³⁰² In **13** the redistribution of CO_2 to the γ position can be considered as a nucleophilic attack on the electrophilic CO_2 carbon by the anionic NacNac ligand. Supporting this reactivity, theoretical calculations on the NacNac anion have demonstrated that there is significant electron density located at the γ -carbon.³⁰³ Arnold reported that while the negative charge is effectively delocalised over the NCCCN part of the

anion, the HOMO and HOMO-1 are located at the α -nitrogen and γ -carbon respectively, which bestows them with nucleophilic properties.¹⁷⁰ This reactivity facet has been utilised by a number of groups in the synthesis of related functionalised NacNac species. Examples include the CO₂ fixation by a scandium complex reported by Piers,²⁹⁴ and Erker's attachment of a nitrile to γ -carbon position following an initial deprotonation reaction.^{304, 305} Harder has recently unveiled a new variation of the DIPPBDI ligand which has been termed DIPPDPM, based upon a related dipyrromethene scaffold.³⁰⁶ In contrast to the negatively charged central backbone carbon found in DIPPBDI offering nucleophilic reactivity, that in DIPPDPM is effectively neutral. This makes it a less nucleophilic and less Brønsted basic molecule, as appropriate for a true spectator ligand.³⁰⁶

Next, we extended our studies to another class of small molecule, namely isocyanates. This seemed a pertinent choice given recent work by Ma *et al.* that explored the activation of small molecules, including isothiocyanates, by a magnesium alkyl NacNac complex.³⁰⁷ We decided to focus our efforts on the isoelectronic isocyanates since these compounds have a similar bonding situation to that in carbon dioxide, with the synthetic advantage that exact stoichiometric amounts of the liquid isocyanates can be easily added to reactions. Insertion of isocyanates into s-block metal complexes is known,^{308, 309} albeit a systematic investigation of isocyanate fixation using lithium NacNac complexes is required to investigate chemoselectivity of such a process.

With this in mind, the parent NacNac(H) ligand was deprotonated using *n*-butyllithium in hexane at 0 °C. To this mixture was added TMEDA, followed by tert-butyliisocyanate (*t*-BuNCO), giving a green suspension. This mixture was heated at reflux for one hour, forming a dark brown solution. Concentrating this solution and cooling at -30 °C, gave colourless crystals of the isocyanate insertion product $[(\text{MeCN-2,6-}i\text{Pr}_2\text{C}_6\text{H}_3)_2\text{C}(\text{CONH}(t\text{-Bu}))]\text{Li.TMEDA}$ (**14**) in 48% isolated yield. Interestingly, in this reaction we did not observe any isocyanate trimerization, which is somewhat surprising given that lithium amides are known to facilitate this process.³¹⁰

X-ray crystallography determined the monomeric arrangement of **14** (Figure 5.2) comprising a deprotonated NacNac scaffold with *t*-BuNCO inserted into the backbone γ -C-H bond to form a new carbon-carbon bond.

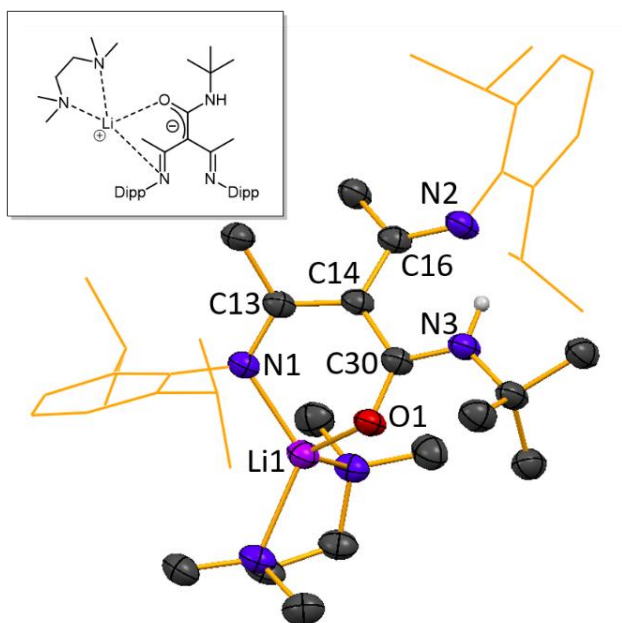
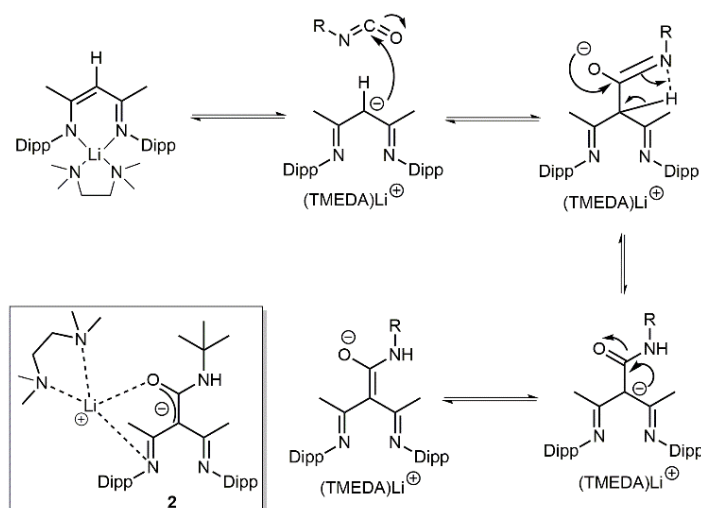


Figure 5.2: Molecular structure of $\{[(\text{MeCN-2,6-}i\text{Pr}_2\text{C}_6\text{H}_3)_2\text{C}(\text{CONH}(t\text{-Bu}))]\text{Li.TMEDA}\}$ (14**) with key atoms labelled. Hydrogen atoms except the amide NH are omitted and the NacNac Dipp groups are shown as wire frame for clarity. Thermal ellipsoids are displayed at 40% probability level. Symmetry transformations used to generate equivalent atoms: $-x, -y, -z$. Inset shows ChemDraw representation showing resonance structure of (**14**) as implied by the X-ray crystallographic metrics.**

The highly distorted tetrahedral lithium [with bond angles ranging from $91.5(2)^\circ$ to $129.6(3)^\circ$ ($\tau_4 = 0.76$)],¹²⁵ coordinates to the oxygen of the *t*-BuNCO unit and one nitrogen of the NacNac ligand, and completes its coordination sphere *via* TMEDA chelation. There is also uncoordinated TMEDA co-crystallised with **14**. The lithium sits κ^2 relative to the ligand, lying closer to the smaller oxygen atom of the *t*-BuNCO unit than the NacNac nitrogen atom [Li-N distance of $1.990(5)$ Å vs. Li-O distance of $1.839(6)$ Å]. The *t*-BuNCO fragment of the complex features secondary amide functionality with a $\text{C}_{30}\text{-O}_1$ bond length of $1.258(3)$ Å and $\text{C}_{30}\text{-N}_3$ bond length of $1.336(5)$ Å. The presence of the amine NH was also established through spectroscopic studies, with a resonance at 11.46 ppm in the ^1H NMR spectrum and a broad stretch at 3413 cm^{-1} in the IR spectrum.

The presence of a hydrogen atom residing in the secondary amide nitrogen can be attributed to a sigmatropic rearrangement from the backbone hydrogen atom of the γ -carbon within the NacNac ligand (Scheme 5.1).



Scheme 5.1: Potential pathway to form products **14 (and **16**) *via* a sigmatropic hydride rearrangement of the backbone γ -carbon proton.**

Such rearrangements have been observed before in small molecule fixation. Notably Fulton *et al.*, used lead and tin NacNac complexes to activate phenyl isocyanate, and Ren and Ma utilised magnesium NacNac complexes to activate phenyl isothiocyanate.^{307, 311} The diimine functionality present within **14** was also confirmed from the C₁₃-N₁ and C₁₆-N₂ bond lengths of 1.299(4) Å and 1.295(5) Å respectively, again comparable with the standard imine C-N bond length of 1.279 Å.³⁰¹ The imine was further confirmed *via* IR spectroscopic studies, which revealed a vibration at 1602 cm⁻¹, attributable to the C=N stretch (see ESI).

Given our group's long standing interest in the polydentate donor molecule Me₆TREN,¹⁰⁸⁻¹¹⁰ we decided to extend the activation of isocyanates to include Me₆TREN, to establish whether its large steric profile would impact upon the resulting structure, and whether all four of its donor arms would be involved in metal ion coordination. For example, one arm is free in the structure of [Me₆TREN-Mg-N(SiMe₃)₂][B{C₆H₃(CF₃)₂}]₄ reported recently by Venugopal.³¹² In this regard, NacNac(H) was deprotonated by the action of *n*-butyllithium in hexane at 0 °C and Me₆TREN was added, causing the formation of a white precipitate. A change to a yellow solution occurred upon adding one equivalent of *t*-BuNCO and heating the mixture at reflux. Concentrating this solution and cooling it to -30 °C led to colourless crystals, identified as [(MeCN-2,6-*i*Pr₂C₆H₃)₂C(O)Li{NH(*t*Bu)CO}]₂ (**15**) in an isolated yield of 68%. This complex is dimeric in the crystal, composed of a deprotonated NacNac ligand, with a *t*-BuNCO moiety inserted into the γ -C-H backbone position and consequently forming a new C-C bond (Figure 5.3). Despite its presence in the reaction mixture, Me₆TREN is absent from the structure. Surprisingly, oxygen has also been inserted into the same γ -C position, leading to the

formation of a new C-O bond with the two lithium cations present forming a planar four-membered (LiO)₂ ring. The equivalence of the lithium centres was also established in the solution state *via* ⁷Li NMR studies (See ESI).

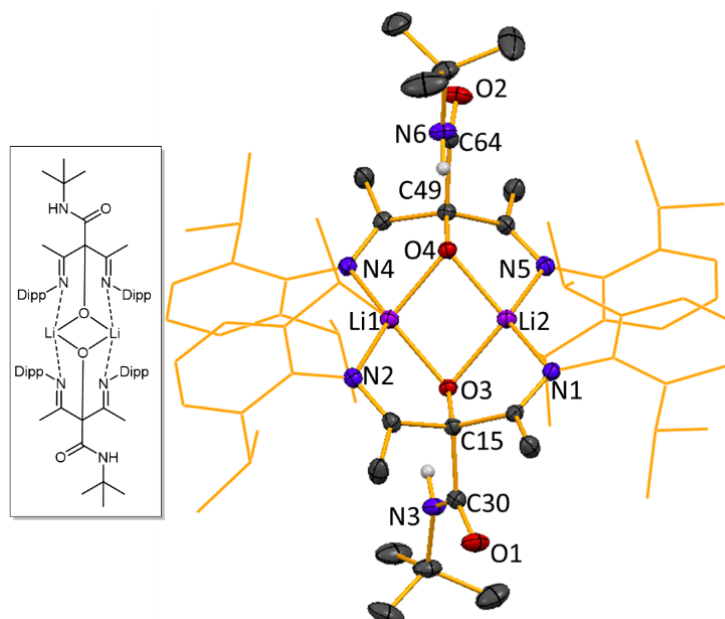


Figure 5.3: Molecular structure of [(MeCN-2,6-*i*Pr₂C₆H₃)₂C(O)Li{NH(*t*Bu)CO}]]₂ (15**). Hydrogen atoms except the amide NH are omitted and the NacNac Dipp groups are shown as wire frame for clarity. Thermal ellipsoids are displayed at 40% probability level. Symmetry transformations used to generate equivalent atoms: $\frac{1}{2} - x, \frac{1}{2} + y, \frac{1}{2} - z; -x, -y, -z; \frac{1}{2} + x, \frac{1}{2} - y, \frac{1}{2} + z$. Inset shows ChemDraw representation showing resonance structure of (**15**) implied by X-ray crystallographic metrics.**

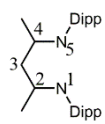
Though crystallographically distinct, the two lithium centres within non-centrosymmetric **15** are essentially equivalent. The Li-O bond lengths in the central core, for example, are identical within experimental error [Li₁-O₃, 1.892(3) Å; Li₁-O₄, 1.894(3) Å; Li₂-O₃, 1.895(3) Å and Li₂-O₄, 1.905(3) Å] and are broadly similar to those seen in **14**. The bond angles subtended at lithium are also broadly similar to each other (N₂-Li₁-N₄, 134.2(1)°; N₁-Li₂-N₅, 129.1(2)°; O₄-Li₁-O₃, 99.4(1)°; O₄-Li₂-O₃, 99.0(1)°). Each lithium is four coordinate, bound to two central oxygen atoms and two nitrogen atoms from the backbone of two separate NacNac ligands, exhibiting distorted tetrahedral geometries (τ_4 = 0.65 and 0.66 respectively).¹²⁵

Mimicking the arrangements in **14**, each *t*-BuNCO fragment has a secondary amide function, characterised by the C-N single bond lengths of 1.329(2) Å (C₆₄-N₆) and 1.328(2) Å (C₃₀-N₃). The C=N bond lengths within the NacNac moiety are generally close to 1.28 Å [N₁-C₁₃, 1.278(2) Å; N₂-C₁₆, 1.277(2) Å; N₄-C₄₇, 1.275(2) Å; N₅-C₅₀, 1.276(2) Å], consistent with the presence of imine C=N double bonds.³⁰¹ Two distinct types of C-O bonds reside within the

structure; namely those of the secondary amide functionality ($C_{30}-O_1$ length of 1.226(2) Å and $C_{64}-O_2$ length of 1.228(2) Å) and those at the centre of the $(LiO)_2$ core ($C_{49}-O_4$ and $C_{15}-O_3$ bond lengths of 1.357(2) and 1.358(2) Å respectively). The presence of the central oxygen anions could be through adventitious hydrolysis, though the reaction is reproducible with yields of around 68 %, or by fixation of molecular oxygen, as has been observed in many other complexes.³¹³⁻³¹⁵ Subsequent experiments have shown that reaction of compound **14** with molecular oxygen *via* a drying tube did not produce **15**, suggesting that adventitious moisture is the source of the oxygen atom. The definite point is that such systems are able to undergo double small molecule fixation within the same system. In any event, the product is unusual for containing not only a newly formed C-C bond between the γ -carbon of the NacNac and the carbon of the *t*-BuNCO but also for containing a new C-O bond at the same γ -carbon position.

Next, we tried to expand the isocyanate scope to less bulky examples, to explore whether the backbone insertion reactivity could be maintained. With this in mind, the parent NacNac(H) ligand was deprotonated using *n*-butyllithium in hexane at 0 °C. To this mixture was added PMDETA, followed by the less bulky isopropyl isocyanate (*i*-PrNCO), forming a green suspension. Addition of THF and gentle heating formed a brown solution, which was concentrated and cooled at -20 °C to obtain colourless crystals of the dimeric isocyanate insertion product $[\{(MeCN-2,6-iPr_2C_6H_3)_2C(CONH(i-Pr))\}Li.THF]_2$ (**16**) in 41% yield. X-ray crystallographic studies established the centrosymmetric dimeric structure adopted by **16** (Figure 5.4).

Table 5.0: Representative bond distances (Å) showing delocalization within NacNac backbone

	Bond	13	14	15	16
	N1-C2	1.269(3)	1.299(3)	1.278(2)	1.311(3)
	C2-C3	1.507(4)	1.451(4)	1.564(2)	1.435(4)
	C3-C4	1.514(4)	1.443(3)	1.561(2)	1.467(3)
	C4-N5	1.286(3)	1.295(4)	1.277(2)	1.298(3)

16 comprises two deprotonated NacNac scaffolds, linked *via* a four-membered $(LiO)_2$ ring, with *i*-PrNCO inserted into the γ -carbon position to form a new C-C bond. The distorted tetrahedral lithium centre is four coordinate, with bond angles ranging from 91.5(2)° to 136.7(3)° ($\tau_4 = 0.72$),¹²⁵ bonded to one nitrogen of the NacNac ligand, the oxygen atoms of two *i*-PrNCO units, and a THF ligand. Respective bond distances are 2.021(6) Å (Li_1-N_2),

1.915(5) Å (Li₁-O₁), 1.896(6) Å (Li₁-O_{1'}) and 1.991(5) Å (Li₁-O₂). A sigmatropic hydride rearrangement is implicated again with the amide functionality discernable from the ¹H NMR spectrum (resonance at 11.0 ppm, see ESI). As in both **14** and **15**, it is the isocyanate (*i*-PrNCO) fragment of the complex which features such secondary amide functionality, as ascertained from the C₃₀-O₁ and C₃₀-N₃ bond lengths of 1.270(4) Å and 1.348(4) Å respectively. Once more, **16** exhibits diimine character based on bond length evidence of 1.298(4) Å for C₁₆-N₂ and 1.310(4) Å for C₁₃-N₁ (see Table 5.0 for a comparison of important NacNac bond lengths highlighting the diimine character in each case). Of note is the fact that complex **16** being dimeric departs from the monomeric structure seen in **14**. This dimerisation is sterically driven due to the use of a less bulky isocyanate. Moreover, as was the case in **15** with Me₆TREN, in **16** the donor PMDETA is not incorporated into the crystal structure. This may indicate that within these sterically congested architectures, the incorporation of larger (than THF or bidentate TMEDA) solvating ligands near the metal ion is prohibited.

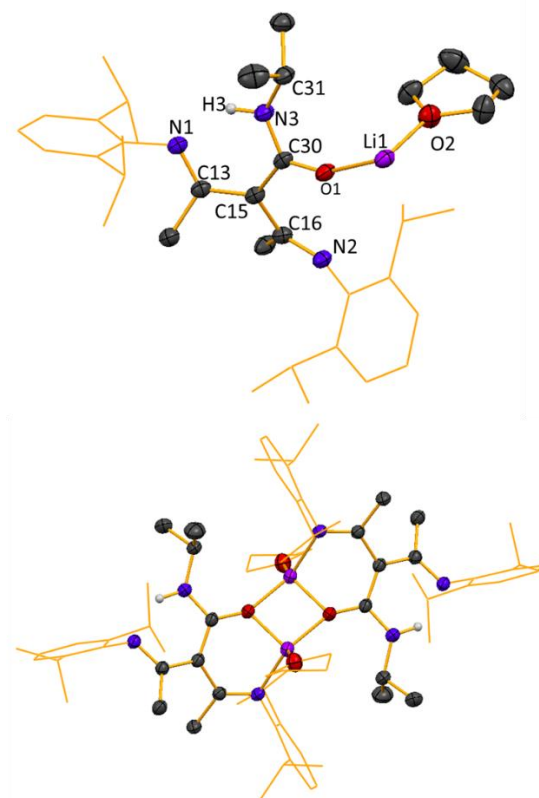


Figure 5.4: Top: Molecular structure of the asymmetric unit of [(MeCN-2,6-*i*Pr₂C₆H₃)₂C(CONH(*i*-Pr))}Li.THF]₂ (**16**) with key atoms labelled; and Bottom: Full dimeric structure of (**16**). Hydrogen atoms except the amide NH are omitted and the NacNac Dipp groups and solvating THF are shown as wire frame for clarity. Thermal ellipsoids are displayed at 40% probability level. Symmetry transformations used to generate equivalent atoms: -x, -y, -z.

This study has uncovered unusual reactivity of a common lithium NacNac complex. Exposing lithium NacNac (Dipp, Me) to carbon dioxide forms a dimeric lithium carboxylate based NacNac product, where the CO₂ has reacted preferentially at the γ -carbon position, which is to the best of our knowledge, the first structurally authenticated example of such reactivity with alkali metal NacNac species. Extending this reactivity to isocyanates results in either monomeric or dimeric structures, depending on the identity/bulk of the isocyanate used. In conclusion, on reacting *t*-BuNCO with LiNacNac and TMEDA, a monomeric structure is obtained, with isocyanate insertion into the γ -carbon position resulting in both amide and imine functionality being present within the complex. When using the higher dentate donor Me₆TREN, a serendipitous double insertion is accomplished comprising an isocyanate molecule and an oxygen atom, both at the same carbon position, establishing such systems as able to undergo dual small molecule activation.

Moving to the less bulky isocyanate, *i*-PrNCO, the reaction with LiNacNac produces a dimeric complex, where the NacNac units are linked *via* Li-O bonds arising from the amido functionality inserted within the γ -carbon position. Future work will explore the reactivity of other alkali metal NacNac type ligands towards a range of small molecules, as well as attempting to apply the newly formed backbone-functionalised NacNac metal complexes as a source of special ditopic ligands in synthesis and homogeneous catalysis. The functionalised ligands are ripe for investigations into their complexation behaviour and further reactivity, which are currently ongoing within our laboratory.

5.6 Extended Discussion and Future Work

Of note within Chapter 5.5 is that all the results involve lithium as the alkali metal within the system. Given the lack of literature on lithium carbamates and backbone insertion into LiNacNac species, it should come as no surprise that there is also a paucity of literature available on NaNacNac carbamate complexes. As discussed in Chapter 3.2, there are no crystallographically verified examples of NaNacNac complexes within the literature. Therefore, it was decided to attempt to obtain a fully characterised backbone inserted complex featuring both a NacNac scaffold and sodium cation. To this end, a transmetallation approach between LiNacNac and NaO^{*t*}Bu was adopted in order to obtain the desired NaNacNac complex. Such an approach is commonly used within organometallic chemistry in

the preparation of organosodium compounds.³¹⁶⁻³¹⁹ The NaNacNac starting ligand is a white powder insoluble in hexane, allowing for easy isolation *via* filtration. This powder was subsequently suspended in fresh hexane, with PMDETA and *t*BuNCO added sequentially in a 1:1 stoichiometric ratio, forming an olive-green suspension. Refluxing this mixture for one hour gave a dark brown solution, which on cooling at -30 °C afforded colourless crystals, identified *via* X-ray diffraction as $[(\text{MeCN-2,6-}i\text{Pr}_2\text{C}_6\text{H}_3)_2\text{C}(\text{CONH}(t\text{-Bu}))]\text{Li.PMDETA}$ (**17**) in a 53% yield.

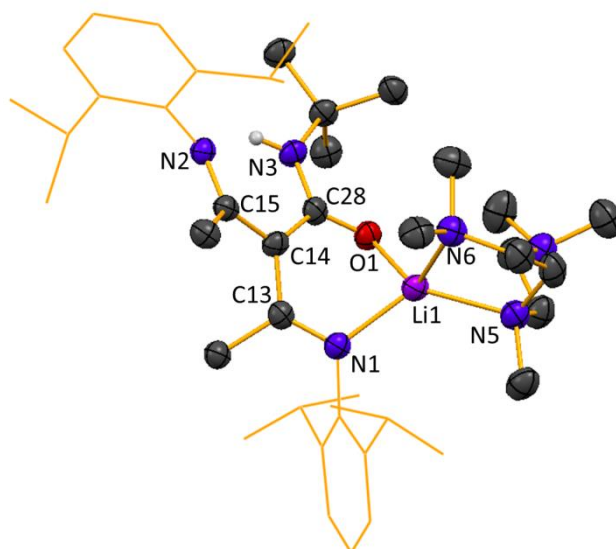


Figure 5.5: Molecular structure of $[(\text{MeCN-2,6-}i\text{Pr}_2\text{C}_6\text{H}_3)_2\text{C}(\text{CONH}(t\text{-Bu}))]\text{Li.PMDETA}$ (17**). Hydrogen atoms except the amide NH are omitted and the NacNac Dipp groups are shown as wire frame for clarity. Thermal ellipsoids are displayed at 40% probability level. Symmetry transformations used to generate equivalent atoms: -x, -y, -z.**

The surprise within this structure is the presence of a lithium centre rather than the expected sodium. While the product is unexpected, the reaction is reproducible, on each occasion forming **17** as opposed to any sodium containing product. While the definitive reason for the failure of the lithium to sodium transformation is unknown, there could perhaps be a chelating effect driven by the isocyanate insertion, which may lead to the preference for formation of **17**. Alternatively, ^7Li NMR spectroscopy carried out on the isolated “NaNacNac” powder revealed a resonance, indicating that there is still lithium present in this isolated powder. There could be several reasons for why a lithium containing species would be present, for example there could be an amount of unreacted LiNacNac starting material,

which then preferentially reacts with the isocyanate to produce complex **17**. Alternatively, there could be some Li present within the ⁿBuNa used to synthesise the NaNacNac in the first place, which would then lead to the formation of LiNacNac rather than the sodium congener. Indeed, further ⁷Li NMR studies of the ⁿBuNa powder synthesised revealed a resonance, indicating the presence of lithium within the powder. This Li presumably remains due to the high reactivity of ⁿBuNa effectively ‘trapping’ some of the ⁿBuLi starting material within the powder.

As can be seen, complex **17** forms a monomeric arrangement in the crystal, composed of a NacNac scaffold with *t*BuN(H)CO bonded to the activated γ -carbon position (Figure 5.5). Here the lithium is coordinated to one nitrogen atom of the NacNac ligand, the oxygen atom of the *t*BuN(H)CO group and only two nitrogen atoms of a possible tridentate PMDETA ligand.^{112, 320-322} A full structural description of **17** is unwarranted given its similarity to complex **14** (Figure 5.2, Page 144). The main feature of note within **17** is the rarely seen bidentate PMDETA, with the lithium κ^2 with respect to the PMDETA and essentially equidistant between the two nitrogen atoms (Li1-N5, 2.121(6) Å and Li1-N6, 2.166(5) Å). The presence of this bidentate-binding PMDETA is unusual, with only a few hits found within the CSD⁸¹ where a bidentate PMDETA specifically coordinates to a lithium cation.³²³

When attempting to obtain **17** in a rational way using LiNacNac, PMDETA and *t*BuNCO, a crystalline degradation product formed instead. The structure of this product consists of a 2,6-diisopropylaniline based ligand, with a new bond between the nitrogen of this ligand and the carbon of the *t*BuNCO fragment. This unexpected result could be due to the presence of unreacted 2,6-diisopropylaniline left over when making the parent NacNac(H) ligand, although GC/MS analysis indicated that there was less than 1 % of unreacted starting amine within the batch of NacNac(H), or *via* degradation of the parent NacNac(H) ligand. To the best of our knowledge no such degradation to the parent 2,6-diisopropylaniline has been seen before, with select examples showing only fragmentation *via* the γ -carbon position.³²⁴⁻
³²⁶ This product was obtained fortuitously and with low quality X-ray data, however repeating the reaction rationally using the parent 2,6-diisopropylaniline, ⁿBuLi, PMDETA and *t*BuNCO gave the same reaction product but in a larger yield (isolated crystalline yield of less than 20 % versus 66 % respectively).

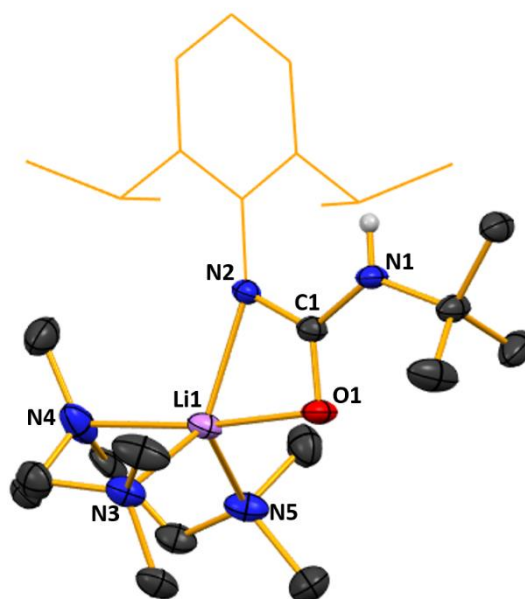


Figure 5.6: Molecular structure of $\{[(2,6\text{-}i\text{Pr}_2\text{C}_6\text{H}_3)]\text{NCON}(t\text{Bu})\text{Li.PMDETA}\}$ (18**). Hydrogen atoms excluding amine NH are omitted and the Dipp group is shown as wire frame for clarity. Thermal ellipsoids are displayed at 40% probability level. Symmetry transformations used to generate equivalent atoms: $-x + \frac{1}{2}, -y, z + \frac{1}{2}$; $x + \frac{1}{2}, -y + \frac{1}{2}, -z$; $-x, y + \frac{1}{2}, -z + \frac{1}{2}$; $-x, -y, -z$; $x - \frac{1}{2}, y, -z - \frac{1}{2}$; $-x - \frac{1}{2}, y - \frac{1}{2}, z$; $x, -y - \frac{1}{2}, z - \frac{1}{2}$.**

The lithium centre here is five-coordinate, interacting with three nitrogen atoms from PMDETA, the nitrogen atom from the 2,6-diisopropylamide ligand and an oxygen atom from the isocyanate. This oxygen atom shows negative character, as suggested by the bond lengths, with the $\text{C}_1\text{-O}_1$ distance of 1.262(2) Å being intermediate between single and double bonds. Despite no backbone γ -proton being present in contrast to the NacNac systems, there is still amine functionality visible in **18**, with this likely arising from the transfer of the proton from DippN(H)Li to the nitrogen atom of the isocyanate.

Specifically looking into the NacNac examples, in terms of how such backbone rearrangements may occur, a ^1H NMR spectroscopic study was carried out in a J Youngs tube to confirm that such a transformation was likely to occur *via* sigmatropic hydride rearrangement. Figure 5.7 shows two comparative spectra, with the ^1H NMR spectrum on the top of LiNacNac alone and that on the bottom being LiNacNac with PMDETA donor added. In both instances the backbone γ -carbon proton is clearly visible at 4.84 ppm and 4.99 ppm respectively.

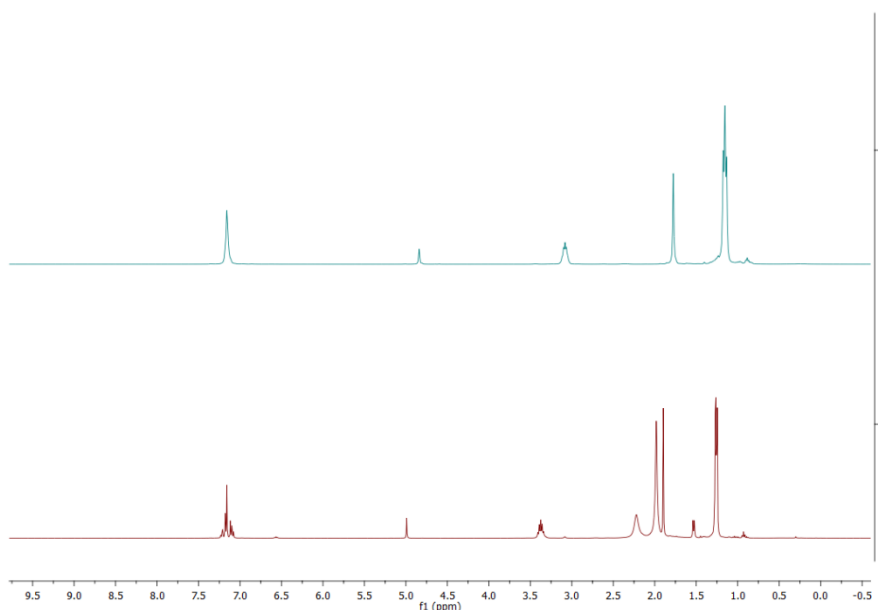


Figure 5.7: Comparative ^1H NMR spectra showing (Top) LiNacNac in C_6D_6 and (Bottom) LiNacNac with PMDETA in C_6D_6 . Note the presence of the backbone γ -proton in both spectra.

Upon addition of $t\text{BuNCO}$, this resonance disappears, implying that the backbone γ -carbon proton has instantaneously rearranged to form the amide functionality seen in the structures described in Chapter 5.5. There is further evidence for this given that a small resonance can be seen in the spectra post isocyanate addition at 11.36 ppm, which would correspond to the NH proton, suggesting the formation of an amine. This signal does not change in terms of size upon heating overnight, suggesting that while the addition of heat may be necessary in order to obtain a solution and hence crystals on the bulk scale, on the NMR scale the rearrangement takes place much quicker, forming the backbone inserted product rapidly.

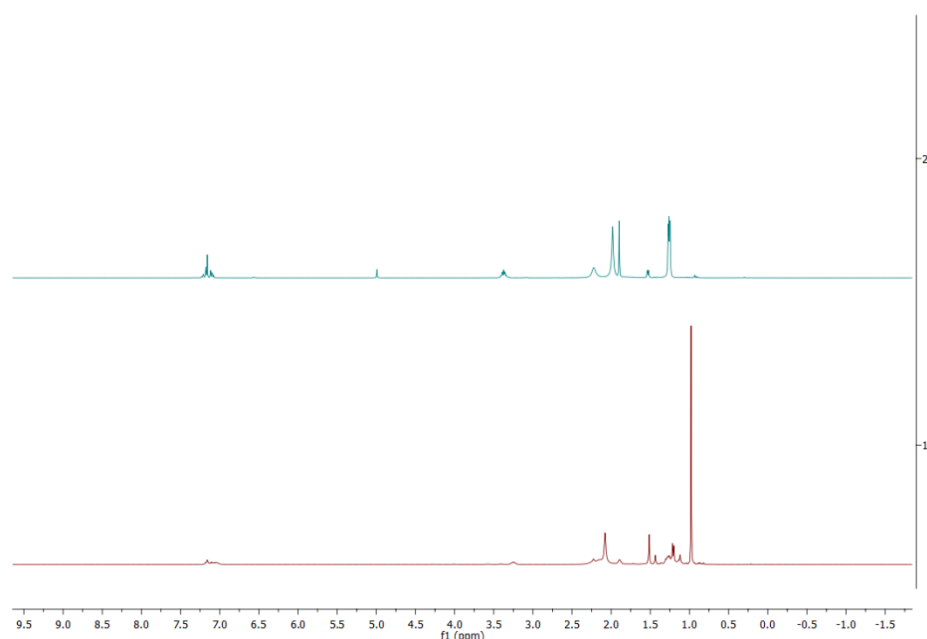
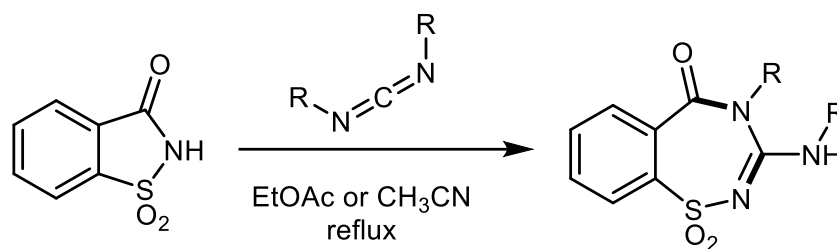


Figure 5.8: Comparative ^1H NMR spectra showing (Top) LiNacNac with PMDETA pre isocyanate addition in C_6D_6 and (Bottom) LiNacNac with PMDETA post isocyanate addition in C_6D_6 . Note the absence of the backbone γ -proton in the bottom spectra.

With these results in hand, we thought to expand the range of small molecules into other examples aside from CO_2 and isocyanates. We came across carbodiimides as potential candidates, given they possess a central $\text{N}=\text{C}=\text{N}$ motif and are thus isoelectronic with CO_2 . We reasoned that if such a compound was reacted with an alkali metal NacNac complex it would be through the γ -carbon of the NacNac ligand towards the central carbon of the carbodiimide, as for CO_2 and isocyanate reagents, with the likely formation of a new carbon-carbon bond. Carbodiimides themselves are versatile reagents, with several recent papers showing their capability to insert into reactive species for synthetic purposes. For example, in 2017 it was shown that carbodiimides could insert into sulfonamides (a previously unknown reaction) which in turn led to a one-pot route for the expansion of a five-membered saccharin rings to seven-membered benzothiadiazepine derivatives.³²⁷



Equation 5.0: General conversion of saccharin ring to benzothiadiazepine *via* carbodiimide insertion.

Other uses for carbodiimides as reagents include the potential to take part in the one-pot palladium catalysed cross coupling with an aromatic carboxylic acid, in a variation of CO₂ extrusion-insertion reactions previously utilised.³²⁸ Despite these examples, there appears to be no literature precedent in terms of the reaction between carbodiimides and alkali metal NacNac complexes.

To this end, it was decided to react LiNacNac with N,N'-Dicyclohexylcarbodiimide (DCC). This is a relatively bulky example of an isocyanate, with two cyclohexyl rings attached to each of the nitrogen atoms. LiNacNac [synthesised *in situ* from the action of ⁿBuLi on NacNac(H)] was suspended in hexane solvent and TMEDA was added to obtain a solution. To this yellow solution was added 1 molar equivalent of DCC, with no obvious visual change upon addition. The solution was concentrated *in vacuo* and placed in the fridge, where colourless crystals formed, identified by X-ray crystallography as the discrete complex [((MeCN-2,6-*i*Pr₂C₆H₃)₂CH}Li.NCN(C₆H₁₁)₂] (**19**), obtained in an 83 % yield.

19 consists of a discrete LiNacNac complex coordinated to a molecule of DCC through one of the nitrogen atoms of the DCC ligand. Unlike the previous examples in Chapter 5.5, no sigmatropic hydride rearrangement process or backbone attack takes place, with the DCC coordinating to the lithium cation at the front of the NacNac molecule as a donor. This is evidenced both in the solid and solution state, with ¹H NMR spectroscopic studies showing a resonance at 5.02 ppm, corresponding to the γ-backbone proton. The planarity of the NacNac backbone is not altered in any way in this structure, with the lithium cation remaining within the NCCCN plane. This was a surprising result, as it was expected that the DCC, similar to CO₂ and isocyanates, would act as an electrophile in the presence of nucleophilic LiNacNac and that addition towards the γ-carbon centre of the LiNacNac from the carbon of the carbodiimide would be seen. Despite attempts to induce rearrangement *via* prolonged heating at reflux temperatures, no such reaction was observed, with **19** consistently being the only product obtained.

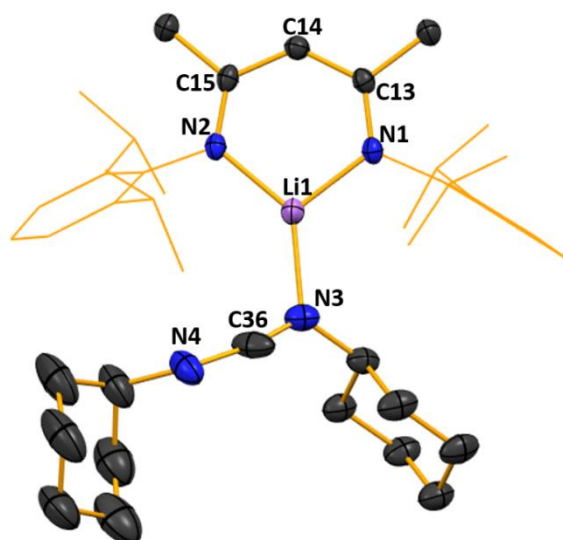


Figure 5.9: Molecular structure of $[(\text{MeCN-2,6-}i\text{Pr}_2\text{C}_6\text{H}_3)_2\text{CH}]\text{Li.NCN}(\text{C}_6\text{H}_{11})_2$ (19**). Hydrogen atoms are omitted and the NacNac Dipp groups are shown as wire frame for clarity. Thermal ellipsoids are displayed at 40% probability level. Symmetry transformations used to generate equivalent atoms: $-x, -y, -z$.**

The lithium centre is in a distorted trigonal planar geometry, with angles ranging from the smallest of $101.4(2)^\circ$ to an obtuse of $135.6(3)^\circ$, while also lying effectively equidistant between the two nitrogen atoms of the NacNac ligand ($\text{Li}_1\text{-N}_1$, $1.898(5)$ Å and $\text{Li}_1\text{-N}_2$, $1.902(5)$ Å). Within the NacNac ligand itself, C-N bond lengths are intermediate between single and double bonds, suggesting significant delocalisation within the NacNac scaffold ($\text{C}_{15}\text{-N}_2$ and $\text{C}_{13}\text{-N}_1$ bond lengths of $1.318(3)$ Å and $1.324(3)$ Å respectively).

The bond lengths on the DCC ligand suggests there is also some delocalisation present here. For example, looking at the C-N bond lengths, one is longer than expected for a C=N double bond and is also longer than the other C-N bond present ($\text{C}_{36}\text{-N}_4$, $1.39(1)$ Å and $\text{C}_{36}\text{-N}_3$, $1.206(4)$ Å). This change suggests that the N-C-N central core of the DCC is no longer symmetrical, presumably as a result of coordination of one of the nitrogen atoms to the lithium centre. This distortion is also seen in the bond angles of the DCC ligand, which are larger than the C-N=C bond angles of 120° normally seen in carbodiimide ligands ($\text{C-N}_4=\text{C}_{36}$, $134.6(8)^\circ$ and $\text{C-N}_3=\text{C}_{36}$, $121.4(3)^\circ$).

Complex **19** was also fully characterised *via* multinuclear NMR spectroscopy. As previously mentioned, the ^1H NMR spectrum clearly shows the backbone γ -hydrogen resonance at 5.02

ppm, with all other resonances in agreement with the solid-state structure, suggesting that its composition is maintained in solution. Of note was the ^7Li NMR, which showed a single resonance corresponding to the single lithium environment present within **19** at 2.61 ppm. This contrasts to the ^7Li spectra obtained for LiNacNac, which shows a resonance at 0.73 ppm, confirming that the Li in **19** remains in a different environment, presumably due to the donating effects of the DCC molecule being maintained in solution.

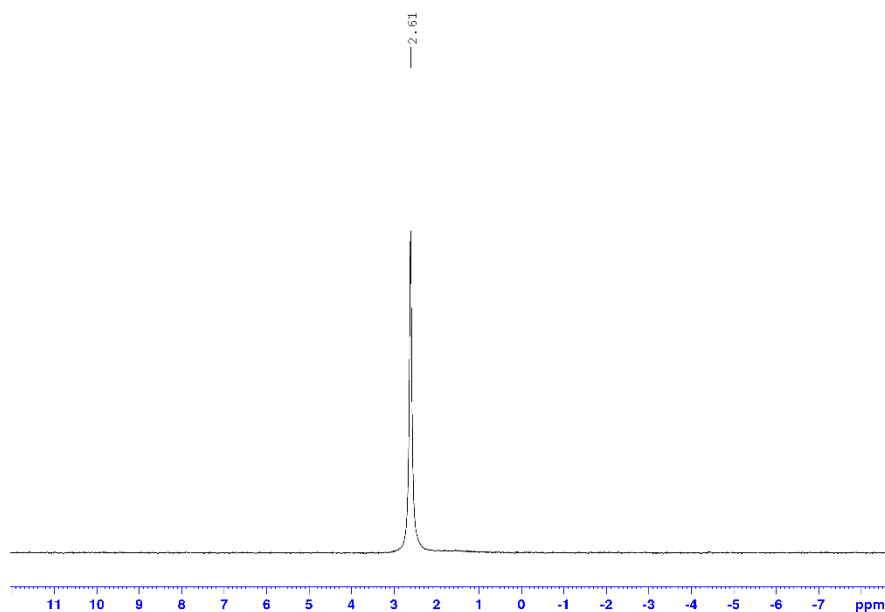


Figure 5.10: ^7Li NMR spectrum of $[(\text{MeCN-2,6-}i\text{Pr}_2\text{C}_6\text{H}_3)_2\text{CH}]\text{Li.NCN}(\text{C}_6\text{H}_{11})_2$ (**19**) in C_6D_6 solution.

With these results showing the effects of nitrogen containing donors, we wondered if donors containing oxygen centres could have a similar effect. The oxygen containing donor settled on was triphenylphosphine oxide. Phosphorus containing molecules have many wide-ranging applications, including in hydrophosphination catalysis, which has recently been explored by our group using mixed-metal lithium aluminate complexes as catalysts.³²⁹ While triphenylphosphine oxide itself has not been utilised in hydrophosphination catalysis per se, it would be advantageous to investigate its bonding interactions with organometallic species such as LiNacNac, which itself has begun to show promise as a potential catalyst for other hydroelementation reactions such as hydroboration and cyanosilylation.²⁸¹ We also pondered whether the polar P=O bond would lend itself to insertion into the backbone γ -carbon of the LiNacNac as seen in CO_2 and isocyanates or if similar reactivity to that of DCC

would be observed. To this end, LiNacNac was synthesised *in situ* from reaction of NacNac(H) with $^n\text{BuLi}$ in hexane. To this mixture was added PMDETA to give a golden yellow solution, with addition of triphenylphosphine oxide giving a colour change to vivid orange. This solution was concentrated *in vacuo* and placed at $-18\text{ }^\circ\text{C}$, whereupon crystals formed overnight, identified *via* X-ray crystallography as $[\{(\text{MeCN-2,6-}i\text{Pr}_2\text{C}_6\text{H}_3)_2\text{CH}\}\text{Li}.\text{OP}(\text{C}_6\text{H}_5)_3]$ (**20**).

Monomeric **20** comprises a LiNacNac scaffold, with a molecule of triphenylphosphine oxide interacting with the lithium cation at the front of the complex, with no backbone attack seen. PMDETA is also not present within the structure, though subsequent experiments have shown that PMDETA addition is necessary in order to obtain crystals. Without adding PMDETA, **20** can still successfully be made as an amorphous powder, with confirmation of success determined *via* multinuclear NMR spectroscopy.

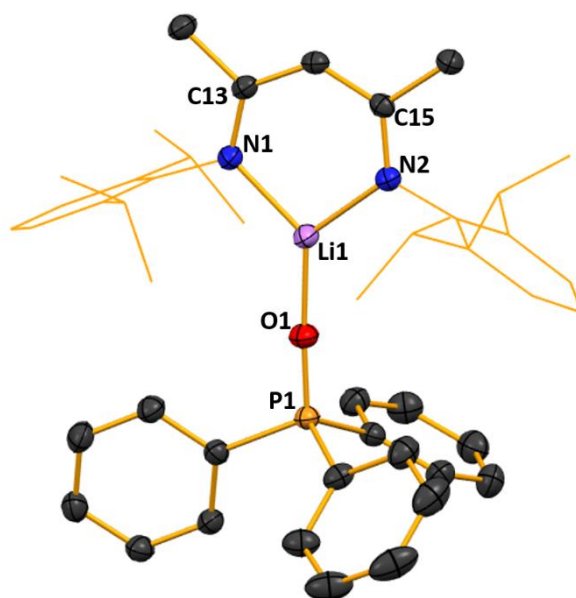


Figure 5.11: Molecular structure of $[\{(\text{MeCN-2,6-}i\text{Pr}_2\text{C}_6\text{H}_3)_2\text{CH}\}\text{Li}.\text{OP}(\text{C}_6\text{H}_5)_3]$ (20**).** Hydrogen atoms, disorder and co-crystallised hexane solvent are omitted and the NacNac Dipp groups are shown as wire frame for clarity. Thermal ellipsoids are displayed at 40% probability level. Symmetry transformations used to generate equivalent atoms: $-x, y, -z + \frac{1}{2}; x + \frac{1}{2}, y + \frac{1}{2}, z; -x + \frac{1}{2}, y + \frac{1}{2}, -z + \frac{1}{2}; -x, -y, -z; x, -y, z - \frac{1}{2}; -x + \frac{1}{2}, -y + \frac{1}{2}, -z; x + \frac{1}{2}, -y + \frac{1}{2}, z - \frac{1}{2}$.

The lithium centre is three-coordinate, bonded to two nitrogen atoms from the bidentate NacNac unit and one oxygen atom from the triphenylphosphine oxide molecule in a distorted trigonal planar geometry, with the smallest angle being $99.8(2)^\circ$ between $\text{N}_1\text{-Li}_1\text{-N}_2$ and an obtuse angle of $131.4(2)^\circ$ between $\text{O}_1\text{-Li}_1\text{-N}_1$. The phosphine oxide retains its double bond in

the solid state, with a P=O bond length of 1.489(1) Å, with the lithium cation sitting equidistant between the nitrogen atoms of the NacNac ligand (N₁-Li₁, 1.925(3) Å and N₂-Li₁, 1.911(3) Å). The P-O-Li bonding arrangement sits within the plane of the NCCCN unit, which in turn is not disturbed from planarity, contrasting to the backbone insertion examples seen in Chapter 5.5. The C-N bonds in the NacNac scaffold are intermediate between single and double bonds (N₁-C₁₃, 1.318(2) Å; N₂-C₁₅, 1.316(2) Å), indicating a degree of delocalisation within the NacNac architecture.

Multinuclear NMR spectroscopy experiments were carried out on **20**, which agreed with the solid-state structure, particularly that the coordination between the phosphine oxide and the LiNacNac is maintained in solution. This can be deduced from the ⁷Li NMR, which shows a resonance at 2.70 ppm, in contrast to that seen for LiNacNac at 0.73 ppm, indicating a change in the lithium environment. The ³¹P NMR also indicates coordination, with the resonance at 23.2 ppm for free uncoordinated triphenylphosphine oxide contrasting to that at 30.80 ppm seen in **20**.

A search of the literature showed that such interactions between triphenylphosphine oxide and lithium cations are known, the CSD revealing 20 hits for triphenylphosphine oxide interacting with a lithium centre *via* the oxygen atom.⁸¹ There are, however, no results involving a LiNacNac scaffold, with many of the 20 hits featuring a lithium cation surrounded by four Ph₃PO units with a counter ion of some description also present.^{330, 331} This result, in conjunction with the result involving DCC (Figure 5.9), shows that coordination of relatively bulky oxygen and nitrogen containing groups to LiNacNac is possible, although for these ligand systems the coordination takes place at the front of the molecule, with the lithium NacNac backbone remaining undisturbed, contrasting with the results obtained with isocyanates and CO₂, where nucleophilic attack takes place *via* the backbone γ-carbon position.

Chapter 6: Conclusions and Outlook

6.1 Conclusions

Previous work within the field of diesel engine deposits has often focused on the problem from an engineering outlook, with the main thrust of earlier efforts being understanding the identity of such deposits. Once these deposits were identified as sodium carboxylate based, it was established that they formed in diesel fuel due to the presence of the sources of both sodium and long chain acids within the fuel, the latter directly added in order to aid performance. Despite identifying the overall nature of the deposits, the community was unable to conclusively identify the exact chemical structures adopted. This was for a number of reasons, the main one being that the long chain acids used within diesel engines reacted to form long chain sodium carboxylates, which are difficult to analyse *via* single crystal X-ray diffraction studies due to the flexibility of the long chain and the tendency of such examples to form amorphous solids or gelatinous material, both of which being unsuitable for X-ray structural determination. Since carboxylates contain CO₂ units within their composition, it was decided to run in parallel a programme exploring CO₂ fixation chemistry which, while studied with many different chemical systems, has never been explored in-depth using alkali metal complexes. Expanding upon previous work carried out within the Mulvey group on structural determination studies featuring alkali metals, the overall programme of this PhD project was to prepare examples of both types of species and investigate the structural motifs they adopt in both the solution and the crystal state *via* multinuclear NMR spectroscopy and single crystal X-ray crystallography where appropriate.

In Chapter 2 it was initially shown that reaction solutions of long chain carboxylates, specifically sodium 2-ethylhexanoate and sodium octanoate, with several heteroatom containing donors, TMEDA, PMDETA, Et₂O, THF, Me₆-TREN, diglyme or various crown ethers were unable to produce crystalline solids. Instead, thick gelatinous suspensions formed, presumably due to the donors being unable to break apart a polymeric sodium carboxylate structure that forms. Solution state NMR spectroscopic studies, in particular DOSY NMR, showed that sodium carboxylates likely form dimeric arrangements in the presence of polar solvents such as water and methanol. Reaction of 2-ethylhexanoic acid with TMP(H) resulted in the formation of a hydrogen bonded dimer, which could be considered as the replacement

of Na^+ by H^+ giving some indication of the dimeric structure likely to be adopted in polar solvents.

Expansion of the work to a more rigid 1,10-phenanthroline system gave success, with two informative crystal structures of sodium 2-ethylhexanoate obtained. The first of these, of formula $[(\text{C}_5\text{H}_{10})(\text{C}_2\text{H}_5)\text{COONa}(1,10\text{-phen})]_\infty$, showed a rarely seen bidentate mode of carboxylate binding, with a polymeric structure propagated *via* unidentate carboxylate binding. The second structure contained a molecule of water, which changed the carboxylate binding mode to unidentate and also affected the propagation of the polymer itself, with the chain forming through hydrogen bonding interactions and π - π stacking interactions between the aromatic rings of the 1,10-phenanthroline. Attempting the slow diffusion method of crystallisation gave the solvent-free and donor-free polymeric $[(\text{C}_5\text{H}_{10})(\text{C}_2\text{H}_5)\text{COO.Na}]_\infty$ complex. This is the longest chain example of such a molecule within the CSD and shows a complexity that cannot be predicted from IR and NMR studies alone. The structure does not pack as a simple layer of hydrophobic and hydrophilic groups, instead the architecture reveals a NaO_2 core section, around which the long hydrophobic alkyl groups wrap. This unusual arrangement is potentially the structure that forms in non-polar solvents, with subsequent deaggregation in the presence of donors such as water and 1,10-phenanthroline. Expansion of this work to the potential drug candidate sodium valproate $[(\text{C}_3\text{H}_7)_2\text{CHCOO.Na.DMSO}]_\infty$ revealed a similar polymeric architecture present, with the sodium now solvated by a DMSO molecule. In contrast to the sodium 2-ethylhexanoate structure however, that of sodium valproate is more of a layered structure, with a hydrophilic layer sandwiched between two organic hydrophobic bilayers. Attempts to further expand this work to high pressure systems, inverse crown systems and mixed metal 'superbase' type systems were unfortunately unsuccessful due to either no crystals being obtained (due to lack of solubility) or no incorporation of the long chain species of interest in systems that did produce crystals.

Consequently, we turned our attention to new ways to synthesise shorter chain examples. Our efforts in this area are detailed in Chapter 4, starting with insertion of CO_2 into lithium alkyl species. Taking *n*-propyllithium and *n*-propylsodium, we were able to show that CO_2 insertion results in the formation of alkali metal carboxylates in both instances. These were characterised *via* DOSY NMR spectroscopy and were shown to exist as either dimers or monomers in polar solvents, depending on the identity of the alkali metal. Testing to see if

such CO₂ capture chemistry could be replicated by using other alkali metal containing species, we discovered such species form a remarkable array of structures, depending on the identity of the species in question and the presence or absence of donor. We uncovered that reacting a relatively simple lithium pyrrole species with CO₂ gave a polymeric structure, composed of an alternating arrangement of four- and eight-membered rings fused together. While such a structural motif is common in lithium amide chemistry this is the first example of such an arrangement within the field of lithium carbamates. Moving on to a commonly used utility amide, namely LDA, CO₂ addition furnishes a product of much greater complexity than the simple insertion product anticipated. Instead a dodecameric structure, consisting of two open cubanes linked by a planar four-membered (LiO)₂ ring, results. Also present within this complex are two intact carbamic acid groups, both found in the X-ray crystallographic determination, which is surprising given the ease with which such groups usually break apart into CO₂ and the parent amine. This result highlights the complexity obtained from relatively simple reaction conditions, with previous work showing a hafnium carbamate DA complex adopting a much simpler structure. Expanding to monometallic HMDS complexes, we found that addition of CO₂ formed an intractable gelatinous material that we were unable to solubilise. It was not until a heterobimetallic HMDS complex was used that CO₂ addition furnished a solution which subsequently deposited crystals, which were elucidated to be a novel polymeric anhydride complex, composed of silylamido-substituted anhydride units. This complex contains an unexpected ditopic arrangement, where the oxygen at the back of the ligand interacts with the sodium cation; whereas the oxygen atoms at the front of the ligand chelate a lithium centre. The failure of LiHMDS or NaHMDS to likewise fix CO₂ suggests that this anhydride species may have a synergistic, mixed-metal, origin.

Having shown that CO₂ insertion reactions were more complicated than expected for common utility amides, we next turned our attention to LiNacNac complexes, widely used throughout chemistry. As detailed in Chapter 5, initial experiments reacting LiNacNac.TMEDA with CO₂ resulted not in the formation of the expected lithium carbamate, but a dimeric lithium carboxylate NacNac based complex where the CO₂ had inserted at the backbone γ -carbon of the NacNac ligand. To the best of our knowledge, this is the first structurally authenticated example of this kind of reactivity with alkali metal NacNac species. Expansion of this work to isoelectronic isocyanate molecules, resulted in similar backbone γ -carbon reactivity, with replacement of CO₂ with *t*BuNCO in the above system resulting in the formation of a monomeric complex featuring both imine and amide functionality. This amide

functionality is thought to arise from a sigmatropic hydride rearrangement process, as implicated by solution state NMR experiments. On changing the donor to Me₆-TREN, a double small molecule activation occurred, with isocyanate and serendipitously oxygen insertion both taking place at the same γ -carbon location. This discovery opens up the potential for such LiNacNac systems to be precursors to more complex NacNac derivatives if this double small molecule insertion process can be applied widely. This backbone reactivity was also found to be common to smaller classes of isocyanate, with *i*PrNCO giving a dimeric complex linked *via* Li-O amido bonds within the structural framework. Attempts to expand the scope of this reaction to heavier alkali metals, namely NaNacNac, instead gave [((MeCN-2,6-*i*Pr₂C₆H₃)₂C(CONH(*t*-Bu)))Li.PMDETA], possibly as a result of the failure of the Li to Na transmetallation reaction, which would lead to the presence of some unreacted LiNacNac that then reacts with the isocyanate. Alternatively, when using ⁿBuNa there may be incorporation of reactive ⁿBuLi within the ⁿBuNa, leading to formation of LiNacNac over NaNacNac. In this complex, which again contains an isocyanate at the γ -carbon position and dual imide and amine functionality, there is no sodium centre, with a lithium cation present instead. Of note is the presence of an unusual bidentate PMDETA ligand, with one arm of this donor free in the crystal state. Reactivity with small molecules is not limited to NacNac ligands, with the parent 2,6-diisopropylaniline also able, once deprotonated by the action of ⁿBuLi, to react with *t*BuNCO, forming an addition complex that also features amine functionality. On extending the range of small molecules to carbodiimides, it was found that the reaction of LiNacNac with N,N'-Dicyclohexylcarbodiimide unexpectedly did not give a backbone inserted product. Instead, the DCC interacted with the lithium centre at the front of the LiNacNac complex, with the backbone not perturbed from planarity in any way. This was surprising, as it was expected that the central N=C=N section of carbodiimides would react in a similar way to CO₂, with the steric bulk of the DCC potentially one reason why such backbone reactivity is not seen. Finally, attempting to react LiNacNac with Ph₃P=O again saw no backbone reactivity, with the oxygen of the phosphine oxide interacting with the lithium centre in a simple donor-acceptor complex. This is also presumably due to sterics, with the presence of the three bulky phenyl rings likely to be too bulky to move into the backbone of the LiNacNac system, although the high oxophilicity of the lithium centre could suggest why the phosphine oxide interacts at the front of the system.

6.2 Outlook and Future Perspectives

The area of research probing the structures of long chain alkali metal carboxylates is of interest to the fuel industry. Given the vast number of vehicles that use diesel as a source of fuel it is vital to understand the chemistry that takes place within their engine system. While this project has uncovered the solution and solid-state structures of a series of representative examples of sodium carboxylates there are many more that could be investigated. For example, the main acid used within diesel engines is the di-acid dodecenylsuccinic acid, meaning that there is potential for more complex and interesting molecular structures to form. Attempts to obtain crystals of such a complex have been an ongoing theme throughout this project, but alas all were unsuccessful, with the lithium and sodium DDSA complexes forming amorphous solids rather than single crystals. This is an obvious area where further research could be directed, with any results obtained representing a breakthrough in the field of diesel deposits. Alternatively, techniques such as small-angle X-ray scattering and small-angle neutron scattering have recently been shown to be effective at providing insight into the molecular packing of gels, which may be useful in this field if no suitable single crystals can be obtained.³³²

Despite recent government announcements stating their intention to ban the sale of diesel cars by 2035,³³³ there is currently no such legislation aimed at diesel use in commercial jet engines for example, therefore it will remain of critical importance to understand the reactive chemistry that takes place within a diesel engine system. This will allow for a more detailed insight to be gained in how to deal with any issues that may arise, as the structure that such deposits adopt may play a major role in relation to their properties. Further work could also be dedicated to gaining a better understanding of the chemical make-up of sodium naphthenate. This is the principal source of sodium in engine testing; however, the chemical structure of this compound is not known. This makes it highly likely that there will be some chemical variation between batches, which suggests that depending on the batch used you may well see different engine test results. For example, it follows that if one batch contains less sodium than another, less deposits would form. The work within this project has shown that even something as straightforward as calculating what the majority species present within sodium naphthenate is proves to be highly problematic. Therefore, in terms of engine testing, it would be prudent to potentially expand the source of sodium used within diesel

engines to other compounds that are more reproducible in their results. This would ultimately allow for more accurate engine testing to be done and hopefully enable a more accurate picture of the chemistry taking place in a diesel engine.

The outlook for small molecule fixation chemistry looks bright with plenty of opportunities for expansion. Many of the examples of alkali metal amides that have been utilised throughout this project have been lithium based, therefore it would be logical to attempt to expand the chemistry to heavier analogues. It would be intriguing to ascertain if such reactivity was maintained down Group 1 or if the sodium, potassium, rubidium and caesium examples of such amides would show more unusual reactivities given their softer nature and greater propensity for engaging in interactions with unsaturated bonds. There is one example in this project which seems to suggest a strong synergistic effect is operating due to the mixing of two different alkali metals within the same HMDS environment. This intriguing finding demands a systematic investigation of all possible permutations of alkali metal HMDS complexes and of other common amide reagents.

The nature of the small molecules used was also expanded to isocyanates. However, there are many more small molecules that could be utilised in this area. For example, it could be conceivable that other gaseous small molecules such as CO and NO₂ could be inserted into utility amides and NacNac complexes in much the same way as CO₂. Such complexes could see similar structural motifs; or could present different architectures depending on which small molecule is used. While the use of organometallic reagents is never alone going to solve the environmental issues associated with CO₂ and such molecules, it is nonetheless intriguing to uncover that such organometallic compounds are capable of transforming the CO₂ into other environmentally benign functional groups such as carboxylates and amides. The chemistry of small molecule activation at NacNac centres is particularly ripe for further development, as it could provide a cheap and easy way to obtain functionalised NacNac ligand systems, obtained *via* hydrolysis of the new systems presented in this thesis. Subsequent metallation of such species could result in the formation of new metal NacNac complex systems, which could prove to be useful in catalysis as novel alternatives to the parent metal NacNac ligand systems. Such systems may well have unusual structural constitutions which may prove to be interesting, as of course in almost all these cases the backbone γ -carbon position has a new functional group attached, which blocks this position

from any further reactivity and in some cases provides new donor coordination centres for attracting metals.

While we have showed through this work that such small molecule activations are possible on a stoichiometric basis, the next major challenge would be to investigate the viability of using the species investigated here as catalysts in such transformations. This would need to involve an ultimate end goal for the molecules captured, for example converting the captured CO₂ to methanol or some other alcohol molecule, but could in the future provide a more sustainable method of CO₂ capture technology than that which is used currently.

With the increased awareness within the chemical community on sustainability it is likely that the new ideas in this ongoing research will be at the forefront of chemical investigations in the field of small molecule activation as cheap, sustainable and easy to synthesise capture agents for CO₂ and other important small molecules.

Chapter 7: Experimental

7.1 General Experimental techniques

7.1.1 Solvent and reagent purification

All reactions unless otherwise stated were performed under a protective argon or nitrogen atmosphere using either standard Schlenk or glove box techniques.³³⁴ Hexane, THF, diethyl ether, methylcyclohexane and toluene were dried by heating to reflux over sodium benzophenone ketyl and then distilled under nitrogen prior to use.³³⁵ C₆D₆, d₈-toluene and d₈-THF were degassed by freeze-pump-thaw methods and stored over activated 4 Å molecular sieves. All reagents were purchased from commercial sources and used as received, unless otherwise stated. TMEDA, PMDETA and 2,6-diisopropylaniline were distilled and stored over activated 4 Å molecular sieves prior to use.

Lithium alkyl reagents such as ⁿBuLi are required to be standardised regularly to ensure the solution is of the correct molarity to be used in any subsequent reactions. The molarity can change over time due to evaporation of solvent or reaction with air to form hydroxides etc.

Standardisation was carried out by dissolving menthol (1 mmol, 0.156 g) and 1,10-phenanthroline (2-3 g) in 2 ml of dry THF. This pale-yellow solution was then titrated with the appropriate lithium alkyl solution (RLi) until the solution was a persistent red colour, at which point the volume of RLi added was noted. The molarity was then calculated using the formula

$$\text{Molarity of RLi} = (Z/Y) \times 1000$$

Where Z is the number of moles of menthol added and Y is the volume of RLi added to induce the colour change.

7.1.2 Analytical techniques

NMR spectra were recorded on a Bruker AV3 or AV400 MHz spectrometer operating 400.13 MHz for ¹H, 155.47 MHz for ⁷Li, 162.0 MHz for ³¹P and 100.62 MHz for ¹³C. All ¹³C NMR spectra were proton decoupled. ¹H, ¹³C{¹H}, ⁷Li and ³¹P chemical shifts are expressed in parts per million (δ, ppm) and where appropriate referenced to residual solvent peaks or external references.

Diffusion Ordered Spectroscopy (DOSY) NMR were recorded on an AV400 MHz spectrometer operating at 400.13 MHz, using either the pulse programs ledbpgp2s or dstegp3s. DOSY experiments were performed following the external calibration method introduced by Stalke.^{82, 336} As such, 30mM concentration solutions of the analyte (0.015 mmol) in either C₆D₆, d₈-THF or MeOD (0.5 ml) and tetramethylsilane or naphthalene (0.015 mmol) as an internal standard.

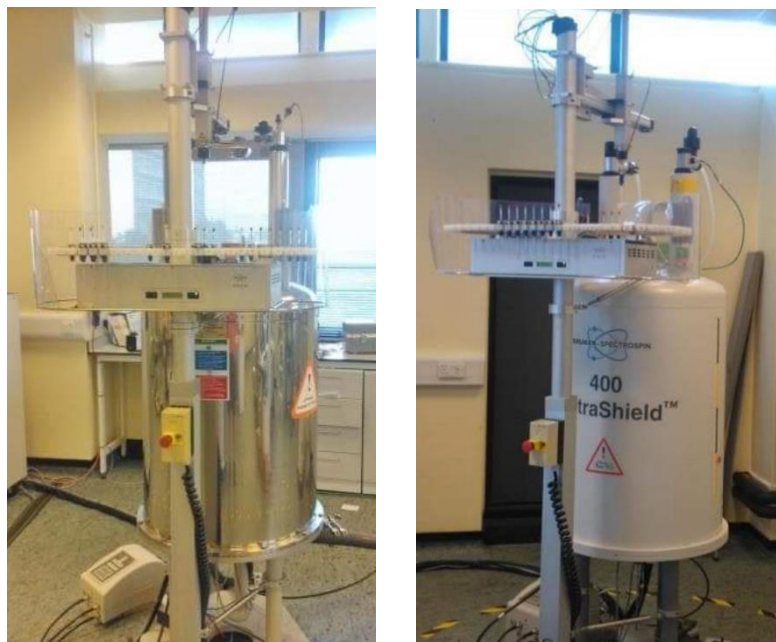


Figure 7.0: (Left) Bruker AV400 and (Right) Bruker AV300 MHz spectrometers used throughout this PhD.

IR spectra were recorded on a Perkin Elmer Spectrum 100 FTIR spectrometer and a ThermoScientific Nicolet iS5 FTIR spectrometer. Samples were prepared as nujol mulls of the isolated crystalline solids or as the isolated solids analysed directly.

Elemental analyses were performed using a Perkin Elmer 2400 elemental analyser. Due to the high sensitivity of several of the newly synthesised species in this thesis, accurate elemental analysis could not always be obtained.



Figure 7.1: (Left) ThermoScientific Nicolet iS5 FTIR and (Right) Perkin Elmer Spectrum 100 FTIR spectrometers used throughout this PhD.

X-ray crystallography data for novel complexes reported in this thesis were collected on Oxford Diffraction Gemini S or Xcalibur E instruments with graphite-monochromated Mo $\kappa\alpha$ ($\lambda = 0.71073 \text{ \AA}$) or Cu $\kappa\alpha$ ($\lambda = 1.54184 \text{ \AA}$) radiation. Data collection and processing used Rigaku and Bruker software.^{337, 338} All structures were solved and refined to convergence on F^2 for all independent reflections by the full-matrix least squares method using SHELXL-2014/7,^{337, 339} or by the Gauss Newton algorithm using OLEX2.³⁴⁰



Figure 7.2: Oxford Diffraction Gemini S instrument used throughout this PhD to obtain X-ray crystallographic data.

7.2 Experimental data for Chapter 2

The full data set underlying this research can be located online at <https://doi.org/10.15129/5dbe129a-acaf-457a-b8a5-52ba7e16fdca>.

Selected crystallographic data are shown in Tables 7.5.1 and 7.5.2 and full details for X-ray diffraction in .cif format are available from CCDC (1984053-1984056) for compounds **1-4**.

7.2.1 Synthesis of compounds

Synthesis of ⁿBuNa

Prepared *via* a literature method.³⁴¹

This was prepared *via* a metathesis reaction. NaOtBu (40 mmol, 3.84 g) was weighed into a Schlenk flask and suspended in hexane (50 ml). The suspension was cooled to 0 °C and ⁿBuLi (40 mmol, 25 ml) was added slowly. The mixture was warmed up to room temperature and left stirring overnight. The solid ⁿBuNa was collected *via* filtration and washed with hexane (3 x 20 ml) to remove the soluble LiOtBu by-product. The white ⁿBuNa solid was dried under reduced pressure and transferred to the glovebox where it was stored. Decomposition of the ⁿBuNa solid could be tracked visually, with off-white or black samples indicating decomposition. Typical yield on average was 70-75 %.

Synthesis of sodium 2-ethylhexanoate: Sodium 2-ethylhexanoate was prepared by addition of 2-ethylhexanoic acid (10 mmol, 1.6 ml) to NaOH (10 mmol, 0.4 g) in ethanol (5 ml) with stirring. Once the exothermic reaction had concluded the ethanol solvent was removed *in vacuo* and the white powder left was dried under reduced pressure (1.41 g, 85 %).

¹H NMR (400.1 MHz, D₂O, 300 K): δ 2.12 (pent, 1H, CH), 1.45 (multiplet, 4H, 2 x CH₂), 1.27 (multiplet, 4H, 2 x CH₂), 0.88 (multiplet, 6H 2 x CH₃) ppm.

¹³C{¹H} NMR (100.6 MHz, D₂O, 300K): δ 186.0 (C_{quaternary}, COO, 2-ethylhexanolate), 50.6 (CH, 2-ethylhexanolate), 31.9 (CH₂, 2-ethylhexanolate) 29.1 (CH₂, 2-ethylhexanolate), 25.6 (CH₂, 2-ethylhexanolate), 21.7 (CH₂, 2-ethylhexanolate), 12.9 (CH₃, 2-ethylhexanolate), 11.3 (CH₃, 2-ethylhexanolate) ppm.

IR ν 2958-2926 (sharp s, aliphatic CH), 1562 (sharp s, anti-symmetric COO), 1413 (sharp s, symmetric COO) cm^{-1}

Table 7.0: ^1H DOSY NMR data for sodium 2-ethylhexanoate

Compound	D [m^2s^{-1}]	MW _{calc} [g/mol]	MW _{est} [g/mol]	Error [%]
Sodium 2-ethylhexanoate	6.547×10^{-10}	435	404	8
Tetramethylsilane	1.578×10^{-9}	88	86	2

The diffusion coefficient of sodium 2-ethylhexanoate in CD_3OD indicates a molecular weight of 404 g mol^{-1} . This result is consistent with the calculate molecular weight for a dimeric structure featuring four solvating water molecules.

Synthesis of sodium octanoate: A similar procedure as above was used to synthesise a sample of sodium octanoate (1.33 g, 80 %).

^1H NMR (400.1 MHz, D_2O , 300 K): δ 2.21 (t, 2H, CH_2), 1.58 (pent, 2H, CH_2), 1.32 (broad m, 8H, 4 x CH_2), 0.90 (t, 3H, CH_3) ppm.

$^{13}\text{C}\{^1\text{H}\}$ NMR (100.6 MHz, D_2O , 300K): δ 183.7 ($\text{C}_{\text{quaternary}}$, COO, octanoate), 37.0 (CH_2 , octanoate), 30.5 (CH_2 , octanoate), 28.2 (CH_2 , octanoate), 27.7 (CH_2 , octanoate), 25.4 (CH_2 , octanoate), 21.5 (CH_2 , octanoate), 12.9 (CH_3 , octanoate) ppm.

IR ν 2919-2852 (br, aliphatic CH), 1558 (sharp s, anti-symmetric COO), 1444 & 1413 (sharp s, symmetric COO) cm^{-1}

Table 7.1: ^1H DOSY NMR data for sodium octanoate

Compound	D [m^2s^{-1}]	MW _{calc} [g/mol]	MW _{est} [g/mol]	Error [%]
Sodium octanoate	8.271×10^{-10}	397	433	-8
Tetramethylsilane	1.578×10^{-9}	88	86	3

The diffusion coefficient of sodium octanoate in CD_3OD indicates a molecular weight of 433 g mol^{-1} . This result is consistent with the calculate molecular weight for a dimeric structure featuring four solvating water molecules.

Synthesis of $[\{\text{TMP(H)}_2\}^+ \{\text{C}_5\text{H}_{10}(\text{C}_2\text{H}_5)\text{COO}\}^-]_2$, (**1**)

Method a)

A Schlenk tube was charged with $n\text{BuNa}$ (2 mmol, 0.16 g) and this was subsequently suspended in hexane (10 ml). TMP(H) (2 mmol, 0.34 ml) was added to the white suspension which was stirred for one hour at room temperature to form a yellow suspension. 2-ethylhexanoic acid (4 mmol, 0.64 ml) was added, forming a colourless solution. This was concentrated *in vacuo* and placed at -30°C . After 24 hours, colourless crystals identified as **1** had formed (yield 0.046 g, 0.16 mmol, 16 %).

Method b)

A Schlenk tube was charged with TMP(H) (1 mmol, 0.17 ml), which was subsequently dissolved in hexane (10 ml). 2-ethylhexanoic acid (1 mmol, 0.16 ml) was then added and the colourless solution concentrated *in vacuo*. This concentrated solution was then placed at -30°C . After a few days, colourless X-ray quality crystals of **1** had formed. (yield 0.191 g, 0.67 mmol, 67 %).

^1H NMR (400.1 MHz, C_6D_6 , 300 K): δ 10.12 (broad s, 2H, NH_2), 2.41 (heptet, 1H, CH,), 1.91 (m, 2H, CH_2 ,), 1.57 (broad m, 6H, CH_2 ,), 1.47 (s, 6H, CH_2 , TMP), 1.33 (s, 12H, CH_3 , TMP), 1.16 (t, 3H, CH_3 ,), 0.97 (t, 3H, CH_3 ,) ppm.

$^{13}\text{C}\{^1\text{H}\}$ NMR (100.6 MHz, C_6D_6 , 300K): δ 180.6 ($\text{C}_{\text{quaternary}}$, COO, 2-ethylhexanolate), 53.9 (TMP), 50.8 (CH, 2-ethylhexanolate), 35.4 (TMP), 33.6 (TMP), 28.0 (CH_2 , 2-ethylhexanolate), 27.1 (CH_2 , 2-ethylhexanolate), 23.5 (CH_2 , 2-ethylhexanolate), 17.4 (TMP), 14.5 (CH_3 , 2-ethylhexanolate), 13.0 (CH_3 , 2-ethylhexanolate) ppm.

IR ν 3082.3 (br s, aliphatic CH), 1631.5 (sharp s, anti-symmetric COO), 1529 (br s, symmetric COO) cm^{-1}

Melting point: 64-66 $^\circ\text{C}$

Elemental analysis Calculated: C: 71.27 %, H: 12.67 %, N: 4.89 %. Found: C: 70.78 %, H: 11.93 %, N: 4.93 %.

Synthesis of $[\{(C_5H_{10})(C_2H_5)COONa.(H_2O)(1,10\text{-phen})\}_2]_{\infty}$, (2)

Sodium 2-ethylhexanoate (1 mmol, 0.166 g) was added to a Schlenk tube and suspended in hexane (5 ml). 1,10-phenanthroline (1 mmol, 0.180 g) was then added *via* solid addition tube and the white suspension thus formed was stirred overnight. THF and gentle heating furnished a colourless solution, which when cooled slowly in a Dewar of hot water deposited colourless crystals of **2** (yield 0.1953 g, 0.27 mmol, 54 %).

1H NMR (400.1 MHz, d_8 -THF, 300 K): δ 9.19 (dd, 2H, CH_2 , 1,10-phen), 8.30 (dd, 2H, CH_2 , 1,10-phen), 7.84 (s, 2H, CH_2 , 1,10-phen), 7.60 (q, 2H, CH_2 , 1,10-phen), 2.74 (s, 2H, H_2O), 1.93 (m, 1H, CH , 2-ethylhexanoate), 1.50 (m, 2H, CH_2 , 2-ethylhexanoate), 1.15 (m, 7H, CH_2 , 2-ethylhexanoate), 0.73 (t, 3H, CH_3 , 2-ethylhexanoate), 0.65 (t, 3H, CH_3 , 2-ethylhexanoate) ppm.

$^{13}C\{^1H\}$ NMR (100.6 MHz, d_8 -THF, 300 K): δ 183.3 ($C_{quaternary}$, COO, 2-ethylhexanoate), 151.1 (CH , 1,10-phen), 147.1 (CH , 1,10-phen), 136.4 (CH , 1,10-phen), 129.4 (CH , 1,10-phen), 127.1 (CH , 1,10-phen), 123.6 (CH , 1,10-phen), 51.2 (CH , 2-ethylhexanoate), 33.4 (CH_2 , 2-ethylhexanoate), 30.9 (CH_2 , 2-ethylhexanoate), 26.7 (CH_2 , 2-ethylhexanoate), 23.7 (CH_2 , 2-ethylhexanoate), 14.3 (CH_3 , 2-ethylhexanoate), 12.8 (CH_3 , 2-ethylhexanoate) ppm.

IR ν 3375.4 (br, H_2O), 1734 (s, C=O stretch), 1580.2 (symmetric COO) cm^{-1}

Melting point: 126-130 °C

Satisfactory elemental analysis was not obtained after multiple attempts due to the sensitivity of this compound.

Synthesis of $[\{(C_5H_{10})(C_2H_5)COO.Na\}_4]_{\infty}$, (3)

A sample of sodium 2-ethylhexanoate (~100 mg) was placed in a small vial and was fully dissolved in acetone. This vial (with the top left off) was then placed into a larger vial and acetonitrile was placed in this vial, which was then sealed. This allowed for the slow diffusion of the acetonitrile into the acetone. After a few weeks, a few small crystals suitable for X-ray structural analysis had formed (yield of crystalline material not measured due to main effort being obtaining material suitable for single crystal X-ray diffraction).

No NMR or further characterisation was carried out on this sample due to the small amount of crystalline material present, as well as the fact that it would essentially be identical to the characterisation of pure sodium 2-ethylhexanoate as seen above.

Synthesis of $[(C_3H_7)(C_4H_9)COONa.(DMSO)]_\infty$, (4)

A similar procedure to that laid out to obtain crystals of **3** was followed. A sample of sodium valproate (~200 mg) was dried in an oven before being transferred to the glovebox. This was then added to 2 ml of a DMF/DMSO mixture and heated until dissolution became apparent. Slow cooling in a hot water Dewar afforded colourless crystals after a few days (yield of crystalline material not measured due to main effort being obtaining material suitable for single crystal X-ray diffraction).

1H NMR (400.1 MHz, D_2O , 300 K): δ 2.26 (pent, 1H, CH, CHCOO), 1.40 (br multiplet, 4H, 2 x CH_2 , valproate), 1.29 (sept, 4H, 2 x CH_2 , valproate), 0.90 (t, 6H, 2 x CH_3 , valproate) ppm.

$^{13}C\{^1H\}$ NMR (100.6 MHz, D_2O , 300 K): δ 186.7 ($C_{quaternary}$, COO, valproate), 48.8 (CHCOO, valproate), 35.3 (CH_2 , valproate), 20.6 (CH_2 , valproate), 13.5 (CH_3 , valproate) ppm.

IR ν 2961-2872 (sharp s, aliphatic CH), 1555 (sharp s, anti-symmetric COO), 1410 (sharp s, symmetric COO) cm^{-1}

Satisfactory elemental analysis was not obtained after multiple attempts.

Synthesis of $[(C_5H_{10})(C_2H_5)COONa(1,10-phen)]_\infty$, (5)

$nBuNa$ (1 mmol, 0.08 g) was added to a Schlenk tube and suspended in hexane (5 ml). To this suspension was added 2-ethylhexanoic acid (1mmol, 0.16 ml) and 1,10-phenanthroline (1 mmol, 0.180 g), forming a white suspension, which was stirred overnight. THF and gentle heating furnished a colourless solution, which was slowly cooled in a Dewar of hot water depositing colourless crystals of **5** (yield 0.236 g, 0.68 mmol, 68 %).

1H NMR (400.1 MHz, C_6D_6 , 300 K): δ 9.26 (dd, 2H, CH_2 , 1,10-phen), 7.52 (dd, 2H, CH_2 , 1,10-phen), 7.20 (s, 2H, CH_2 , 1,10-phen), 7.03 (q, 2H, CH_2 , 1,10-phen), 2.39 (m, 1H, CH, 2-ethylhexanoate), 1.90 (m, 2H, CH_2 , 2-ethylhexanoate), 1.67 (m, 2H, CH_2 , 2-ethylhexanoate),

1.39 (m, 2H, CH_2 , 2-ethylhexanoate), 1.27 (q, 2H, CH_2 , 2-ethylhexanoate) 1.11 (t, 3H, CH_3 , 2-ethylhexanoate), 0.84 (t, 3H, CH_3 , 2-ethylhexanoate) ppm.

$^{13}\text{C}\{^1\text{H}\}$ NMR (100.6 MHz, C_6D_6 , 300 K): δ 178.7 ($\text{C}_{\text{quaternary}}$, COO, 2-ethylhexanoate), 150.1 (CH, 1,10-phen), 146.4 (CH, 1,10-phen), 134.6 (CH, 1,10-phen), 127.8 (CH, 1,10-phen), 125.6 (CH, 1,10-phen), 122.1 (CH, 1,10-phen), 50.2 (CH, 2-ethylhexanoate), 32.2 (CH_2 , 2-ethylhexanoate), 29.9 (CH_2 , 2-ethylhexanoate), 25.6 (CH_2 , 2-ethylhexanoate), 22.7 (CH_2 , 2-ethylhexanoate), 13.5 (CH_3 , 2-ethylhexanoate), 12.0 (CH_3 , 2-ethylhexanoate) ppm.

Satisfactory elemental analysis was not obtained after multiple attempts due to the sensitivity of this compound.

Synthesis of $[\{\text{NaMg}[\text{N}(\text{iPr})_2]_2\text{OC}_2\text{H}_3(\text{C}_2\text{H}_5)\text{C}_4\text{H}_9\}_2]$, (7)

$^n\text{BuNa}$ (2 mmol, 0.16 g) was suspended in methylcyclohexane (20 ml), which was sonicated for 20 minutes to aid dissolution. To this was added Bu_2Mg (2 mmol, 2 ml) and iPrNH_2 (6 mmol, 0.84 ml), forming a yellow solution which was stirred for 30 minutes. 2-ethylhexanol (2 mmol, 0.31 ml) was added with exothermic reaction, forming a colourless solution. This was concentrated *in vacuo* and placed at $-30\text{ }^\circ\text{C}$, forming colourless crystals after a few days (yield 0.4146 g, 0.40 mmol, 40 %).

^1H NMR (400.1 MHz, C_6D_6 , 300 K): δ 3.96 (d, 1H CHO , 2-ethylhexanolate), 3.36 (pent, 1H, CHMe_2 , crown), 1.38 (m, 2H, CH_2 , 2-ethylhexanolate), 1.23 (m, 6H, CH_2Me , crown), 0.94 (t, 3H, CH_3 , 2-ethylhexanolate) ppm.

$^{13}\text{C}\{^1\text{H}\}$ NMR (100.6 MHz, C_6D_6 , 300 K): δ 64.9 (CH_2O , 2-ethylhexanolate), 45.5 (CHMe , crown), 42.3 (CH, 2-ethylhexanolate), 30.6 (CH_2 , 2-ethylhexanolate), 29.5 (CHMe_2 , crown), 23.8 (CH_2 , 2-ethylhexanolate), 23.5 (CH_2 , 2-ethylhexanolate), 22.5 (CH_2 , 2-ethylhexanolate), 14.3 (CH_3 , 2-ethylhexanolate), 11.4 (CH_3 , 2-ethylhexanolate) ppm.

Satisfactory elemental analysis was not obtained after multiple attempts due to the sensitivity of this compound.

Synthesis of $[(\text{PhNNa})_2(\text{Py})_3 \cdot 0.5(\text{THF}/\text{Py})]$, (**9**)

2-ethylhexanol (1 mmol, 0.16 ml) was added to a Schlenk tube containing hexane (5 ml). $^n\text{BuLi}$ (1.1 mmol, 0.70 ml) and NaNPh_2 (1 mmol, 0.1912 g) were added at 0 °C, forming a dark green suspension. Pyridine (2 mmol, 0.16 ml) was added to this, forming a lighter green suspension. This was stirred overnight and then heated to reflux at 85 °C, with no obvious visual change in the nature of the suspension. THF (0.6 ml) and gentle heating furnished a green solution, which was placed in a freezer operating at -20 °C. After a few days colourless crystals had formed, identified as $[(\text{PhNNa})_2(\text{Py})_3 \cdot 0.5(\text{THF}/\text{Py})]$ (**9**) (yield 0.2087 g, 0.3 mmol, 60 %).

^1H NMR (400.1 MHz, C_6D_6 , 300 K): δ 8.38 (m, 2H, 2 x CH, pyridine), 7.22 (t, 3H, 2 x CH_2 , PhNNa), 6.96 (tt, 1H, CH, PhNNa), 6.76 (t, 1H, CH, pyridine), 6.65 (m, 2H, CH_2 , PhNNa), 3.51 (t, 1H, CH_2 , THF), 1.40 (t, 1H, CH_2 , THF) ppm.

$^{13}\text{C}\{^1\text{H}\}$ NMR (100.6 MHz, C_6D_6 , 300 K): δ 150.2 (CH, pyridine), 135.5 ($\text{C}_{\text{quaternary}}$, Ph_2NNa), 130.0 (CH, Ph_2NNa), 123.6 (CH, Ph_2NNa), 118.8 (Ph_2NNa , Ph_2NNa), 67.9 (CH_2 , THF), 25.7 (CH_2 , THF) ppm.

Satisfactory elemental analysis was not obtained after multiple attempts due to the sensitivity of this compound.

7.3 Experimental data for Chapter 4

The full data set underlying this research can be located online at <http://dx.doi.org/10.15129/1ae0a46f-614f-4994-9d61-9473bab1807b>. Selected crystallographic data are shown in Table 7.5.3 and full details of X-ray diffraction in .cif format are available from CCDC (1873068 – 1873070). Two molecules of hexane co-crystallised in the unit cell of complex **11**, with the corresponding electron density removed using the SQUEEZE routine implemented within the software program PLATON.³⁴² Approximately 102 electron equivalents were removed from 818 Å³ of unit cell volume. Compound **12** was refined as an inversion twin, Flack parameter 0.27(6).

7.3.1 Synthesis of compounds

Synthesis of $[(\text{THF})\cdot\text{Li}(\text{CO}_2\text{NC}_4\text{H}_4)]_\infty$, (**10**)

ⁿBuLi (0.69 mL, 1.6 M in hexane, 1.1 mmol) was added *via* syringe to a cooled solution of 1H-pyrrole (0.07 mL, 1.0 mmol) in hexane (5 mL) at 0 °C, furnishing a grey suspension. After stirring for 15 minutes, CO₂ was bubbled through this suspension *via* a cannula and gas distribution tube from an adjacent Schlenk tube filled with dry ice. This formed a white precipitate with an exothermic reaction. After 10 minutes, the gas distribution tube was removed and THF was added with gentle heating to furnish a grey coloured solution. Upon cooling in a hot water Dewar overnight, a crop of X-ray quality colourless crystals had deposited (yield 0.0791 g, 0.42 mmol, 42 %).

¹H NMR (400.1 MHz, d₈-THF, 300 K): δ 7.27 (t, J = 2.2Hz, 2 H, CH₂), 5.94 (t, J = 2.2Hz, 2 H, CH₂), 3.61 (t, J = 6.64Hz, 4 H, 2 x CH₂), 1.77 (t, J = 6.62 Hz 4 H, 2 x CH₂) ppm.

¹³C{¹H} NMR (100.6 MHz, d₈-THF, 300 K): δ 155.1 (s, COO), 120.8 (s, CH₂), 109.2 (s, CH₂) ppm.

⁷Li NMR (155.5 MHz, d₈-THF, 300 K): δ 2.18 (s) ppm.

IR ν 1623 (br s, anti-symmetric COO), 1261.3 (s, symmetric COO) cm⁻¹

Due to the extreme air- and moisture-sensitivity of this complex, satisfactory elemental analysis could not be obtained despite multiple attempts.

Synthesis of $[(iPr_2NCOOLi)_{12}(iPr_2NCOOH)_2]$, (11)

$nBuLi$ (0.69 mL, 1.6 M in hexane, 1.1 mmol) was added *via* syringe to a cooled solution of diisopropylamine (0.14 mL, 1 mmol) in hexane (5 mL) at 0 °C, furnishing a white precipitate. After stirring for 15 minutes, PMDETA (0.21 mL, 1 mmol) was added, furnishing a pale green solution. Upon stirring for a further 15 minutes, CO_2 was bubbled through this solution *via* a cannula and gas distribution tube from an adjacent Schlenk tube filled with dry ice. This furnished a homogenous colourless solution with exothermic reaction, which was subsequently placed at -33 °C. After a few days, colourless crystals had formed (yield 0.0580 g, 0.023 mmol, 33 % based on diisopropylamine).

1H NMR (400.1 MHz, C_6D_6 , 300 K): δ 2.79 (quintet, $J = 5.92$ Hz, 1H, CH), 0.95 (d, $J = 6.16$ Hz, 6H, CH_3) ppm.

$^{13}C\{^1H\}$ NMR (100.6 MHz, C_6D_6 , 300 K): δ 45.4 (s, CH), 23.8 (s, CH_3) ppm.

7Li NMR (155.5 MHz, d_8 -toluene, 300 K): δ 0.50 (br s) ppm.

7Li NMR (155.5 MHz, d_8 -toluene, 350 K): δ 0.36 (s), 0.45 (s), 0.58 (s) ppm.

IR ν 1594.3 + 1545 (s, anti-symmetric COO), 1360 + 1265.6 (s, symmetric COO) cm^{-1}

Due to the extreme air- and moisture-sensitivity of this complex, satisfactory elemental analysis could not be obtained despite multiple attempts.

Synthesis of $[(Me_3Si)NC(=O)OC(=O)N(H)(SiMe_3)]_2LiNa(THF)_4$, (12)

LiHMDS (1 mmol, 0.1673 g) and NaHMDS (1 mmol, 0.1834 g) were added to a Schlenk within an Argon filled glovebox. They were then dissolved in THF (5 ml), giving a pale-yellow solution which was stirred for 30 minutes. This solution was then cooled to -78 °C. Upon stirring for a further 15 minutes, CO_2 was bubbled through this solution *via* a cannula and gas distribution tube from an adjacent Schlenk tube filled with dry ice. This furnished a slightly more viscous solution, which was allowed to warm slowly to room temperature, whereupon a pale-yellow solution reformed. This was placed at -33 °C. After a period of five days, a crop of X-ray quality colourless crystals had formed (yield 0.3746 g, 0.47 mmol, 51 %).

^1H NMR (400.1 MHz, d_8 -THF, 300 K): δ 0.07 (s, 6 H, Me_3Si) ppm.

$^{13}\text{C}\{^1\text{H}\}$ NMR (100.6 MHz, d_8 -THF, 300 K): δ 1.79 (s, Me_3Si) ppm.

^7Li NMR (155.5 MHz, d_8 -THF, 300 K): δ -0.34 (s) ppm.

IR ν 3420.4 (broad, NH), 2245.5 (s, C-N), 1651.8 (s, C=O) cm^{-1}

Due to the extreme air- and moisture-sensitivity of this complex, satisfactory elemental analysis could not be obtained despite multiple attempts.

Synthesis of lithium butanoate using CO_2

n-Propyllithium (2 mmol, 2 ml) was dissolved in a Schlenk tube containing hexane solvent (5 ml). This was cooled to -50°C and CO_2 was bubbled through this solution *via* a cannula and gas distribution tube from an adjacent Schlenk tube filled with dry ice, forming a white suspension. The solvent was removed *in vacuo* and the white solid left behind was analysed *via* ^1H NMR spectroscopy (yield 0.147 g, 1.6 mmol, 78 %).

^1H NMR (400.1 MHz, MeOD, 300 K): δ 2.03 (t, 2H, CH_2COO), 1.51 (hex, 2H, CH_3), 0.83 (t, 3H, CH_3) ppm.

$^{13}\text{C}\{^1\text{H}\}$ NMR (100.6 MHz, MeOD, 300 K): δ 183.9 (s, COO), 39.4 (s, CH_2COO), 19.1 (s, CH_2), 13.0 (s, CH_3) ppm.

Table 7.2: ^1H DOSY NMR data for lithium butanoate

Compound	$D [\text{m}^2\text{s}^{-1}]$	$\text{MW}_{\text{calc}} [\text{g/mol}]$	$\text{MW}_{\text{est}} [\text{g/mol}]$	Error [%]
Lithium butanoate	8.775×10^{-10}	316	306	3
naphthalene	1.691×10^{-9}	128	129	-1

The diffusion coefficient of lithium butanoate in CD_3OD indicates a molecular weight of 306 g mol^{-1} . This result is consistent with the calculate molecular weight for a dimeric structure featuring four solvating methanol molecules.

Synthesis of sodium butanoate using CO₂

n-Propylsodium was synthesised *in situ* from *n*-propyllithium (2 mmol, 2 ml) and Na^tOBu (2 mmol, 0.192 g). This was filtered to remove the Li^tOBu by product and the solid *n*-propylsodium was suspended in a Schlenk tube containing hexane solvent (5 ml). This was cooled to -50 °C and CO₂ was bubbled through this solution *via* a cannula and gas distribution tube from an adjacent Schlenk tube filled with dry ice, forming a thicker white suspension. The solvent was removed *in vacuo* and the solid left behind analysed *via* NMR spectroscopy (yield 0.143 g, 1.3 mmol, 65 %).

¹H NMR (400.1 MHz, MeOD, 300 K): δ 2.06 (t, 2H, CH₂COO), 1.55 (hex, 2H, CH₃), 0.87 (t, 3H, CH₃) ppm.

¹³C{¹H} NMR (100.6 MHz, MeOD, 300 K): δ 183.7 (s, COO), 39.6 (s, CH₂COO), 19.4 (s, CH₂), 13.2 (s, CH₃) ppm.

Table 7.3: ¹H DOSY NMR data for sodium butanoate

Compound	D [m ² s ⁻¹]	MW _{calc} [g/mol]	MW _{est} [g/mol]	Error [%]
Sodium butanoate	9.090x10 ⁻¹⁰	307	302	-2
naphthalene	1.754x10 ⁻⁹	128	126	2

The diffusion coefficient of sodium butanoate in CD₃OD indicates a molecular weight of 302 g mol⁻¹. This result is consistent with the calculated molecular weight for a monomeric structure featuring six solvating methanol molecules.

7.4 Experimental data for Chapter 5

The full data set underlying this research can be located online at <http://dx.doi.org/10.15129/a4116ecb-94bf-4664-8d25-d2f2bae50825>. Selected crystallographic data are shown in Tables 7.5.4 and 7.5.5 and full details of X-ray diffraction in .cif format are available from CCDC (1947186-1947189) for compounds **13-16**.

7.4.1 Synthesis of compounds

Synthesis of NacNac(H)

Prepared *via* a literature method.¹⁷²

2,4-pentanedione (44.44 mmol, 4.45 g) and 2,6-diisopropylaniline (107 mmol, 19.1 g) were added to a round bottom flask containing ethanol (200 ml). Concentrated 12 M HCl (5 ml) was then added and the solution heated at reflux for 3 days. After this length of time the solvent was removed *in vacuo* and the pink residue left was suspended in hexane (300 ml) and heated at reflux for one hour. The slurry left was then filtered, and the white solid salt was subsequently treated with aqueous Na₂CO₃ (200 ml) and dichloromethane (300 ml). The slurry was stirred until the solid dissolved and the organic layer was then separated, dried with MgSO₄ and filtered. The solvent was removed *in vacuo* and the product washed with cold methanol (50 ml). The pure NacNac(H) ligand was dried under reduced pressure to remove any residual solvent, giving a yield of 70 % on average.

¹H NMR (400.1 MHz, CDCl₃, 300 K): δ 12.25 (s, 1H, NH), 7.13 (m, 6H, CH, Ar*), 5.01 (s, 1H, CH, γ -CH), 3.26 (pent, 4H, 4 x CH, iPr), 1.86 (s, 6H, 2 x CH₃, Me), 1.36 (d, 12H, 4 x CH₃, iPr), 1.26 (d, 12H, 4 x CH₃, iPr) ppm.

¹³C{¹H} NMR (100.6 MHz, CDCl₃, 300 K): δ 161.3 (C-CH₃, NacNac), 142.6 (C_{quaternary}, Ar*), 140.9 (CH, Ar*), 125.2 (CH, Ar*), 123.2 (CH, Ar*), 93.4 (CH, NacNac), 28.3 (CH, iPr), 24.4 (CH, iPr), 23.4 (C-CH₃, NacNac), 20.9 (CH₃, NacNac) ppm.

Synthesis of Me₆-TREN

Prepared *via* a literature method.³⁴³

Acetic acid (135 ml) and tren (19.9 mmol, 3 ml) were dissolved in acetonitrile (600 ml). To this was added aqueous formaldehyde (660 mmol, 49 ml) and the solution was allowed to

stir for one hour. This was then cooled to 0 °C and sodium borohydride (13.4 mmol, 10 g) was added slowly. The mixture was stirred for 48 hours and the solvent was removed *in vacuo*. The residue was made strongly basic with aqueous sodium hydroxide (3 M) and extracted with DCM. These extracts were combined, dried with MgSO₄ and the solvent removed. The residue was dissolved in pentane, filtered and the filtrate reduced to dryness to give Me₆-TREN as a pale-yellow oil. The average yield was 3.9 g, 85 %.

¹H NMR (400.1 MHz, CDCl₃, 300 K): δ 2.44 (m, 6H, CH₂NMe₂), 2.21 (m, 6H, NCH₂CH₂NMe), 2.07 (s, 18H, CH₃) ppm.

Synthesis of [{(MeCN-2,6-*i*Pr₂C₆H₃)₂CH(CO₂)}Li.TMEDA]₂, (13)

A Schlenk tube was charged with NacNac(H) (0.41 g, 1 mmol) and this was subsequently dissolved in hexane (10 ml). ⁿBuLi (0.69 ml, 1.6 M in hexane, 1.1 mmol) was added to the cooled solution at 0 °C and the yellow solution thus formed was stirred for one hour at room temperature. TMEDA (0.15 ml, 1 mmol) was added, forming a dark solution which was stirred for one hour. This solution was then cooled to -50 °C. CO₂ was then bubbled through this solution *via* a cannula and gas distribution tube from an adjacent Schlenk tube filled with dry ice. This furnished a pale-yellow solution, which was concentrated *in vacuo* until a colour change to green was observed. This green solution was then placed at -20 °C. After a period of two weeks, a crop of X-ray quality colourless crystals had formed (yield 0.538 g, 0.46 mmol, 46 %).

¹H NMR (400.1 MHz, C₆D₆, 300 K): δ 7.17 (broad m, 1H, CH, Ar*), 7.12 (broad m, 5H, CH, Ar*), 4.80 (s, 1H, CH, NacNac), 3.27 (q, 2H, CH, ⁱPr), 3.08 (broad q, 2H, CH, ⁱPr), 2.11 (s, 12H, CH₃, TMEDA), 2.07 (s, 4H, CH₂, TMEDA), 1.97 (s, 3H, CH₃, NacNac), 1.19 (broad m, 24H, CH₃, ⁱPr) ppm.

¹³C{¹H} NMR (100.6 MHz, C₆D₆, 300 K): δ 170.2 (C_{quaternary}, COO), 161.5 (C-CH₃, NacNac), 142.8 (C_{quaternary}, Ar*), 125.9 (CH, Ar*), 123.6 (CH, Ar*), 123.3 (CH, Ar*), 94.3 (CH, NacNac), 57.4 (CH, TMEDA), 46.0 (CH, TMEDA), 28.7 (CH, ⁱPr), 24.5 (CH, ⁱPr), 23.4 (CH₃, NacNac), 20.8 (CH₃, NacNac) ppm.

⁷Li NMR (155.5 MHz, C₆D₆, 300K): δ 0.86 (s) ppm.

IR γ 1636.4 (br s, anti-symmetric COO), 1591 (s, C=N) cm⁻¹

Melting point: 117-120 °C

Elemental analysis *Calculated:* C: 73.94 %, H: 9.82 %, N: 9.58 %. *Found:* C: 73.91 %, H: 9.76 %, N: 8.61 %.

Synthesis of $\{[(\text{MeCN-2,6-}i\text{Pr}_2\text{C}_6\text{H}_3)_2\text{C}(\text{CONH}(t\text{-Bu}))]\text{Li.TMEDA}\}$, (14)

A Schlenk tube was charged with NacNac(H) (0.41 g, 1 mmol) and this was subsequently dissolved in hexane (10 ml). $n\text{BuLi}$ (0.69 ml, 1.6 M in hexane, 1.1 mmol) was added to the cooled solution at 0 °C and the yellow solution thus formed was stirred for one hour at room temperature. TMEDA (0.15 ml, 1 mmol) and $t\text{-BuNCO}$ (0.11 ml, 1 mmol) was then added, forming a brown suspension. This was then heated at reflux for one hour at 85 °C, forming a dark brown solution, which was subsequently placed at -30 °C. After a few days, colourless crystals had formed (yield 0.363 g, 0.48 mmol, 48 %).

^1H NMR (400.1 MHz, C_6D_6 , 300 K): δ 11.46 (s, 1H, NH, CONH), 7.29 (d, 2H, CH, Ar*), 7.19 (m, 3H, CH, Ar*), 7.09 (m, 1H, CH, Ar*), 3.35 (m, 4H, CH, $i\text{Pr}$), 2.04 (s, 4H, CH_2 , TMEDA), 1.99 (s, 12H, CH_3 , TMEDA), 1.83 (br s, 3H, CH_3 , NacNac), 1.62 (s, 9H CH_3 , $t\text{-Bu}$), 1.38 (d, 6H, $i\text{Pr}$), 1.32 (d, 6H $i\text{Pr}$), 1.26 (d, 6H $i\text{Pr}$), 1.21 (d, 6H $i\text{Pr}$) ppm.

$^{13}\text{C}\{^1\text{H}\}$ NMR (100.6 MHz, C_6D_6 , 300 K): δ 171.1 ($\text{C}_{\text{quaternary}}$, CON), 169.6 (C- CH_3 , NacNac), 139.3 (CH, Ar*), 123.5 ($\text{C}_{\text{quaternary}}$, Ar*), 123.3 ($\text{C}_{\text{quaternary}}$, Ar*), 122.4 ($\text{C}_{\text{quaternary}}$, Ar*), 100.7 (CH, NacNac), 56.7 (CH, TMEDA), 49.8 ($\text{C}_{\text{quaternary}}$, $t\text{-BuNHCO}$), 45.4 (CH, TMEDA), 30.1 (CH_3 , $t\text{-BuNHCO}$), 28.5 (CH, $i\text{Pr}$), 24.8 (CH, $i\text{Pr}$), 23.2 (CH, $i\text{Pr}$), 14.4 (CH_3 , NacNac) ppm.

^7Li NMR (155.5 MHz, C_6D_6 , 300K): δ 1.28 (s) ppm.

IR γ 3413 (br, NH stretch), 1602 (s, C=N), 1550 (s, C=N) cm^{-1}

Melting point: 142-145 °C

Elemental analysis *Calculated:* C: 74.96 %, H: 10.54 %, N: 10.93 %. *Found:* C: 74.82 %, H: 10.47 %, N: 10.82 %.

Synthesis of $[(\text{MeCN-2,6-}i\text{Pr}_2\text{C}_6\text{H}_3)_2\text{C(O)Li}\{\text{NH}(\text{tBu})\text{CO}\}]_2$, (**15**)

A Schlenk tube was charged with NacNac(H) (0.41 g, 1 mmol) and this was subsequently dissolved in hexane (5 ml). $n\text{BuLi}$ (0.69 ml, 1.6 M in hexane, 1.1 mmol) was added to the cooled solution at 0 °C and the yellow solution thus formed was stirred for one hour at room temperature. Me_6TREN (0.26 ml, 1 mmol) was added to form a white suspension. Addition of $t\text{-BuNCO}$ (0.11 ml, 1 mmol) formed a pale-yellow suspension, which was heated at reflux for one hour at 85 °C, forming a pale-yellow solution, which was subsequently placed at -30 °C. After a few days, colourless crystals identified as **15** had formed (yield 0.368 g, 0.68 mmol, 68 %).

^1H NMR (400.1 MHz, C_6D_6 , 300 K): δ 8.51 (s, 1H, NH, CONH), 7.05 (t, 4H, CH, Ar*), 6.95 (t, 2H, CH, Ar*), 2.90 (broad m, 4H, CH, $i\text{Pr}$), 1.92 (s, 5H, CH_3 , NacNac), 1.30 (s, 9H, CH_3 , $t\text{-Bu}$), 1.13 (d, 11H, CH_3 , $i\text{Pr}$), 1.07 (broad d, 12H, CH_3 , $i\text{Pr}$) ppm.

$^{13}\text{C}\{^1\text{H}\}$ NMR (100.6 MHz, C_6D_6 , 300 K): δ 146.9 (C- CH_3 , NacNac), 137.2 (CH, Ar*), 124.1 ($\text{C}_{\text{quaternary}}$, Ar*), 123.4 ($\text{C}_{\text{quaternary}}$, Ar*), 51.1 ($\text{C}_{\text{quaternary}}$, $t\text{-BuNHCO}$), 28.8 (CH_3 , $t\text{-BuNHCO}$), 28.2 (CH, $i\text{Pr}$), 23.6 (CH, $i\text{Pr}$), 23.4 (CH, $i\text{Pr}$) ppm.

^7Li NMR (155.5 MHz, C_6D_6 , 300 K): δ 2.23 (s) ppm.

IR ν 3409.6 (s, NH stretch), 3285.2 (s, NH stretch), 1665.6 (s, C=N), 1614.4 (s, C=N), 1263.5 (s, C-O) cm^{-1}

Melting point: 121-125 °C

Elemental analysis *Calculated:* C: 75.66 %, H: 9.34 %, N: 7.79 %. *Found:* C: 66.69 %, H: 9.27 %, N: 7.35 %. Due to the air- and moisture sensitivity of the samples, more accurate elemental analysis could not be obtained.

Synthesis of $[(\text{MeCN-2,6-}i\text{Pr}_2\text{C}_6\text{H}_3)_2\text{C(CONH}(i\text{-Pr}))\text{Li.THF}]_2$, (**16**)

A Schlenk tube was charged with NacNac(H) (0.41 g, 1 mmol) and this was subsequently dissolved in hexane (5 ml). $n\text{BuLi}$ (0.69 ml, 1.6 M in hexane, 1.1 mmol) was added to the cooled solution at 0 °C and the yellow solution thus formed was stirred for one hour at room temperature. PMDETA (0.21 ml, 1 mmol) was added, forming a green suspension. After one hour, $i\text{-PrNCO}$ (0.10 ml, 1 mmol) was added, forming a slightly darker green suspension.

Addition of ~ 2 ml of THF and gentle heating gave a brown solution, which was subsequently placed at -30 °C. After a few days, colourless crystals had formed (yield 0.251 g, 0.20 mmol, 41 %).

¹H NMR (400.1 MHz, d₈-THF, 300 K): δ 10.95 (d, 1H, NH, CONH), 7.00 (broad m, 4H, CH, Ar*), 6.85 (m, 2H, CH, Ar*), 4.03 (m, 1H, CHiPr), 3.09 (m, 3H, CH, ⁱPr), 1.13 (d, 12H, CH₃, ⁱPr), 1.08 (d, 12H, CH₃, ⁱPr) ppm.

¹³C{¹H} NMR (100.6 MHz, d₈-THF, 300 K): δ 169.2 (C_{quaternary}, CON), 149.0 (CH, Ar*), 126.0 (C_{quaternary}, Ar*), 123.7 (C_{quaternary}, Ar*), 123.5 (C_{quaternary}, Ar*), 99.9 (CH, NacNac), 68.1 (C_{quaternary}, ⁱPrCN), 57.2 (CH₂, PMDETA), 46.2 (CH₂, PMDETA), 41.0 (CH₃, PMDETA), 28.2 (CH, ⁱPr), 26.1 (CH₃, ⁱPrNHCO), 23.6 (CH, ⁱPr), 22.6 (CH, ⁱPr), 18.3 (CH₃, NacNac) ppm.

⁷Li NMR (155.5 MHz, d₈-THF, 300 K): δ 0.70 (s) ppm.

IR γ 3377.5 (br, NH), 1587.9 (s, C=N), 1537.5 (s, C=N) cm⁻¹

Melting point: 150-156 °C

Elemental analysis *Calculated:* C: 76.25 %, H: 9.86 %, N: 7.21 %. *Found:* C: 66.64 %, H: 9.46 %, N: 7.72 %. Due to the air- and moisture sensitivity of the samples, more accurate elemental analysis could not be obtained.

Synthesis of [{(MeCN-2,6-ⁱPr₂C₆H₃)₂C(CONH(*t*-Bu))}]Li.PMDETA, (**17**)

NacNac(H) (1 mmol, 0.41 g) was placed in a Schlenk tube and dissolved in hexane (5 ml). ⁿBuLi (1.1 mmol, 0.69 ml) was added at 0 °C, followed by NaO^tBu (1 mmol, 0.096 g). The solid formed was filtered and washed with hexane. This solid was suspended in hexane (5 ml) and PMDETA (1 mmol, 0.21 ml) was added, forming a dark solution. To this was added ^tBuNCO (1 mmol, 0.11 ml), forming an olive-green suspension. This was heated at reflux for one hour, resulting in the formation of a golden-brown solution. This was concentrated *in vacuo* and placed in a freezer operating at -26 °C, which led to the formation of colourless crystals identified as [{(MeCN-2,6-ⁱPr₂C₆H₃)₂C(CONH(*t*-Bu))}]Li.PMDETA (**17**) (yield 0.3694 g, 0.53 mmol, 53 %).

¹H NMR (400.1 MHz, C₆D₆, 300 K): δ 11.48 (s, 1H, NH, CONH), 7.27 (m, 2H, 2 x CH, Ar*), 7.22 (m, 2H, 2 x CH, Ar*), 7.07 (m, 2H, 2 x CH, Ar*), 3.27 (broad m, 4H, CH, ⁱPr), 2.09 (s, 3H, CH₃, ⁱPr), 1.92 (s, 3H, CH₃, ⁱPr) ppm.

(s, 5H, CH₃, NacNac), 1.59 (s, 9H, CH₃, tBu), 1.21 (m, 13H, CH₃, ⁱPr), 1.13 (m, 11H, CH₃, ⁱPr) ppm.

¹³C{¹H} NMR (100.6 MHz, C₆D₆, 300 K): δ 169.4 (C_{quaternary}, CON), 138.6 (CH, Ar*), 125.9 (C_{quaternary}, Ar*), 123.6 (C_{quaternary}, Ar*), 123.4 (C_{quaternary}, Ar*), 100.8 (CH, NacNac), 65.9 (C_{quaternary}, ⁱPrCN), 58.1 (CH₂, PMDETA), 56.6 (CH₂, PMDETA), 49.7 (CH₃, PMDETA), 30.1 (CH, ⁱPr), 28.7 (CH₃, ⁱPrNHCO), 24.9 (CH, ⁱPr), 22.6 (CH, ⁱPr), 15.6 (CH₃, NacNac) ppm.

⁷Li NMR (155.5 MHz, C₆D₆, 300 K): δ 1.25 (s) ppm.

Due to the extreme air- and moisture-sensitivity of this complex, satisfactory elemental analysis could not be obtained despite multiple attempts.

Synthesis of [{(2,6-*i*Pr₂C₆H₃)}NCON(*t*Bu)Li.PMDETA], (18)

2,6-diisopropylamine (1 mmol, 0.19 ml) was added to a Schlenk tube and dissolved in hexane (5 ml). To this solution was added ⁿBuLi (1.1 mmol, 0.69 ml) and PMDETA (1 mmol, 0.21 mmol), forming a yellow solution. Addition of *t*BuNCO (1 mmol, 0.11 ml) formed a cream suspension, which upon heating to reflux for 30 minutes formed a red solution. This was concentrated until the product precipitated, before being heated and left in a hot water Dewar overnight, whereupon crystals suitable for a single crystal X-ray diffraction study were deposited (yield 0.214 g, 0.47 mmol, 47 %).

¹H NMR (400.1 MHz, C₆D₆, 300 K): δ 11.48 (s, 1H, NH, CONH), 7.10 (m, 3H, 3 x CH, Ar*), 7.07 (m, 2H, 2 x CH, Ar*), 3.32 (broad m, 2H, CH, ⁱPr), 2.20 (br s, 3H, CH₃, PMDETA), 2.07 (br s, 12H, 4 x CH₃, PMDETA), 1.97 (br m, 8H, 4 x CH₂, PMDETA), 1.58 (s, 9H, CH₃, *t*Bu), 1.27 (br m, 11H, CH₃, ⁱPr), 1.18 (br m, 11H, CH₃, ⁱPr) ppm.

¹³C{¹H} NMR (100.6 MHz, C₆D₆, 300 K): δ 169.4 (C_{quaternary}, CON), 138.6 (CH, Ar*), 125.9 (C_{quaternary}, Ar*), 123.5 (C_{quaternary}, Ar*), 123.3 (C_{quaternary}, Ar*), 56.5 (CH₂, PMDETA), 55.8 (CH₂, PMDETA), 49.7 (CH₃, PMDETA), 28.4 (CH₃, ⁱPrNHCO), 25.0 (CH, ⁱPr), 22.6 (CH, ⁱPr) ppm.

⁷Li NMR (155.5 MHz, C₆D₆, 300 K): δ 1.25 (s) ppm.

Due to the extreme air- and moisture-sensitivity of this complex, satisfactory elemental analysis could not be obtained despite multiple attempts.

Synthesis of $\{[(\text{MeCN-2,6-}i\text{Pr}_2\text{C}_6\text{H}_3)_2\text{CH}]\text{Li.NCN}(\text{C}_6\text{H}_{11})_2\}$, (19)

NacNac(H) (1 mmol, 0.41 g) was added to a Schlenk flask and dissolved in hexane (5 ml). This was cooled to 0 °C and $n\text{BuLi}$ (1.1 mmol, 0.72 ml) and TMEDA (1 mmol, 0.15 ml) added to form a yellow solution. DCC (1 mmol, 0.206 g) was added and the yellow solution was concentrated and cooled in the fridge. This formed small colourless crystals within 24 hours (yield 0.523 g, 0.83 mmol, 83 %).

^1H NMR (400.1 MHz, C_6D_6 , 300 K): δ 7.12 (d, 4H, CH, Ar*), 7.02 (t, 2H, CH, Ar*), 7.09 (m, 1H, CH, Ar*), 5.02 (s, 1H, $\gamma\text{-CH}$, NacNac), 3.43 (pent, 4H, CH, $i\text{Pr}$), 2.28 (s, 2H, CH_2 , TMEDA), 1.88 (s, 6H, CH_3 , TMEDA), 1.88 (s, 6H, 2 x CH_3 , NacNac), 1.27 (quart, 26H, 6 x $i\text{Pr}$, NacNac) ppm.

$^{13}\text{C}\{^1\text{H}\}$ NMR (100.6 MHz, C_6D_6 , 300 K): δ 163.8 (C- CH_3 , NacNac), 141.1 (CH, Ar*), 123.6 ($\text{C}_{\text{quaternary}}$, Ar*), 123.3 ($\text{C}_{\text{quaternary}}$, Ar*), 122.9 ($\text{C}_{\text{quaternary}}$, Ar*), 93.2 (CH, NacNac), 55.8 (CH, TMEDA), 35.0 (CH, TMEDA), 28.3 (CH, $i\text{Pr}$), 24.6 (CH, $i\text{Pr}$), 23.7 (CH, $i\text{Pr}$), 14.3 (CH_3 , NacNac) ppm.

^7Li NMR (155.5 MHz, C_6D_6 , 300K): δ 2.61 (s) ppm.

Due to the extreme air- and moisture-sensitivity of this complex, satisfactory elemental analysis could not be obtained despite multiple attempts.

Synthesis of $\{[(\text{MeCN-2,6-}i\text{Pr}_2\text{C}_6\text{H}_3)_2\text{CH}]\text{Li.OP}(\text{C}_6\text{H}_5)_3\}$, (20)

NacNac(H) (1 mmol, 0.41 g) was added to a Schlenk flask and dissolved in hexane (5 ml). This was cooled to 0 °C and $n\text{BuLi}$ (1.1 mmol, 0.75 ml) and PMDETA (1 mmol, 0.21 ml) added to form a yellow solution. Ph_3PO (1 mmol, 0.278 g) was added, forming an orange solution which was concentrated and cooled to -18 °C. This formed small colourless crystals within 24 hours (yield 0.55 g, 0.78 mmol, 78 %).

^1H NMR (400.1 MHz, C_6D_6 , 300 K): δ 7.18 (d, 2H, 2 x CH, Ar* NacNac), 7.12 (m, 4H, CH_2 , Ar* NacNac), 6.97 (br m, 15H, CH, Ph), 5.03 (s, 1H, CH, $\gamma\text{-CH}$), 3.53 (pent, 4H, 4 x CH, $i\text{Pr}$), 1.91 (s, 6H, 2 x CH_3 , Me), 1.26 (d, 12H, 4 x CH_3 , $i\text{Pr}$), 1.01 (d, 12H, 4 x CH_3 , $i\text{Pr}$) ppm.

$^{13}\text{C}\{^1\text{H}\}$ NMR (100.6 MHz, C_6D_6 , 300 K): δ 163.4 (C- CH_3 , NacNac), 141.4 (CH, Ar*), 132.3 (CH, Ar Ph_3PO), 132.0 (CH, Ar Ph_3PO), 128.9 (CH, Ar Ph_3PO), 125.9 (CH, Ar Ph_3PO), 123.6 ($\text{C}_{\text{quaternary}}$,

Ar*), 123.2 (C_{quaternary}, Ar*), 122.5 (C_{quaternary}, Ar*), 92.9 (CH, NacNac), 28.2 (CH, ⁱPr), 24.7 (CH, ⁱPr), 23.6 (CH, ⁱPr), 14.3 (CH₃, NacNac) ppm.

⁷Li NMR (155.5 MHz, C₆D₆, 300 K): δ 2.70 (s) ppm.

³¹P NMR (104.2 MHz, C₆D₆, 300K): δ 30.8 ppm.

Due to the extreme air- and moisture-sensitivity of this complex, satisfactory elemental analysis could not be obtained despite multiple attempts.

7.5 Crystal structure data and refinement details for compounds reported in this thesis

Table 7.5.1: Chapter 2 – compounds 1-4

Compound	$\{[TMP(H)_2]^+ [C_5H_{10}(C_2H_5)COO]^{-}\}_2$, 1	$\{[(C_5H_{10})(C_2H_5)COONa \cdot (H_2O)[1,10\text{-phen}]]_2\}_\infty$, 2	$\{[(C_5H_{10})(C_2H_5)COO \cdot Na]\}_\infty$, 3	$\{[(C_3H_7)(C_4H_8)COONa \cdot (DMSO)]_\infty\}$, 4
Empirical Formula	$C_{17}H_{35}NO_2$	$C_{40}H_{50}Na_2N_4O_6$	$C_8H_{15}O_2Na$	
Molecular Mass	285.46	728.82	166.19	244.32
λ	Cu K α ($\lambda = 1.54184$)	Cu K α ($\lambda = 1.54184$)	Mo K α ($\lambda = 0.71073$)	Cu K α ($\lambda = 1.54184$)
Space Group	P-1	P-1	P-4 ₂ C	P-1
Crystal system	Triclinic	Triclinic	Tetragonal	Triclinic
a/Å	8.3504(4)	6.8138(8)	17.5765(11)	5.8415(4)
b/Å	10.2287(5)	10.8522(13)	17.5765(11)	10.4932(8)
c/Å	11.3640(7)	14.0979(16)	6.0509(11)	11.9836(9)
$\alpha/^\circ$	77.036(5)	77.786(10)	90	102.165(7)
$\beta/^\circ$	75.973(5)	83.321(9)	90	94.355(6)
$\gamma/^\circ$	76.879(4)	71.838(10)	90	105.885(6)
Volume/Å ³	902.27(9)	966.7(2)	1869.3(4)	682.40(9)
Z	2	1	8	2
Measured Reflections	7444	7829	8829	6418
Unique Reflections	3533	3807	2120	2672
R _{int}	0.0209	0.0369	0.0541	0.0311
Observed Reflections [$I > 2\sigma I$]	3088	3008	1420	2276
Goodness of Fit	1.122	1.034	1.023	1.069
R [on F, obs refs only]	0.0585	0.0592	0.0496	0.0536
ωR [on F ² , all data]	0.1792	0.1834	0.1325	0.1599
Largest diff. peak /hole/Å ⁻³	0.48/-0.22	0.37/-0.30	0.19/-0.17	0.54/-0.53

Table 7.5.2: Chapter 2- Compounds 5, 7 and 9

Compound	$[(C_5H_{10})(C_2H_5)COONa(1,10\text{-phen})]_{\infty}$, 5	$[NaMg[N(iPr)_2]_2OC_2H_3(C_2H_5)C_4H_9]_2$, 7	$[(Ph_2NNA)_2(Py)_3 \cdot 0.5(THF/Py)]$, 9
Empirical Formula	$C_{20}H_{23}N_2O_2Na$	$C_{20}H_{25}N_2OMgNa$	$C_{43.5}H_{41.5}ON_{5.5}Na_2$
Molecular Mass	346.39	356.72	695.17
λ	Cu K α ($\lambda = 1.54184$)	Cu K α ($\lambda = 1.54184$)	Cu K α ($\lambda = 1.54184$)
Space Group	Ia	I2	P21
Crystal system	Monoclinic	Monoclinic	Monoclinic
a/Å	6.9269(17)	11.8984(4)	10.0102(2)
b/Å	15.085(4)	16.7271(6)	18.6593(4)
c/Å	17.616(4)	12.2368(5)	10.3074(2)
$\alpha/^\circ$	90	90	90
$\beta/^\circ$	90.88(2)	99.821(3)	98.346(2)
$\gamma/^\circ$	90	90	90
Volume/Å ³	1840.5(8)	2399.74(16)	1904.86(7)
Z	4	4	2
Measured Reflections	6235	9922	9089
Unique Reflections	3111	4608	5910
R _{int}	0.0877	0.0310	0.0457
Observed Reflections [$I > 2\sigma I$]	2047	3872	5681
Goodness of Fit	1.368	2.065	1.047
R [on F, obs refs only]	0.1221	0.1557	0.0504
ωR [on F ² , all data]	0.4008	0.4387	0.1419
Largest diff. peak /hole/Å ⁻³	0.80/-0.41	2.00/-0.85	0.30/-0.20

Table 7.5.3: Chapter 4- Compounds 10-12

Compound	$[(\text{THF})\cdot\text{Li}(\text{CO}_2\text{NC}_4\text{H}_4)]_\infty$, 10	$\{(\text{iPr}_2\text{NCOOLi})_{12}(\text{iPr}_2\text{NCOOH})_2\}$, 11	$[(\text{Me}_3\text{Si})\text{NC}(=\text{O})\text{OC}(=\text{O})\text{N}(\text{H})(\text{SiMe}_3)]_2\text{LiNa}(\text{THF})_4$, 12
Empirical Formula	$\text{C}_9\text{H}_{12}\text{LiNO}_3$	$\text{C}_{98}\text{H}_{198}\text{Li}_{12}\text{N}_{14}\text{O}_{28}$	$\text{C}_{28}\text{H}_{62}\text{LiN}_4\text{NaO}_9\text{Si}_4$
Molecular Mass	189.14	2104.02	741.10
λ	Mo K α ($\lambda = 0.71073$)	Cu K σ ($\lambda = 1.54184$)	Cu K σ ($\lambda = 1.54184$)
Space Group	P-1	P-1	C2
Crystal system	Triclinic	Triclinic	Monoclinic
a/Å	5.4312(10)	14.8500(7)	22.2504(11)
b/Å	7.6252(16)	15.5422(6)	13.1969(5)
c/Å	12.092(2)	17.5104(7)	17.7522(8)
$\alpha/^\circ$	84.577(15)	110.729(4)	90
$\beta/^\circ$	87.445(14)	95.790(3)	112.116(5)
$\gamma/^\circ$	76.369(17)	98.130(4)	90
Volume/Å ³	484.37(16)	3691.8(3)	4829.2(4)
Z	2	1	4
Measured Reflections	2777	34191	11971
Unique Reflections	1891	14449	6709
R _{sigma}	0.0749	0.0799	0.0509
R _{int}	0.0239	0.0892	0.0400
Observed Reflections [$I > 2\sigma I$]	1145	9486	5340
Goodness of Fit	1.098	0.992	1.054
R [on F, obs refs only]	0.0641	0.0957	0.0891
ωR [on F ² , all data]	0.1939	0.3087	0.2660
Largest diff. peak /hole/Å ⁻³	0.38/-0.41	0.73/-0.56	0.68/-0.49

Table 7.5.4: Chapter 5- Compounds 13-16

Compound	[[{(NacNac)CO ₂ .Li.TMEDA)} ₂], 13	[[{(MeCN-2,6-iPr ₂ C ₆ H ₃) ₂ C(CONH(<i>t</i> -Bu))}Li.TMEDA], 14	[(MeCN-2,6-iPr ₂ C ₆ H ₃) ₂ C(O)Li{NH(<i>t</i> -Bu)CO}], 15	[[{(MeCN-2,6-iPr ₂ C ₆ H ₃) ₂ C(CONH(<i>i</i> -Pr))}Li.THF] ₂ , 16
Empirical Formula	C ₇₂ H ₁₁₄ Li ₂ N ₈ O ₄	C ₈₃ H ₁₄₂ Li ₂ N ₁₁ O ₂	C ₆₈ H ₁₀₀ Li ₂ N ₆ O ₄	C ₇₈ H ₁₂₀ Li ₂ N ₆ O ₅
Molecular Mass	1169.59	669.97	1079.41	1235.67
λ	Mo Kα (λ = 0.71073)	Cu Kσ (λ = 1.54184)	Cu Kσ (λ = 1.54184)	Cu Kσ (λ = 1.54184)
Space Group	P-1	P-1	P2 1/n	P-1
Crystal system	Triclinic	Triclinic	Monoclinic	Triclinic
a/Å	11.6560(8)	9.7020(9)	19.0144(3)	12.7236(8)
b/Å	11.6966(7)	15.2850(12)	15.9590(2)	13.2270(10)
c/Å	15.0959(11)	16.9986(14)	21.6141(3)	14.0962(11)
α/°	76.954(6)	66.491(7)	90	102.165(7)
β/°	67.567(7)	88.941(7)	96.2960(10)	105.011(6)
γ/°	85.816(5)	75.350(7)	90	113.070(7)
Volume/Å ³	1853.1(2)	2226.8(4)	6519.26(16)	1973.7(3)
Z	1	2	4	1
Measured Reflections	17316	16164	31370	16204
Unique Reflections	6498	8141	12812	7736
R _{int}	0.0674	0.0910	0.0343	0.0560
Observed Reflections [I>2σI]	2881	4681	10063	5024
Goodness of Fit	1.003	0.933	1.024	1.013
R [on F, obs refs only]	0.0640	0.0867	0.0556	0.0763
ωR [on F ² , all data]	0.1657	0.2451	0.1604	0.2391
Largest diff. peak /hole/Å ⁻³	0.15/-0.17	0.69/-0.47	0.61/-0.27	0.66/-0.25

Table 7.5.5: Chapter 5- Compounds 17-20

Compound	$\{[(\text{MeCN-2,6-}i\text{Pr}_2\text{C}_6\text{H}_3)_2\text{C}(\text{CONH}(\text{t-Bu}))]\text{Li.PMDETA}\}$, 17	$\{[(2,6\text{-}i\text{Pr}_2\text{C}_6\text{H}_3)]\text{NCON}(\text{tBu})\text{Li.PMDETA}\}$, 18	$\{[(\text{MeCN-2,6-}i\text{Pr}_2\text{C}_6\text{H}_3)_2\text{CH}]\text{Li.NCN}(\text{C}_6\text{H}_{11})_2\}$, 19	$\{[(\text{MeCN-2,6-}i\text{Pr}_2\text{C}_6\text{H}_3)_2\text{CH}]\text{Li.OP}(\text{C}_6\text{H}_5)_3\}$, 20
Empirical Formula	$\text{C}_{43}\text{H}_{73}\text{N}_6\text{OLi}$	$\text{C}_{26}\text{H}_{50}\text{N}_5\text{OLi}$	$\text{C}_{42}\text{H}_{63}\text{N}_4\text{Li}$	$\text{C}_{100}\text{H}_{126}\text{N}_4\text{O}_2\text{P}_2\text{Li}_2$
Molecular Mass	697.01	455.65	630.90	1491.86
λ	Cu $K\alpha$ ($\lambda = 1.54184$)	Cu $K\alpha$ ($\lambda = 1.54184$)	Cu $K\alpha$ ($\lambda = 1.54184$)	Cu $K\alpha$ ($\lambda = 1.54184$)
Space Group	P-1	Pbca	P-1	C2/c
Crystal system	Triclinic	Orthorhombic	Triclinic	Monoclinic
a/Å	10.5100(10)	17.9191(3)	12.4391(5)	20.0377(3)
b/Å	13.0187(11)	17.1132(3)	14.1774(7)	16.6030(3)
c/Å	16.7220(16)	18.9522(3)	24.4260(8)	27.2162(3)
$\alpha/^\circ$	89.090(7)	90	92.321(3)	90
$\beta/^\circ$	77.888(8)	90	102.549(3)	92.9420(10)
$\gamma/^\circ$	75.904(8)	90	97.521(4)	90
Volume/Å ³	2168.2(4)	5811.75(17)	4158.0(3)	9042.5(2)
Z	2	8	4	4
Measured Reflections	17231	14119	34426	22030
Unique Reflections	7872	5684	15647	8878
R _{int}	0.0772	0.0346	0.0725	0.0310
Observed Reflections [I>2σI]	4668	4762	8349	7056
Goodness of Fit	1.065	1.040	0.881	1.030
R [on F, obs refs only]	0.0799	0.0544	0.0718	0.0506
ωR [on F ² , all data]	0.2762	0.1530	0.2031	0.1452
Largest diff. peak /hole/Å ⁻³	0.36/-0.28	0.39/-0.26	0.67/-0.32	0.42/-0.28

References

1. J. Barker, C. Snape and D. Scurr, presented in part at the 9th International Colloquium Fuels Conventional and Future Energy for automobiles, Stuttgart/Ostfildern, 2013.
2. J. Reid, S. Cook and J. Barker, *SAE Int. J. Fuels Lubr.*, 2014, **7**, 436-444.
3. Economic and Market Report: EU Automotive Industry, http://www.acea.be/uploads/statistic_documents/Economic_and_Market_Report_Q2_2016.pdf, (accessed 20th October, 2016).
4. *Diesel Fuels Technical Review*, Chevron, 2007.
5. W. Dabelstein, A. Reglitzky, A. Schutze, K. Reders and A. Brunner, *Ullmanns Encyclopedia of Industrial Chemistry*, 2016, 1-41.
6. J. T. Joseph, *FUEL*, 2015, 66-68.
7. E. M. Tyapochkin and E. I. Kozliak, *J. Mol. Catal. A: Chem.*, 2003, **203**, 37-51.
8. J. Bennet, in *Alternative Fuels and Advanced Vehicle Technologies for Improved Environmental Performance: Towards Zero Carbon Transportation* ed. R. Folkson, Woodhead Publishing, 2014, ch. 7, pp. 165-194.
9. I. Martinez, *Fuel Properties*, 1-22.
10. Shell, *Safety Data Sheet for diesel (ULSD/Gasoline)*, 2014, 1-18.
11. K. Ravindra, R. Sokhi and R. Van Grieken, *Atmospheric Environment*, 2008, **42**, 2895-2921.
12. E. H. Stenby and W. Yan, in *Encyclopedia of Hydrocarbons: Exploration, production and transport*, ENI, 2005, vol. 1, ch. 1.1, pp. 31-64.
13. A. Marcus, in *PassageMaker*, Annapolis, Maryland, USA, 1999, vol. 4, pp. 1-6.
14. J. McMurry, in *Organic Chemistry*, Thomson Brooks/Cole, 7th edn., 2008, ch. 3, p. 92.
15. P. Atkins and J. De Paula, *Physical Chemistry*, Oxford University Press, Oxford, 9th edn., 2010.
16. C. Schaschke, I. Fletcher and N. Glen, *Processes*, 2013, **1**, 30-48.
17. D. E. Winterbone and A. Turan, in *Advanced Thermodynamics for Engineers*, Elsevier, 2nd edn edn., 2015, ch. 10, pp. 207-234.

18. M. Boot, C. Luijten, B. Somers, R. Baert, A. Donkerbroek, R. J. H. Klein-Dowel and N. Dam, *Energy & Fuels*, 2009, **23**, 1808-1817.
19. Fuel Additives: Use and Benefits, <https://www.atc-europe.org/public/Doc113%202013-10-01.pdf>, (accessed 17th October, 2016).
20. R. C. Santana, P. T. Do, M. Santikunaporn, W. E. Alvarez, J. D. Taylor, E. L. Sughrue and D. E. Resasco, *Fuel*, 2006, **85**, 643-656.
21. G. R. Ivanis, I. R. Radovic, V. B. Veljkovic and M. L. Kijevcanin, *Fuel*, 2016, **184**, 277-288.
22. M. Bubalik, A. Beck, J. Baladincz and J. Hancsok, *Petroleum & Coal*, 2009, **51**, 167-175.
23. IUPAC, *Compendium of Chemical Terminology*, Blackwell Scientific Publications, Oxford, 2nd edn., 1997.
24. E. S. Forbes and G. R. Neustadter, *Tribology*, 1972, **5**, 72-77.
25. S. Pirouz, Y. Wang, J. M. Chong and J. Duchamel, *J. Phys. Chem. B*, 2015, **119**, 12202-12211.
26. J. Galante-Fox and J. Bennett, in *Afton Chemical Corporation*, 2012, pp. 157-166.
27. J. Barker, J. Reid, C. Snape, D. Scurr and W. Meredith, *SAE Int. J. Fuels Lubr.*, 2014, **7**.
28. S. Cook, J. Barker, J. Reid and P. Richards, *SAE Int. J. Fuels Lubr.*, 2012, **5**.
29. N. M. Ribeiro, A. C. Pinto, C. M. Quintella, G. O. da Rocha, L. S. G. Teixeira, L. L. N. Guarieiro, M. d. C. Rangel, M. C. C. Veloso, M. J. C. Rezende, R. S. da Cruz, A. M. de Oliveira, E. A. Torres and J. B. de Andrade, *Energy & Fuels*, 2007, **21**, 2433-2445.
30. J. R. Kanicky and D. O. Shah, *J. Colloid Interface Sci.*, 2002, **256**, 201-207.
31. D. Claydon, *Goriva i Maziva*, 2014, **53**, 342-353.
32. J. Reid and J. Barker, *SAE International*, 2013.
33. P. Lacey, S. Gail, J. M. Kientz, G. Benoist, P. Downes and C. Daveau, *SAE Int. J. Fuels Lubr.*, 2012, **5**.
34. M. D. C. Almena, O. L. Esperilla, F. M. Manzanero, Y. M. Duarte, L. C. Q. Toscano and G. Wolff, *SAE International*, 2012.
35. J. Barker, S. Cook and P. Richards, *SAE Int. J. Fuels Lubr.*, 2013, **6**.
36. P. G. Mahaffy, B. Bucat, R. Tasker, J. C. Kotz, P. M. Treichel, G. C. Weaver and J. McMurtry, *Chemistry: Human activity, chemical reactivity*, Nelson Education, First International Edition edn., 2011.
37. J. Barker, C. Snape and D. Scurr, *SAE Int. J. Fuels Lubr.*, 2012, **5**, 1155-1164.

38. K. S. Markley, in *Fatty Acids: Their Chemistry, Properties, Production and Uses.*, ed. K. S. Markley, Interscience Publishers, Inc, New York, 2nd edn., 1961, vol. 2, ch. 8, pp. 715-757.
39. R. C. Mehrotra and R. Bohra, *Metal Carboxylates*, Academic Press Inc., London, 1st edn., 1983.
40. E. Kissa, *Journal of Colloid Science*, 1962, **17**, 857-864.
41. E. Kissa, *Journal of Colloid Science*, 1964, **19**, 279-289.
42. R. C. Pink, *J. Chem. Soc.*, 1938, 1252-1254.
43. J. McMurry, in *Organic Chemistry*, Thomson Brooks/Cole, 7th edn., 2008, ch. 21, p. 810.
44. R. A. Grayburn, M. Dowsett, M. De Keersmaecker, D. Banerjee, S. Brown and A. Adrians, *Heritage Science*, 2014, **2**, 1-9.
45. R. A. Grayburn, M. G. Dowsett and A. Adriaens, *Heritage Science*, 2016, **4**, 1-3.
46. R. G. Bossert, *J. Chem. Educ.*, 1950, **27**, 10-15.
47. The use of sodium laureth-11 carboxylate in cosmetics,
https://www.ewg.org/skindeep/ingredient/723780/SODIUM_LAURETH-11_CARBOXYLATE/, (accessed 28th November, 2016).
48. J. J. Shipp, in *Chemistry and Technology of the Cosmetics and Toiletries Industry*, eds. D. F. Williams and W. H. Schmitt, Springer Science+Business Media, New York, 2012, ch. 2, p. 36.
49. Y. F. Han, D. Kumar, C. Sivadinaragana and D. W. Goodman, *J. Catal.*, 2004, **224**, 60-68.
50. G. Ayrey, R. C. Poller and I. H. Siddiqui, *Polymer*, 1972, **13**, 299.
51. W. H. C. Rueggeberg, *Journal of Physical and Colloid Chemistry*, 1948, **52**, 1444-1460.
52. P. N. Nelson and H. A. Ellis, *J. Mol. Struct.*, 2014, **1075**, 299-310.
53. P. N. Nelson, H. A. Ellis and N. A. White, *Spectrochimica Acta Part A: Molecular and Biomolecular Spectroscopy*, 2015, **145**, 440-453.
54. F. A. Cotton, G. Wilkinson, C. A. Murillo and M. Bochmann, *Advanced Inorganic Chemistry*, John Wiley & Sons, Inc., New York, 6th edn., 1999.
55. Y. Koga and R. Matuura, *Memoirs of the faculty of science, Kyushu University, Series C Chemistry*, 1961, **4**.

56. K. Qian, W. K. Robbins, C. A. Hughey, H. J. Cooper, R. P. Rodgers and A. G. Marshall, *Energy & Fuels*, 2001, **15**, 1505-1511.
57. J. S. Clemente and P. M. Fedorak, *Chemosphere*, 2005, **60**, 585-600.
58. U. Wietelmann and J. Klett, *Z. Anorg. Allg. Chem.*, 2018, **644**, 194-204.
59. M. Pérez, M. Fañanás-Mastral, P. H. Bos, A. Rudolph, S. R. Harutyunyan and B. L. Feringa, *Nat. Chem.*, 2011, **3**, 377-381.
60. G. Wu and M. Huang, *Chem. Rev.*, 2006, **106**, 2596-2616.
61. D. B. Collum, *Acc. Chem. Res.*, 1993, **26**, 227-234.
62. W. Schlenk and J. Holtz, *Ber. Dtsch. Chem. Ges.*, 1917, **50**, 262-274.
63. D. Seyferth, *Organometallics*, 2006, **25**, 2-24.
64. D. Seyferth, *Organometallics*, 2009, **28**, 2-33.
65. R. E. Mulvey, *Chem. Soc. Rev.*, 1991, **20**, 167-209.
66. P. Hubberstey, *Coord. Chem. Rev.*, 1988, **85**, 1-85.
67. H. N. C. Wong, *Nat. Catal.*, 2019, **2**, 282-283.
68. E. Nakamura and K. Sato, *Nat. Mater.*, 2011, **10**, 158-161.
69. N. Yabuuchi, K. Kubota, M. Dahbi and S. Komaba, *Chem. Rev.*, 2014, **114**, 11636-11682.
70. *The Nobel Prize in Chemistry 2019*. NobelPrize.org. Nobel Media AB 2019. Wed. 4 Dec 2019., <https://www.nobelprize.org/prizes/chemistry/2019/summary/>.
71. N. Tanibata, Y. Kondo, S. Yamada, M. Maeda, H. Takeda, M. Nakayama, T. Asuka, A. Kitajou and S. Okada, *Sci. Rep.*, 2018, **8**, doi:10.1038/s41598-41018-35608-41599.
72. S. Asako, H. Nakajima and K. Takai, *Nat. Catal.*, 2019, **2**, 297-303.
73. M. Fairley, L. Davin, A. Hernán-Gómez, J. García-Álvarez, C. T. O'Hara and E. Hevia, *Chem. Sci.*, 2019, **10**, 5821-5831.
74. I. Banerjee, A. Harinath and T. K. Panda, *Eur. J. Inorg. Chem.*, 2019, 2224-2230.
75. G. Liu, P. J. Walsh and J. Mao, *Org. Lett.*, 2019, **21**, 8514-8518.
76. R. McLellan, M. Uzelac, L. J. Bole, J. M. Gil-Negrete, D. R. Armstrong, A. R. Kennedy, R. E. Mulvey and E. Hevia, *Synthesis*, 2019, **51**, 1207-1215.
77. M. Ángeles Fuentes, A. J. Martínez-Martínez, A. R. Kennedy and R. E. Mulvey, *Chem. Commun.*, 2016, **52**, 12199-12201.
78. R. M. Gault, A. R. Kennedy, R. McLellan, J. Barker, J. Reid and R. E. Mulvey, *Chem. Commun.*, 2019, **55**, 1478-1481.

79. R. M. Gault, R. McLellan, A. R. Kennedy, J. Barker, J. Reid and R. E. Mulvey, *Chem. Eur. J.*, 2019, **25**, 14728-14734.
80. M. Berton, R. Mello, P. G. Williard and M. E. González-Núñez, *J. Am. Chem. Soc.*, 2017, **139**, 17414-17420.
81. C. R. Groom, I. J. Bruno, M. P. Lightfoot and S. C. Ward, *Acta Cryst.*, 2016, **B72**, 171-179.
82. R. Neufeld and D. Stalke, *Chem. Sci.*, 2015, **6**, 3354-3364.
83. S. Bachmann, R. Neufeld, M. Dzemski and D. Stalke, *Chem. Eur. J.*, 2016, **22**, 8462-8465.
84. R. Neufeld, M. John and D. Stalke, *Angew. Chem. Int. Ed.*, 2015, **54**, 6994-6998.
85. D. Li, G. Kagan, R. Hopson and P. G. Williard, *J. Am. Chem. Soc.*, 2009, **131**, 5627-5634.
86. G. Kagan, W. Li, R. Hopson and P. G. Williard, *Org. Lett.*, 2010, **12**, 520-523.
87. S. E. Baillie, W. Clegg, P. García-Álvarez, E. Hevia, A. R. Kennedy, J. Klett and L. Russo, *Organometallics*, 2012, **31**, 5131-5142.
88. O. Tai, R. Hopson and P. G. Williard, *J. Org. Chem.*, 2017, **82**, 6223-6231.
89. O. Tai, R. Hopson and P. G. Williard, *Org. Lett.*, 2017, **19**, 3966-3969.
90. S. Bachmann, B. Gernert and D. Stalke, *Chem. Commun.*, 2016, **52**, 12861-12864.
91. J. M. Gruver, L. R. Liou, A. J. McNeil, A. Ramirez and D. B. Collum, *J. Org. Chem.*, 2008, **73**, 7743-7747.
92. B. Gehrhus, P. A. Hitchcock, A. R. Kennedy, M. F. Lappert, R. E. Mulvey and P. J. A. Rodger, *J. Organomet. Chem.*, 1999, **587**, 88-92.
93. J. Bernstein, R. E. Davis, L. Shimon and N.-H. Chang, *Angew. Chem. Int. Ed.*, 1995, **34**, 1555-1573.
94. W. H. Zachariasen, *J. Am. Chem. Soc.*, 1940, **62**, 1011-1013.
95. C. Ahlers and M. H. Dickmann, *Inorg. Chem.*, 1998, **37**, 6337-6340.
96. V. Kettmann, E. Kello, V. Vrabel, J. Garaj, M. Karvas, M. Goghova and J. Durmis, *Acta Cryst.*, 1989, **45**, 787-791.
97. E. Kello, V. Kettmann, V. Vrabel, J. Lokaj and M. Karvas, *Acta Cryst.*, 1989, **C45**, 1924-1926.
98. S. Breitung, H.-W. Lerner and M. Bolte, *Acta Cryst.*, 2003, **E59**, o445-o446.
99. W. Clegg, S. T. Liddle, R. E. Mulvey and A. Robertson, *Chem. Commun.*, 1999, 511-512.

100. Y. Tanabe, Y. Mizuhata and N. Tokitoh, *Pure Appl. Chem.*, 2010, **82**, 879-890.
101. E. E. Benson and C. P. Kubiak, *Chem. Commun.*, 2012, **48**, 7374-7376.
102. M. Curcio, J. R. Pankhurst, S. Sproules, D. Mignard and J. B. Love, *Angew. Chem. Int. Ed.*, 2017, **56**, 7939-7943.
103. K. B. Olsen, E. Taubøll and L. Gjerstad, *Acta. Neurol. Scand.*, 2007, **115**, 51-54.
104. D. S. Ziegler, B. Wei and P. Knochel, *Chem. Eur. J.*, 2019, **25**, 2695-2703.
105. L. Britton, J. H. Docherty, A. P. Dominey and S. P. Thomas, *Molecules*, 2020, **25**, 905-916.
106. P. N. Nelson and R. A. Taylor, *Appl Petrochem Res*, 2014, **4**, 253-285.
107. F. J. Martínez Casado, M. Ramos Riesco, M. V. García Pérez, M. I. Redondo, S. López-Andrés and J. A. Rodríguez Cheda, *J. Phys. Chem. B*, 2009, **113**, 12896-12902.
108. D. R. Armstrong, M. G. Davidson, D. Garcia-Vivo, A. R. Kennedy, R. E. Mulvey and S. D. Robertson, *Inorg. Chem.*, 2013, **52**, 12023-12032.
109. A. R. Kennedy, R. McLellan, G. J. McNeil, R. E. Mulvey and S. D. Robertson, *Polyhedron*, 2016, **103**, 94-99.
110. A. I. Ojeda-Amador, A. J. Martínez-Martínez, A. R. Kennedy and C. T. O'Hara, *Inorg. Chem.*, 2015, **54**, 9833-9844.
111. D. R. Armstrong, D. Barr, W. Clegg, S. M. Hodgson, R. E. Mulvey, D. Reed, R. Snaith and D. S. Wright, *J. Am. Chem. Soc.*, 1989, **111**, 4719-4727.
112. P. C. Andrews, W. Clegg and R. E. Mulvey, *Angew. Chem. Int. Ed. Engl.*, 1990, **29**, 1440-1441.
113. A. G. Avent, M. R. Crimmin, M. S. Hill and P. B. Hitchcock, *J. Organomet. Chem.*, 2006, **691**, 1242-1250.
114. K. J. Drewette, K. W. Henderson, A. R. Kennedy, R. E. Mulvey, C. T. O'Hara and R. B. Rowlings, *Chem. Comm.*, 2002, 1176-1177.
115. A. J. Martínez-Martínez, D. R. Armstrong, B. Conway, B. J. Fleming, J. Klett, A. R. Kennedy, R. E. Mulvey, S. D. Robertson and C. T. O'Hara, *Chem. Sci.*, 2014, **5**, 771-781.
116. A. R. Kennedy, R. E. Mulvey and R. B. Rowlings, *J. Am. Chem. Soc.*, 1998, **120**, 7816-7824.
117. I. Haiduc and E. R. T. Tiekink, *Inverse Coordination Chemistry: A Novel Chemical Concept*, Sunway University Press, 2020.
118. R. E. Mulvey, *Chem. Commun.*, 2001, 1049-1056.

119. R. E. Mulvey, *Organometallics*, 2006, **25**, 1060-1075.
120. K. J. Drewette, K. W. Henderson, A. R. Kennedy, R. E. Mulvey, C. T. O'Hara and R. B. Rowlings, *Chem. Commun.*, 2002, 1176-1177.
121. A. R. Kennedy, J. G. MacLellan, R. E. Mulvey and A. Robertson, *J. Chem. Soc., Dalton Trans.*, 2000, 4112-4116.
122. M. Schlosser, *Angew. Chem. Int. Ed.*, 2005, **44**, 376-393.
123. M. Schlosser and S. Strunk, *Tetrahedron Lett.*, 1984, **25**, 741-744.
124. P. Benrath, M. Kaiser, T. Limbach, M. Mondeshki and J. Klett, *Angew. Chem. Int. Ed.*, 2016, **55**, 10886-10889.
125. L. Yang, D. R. Powell and R. P. Houser, *Dalton Trans.*, 2007, 955-964.
126. S. R. Battten, N. R. Champness, X.-M. Chen, J. Garcia-Martinez, S. Kitagawa, L. Öhrström, M. O'Keeffe, M. P. Suh and J. Reedijk, *Pure Appl. Chem.*, 2013, **85**, 1715-1724.
127. D. Nunes, A. Pimental, L. Santos, P. Barquinha, L. Pereira, E. Fortunato and R. Martins, in *Metal Oxide Nanostructures: Synthesis, Properties and Applications* Elsevier, 2019.
128. D. A. Skoog, D. M. West, F. J. Holler and S. R. Crouch, *Fundamentals of Analytical Chemistry (9th ed.)*, Brooks/Cole, 2014.
129. D. B. Dell'Amico, F. Calderazzo, L. Labella, F. Marchetti and G. Pampaloni, *Chem. Rev.*, 2003, **103**, 3857-3898.
130. D. R. Feldman, W. D. Collins, P. J. Gero, M. S. Torn, E. J. Mlawer and T. R. Shippert, *Nature*, 2015, **519**, 339-343.
131. A. D. Curzons, D. N. Mortimer, D. J. Constable and V. L. Cunningham, *Green Chem.*, 2001, **3**, 1-6.
132. B. Dutcher, M. Fan and A. G. Russell, *ACS Appl. Mater. Interfaces*, 2015, **7**, 2137-2148.
133. P. Falkowski, R. J. Scholes, E. Boyle, J. Canadell, D. Canfield, J. Elser, N. Gruber, K. Hibbard, P. Höglberg, S. Linder, F. T. Mackenzie, B. Moore III, T. Pedersen, Y. Rosenthal, S. Seitzinger, V. Smetacek and W. Steffen, *Science*, 2000, **290**, 291-296.
134. W. Leitner, *Angew. Chem. Int. Ed. Engl.*, 1995, **34**, 2207-2221.
135. C. M. Rayner, *Org. Process Res. Dev.*, 2007, **11**, 121-132.
136. A. G. Gershikov and V. P. Spiridonov, *J. Mol. Struct.*, 1982, **96**, 141-149.

137. M. Aresta, in *Activation of Small Molecules: Organometallic and Bioinorganic Perspectives*, ed. W. B. Tolman, WILEY-VCH Verlag GmbH & Co. KGaA, Weinheim, 2006, ch. 1, pp. 1-41.
138. A. Paparo and J. Okuda, *Coord. Chem. Rev.*, 2017, **334**, 136-149.
139. W. B. Tolman, *Activation of Small Molecules: Organometallic and Bioinorganic Perspectives*, WILEY-VCH Verlag GmbH & Co. KGaA, Weinheim, 2006.
140. D. J. Darensbourg and M. S. Zimmer, *Macromolecules*, 1999, **32**, 2137-2140.
141. L. J. Murphy, K. N. Robertson, R. A. Kemp, H. M. Tuononen and J. A. C. Clyburne, *Chem. Commun.*, 2015, **51**, 3942-3956.
142. K. Hirotsu, S. Kamitori, T. Higuchi, I. Tabushi, K. Yamamura and H. Nonoguchi, *J. Inclusion Phenom.*, 1984, **2**, 215-222.
143. H. Kim, Y. Kim, M. Toon, S. Lim, S. M. Parks, G. Seo and K. Kim, *J. Am. Chem. Soc.*, 2010, **132**, 12200-12202.
144. K. A. Udachin, I. L. Moudrakovski, G. D. Enright, C. I. Ratcliffe and J. A. Ripmeester, *Phys. Chem. Chem. Phys.*, 2008, **10**, 4636-4643.
145. H. B. Wright and M. B. Moore, *J. Am. Chem. Soc.*, 1948, **70**, 3865-3866.
146. E. Jo, Y. H. Jhon, S. B. Choi, J.-G. Shim, J.-H. Kim, J. H. Lee, I.-Y. Lee, K.-R. Jang and J. Kim, *Chem. Commun.*, 2010, **46**, 9158-9160.
147. M. Aresta, D. Ballivet-Tkatchenko, D. B. Dell'Amico, M. C. Bonnet, D. Boschi, F. Calderazzo, R. Faure, L. Labella and F. Marchetti, *Chem. Commun.*, 2000, 1099-1100.
148. A. Berkessel, K. Roland, M. Schröder, J. M. Neudörfl and J. Lex, *J. Org. Chem.*, 2006, **71**, 9312-9318.
149. M. Ruben, D. Walther, R. Knake, H. Görls and R. Beckert, *Eur. J. Inorg. Chem.*, 2000, 1055-1060.
150. A. R. Kennedy, R. E. Mulvey, D. E. Oliver and S. D. Robertson, *Dalton Trans.*, 2010, **39**, 6190-6197.
151. R. P. Davies, P. R. Raithby and R. Snaith, *Organometallics*, 1996, **15**, 4355-4356.
152. D. B. Dell'Amico, F. Calderazzo, L. Labella and F. Marchetti, *Inorg. Chem.*, 2008, **47**, 5372-5376.
153. T. Haberer, H. Nöth and R. T. Paine, *Eur. J. Inorg. Chem.*, 2007, 4298-4305.
154. J. Klunker, M. Biedermann, W. Schäfer and H. Hartung, *Z. Anorg. Allg. Chem.*, 1998, **624**, 1503-1508.

155. G. A. Horley, M. F. Mahon and K. C. Molloy, *Inorg. Chem.*, 2002, **41**, 5052-5058.
156. G. Ménard, T. M. Gilbert, J. A. Hatnean, A. Kraft, I. Krossing and D. W. Stephan, *Organometallics*, 2013, **32**, 4416-4422.
157. G. Ménard and D. W. Stephan, *J. Am. Chem. Soc.*, 2010, **132**, 1796-1797.
158. C. M. Mömming, E. Otten, G. Kehr, R. Fröhlich, S. Grimme, D. W. Stephan and G. Erker, *Angew. Chem. Int. Ed.*, 2009, **48**, 6643-6646.
159. A. L. Arduengo, R. L. Harlow and M. Kline, *J. Am. Chem. Soc.*, 1991, **113**, 361-363.
160. H. A. Duong, T. N. Tekavec, A. M. Arif and J. Louie, *Chem. Commun.*, 2004, 112-113.
161. A. Álvarez, M. Borges, J. J. Corral-Pérez, J. G. Oleina, L. Hu, D. Cornu, R. Huang, D. Stoian and A. Urakawa, *ChemPhysChem*, 2017, **18**, 3135-3141.
162. F. Solymosi, *J. Mol. Catal.*, 1991, **65**, 337-358.
163. J. Costamagna, G. Ferraudi, J. Canales and J. Vargas, *Coord. Chem. Rev.*, 1996, **148**, 221-248.
164. N. Kitajima, K. Fujisawa, T. Koda, S. Hikichi and Y. Moro-Oka, *J. Chem. Soc., Chem. Commun.*, 1990, 1357-1358.
165. Q. Qin, Z. Guo and X. Wei, *Journal of Molecular Structure*, 2016, **1114**, 156-160.
166. T. Haberer, H. Noth and R. T. Paine, *Eur. J. Inorg. Chem.*, 2007, **27**, 4298-4305.
167. K.-C. Yang, C.-C. Chang, C.-S. Yeh, G.-H. Lee and S.-M. Peng, *Organometallics*, 2001, **20**, 126-137.
168. K. Knabel, I. Krossing, H. Noth, H. Schwenk-Kircher, M. Schmidt-Amelunxen and T. Seifert, *Eur. J. Inorg. Chem.*, 1998, 1095-1114.
169. L. Bourget-Merle, M. F. Lappert and J. R. Severn, *Chem. Rev.*, 2002, **102**, 3031-3065.
170. C. Camp and J. Arnold, *Dalton Trans.*, 2016, **45**, 14462-14498.
171. Y. C. Tsai, *Coord. Chem. Rev.*, 2012, **256**, 722-758.
172. M. Stender, R. J. Wright, B. E. Eichler, J. Prust, M. M. Olmstead, H. W. Roesky and P. Power, *J. Chem. Soc., Dalton Trans.*, 2001, 3465-3469.
173. W. J. Barry, I. L. Finar and E. F. Mooney, *Spectrochim. Acta*, 1965, **21**, 1095-1099.
174. L. C. Dorman, *Tetrahedron Lett.*, 1966, **4**, 459-464.
175. C. Chen, S. M. Bellows and P. L. Holland, *Dalton Trans.*, 2015, **44**, 16654-16670.
176. G. S. Girolami and A. P. Sattelberger, *Inorganic Syntheses*, John Wiley & Sons, Inc, New Jersey, 2014.
177. C. Cui, H. W. Roesky, H.-G. Schmidt, M. Noltemeyer, H. Hao and F. Cimpoesu, *Angew. Chem. Int. Ed.*, 2000, **39**, 4274-4276.

178. P. B. Hitchcock, M. F. Lappert and D.-S. Liu, *J. Chem. Soc., Chem. Commun.*, 1994, 1699-1700.
179. F. S. Mair, D. Scully, A. J. Edwards, P. R. Raithby and R. Snaith, *Polyhedron*, 1995, **14**, 2397-2401.
180. W. Clegg, E. K. Cope, A. J. Edwards and F. S. Mair, *Inorg. Chem.*, 1998, **37**, 2317-2319.
181. D. A. Dougherty, *Science*, 1996, **271**, 163-168.
182. R. B. King, *Polyhedron*, 2002, **21**, 2347-2350.
183. S. P. Green, C. Jones and A. Stasch, *Science*, 2007, **318**, 1754-1757.
184. A. Stasch and C. Jones, *Dalton Trans.*, 2011, **40**, 5659-5672.
185. J. Hicks, M. Juckel, A. Paparo, D. Dange and C. Jones, *Organometallics*, 2018, **37**, 4810-4813.
186. M. Zhu, L. Liu, H.-T. Yu, W.-X. Zhang and Z. Xi, *Chem. Eur. J.*, 2018, **24**, 19122-19135.
187. C. Weetman, M. S. Hill and M. F. Mahon, *Chem. Eur. J.*, 2016, **22**, 7158-7162.
188. A. S. S. Wilson, M. S. Hill and M. F. Mahon, *Organometallics*, 2019, **38**, 351-360.
189. S. E. Baillie, V. L. Blair, T. D. Bradley, W. Clegg, J. Cowan, R. W. Harrington, A. Hernán-Gómez, A. R. Kennedy, Z. Livingstone and E. Hevia, *Chem. Sci.*, 2013, **4**, 1895-1905.
190. L. Davin, R. McLellan, A. R. Kennedy and E. Hevia, *Chem. Commun.*, 2017, **53**, 11650-11653.
191. M. S. Hill, D. J. Liptrot and C. Weetman, *Chem. Soc. Rev.*, 2016, **45**, 972-988.
192. S. Harder, *Chem. Rev.*, 2010, **110**, 3852-3876.
193. A. G. M. Barrett, M. R. Crimmin, M. S. Hill and P. A. Procopiu, *Proc. R. Soc. London Ser. A*, 2010, **466**, 927-963.
194. C. Weetman, M. D. Anker, M. Arrowsmith, M. S. Hill, G. Kociok-Köhn, D. J. Liptrot and M. F. Mahon, *Chem. Sci.*, 2016, **7**, 628-641.
195. C. Weetman, M. S. Hill and M. F. Mahon, *Polyhedron*, 2016, **103**, 115-120.
196. J. Pahl, S. Brand, H. Elsen and S. Harder, *Chem. Commun.*, 2018, **54**, 8685-8688.
197. J. Pahl, A. Friedrich, H. Elsen and S. Harder, *Organometallics*, 2018, **37**, 2901-2909.
198. J. Pahl, T. E. Stennett, M. Volland, D. Guldi and S. Harder, *Chem. Eur. J.*, 2018, **25**, 2025-2034.
199. S. Brand, H. Elsen, J. Langer, W. A. Donaubauer, F. Hampel and S. Harder, *Angew. Chem. Int. Ed.*, 2018, **57**, 14169-14173.

200. B. Rösch, T. X. Gentner, H. Elsen, C. A. Fischer, J. Langer, M. Wiesinger and S. Harder, *Angew. Chem. Int. Ed.*, 2019, **58**, 5396-5401.
201. T. X. Gentner, B. Rösch, G. Ballmann, J. Langer, H. Elsen and S. Harder, *Angew. Chem. Int. Ed.*, 2019, **58**, 607-611.
202. A. L. Kenward, J. A. Ross, W. E. Piers and M. Parvez, *Organometallics*, 2009, **28**, 3625-3628.
203. M. Arrowsmith, B. Maitland, G. Kociok-Köhn, A. Stasch, C. Jones and M. S. Hill, *Inorg. Chem.*, 2014, **53**, 10543-10552.
204. T. X. Gentner, B. Rösch, K. Thum, J. Langer, G. Ballmann, J. Pahl, W. A. Donaubauer, F. Hampel and S. Harder, *Organometallics*, 2019, **38**, 2485-2493.
205. S. Harder and J. Brettar, *Angew. Chem. Int. Ed.*, 2006, **45**, 3474-3478.
206. J. Spielmann and S. Harder, *Chem. Eur. J.*, 2007, **13**, 8928-8938.
207. J. J. Berzelius, *Journal für Chemie und Physik*, 1817, **21**, 44-48.
208. H. Dietrich, *Acta Cryst.*, 1963, **16**, 681-689.
209. E. Weiss and E. A. C. Lucken, *J. Organomet. Chem.*, 1964, **2**, 197-205.
210. E. Weiss, *Angew. Chem. Int. Ed. Engl.*, 1993, **32**, 1501-1523.
211. T. Kottke and D. Stalke, *Angew. Chem. Int. Ed.*, 1993, **32**, 580-582.
212. T. Kottke and D. Stalke, *J. Appl. Cryst.*, 1993, **26**, 615-619.
213. M. A. Nichols and P. G. Williard, *J. Am. Chem. Soc.*, 1993, **115**, 1568-1572.
214. C. Strohmam and V. H. Gessner, *Angew. Chem. Int. Ed.*, 2007, **46**, 4566-4569.
215. R. E. Mulvey and S. D. Robertson, *Angew. Chem. Int. Ed.*, 2013, **52**, 11470-11487.
216. N. D. R. Barnett, R. E. Mulvey, W. Clegg and P. A. O'Neil, *J. Am. Chem. Soc.*, 1991, **113**, 8187-8188.
217. P. G. Williard and J. M. Salvino, *J. Org. Chem.*, 1993, **58**, 1-3.
218. M. P. Bernstein, F. E. Romesberg, D. J. Fuller, A. T. Harrison, D. B. Collum, Q.-Y. Lui and P. G. Williard, *J. Am. Chem. Soc.*, 1992, **114**, 5100-5110.
219. P. C. Andrews, N. D. R. Barnett, R. E. Mulvey, W. Clegg, P. A. O'Neil, D. Barr, L. Cowton, A. J. Dawson and B. J. Wakefield, *J. Organomet. Chem.*, 1996, **518**, 85-95.
220. W. Clegg, S. Kleditzsch, R. E. Mulvey and P. O'Shaughnessy, *J. Organomet. Chem.*, 1998, **558**, 193-196.
221. R. O. Sauer, *J. Am. Chem. Soc.*, 1944, **66**, 1707-1710.
222. A. Streitwieser, A. Facchetti, L. Xie, X. Zhang and E. C. Wu, *J. Org. Chem.*, 2012, **77**, 985-990.

223. D. Mootz, A. Zinnius and B. Böttcher, *Angew. Chem. Int. Ed. Engl.*, 1969, **8**, 378-379.
224. R. D. Rogers, J. L. Atwood and R. Grüning, *J. Organomet. Chem.*, 1978, **157**, 229-237.
225. L. M. Engelhardt, B. S. Jolly, P. C. Junk, C. L. Raston, B. W. Skelton and A. H. White, *Aust. J. Chem.*, 1986, **39**, 1337-1345.
226. K. W. Henderson, A. E. Dorigo, Q.-Y. Liu and P. G. Williard, *J. Am. Chem. Soc.*, 1997, **119**, 11855-11863.
227. R. Grüning and J. L. Atwood, *J. Organomet. Chem.*, 1977, **137**, 101-111.
228. J. Knizek, I. Krossing, H. Nöth, H. Schwenk and T. Seifert, *Chem. Ber.*, 1997, **130**, 1053-1062.
229. M. Driess, H. Pritzkow, M. Skipinski and U. Winkler, *Organometallics*, 1997, **16**, 5108-5112.
230. M. Karl, G. Seybert, W. Massa, K. Harms, S. Agarwal, R. Maleika, W. Stelter, A. Greiner, W. Heitz, B. Neumüller and K. Dehnicke, *Z. Anorg. Allg. Chem.*, 1999, **625**, 1301-1309.
231. Y. Sarazin, S. J. Coles, D. L. Hughes, M. B. Hursthouse and M. Bochmann, *Eur. J. Inorg. Chem.*, 2006, 3211-3220.
232. P. G. Williard and M. A. Nichols, *J. Am. Chem. Soc.*, 1991, **113**, 9671-9673.
233. P. G. Williard, *Acta Crystallogr. Sect. C*, 1988, **44**, 270-272.
234. G. C. Forbes, A. R. Kennedy, R. E. Mulvey, B. A. Roberts and R. B. Rowlings, *Organometallics*, 2002, **21**, 5115-5121.
235. M. G. Davidson, D. García-Vivo, A. R. Kennedy, R. E. Mulvey and S. D. Robertson, *Chem. Eur. J.*, 2011, **17**, 3364-3369.
236. K. F. Tesh, T. P. Hanusa and J. C. Huffman, *Inorg. Chem.*, 1990, **29**, 1584-1586.
237. A. P. N. Franchimont and H. Friedmann, *Recl. Trav. Chim.*, 1905, **24**, 404-418.
238. D. Kampmann, G. Stuhlmüller, R. Simon, F. Cottet, F. Leroux and M. Schlosser, *Synthesis*, 2005, 1028-1029.
239. M. F. Lappert, M. J. Slade, A. Singh, J. L. Atwood, R. D. Rogers and R. Shakir, *J. Am. Chem. Soc.*, 1983, **105**, 302-304.
240. D. R. Armstrong, P. García-Álvarez, A. R. Kennedy, R. E. Mulvey and S. D. Robertson, *Chem. Eur. J.*, 2011, **17**, 6725-6730.
241. P. G. Williard and Q.-Y. Liu, *J. Am. Chem. Soc.*, 1993, **115**, 3380-3381.
242. D. R. Armstrong, D. V. Graham, A. R. Kennedy, R. E. Mulvey and C. T. O'Hara, *Chem. Eur. J.*, 2008, **14**, 8025-8034.

243. T. Haberer, H. Nöth and R. T. Paine, *Eur. J. Inorg. Chem.*, 2007, **27**, 4298-4305.
244. T.-T. Wu, J. Huang, N. D. Arrington and G. M. Dill, *J. Agric. Food Chem.*, 1987, **35**, 817-823.
245. D. C. D. Butler and H. Alper, *Chem. Commun.*, 1998, 2575-2576.
246. A. L. Rheingold and R. A. Kemp, *CSD Communication*, 2015.
247. S. C. Ball, M. G. Davidson, R. P. Davies, A. J. Edwards, I. Lopez-Solera, P. R. Raithby and R. Snaith, *Angew. Chem. Int. Ed. Engl.*, 1995, 921-923.
248. X. Shao, Z. Li, X. Qian and X. Xu, *J. Agric. Food Chem.*, 2009, **57**, 951-957.
249. Y. Yang, Q. Zhang, J. Zheng and S. Zhang, *Polymer*, 2013, **54**, 3254-3260.
250. J. A. Garden, A. R. Kennedy, R. E. Mulvey and S. D. Robertson, *Dalton Trans.*, 2011, **40**, 11945-11954.
251. B. Milani, G. Licini, E. Clot and M. Albrecht, *Dalton Trans.*, 2016, **45**, 14419-14420.
252. S. M. Mansell, N. Kaltsoyannis and P. L. Arnold, *J. Am. Chem. Soc.*, 2011, **133**, 9036-9051.
253. K. Ray, F. F. Pfaff, B. Wang and W. Nam, *J. Am. Chem. Soc.*, 2014, **136**, 13942-13958.
254. R. M. Wells, V. Tetens and T. Brittain, *Nature*, 1983, **306**, 500-502.
255. C. Thomas and A. B. Lumb, *Continuing Education in Anaesthesia Critical Care & Pain*, 2012, **12**, 251-256.
256. X. Yin and J. R. Moss, *Coord. Chem. Rev.*, 1999, **181**, 27-59.
257. Q. Qin, Z. Guo and X. Wei, *J. Mol. Struct.*, 2016, **1114**, 156-160.
258. M. Hamell and R. Levine, *J. Org. Chem.*, 1950, 162-168.
259. R. Neufeld, M. John and D. Stalke, *Angew. Chem. Int. Ed.*, 2015, **54**, 6994-6998.
260. Y. Zhao, C. Mao, Y. Li, P. Zhang, Z. Huang, F. Bi, R. Huang and Q. Wang, *J. Agric. Food Chem.*, 2008, **56**, 7326-7332.
261. G. La Regina, A. Coluccia, A. Brancale, F. Piscitelli, V. Gatti, G. Maga, A. Samuele, C. Pannecoque, D. Schols, J. Balzarini, E. Novellino and R. Silvestri, *J. Med. Chem.*, 2011, **54**, 1587-1598.
262. F. Engelhardt, C. Maaß, D. M. Andrada, R. Herbst-Irmer and D. Stalke, *Chem. Sci.*, 2018, **9**, 3111-3121.
263. R. E. Mulvey, *Chem. Soc. Rev.*, 1998, **27**, 339-346.
264. D. R. Armstrong, D. Darr, R. Snaith, W. Clegg, R. E. Mulvey, K. Wade and D. Reed, *J. Chem. Soc. Dalton Trans.*, 1987, 1071-1081.

265. H. Chen, R. A. Bartlett, H. V. Rasika Dias, M. M. Olmstead and P. P. Power, *Inorg. Chem.*, 1991, **30**, 2487-2494.
266. W. Clegg, S. H. Dale, D. V. Graham, R. W. Harrington, E. Hevia, L. M. Hogg, A. R. Kennedy and R. E. Mulvey, *Chem. Commun.*, 2007, 1641-1643.
267. C. Willemann, R. Gruenert, P. J. Bednarski and R. Troschuetz, *Bioorganic Med. Chem.*, 2009, **17**, 4406-4419.
268. X. Li and R. Vince, *Bioorganic Med. Chem.*, 2006, **14**, 2942-2955.
269. A. Berkessel, K. Roland, M. Schröder, J. M. Neudörfl and J. Lex, *J. Org. Chem.*, 2006, **71**, 9312-9318.
270. A. Esparza-Ruiz, C. Herrmann, J. Chen, B. O. Patrick, E. Polishchuk and C. Orvig, *Inorganica Chim. Acta*, 2012, **393**, 276-283.
271. F. Calderazzo, S. Ianelli, G. Pampaloni, G. Pelizzi and M. Sperrle, *J. Chem. Soc. Dalton Trans.*, 1991, 693-698.
272. R. Neufeld, R. Michel, R. Herbst-Irmer, R. Schöne and D. Stalke, *Chem. Eur. J.*, 2016, **22**, 12340-12346.
273. C. Camp, L. Chatelain, C. E. Kefalidis, J. Pécaut, L. Maron and M. Mazzanti, *Chem. Commun.*, 2015, **51**, 15454-15457.
274. D. A. Dickie, K. B. Gislason and R. A. Kemp, *Inorg. Chem.*, 2012, **51**, 1162-1169.
275. J. J. Morris, B. C. Noll and K. W. Henderson, *Acta. Cryst. Sect. E*, 2007, **63**, m2477.
276. D. R. Armstrong, A. R. Kennedy, R. E. Mulvey and S. D. Robertson, *Chem. Eur. J.*, 2011, **17**, 8820-8831.
277. A. D. Kirilin, L. O. Belova, A. V. Lega, A. S. Maksimov, S. V. Petrov and E. A. Chernyshev, *Russ. J. Gen. Chem.*, 2005, **75**, 1163-1164.
278. J. F. M. Hewitt, L. Williams, P. Aggarwal, C. D. Smith and D. J. France, *Chem. Sci.*, 2013, **4**, 3538-3543.
279. A. Nagaki, Y. Takahashi and J.-I. Yoshida, *Chem. Eur. J.*, 2014, **20**, 7931-7934.
280. J. Davies, T. D. Svejstrup, D. F. Reina, N. S. Sheikh and D. Leonori, *J. Am. Chem. Soc.*, 2016, **138**, 8092-8095.
281. M. K. Bisai, T. Das, K. Vanka and S. S. Sen, *Chem. Commun.*, 2018, **54**, 6843-6846.
282. M. Asay, C. Jones and M. Driess, *Chem. Rev.*, 2010, **111**, 354-396.
283. S. P. Sarish, S. Nembenna, S. Nagendran and H. W. Roesky, *Acc. Chem. Res.*, 2011, **44**, 157-170.
284. R. L. Webster, *Dalton Trans.*, 2017, **46**, 4483-4498.

285. O. A. Mironova, T. S. Sukhikh, S. N. Konchenko and N. A. Pushkarevsky, *Polyhedron*, 2019, **159**, 337-344.
286. D. J. Mindiola, *Angew. Chem. Int. Ed.*, 2009, **48**, 6198-6200.
287. M. Magre, B. Maity, A. Falconnet, L. Cavallo and M. Rueping, *Angew. Chem. Int. Ed.*, 2019, DOI: 10.1002/anie.201902188.
288. Y. Liu, J. Li, X. Ma, Z. Yang and H. W. Roesky, *Coord. Chem. Rev.*, 2018, **374**, 387-415.
289. P. G. Hayes, W. E. Piers and M. Parvez, *Chem. Eur. J.*, 2007, **13**, 2632-2640.
290. P. G. Hayes, W. E. Piers and M. Parvez, *J. Am. Chem. Soc.*, 2003, **125**, 5622-5623.
291. A. Friedrich, J. Pahl, H. Elsen and S. Harder, *Dalton Trans.*, 2019, DOI: 10.1039/c1038dt03576h.
292. J. Lewiński, J. Zachara, P. Goś, E. Grabska, T. Kopeć, I. Madura, W. Marciniak and I. Prowotorow, *Chem. Eur. J.*, 2000, **17**, 3215-3227.
293. H. Zhu, J. Chai, V. Jancik, H. W. Roesky, W. A. Merrill and P. P. Power, *J. Am. Chem. Soc.*, 2005, **127**, 10170-10171.
294. F. A. LeBlanc, A. Berkefeld, W. E. Piers and M. Parvez, *Organometallics*, 2012, **31**, 810-818.
295. W.-K. Kim, M. J. Fevola, L. M. Liable-Sands, A. L. Rheingold and K. H. Theopold, *Organometallics*, 1998, **17**, 4541-4543.
296. P. H. M. Budzelaar, A. Bart van Oort and A. Guy Orpen, *Eur. J. Inorg. Chem.*, 1998, 1485-1494.
297. F. Basuli, R. L. Clark, B. C. Bailey, D. Brown, J. C. Huffman and D. J. Mindiola, *Chem. Commun.*, 2005, 2250-2252.
298. J. R. Hagadorn, L. Que Jr and W. B. Tolman, *J. Am. Chem. Soc.*, 1998, **120**, 13531-13532.
299. D. Banerjee, S. J. Kim and J. B. Parise, *Cryst. Growth Des.*, 2009, **9**, 2500-2503.
300. S. V. Kulangara, C. Mason, M. Juba, Y. Yang, I. Thapa, S. Gambarotta, I. Korobkov and R. Duchateau, *Organometallics*, 2012, **31**, 6438-6449.
301. F. H. Allen, O. Kennard, D. G. Watson, L. Brammer, A. Guy Orpen and R. Taylor, *J. Chem. Soc., Perkin Trans. 2*, 1987, S1-S19.
302. N. J. Hartmann, G. Wu and T. W. Hayton, *Dalton Trans.*, 2016, **45**, 14508-14510.
303. D. W. Randall, S. D. George, P. L. Holland, B. Hedman, K. O. Hodgson, W. B. Tolman and E. I. Solomon, *J. Am. Chem. Soc.*, 2000, **122**, 11632-11648.

304. R. S. Rojas, A. R. Cabrera, B. C. Peoples, K. Spannhoff, M. Valderrama, R. Fröhlich, G. Kehr and G. Erker, *Dalton Trans.*, 2012, **41**, 1243-1251.
305. A. R. Cabrera, Y. Schneider, M. Valderrama, R. Fröhlich, G. Kehr, G. Erker and R. S. Rojas, *Organometallics*, 2010, **29**, 6104-6110.
306. G. Ballmann, S. Grams, H. Elsen and S. Harder, *Organometallics*, 2019, DOI: 10.1021/acs.organomet.1029b00334.
307. W. Ren, S. Zhang, Z. Xu and X. Ma, *Dalton Trans.*, 2019, **48**, 3109-3115.
308. A. G. M. Barrett, T. C. Boorman, M. R. Crimmin, M. S. Hill, G. Kociok-Köhn and P. A. Procopiou, *Chem. Commun.*, 2008, 5206-5208.
309. A. Hernán-Gómez, T. D. Bradley, A. R. Kennedy, Z. Livingstone, S. D. Robertson and E. Hevia, *Chem. Commun.*, 2013, **49**, 8659-8661.
310. J. Shi, Z. Guo, X. Wei, D. Liu and M. F. Lappert, *Synlett*, 2011, 1937-1939.
311. L. A.-M. Harris, E. C. Y. Tam, M. P. Coles and J. R. Fulton, *Dalton Trans.*, 2014, **43**, 13803-13814.
312. S. Banerjee, Ankur, A. P. Andrews, B. Varghese and A. Venugopal, *Dalton Trans.*, 2019, **48**, 7313-7319.
313. G. Henrici-Olivé and S. Olivé, *J. Organomet. Chem.*, 1973, **52**, 49-50.
314. M. P. Lanci, V. V. Smirnov, C. J. Cramer, E. V. Gauchenova, J. Sundermeyer and J. P. Roth, *J. Am. Chem. Soc.*, 2007, **129**, 14697-14709.
315. G. Lyashenko, G. Saischek, A. Pal, R. Herbst-Irmer and N. C. Mösch-Zanetti, *Chem. Commun.*, 2007, 701-703.
316. W. Clegg, B. Conway, A. R. Kennedy, J. Klett, R. E. Mulvey and L. Russo, *Eur. J. Inorg. Chem.*, 2011, 721-726.
317. R. Campbell, L. M. Carrella, W. Clegg, R. E. Mulvey, E. Rentschler, S. D. Robertson and L. Russo, *Inorg. Chem.*, 2011, **50**, 4656-4659.
318. S. A. Orr, A. R. Kennedy, J. J. Liggat, R. McLellan, R. E. Mulvey and S. D. Robertson, *Dalton Trans.*, 2016, **45**, 6234-6240.
319. S. K. Gupta and A. Kelkar, *Main Group Chemistry*, 2005, **4**, 201-207.
320. C. P. Sindlinger and A. Stasch, *Dalton Trans.*, 2014, **43**, 14334-14345.
321. D. V. Graham, E. Hevia, A. R. Kennedy, R. E. Mulvey and C. T. O'Hara, *Chem. Commun.*, 2006, **4**, 417-419.

322. W. Clegg, B. J. Fleming, P. Garcia-Álvarez, L. M. Hogg, A. R. Kennedy, J. Klett, A. J. Martínez-Martínez, R. E. Mulvey, L. Russo and C. T. O'Hara, *Dalton Trans.*, 2013, **42**, 2512-2519.
323. P. Jutzi, E. Schlüter, C. Krüger and S. Pohl, *Angew. Chem. Int. Ed. Engl.*, 1983, **22**, 994.
324. S. Yokota, Y. Tachi and S. Itoh, *Inorg. Chem.*, 2002, **41**, 1342-1344.
325. K. D. Conroy, W. E. Piers and M. Parvez, *Organometallics*, 2009, **28**, 6228-6233.
326. A. Kalita, V. Kumar and B. Mondal, *RSC Adv.*, 2015, **5**, 643-649.
327. D. Tan and T. Frišić, *Chem. Commun.*, 2017, **53**, 901-904.
328. Y. Yang, A. Noor, A. J. Canty, A. Ariafard, P. S. Donnelly and R. A. J. O'Hair, *Organometallics*, 2019, **38**, 424-435.
329. V. A. Pollard, A. Young, R. McLellan, A. R. Kennedy, T. Tuttle and R. E. Mulvey, *Angew. Chem. Int. Ed.*, 2019, **58**, 12291-12296.
330. E. Hashem, T. McCabe, C. Schulzke and R. J. Baker, *Dalton Trans.*, 2014, **43**, 1125-1131.
331. J. P. Fackler Jr, C. A. López and R. E. P. Winpenny, *Acta Cryst.*, 1992, **C48**, 2218-2220.
332. E. R. Draper, B. Dietrich, K. McAulay, C. Brasnett, H. Abdizadeh, I. Patmanidis, S. J. Marrink, H. Su, H. Cui, R. Schweins, A. Seddon and D. J. Adams, *Matter*, 2020, **2**, 764-778.
333. UK could ban sale of petrol and diesel cars in 12 years, says Shapps, <https://www.theguardian.com/environment/2020/feb/12/uk-ban-sale-petrol-diesel-cars-shapps-transport>, (accessed 3rd April, 2020).
334. D. F. Shriver and M. A. Drezdon, *The Manipulation of Air-Sensitive Compounds*, J. Wiley and Sons, New York, 1986.
335. J. Leonard, B. Lygo and G. Proctor, *Advanced Practical Organic Chemistry*, CRC Press, Boca Raton, 2013.
336. A.-K. Kreyenschmidt, S. Bachmann, T. Niklas and D. Stalke, *ChemistrySelect*, 2017, **2**, 6957-6960.
337. G. M. Sheldrick, *Acta Crystallogr.*, 2008, **A64**, 112-122.
338. G. M. Sheldrick, *Acta Crystallogr.*, 2015, **C71**, 3-8.
339. A. P. Dove, V. C. Gibson, E. L. Hormnirun, E. L. Marshall, J. A. Segal, A. J. P. White and D. J. Williams, *Dalton Trans.*, 2003, 3088-3097.

- 340. O. V. Dolomanov, L. J. Bourhis, R. J. Gildea, J. A. K. Howard and H. Puschmann, *J. Appl. Cryst.*, 2009, **42**, 339-341.
- 341. C. Schade, W. Bauer and P. V. R. Schleyer, *J. Organomet. Chem*, 1985, **295**, 25-28.
- 342. A. L. Spek, *Acta Crystallogr., Sect. C*, 2015, **71**, 9-18.
- 343. G. J. P. Britovsek, J. England and A. J. P. White, *Inorg. Chem.*, 2005, **44**, 8125-8134.